University College London

Department of Chemical Engineering

Zeolite Microstructured Reactors

Yu Shan Susanna Wan

July 2003

A Thesis Submitted for the Degree of Doctor of Philosophy

of the University College London

ProQuest Number: 10010374
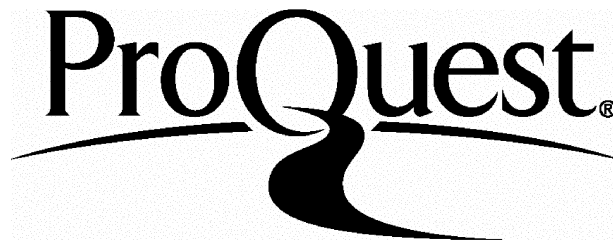
ProQuest®

ProQuest 10010374

To my family

Zeolite Microstructured Reactors

Abstract

Microreactors can provide better energy and material utilization leading to efficient chemical production. Due to the large surface area to volume ratio, the heat and mass transfer efficiency can be maximized. Reactions can also be performed under safe and automated conditions ensuring minimal environmental impact.

Zeolites can be precisely tailored up to the sub-nanometer scale. They are of great interest in catalysis and separation, which serve as the best candidate material for incorporation in microchemical systems. Titanium silicalite-1 zeolite (TS-1) is known to be an efficient catalyst for selective oxidation of alcohols, epoxidation of alkenes and hydroxylation of aromatics.

The techniques to incorporate zeolite in microchemical devices were pioneered. Zeolites (Silicalite-1, ZSM-5 and TS-1) can be employed as catalysts, membrane or structural materials. Traditional semiconductor fabrication technology was employed in micromachining the device architecture. Three novel strategies for manufacturing zeolite microchemical devices have been successfully demonstrated: localized zeolite growth, etching of zeolite-silicon composite film and free-standing zeolite membrane in microseparator.

The first prototype of zeolite-based single channel microreactor was successfully experimented for 1-pentene epoxidation over TS-1 catalyst. A simple computation model was developed to study the influence of reactor geometry, catalyst properties and reaction conditions to improve the microreactor performance. TS-1 coatings with different titanium-contents and crystal grain sizes were studied. Short-term deactivation of TS-1 was observed due to the formation of organic compounds and presence of water by product. Long-term deactivation by titanium leaching was irreversible.

In order to selectively remove water, which is one of the byproducts, a multi-channel membrane microreactor was designed and fabricated. The reaction studied was TS-1 catalysed selective oxidation of aniline while the membrane material was hydrophilic ZSM-5. Deactivation of the catalyst was reduced with improved product selectivity.

In this thesis, different strategies for incorporating zeolite in microreactors were studied. The microreactors were successfully tested and their various applications have been demonstrated. These results have provided an insight to improve the design of zeolite microstructured reactors.

Acknowledgements

First of all I would like to thank the Croucher Foundation for my scholarship. This work would not have been possible without the financial support from the Trustees.

I would like to express my sincere gratitude to my supervisor, Dr. Asterios Gavriilidis for his continuous guidance and encouragement throughout my PhD study. His helpful comments and advice inspired me a lot. I would like to thank my subsidiary supervisory, Dr. George Manos for his help and support.

I would also like to appreciate Dr. King Lun Yeung and Dr. Joseph Chau from the Hong Kong University of Science and Technology for the collaboration of this research. This work would not have happened so smoothly without their guidance and contribution. I am truly grateful for them.

Special thanks should go to Prof. Paul Barnes and Prof. Graham Hutchings for serving as my examiners.

I would like to express my warmest thoughts to all my friends in UCL and HKUST for their encouragement and friendship. I would also like to thank my research colleagues and technicians for their technical support. They make my research life enjoyable and memorable. I treasure every moment with them. I wish them all the best in the future.

Finally, I would like to thank my parents and granny for their unconditional love. I would also like to express my love to Cecilia and Simon back home. We have great fun together. I wish Cecilia happiness all her life and I believe Simon will be a great photographer one day. May God bless them.

Table of contents

Chapter 3

Instrumentation and methodology   85

Chapter 4

Chapter 5

Chapter 6

Chapter 7

Zeolite membrane microreactor for selective oxidation of aniline   209

List of figures

14

16

of the zeolite membrane grown within T-reactor channel (d)

A picture of the recess fabricated at the back of wafer with

the exposed zeolite membrane

70°C, H_2O_2/aniline=0.2

List of tables

Nomenclature

A	total external surface area of catalyst	m^2
c	dimensionless concentration of hydrogen peroxide used in Femlab model	-
C	concentration of hydrogen peroxide	$molm^{-3}$
C_{AS}	concentration of species A at the external surface of the catalyst	$molm^{-3}$
d	depth of channel	μm
D_{bulk}	diffusion coefficient of bulk fluid	m^2s^{-1}
$D_{eff(intra)}$	intra effective diffusitivity inside crystal	m^2s^{-1}
$D_{eff(inter)}$	inter effective diffusivity of catalyst	m^2s^{-1}
k_1	kinetic constant of first order reaction per unit surface area	ms^{-1}
k_2	kinetic constant of second order reaction per unit surface area	$m^4mol^{-1}s^{-1}$
k'_1	kinetic constant of first order reaction per unit volume	s^{-1}
k'_2	kinetic constant of second order reaction per unit volume	$m^3mol^{-1}s^{-1}$
l	channel length	mm
m	slope of reaction kinetic graph	s^{-1}
n	reaction order	-
Pe	Peclet number	-

Q	volumetric flowrate	m^3s^{-1}
r	rate of hydrogen peroxide conversion per unit catalyst surface area	$molm^{-2}s^{-1}$
r'	rate of hydrogen peroxide conversion	$molm^{-3}s^{-1}$
r''	dimensionless reaction rate used in Femlab model	-
R	radius of channel	m
S_a	surface area per unit mass of catalyst	m^2g^{-1}
T	reaction temperature	K
t	time	s
u	dimensionless velocity used in Femlab model	-
U_m	mean velocity	ms^{-1}
U_y	fluid velocity along the y axis	ms^{-1}
V	volume of reactor	m^3
W	catalyst weight	g
w	channel width	µm
x	transverse dimension	m
x'	dimensionless co-ordinate in x direction	-
y	dimension along channel length	m
y'	dimensionless co-ordinate in y direction	-
$[H_2O_2]$	concentration of hydrogen peroxide	$molm^{-3}$
$[C_5]$	concentration of 1-pentene	$molm^{-3}$

Greek Letters

Δ	difference	-
ΔP	pressure drop	Pa
β	titanium-content	at.%
τ	residence time	s
ε	crystal grain size	µm
ρ	catalyst density	gm^{-3}
δ	catalyst layer thickness	µm
θ	stoichiometric ratio of 1-pentene to hydrogen peroxide	-
χ	conversion of hydrogen peroxide	-
ϕ_n	Thiele modulus	-
μ	viscosity	Nsm^{-2}
Φ	Weisz-Prater parameter	-
Ψ	overall yield of epoxypentane	%

Subscripts

n	reaction order
0	initial condition
x	transverse dimension
y	dimension along channel length

Chapter 1

Introduction

1.1 Microreaction technology

Miniaturization of chemical systems has been gaining much attention for a variety of chemical and biological applications. The technology emerged from the expanding field of MicroElectroMechanical Systems (MEMS), which initially developed from integrated circuitry, representing miniaturized versions of mechanical machinery such as motors, turbines, pumps and actuators (Dutta, 1970). Nowadays, they also include sensors, heat exchangers and fluid handling devices. Recent advances in the design and fabrication of micromixers, microseparators and microreactors bring closer the reality of desktop miniature factories and micro-pharmaceutical synthesis (Dutta, 1970; Kawahara et al., 1996).

Research into miniaturization is driven by the need to minimize serious safety and environmental problems encountered presently in huge chemical plants (Ajmera et al., 2001). Cost implications can be reduced through better energy and material utilization. Smart, integrated microchemical systems are expected to bring into realization a distributed, on-site and on-demand production network for high value added products (Gavriilidis et al., 2002). By employing the most advanced green technology, minimal environmental impact can be ensured under safe and automated conditions (Quiram et al., 2000).

Besides academic and research institutes, developments in microreaction technology have become prevalent among numerous industrial bodies like DuPont,

BASF, Shell, Merck, Bayer, Axiva, etc. Microreactors offer great advantages such as safety, flexibility and pollution abatement (Löwe and Ehrfeld, 1999). The large surface area to volume ratio has proved it can provide excellent heat and mass transfer efficiency providing well-defined and uniform processes to increase product conversion and selectivity (Hardt et al., 2000). They provide significant improvement for rapid catalyst testing in high throughput experimentations (Haswell et al., 2001 and Greenway et al., 2000). The ability to accommodate completely new operating regimes serves as a great tool to locate optimal reaction conditions that are not accessible by conventional means (Wörz et al., 2001). Higher process yields can be attained (Wörz et al., 1998) by applying new process implementation. Explosion proof oxidation can also be now safely operated using microreactors (Jensen, 2001).

1.2 Application of zeolites

Zeolites, known as molecular sieves, are microporous tectosilicates with different pore sizes. They can be precisely tailored up to the sub-nanometer scale with desired arrangement and properties, which are of great interest in the field of catalysis, ion-exchange, separation and extraction (Davis and Lobo, 1992; Davis, 1998; Caro et al., 2000). Nowadays, they are widely employed in the synthesis of fine chemicals and pharmaceuticals (Hölderich and van Bekkum, 1991; Derouane at al., 2000), pollution abatement (Nishizaka and Misono, 1993; Sato et al., 1991), membranes (Coronas and Santamaria, 1999a) and membrane reactors (Casanave et al., 1995; Coronas and Santamaria, 1999b).

In the last decade, zeolite-support composites have been reported showing enormous potential in industry (Suzuki, 1987). Zeolite membranes possess the advantages of shape selectivity, sorption and catalysis properties, which serve as an excellent choice for application in chemical synthesis, catalyst regeneration, product separation, solvent recovery, liquid/liquid extraction and waste minimisation (van Bekkum et al., 1994; Jansen et al., 1994; Tsapatsis, 1999; Chau et al., 2000). The chemical environment within the zeolite pore channel can be manipulated to influence the molecular transport of diffusing species during separation. In addition, its unique framework chemistry and high internal surface area offer an excellent catalytic environment for many chemical reactions.

Recently, a miniature MFI type zeolite film (sicalite-1, ZSM-5) was successfully fabricated using traditional semiconductor technology (den Exter et al., 1997; Rebrov et al., 2001). This opens up the door to incorporate zeolites into microelectromechanical systems (MEMS). Zeolites, with their great thermal and chemical stability, offer a great choice for integration in microsystems. Their structures can be tuned and engineered precisely for design and application in nano devices (Yan and Bein, 1995). Novel thoughts of integrated membrane reactors can provide chemical reaction and product separation simultaneously (Schmidt et al., 1998; Martin et al., 1999).

1.3 Objectives

The main objective of this work is to investigate the fabrication strategies and design operating parameters of zeolite catalytic microreactors, membrane microreactors and membrane microseparators by subsequent testing through simulation and experiments. Traditional semiconductor fabrication methodology along with zeolite thin film technology were developed to incorporate MFI type zeolites into microreactor design as structural materials, catalysts or membranes. The microstructure and chemistry of these zeolites were tailor-made to satisfy the application requirements.

A first prototype of a zeolite microreactor was successfully tested. Detailed simulation was conducted as a design and data interpretation tool to examine the microreactor performance. A multi-channel membrane microreactor was also developed utilizing the molecular sieving effect of a zeolite. This novel technology, to fabricate zeolite microreactors, opens up a new horizon to incorporate zeolites in microstructured reactors for various chemical applications.

1.4   Thesis Outline

The novel concept of microreaction technology is introduced in Chapter 1. The development of miniaturized chemical systems and their advantages are discussed. The potential applications of zeolites as catalyst and membrane material in microreactors are suggested. The main objective of this work is also presented.

Chapter 2 contains a broad literature survey on zeolites and microsystem technology. The characteristics of zeolites and their applications as catalysts and membranes are illustrated. The advantages of microreactors and their further applications are discussed in detail.

Chapter 3 outlines the instrumentation and methodology employed in this work. Preparation of colloidal zeolite and zeolite membranes are introduced. Microchannel fabrication and characterisation methods are presented. Details for microreactor testing are illustrated.

Novel fabrication techniques to incorporate MFI zeolites in microchemical systems are discussed in Chapter 4. Complex microchannel geometry and networks, as well as zeolite arrays successfully fabricated, are illustrated. Blueprints for zeolite-based microchemical systems are presented and the structural details of the microdevices are analysed.

In Chapter 5, design and fabrication of zeolite-based microreactors and membrane microseparators are presented. Strategies for the manufacture of zeolite catalytic microreactors are discussed: zeolite powder coating, uniform zeolite film growth, localized zeolite growth, and etching of zeolite-silicon composite films. The preparation of free-standing membranes for zeolite membrane microseparators is also presented.

Chapter 6 presents the testing of a TS-1 microreactor for 1-pentene epoxidation, which has been selectively incorporated within the microreactor channel using a new synthesis procedure. A simple computation model is developed to simulate the reaction in the single-channel microreactor. The result obtained from computer simulation acts as a guideline to improve the reactor performance. The technique to engineer the catalyst microstructure and chemistry is demonstrated. Catalyst deactivation study was carried out on the TS-1 microreactor. Titanium leaching from the zeolite framework was also observed in the experiment.

A multi-channel membrane microreactor is then developed for selective removal of water. Chapter 7 presents the preliminary experimental result of the TS-1 catalysed selective oxidation of aniline. The product yield and selectivity are compared with performance of normal microreactors.

Finally, the conclusions and suggestions for future work are outlined in chapter 8. The practical implications of the thesis research are discussed. Applications

of zeolite-based microchemical devices in various research areas and industrial

processes are suggested.

Chapter 2

Literature Survey

2.1 General Background on Zeolites

Molecular sieve zeolites are crystalline alumino-silicalites in which the aluminum and silicon atoms are present in the form of AlO_4 or SiO_4 tetrahedra (Thompson, 1998). A Swedish mineralogist, Cronstedt, discovered the first zeolite in 1756, who found that the mineral lost water rapidly upon heating and thus seemed to boil (Cronstedt, 1756). The name "zeolite" comes from the Greek words *zeo* (to boil) and *lithos* (stone). In this project, we will focus on the study of MFI type zeolites.

2.1.1 Zeolite Structure

The fundamental building block of all zeolites is a tetrahedron of four oxygen anions surrounding a small silicon or aluminum ion. They are arranged so that each of the four oxygen anions is shared in turn with another silica or alumina tetrahedron. Figure 2.1 presents the primary building blocks of a zeolite. The cations required to maintain electrical neutrality are usually sodium in the zeolites as initially prepared, but they can be readily replaced by ion exchange which is the most direct and useful method for the modification of zeolite properties (Bhatia, 1990).

silica tetrahedron   alumina tetrahedron
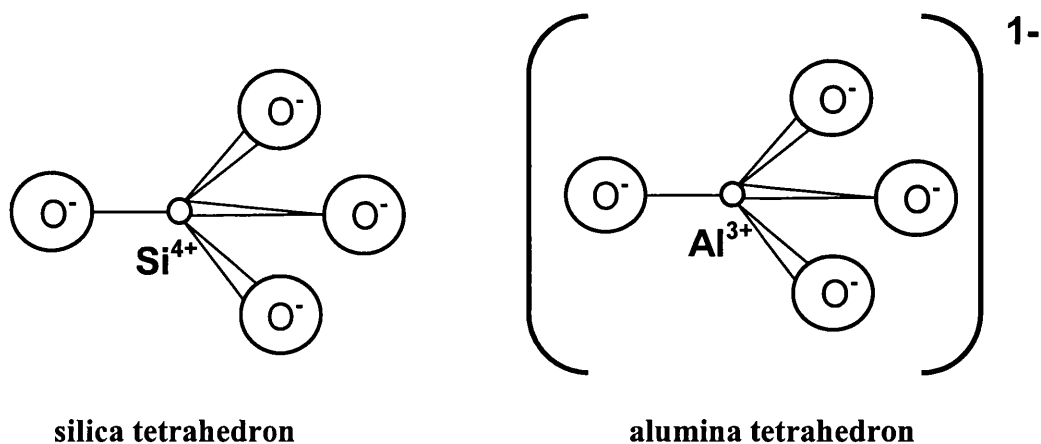
Figure 2.1   Primary building blocks of zeolites

(The IZA Structure Commission, 2003)

The silica and alumina tetrahedra are combined into more complicated secondary units, forming the building blocks of the framework zeolite crystal structures. The unit cell formula is usually written as $Mn^+_{x/n}[(AlO_2^-)(SiO_2)_y]_z\,H_2O$ whereas Mn stands for metal cations. For MFI type zeolites, for example ZSM-5, the unit cell formula is $Na_n[Al_nSi_{96-n}O_{192}] \sim 16\ H_2O$ with n < 27 (Kokotailo et al., 1978). ZSM-5 zeolite is orthorhombic with a framework density of 18.4 T/1000 Å^3 where T is an aluminium or silicon atom. Materials with the same topology include silicalite-1 (Flanigen et al., 1978) and TS-1 (Taramasso et al., 1983).

All known zeolite framework types can be characterized in terms of finite and infinite (i.e., chain or layer like) component units. A unit cell contains an integral number of secondary building units (SBUs) as shown in figure 2.2. Many of the

frameworks can be built from several different SBUs. These SBUs for each zeolite structure type are designated using the conventional three-letter code. The codes are assigned by the International Zeolite Association (IZA) Structure Commission on behalf of IUPAC, denoting the topology or connectivity of a tetrahedral zeolite-type framework (Meier and Baerlocher, 1999).

Framework density (FD) represents the number of tetrahedrally coordinated atoms (T-atoms) per 1000 Å^3. FD values of at least 19 to 21 T/1000 Å^3 are generally obtained for non-zeolite framework structures while for zeolite with fully crosslinked frameworks, the values range from 12.1 to 20.6. (Meier and Baerlocher, 1999; Baerlocher et al., 2001). Table 2.1 lists the constituent units of zeolite structure types (Bhatia, 1990).
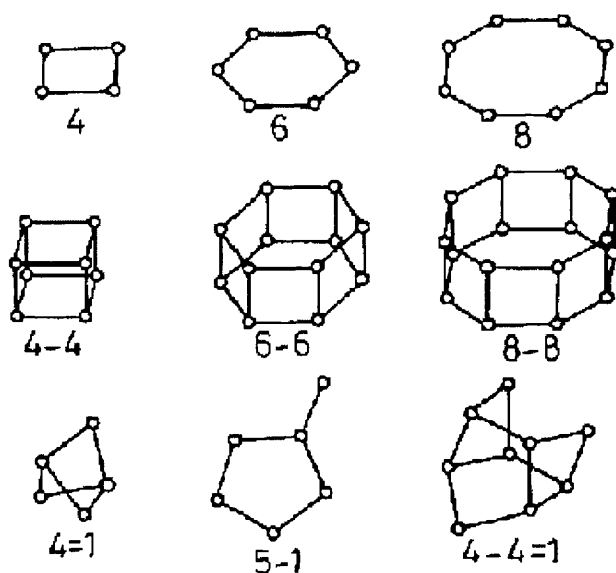
Figure 2.2   Secondary building units (The IZA Structure Commission, 2003)

38

Structure type		Secondary building units				Selected isotypes	Framework density
Code	**Full name**						
FAU	Faujasite	4	6		6-6	X, Y	12.7
LTA	Linde type A	4	6	8	4-4	SAPO-42, ZK-4,	12.9
RHO	Rho	4	6	8	8-8	Pahasapaite	14.3
CHA	Chabazite	4	6		6-6	AlPO-34, Phi	14.6
KFI	ZK-5	4	6	8	6-6	P, Q	14.7
OFF	Offretite		6			TMA-O, LZ-217	15.5
PHI	Phillipsite	4		8		Harmotome	15.8
ERI	Erionite	4	6			AlPO-17, LZ220	15.6
LTL	Linde type L		6			Perlialite	16.4
MOR	Mordenite		5-1			Ca-Q, LZ-211	17.2
MEL	ZSM-11		5-1			Silicalite-2, TS-2	17.7
MFI	ZSM-5		5-1			Silicalite-1, TS-1	17.9

Table 2.1   Constituent units of zeolite structure types

(Database of zeolite structures, 2003)

The characteristic channel systems in zeolite frameworks are usually described as 1-, 2- and 3-dimensional. Each system of equivalent channels can be distinguished by the channel direction, the number of T-atoms forming the rings controlling diffusion through the channels, and the crystallographic free diameters of the channels (Database of zeolite structures, 2003). The size and shape of the apertures vary in a different way depending on the ring opening structure. MFI

zeolites have a 3-dimensional system of 10-ring channels with a network of intersecting straight and sinusoidal channels. Figure 2.3 displays the crystal plane illustration of MFI zeolite with the framework viewed along the straight channel and zigzag channels (Olson et al., 1981; van Koningsveld, 1987).

(a)   <010> straight channel

<100> sinusoidal channel

<001>

(b) Framework viewed along [100]   (c) Framework viewed along [010]
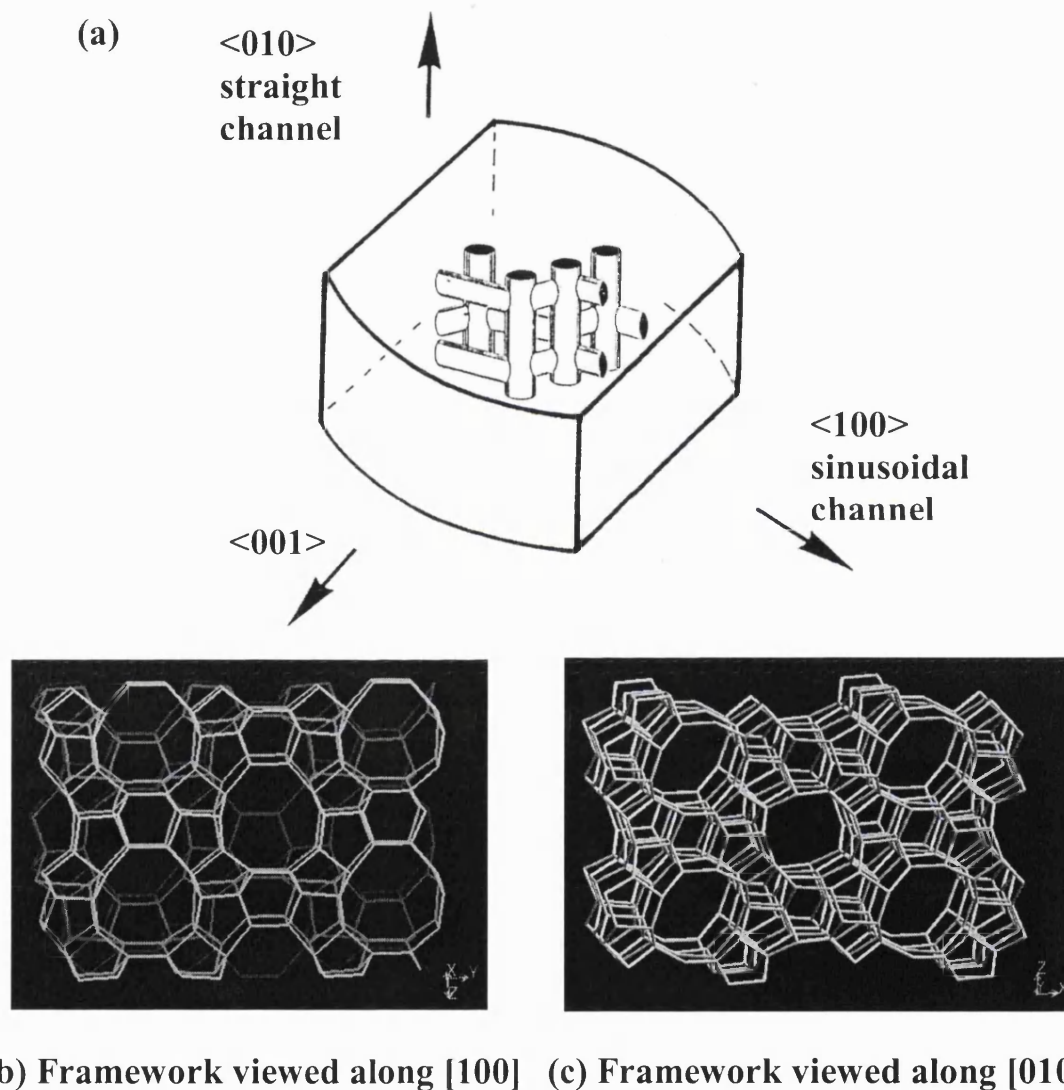
Figure 2.3   Schematic diagram of MFI zeolite (a) crystal plane illustration, (b) framework viewed along [100] and (c) framework viewed along [010] (Database of zeolite structures, 2003)

The 10-ring apertures of MFI zeolites are illustrated in figure 2.4 viewed along different channels and projections. The sinusoidal channel along the <100> direction exhibits an elliptical pore, 5.1Å × 5.5 Å diameters, while the more circular apertures running along the straight channel [010] have a pore size of 5.3Å × 5.6 Å.
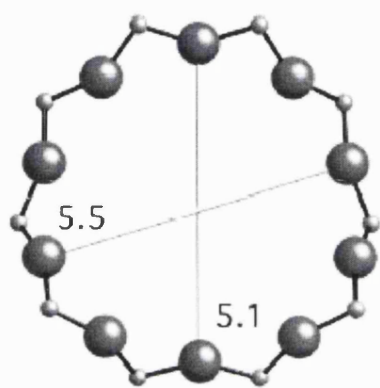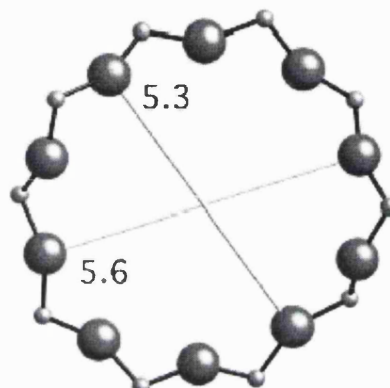
(a) 10-ring viewed along [100]   (b) 10-ring viewed along [010]

Figure 2.4   Schematic diagram of MFI zeolite (a) 10-ring viewed along [100] and (b) 10-ring viewed along [010] (Database of zeolite structures, 2003)

2.1.2   Crystal Growth

The mechanism of zeolite crystallization is very complex. The routes by which crystals are formed involve numerous simultaneous and interdependent equilibria and condensation steps (Burkett and Davis, 1994). Crystalline zeolites are produced from an amorphous alumninosilicate gel. For silicate-1 (MFI topology),

41

tetraethyl orthosilicate (TEOS) and tetrapropylammonium hydroxide (TPAOH) are used as the silica source and the template respectively.

The tetrapropylammonium (TPA) cation acts in an organic structure-directing role in zeolite synthesis. The TPA molecules are located at the channel intersections with propyl chains extending into both linear and sinusoidal channels (Chao et al, 1986). The molecules are held tightly at these sites and cannot diffuse in or out of the structure, and can only be removed by calcination. This suggests that the TPA molecules must be incorporated into the silicate structure during crystal growth.

The mechanism of structure direction and self-assembly for the TPA-mediated synthesis of Si-ZSM-5 is illustrated in figure 2.5. Burkett and co-workers (1994, 1995) have reported the existence of specific, intermolecular interactions within pre-organized, inorganic-organic composite structures during the synthesis of Si-ZSM-5. Structure direction is determined by the van der Waals interactions between the alkyl chains of the organic species and the hydrophobic silicate species, which give rise to the geometric correspondence between the structure-directing agent and the zeolite pore architecture. These structure-directing interactions have broad implications for the design and synthesis of new molecular sieve materials.
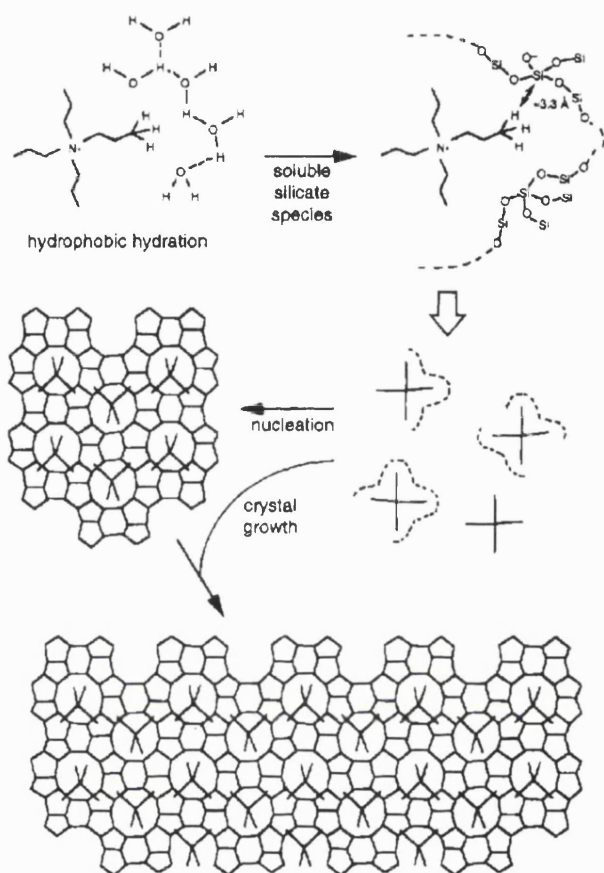
Figure 2.5   Schematic diagram of the proposed mechanism of structure direction and crystal growth involving inorganic-organic composite species in the TPA-mediated synthesis of MFI zeolite (Burkett et al., 1994, 1995).

2.2   Zeolite Catalysis

Zeolites are important catalysts in a wide range of chemical and petrochemical processes over the last two decades. Recently, they have been applied in the synthesis of intermediates and fine chemicals (Hölderich and van Bekkum, 1991; Maxwell and Stork, 1991; van Bekkum et al., 1994; Armor, 1999). The aluminum containing MFI zeolite, Al-ZSM-5 is used to catalyse hydrogenation, disproportionation, isomerisation and alkylation reactions (Jacobs and Martens, 1991). TS-1 zeolite is known to be an efficient catalyst for selective oxidation of alcohols (Maspero and Romano, 1994), epoxidation of alkenes (Clerici et al., 1991) and hydroxylation of aromatics (van der Pol et al., 1992), etc.

Zeolites can be precisely tailored up to sub-nanometer scale for successful applications. They can act as a very robust material to synthesize and withstand severe reaction conditions (Feast and Lercher, 1996). In comparison with macro- and mesoporous oxides, zeolites offer the advantages of high concentration of active sites resulting in very active catalysts and their chemical properties can be better modified. Their tuneable pore size and tortuosity can also determine the space available for transition states and diffusivities of reactants and products.

The rate and selectivity of catalysed reactions over molecular sieves catalysts are determined by their chemical induced selectivity (surface interface chemistry) and shape selectivity (steric limitations). Molecular sieve catalysts can be tuned over a

wide range of acidity and basicity. Many cations can be introduced by ion exchange and isomorphous substitution (Jacobs and Martens, 1991). They can also provide sites or be the site carriers allowing valence changes in redox processes. Metal crystallites and metal complexes can be entrapped within the zeolite framework offering a unique steric and chemical environment (Lunsford, 1987; Hölderich et al., 1991,).

2.2.1 Molecular sieves as acid and base

The medium pore sized zeolite, ZSM-5, is widely used as acid catalysts in hydrocarbon reactions (Jacobs and Martens, 1991). As described, each of the four oxygen anions is shared in turn with another silica or alumina tetrahedron. Isomorphous substitution of Si^{4+} by a trivalent ion (Al^{3+}) will result in a negative lattice charge and is compensated by a cation, usually sodium as shown in figure 2.6.
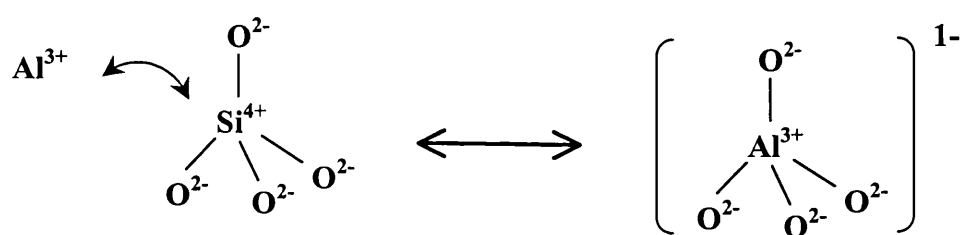
Figure 2.6   Isomorphous substitution of ZSM-5 primary building block

The high excess charge with the zeolite lattice provides strong Brønsted acidity (Kieboom et al, 1999). The catalytic activity increases with the Al/Si ratio and the proton content of zeolite as deprotonation energy is a strong function of Al/Si ratio. Catalytic cracking shown in figure 2.7 is one of the reactions catalysed by ZSM-5. Other reactions include metal catalysed CH activation and protonation of alkenes.

$$R-\overset{+}{\underset{R}{C}}-CH_2CH_2R \longrightarrow H_3C-\overset{+}{\underset{R}{CH}} + \underset{H_2}{C}=\underset{H}{C}-R$$
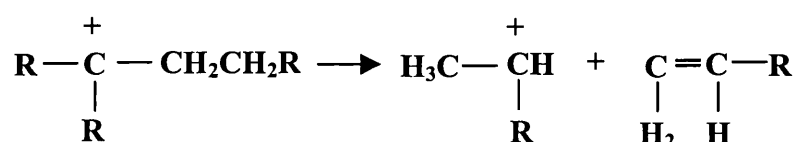
Figure 2.7   Catalytic cracking catalysed by ZSM-5 zeolite

2.2.2   Titanium containing molecular sieves

Titanosilicalite, TS-1, in which 0.1 to 2.5% of the Si atoms are replaced by Ti is the most successfully isomorphously substituted zeolite (Tuel et al., 1990). The presence of the acid sites determines the selectivity of the catalyst. TS-1 is found to catalyse a variety of reactions such as the conversion of alkenes to epoxide, alcohols to aldehydes, alkanes to secondary alcohols and ketones, phenol to hydroquinone and catechol and amines to hydroxylamines. (Langhendries et al., 1999, Davies et al, 2000, Schmidt et al, 2000, Uguina et al., 2000, Jenzer et al, 2001).
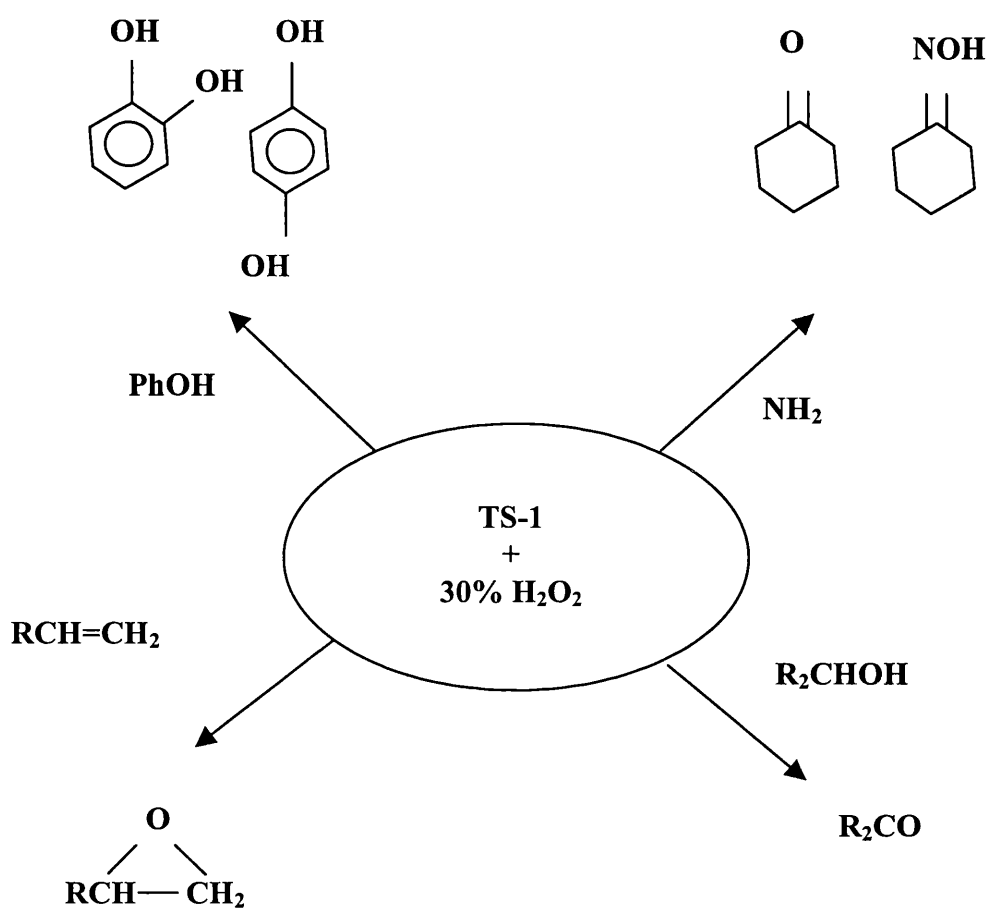
Figure 2.8   TS-1 catalysed oxidation with H₂O₂ (Sheldon, 1997)

47

2.3   Titanium silicalite-1 catalysts

2.3.1   TS-1 synthesis

Titanium silicalite-1 (TS-1) was first discovered by researchers in Enichem (Taramasso et al., 1983). The original method ("mixed alkoxides" method) is based on controlled hydrolysis of an aqueous solution containing tetraethyl orthosilicate (TEOS), tetraethyl orthotitanate (TEOT) and the organic templating agent, tetrapropylammonium hydroxide (TPAOH) (Taramasso et al., 1983). The procedure was illustrated in figure 2.9. TPAOH was added gradually to the hydrolysis mixture of TEOT and TEOS. The hydrolysis step should be done carefully to ensure that all apparatus are free of water. This is due to the fact that the titanium compounds will undergo hydrolysis once they get into contact with even a very small amount of water. The synthesis will fail as the compounds will polymerise and precipitate in the form of hydrated TiO_2. The synthesis solution then undergoes hydrothermal synthesis in a stainless steel autoclave heated at 175°C for 10 days.

Another method, involving the use of H_2O_2 to complex Ti, is called the "dissolved titanium" method (figure 2.9). Hydrogen peroxide is added to the titanium-containing solution to form stable peroxo-complexes. Colloidal SiO_2 will then be added which acts as the silica source. The complexes will slowly release the metal ions into the synthesis solution during hydrothermal treatment (Perego et al, 1998).

48

Other synthesis procedures, such as the use of low pH reactant mixture containing fluoride ions as mineralizing agent and the use of mixture of TPAOH and tetraethylammonium hydroxide (TEAOH), have been proposed (Carati et al., 1999). Instead of conventional oven heating, microwave heating of SiO_2-TiO_2 xerogel dry-impregnated with template was reported recently (Ahn et al., 2001).

"Mixed alkoxides"   **"Dissolved titanium"**
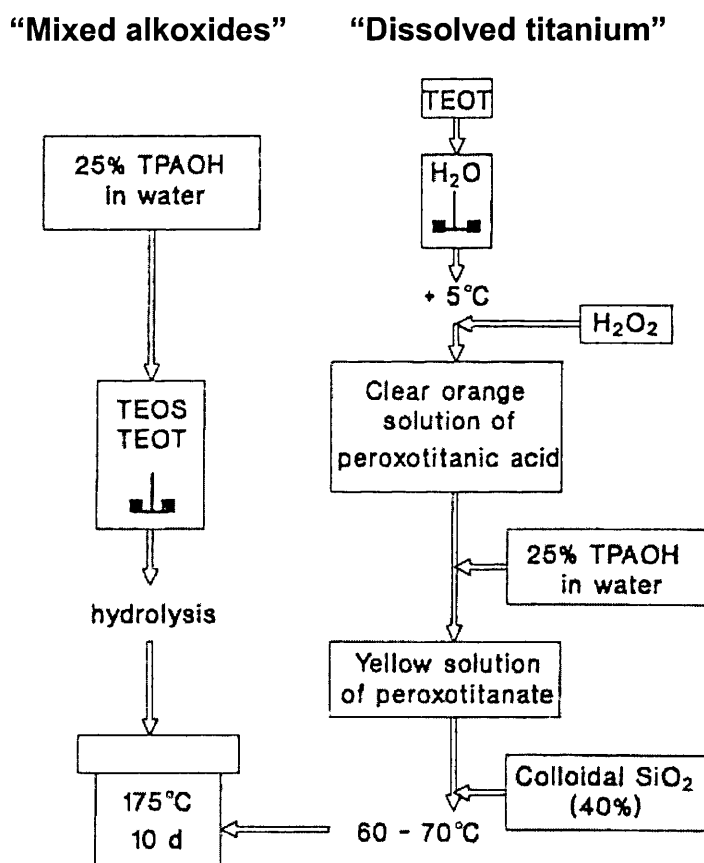
Figure 2.9   Synthesis procedure for TS-1 (Perego et al, 1998)

2.3.2 Catalytic properties

TS-1 is hydrophobic and high product selectivity is obtained in oxidation with hydrogen peroxide. The catalytic properties of titanium silicalite-1 are unique. TS-1 is characterized by its excellent selectivity, sterospecificity, and electrophilic behaviour (Cleric and Ingallina, 1993). Only a slight loss of hydrogen peroxide is observed from decomposition to H_2O and O_2 in a variety of liquid-phase oxidation reaction of H_2O_2 with alcohols, ketones and alkanes (Grzybowska-Swierkosz and Haber, 1994).

TS-1 serves as the catalyst to activate hydrogen peroxide, which is the oxidizing agent, via the formation of a surface peroxotitanate species, either in hydroxylated or dehydrated state (Figure 2.10). Activation involves weakening or polarizing the peroxidic bond to induce electrophilic properties in the oxidant (Feast and Lercher, 1996). Oxidation then occurs by subsequent oxygen transfer from the peroxotitanate to the reactant.
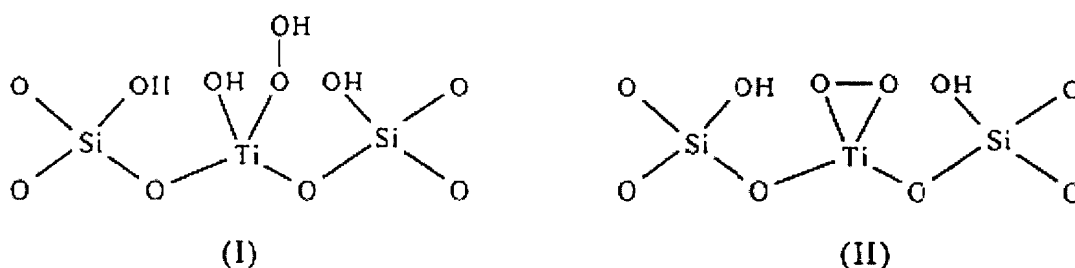
Figure 2.10   Two possible active peroxotitanates species;

(I) hydroxylated or (II) dehydrated

50

2.3.3 Oxidation reactions

Examples of oxidation reactions catalysed by TS-1 are ammonia oxidation, cyclohexanone ammoximation (Mantegazza et al., 1999), selective oxidation of aniline (Gontier and Tuel, 1994), oxidation of glycerol (McMorn et al., 1999) and oxidation of primary and secondary alcohols (Maspero and Romano, 1994). Due to its remarkable high efficiency and molecular selectivity, TS-1 is widely employed in many chemical processes. TS-1 was used to catalyse cyclohexanone ammoximation in the industrial production of Nylon 6.

TS-1 is also an efficient catalyst for epoxidation reactions like lower olefins to epoxides (Clerici and Ingallina, 1993), allyl chloride to epichlorohydrin (Gao et al., 1996), allyl alcohol to glycidol (Hutchings et al., 1995), styrene to phenylacetaldehyde (Kumar et al., 1995) and propylene to propylene oxide (Chen et al, 1998). It is characterized by its excellent selectivity, stereospecificity, and electrophilic behaviour (Cleric and Ingallina, 1993). The following table lists the details of each example of epoxidation reactions catalysed by TS-1 (Table 2.2).

Epoxidation reaction	By product	Solvent	TS-1 (g/l)	Reactant (M)	$[H_2O_2]$ (M)	t (min)	Temp (°C)	H_2O_2 conversion (%)	H_2O_2 selectivity to product (%)
allyl chloride to epichlorohydrin (ECH)	glycol	methanol	10.00	1.214	0.517	60	45	98.7	97.8
epoxidation of styrene and further isomerisation to phenylacetaldehyde	Benzaldehyde and styrene epoxide	acetone	40.0	2	0.5	360	80	78[a]	77.5[a]
propylene to propylene oxide	propylene diol and mono-methylethers	methanol	10.0	1.5wt%	1	60	25	$4.9\,min^{-1}$[b]	97.7

Epoxidation reaction	By product	Solvent	TS-1 (g/l)	Reactant (M)	[H₂O₂] (M)	t (min)	Temp (°C)	H₂O₂ conversion (%)	H₂O₂ selectivity to product (%)
1-pentene to 1,2-epoxypentane	Glycols and glycol mono-methylethers	methanol	6.2	0.9	1.8	60	25	94	91
allyl alcohol to glycidol	Glycerol, 3-ethyl-1,2-propanediol and 2-ethyl-1,3-propanediol	ethanol	11.1	2.22	2.22	360	65	56.6 [c]	52.8
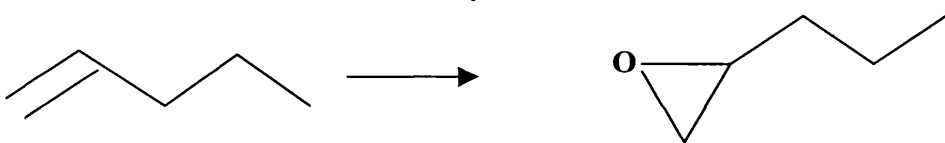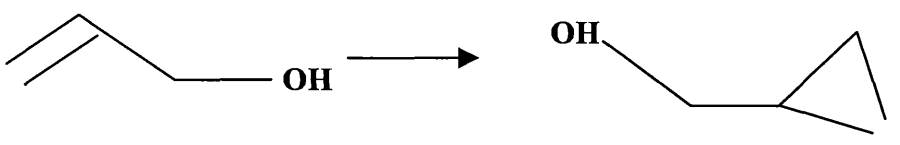
[a] w.r.t. styrene conversion (theoretical)

[b] the turnover frequency (TOF) of H_2O_2 is used to represent the reaction rate. TOF is defined as number of moles of H_2O_2 converted per mole of titanium in the catalyst per minute.

[c] allyl alcohol conversion

Table 2.2   Oxidation reactions catalysed by TS-1

2.3.4 Reactions considered in this work

Epoxidation of lower olefins with hydrogen peroxide

Olefin epoxidation is a key transformation in organic synthesis (Sheldon, 1996; Sienel et al, 1999). The use of aqueous hydrogen peroxide as the oxidant is inexpensive, safer and easier to handle when compared with the Prilezhaev reaction of olefins with percaboxylic acids (Swern, 1971). Titanium silcalite-1 has an average pore diameter of 0.55nm where the active site is situated inside the channel system. Internal mass transfer resistance is likely to occur across the catalyst layer. Therefore, branched and cyclic alkenes tend to react more slowly than straight chain alkenes (Clerici and Ingallina, 1993). 1-Pentene epoxidation is chosen for the preliminary study of the microreactor due to its faster reaction rate among TS-1 catalysed epoxidations.

The epoxidation of 1-pentene with hydrogen peroxide as the oxidizing agent is shown below yielding 1,2-epoxypentane. The stoichiometry of pentene, hydrogen peroxide to epoxide is 1. The principal by-products formed are glycols and glycol monoethylethers (Clerici and Ingallina, 1993).

$$CH_3CH_2CH_2CH=CH_2 \quad + \quad H_2O_2 \quad \longrightarrow \quad \underset{O}{CH_2\!\!\diagup\!\!\diagdown\!CHCH_2CH_2CH_3}$$
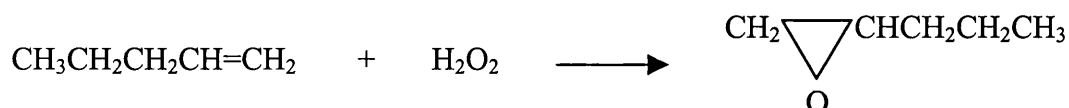
The chosen reaction for TS-1 catalysis is the epoxidation of 1-pentene to form 1,2-epoxypentane using 33% by weight hydrogen peroxide as oxidant (Clerici and Ingallina, 1993). The reaction can be performed at near room temperature with selectivity up to 98% on hydrogen peroxide. Some of the literature values for the reaction for C5-C8 olefins are listed in table 2.3.

n	Olefin	$[H_2O_2]_n$ (M)	T (°C)	t (min)	H_2O_2 (conv. %)	Selectivity (% on H_2O_2)	$t_{1/2}$
1	1-Pentene	0.18	25	60	94	91	5
2	1-Hexene	0.18	25	70	88	90	8
3	1-Hexene[b]	0.18	25	70	68	90	14
4	1-Octene	0.17	45	45	81	91	5

[a] Olefins, 0.90M; TS-1, 6.2 g/l; solvent, methanol; $t_{1/2}$ is the time required for 50% H_2O_2 conversion.
[b] [1-Hexene] 0.18M.

Table 2.3   Epoxidation of C5-C8 olefins (Clerici and Ingallina, 1993)

2.4   Zeolite Membranes

Zeolites and molecular sieves are excellent materials for inorganic membranes (Jansen et al., 1994). The pore structure of the zeolite restricts the size and shape of the molecules that can enter and leave the channels. This gives rise to molecular sieving effects observed in many separation and reaction processes (Jansen et al., 1994). Unlike most microporous metal oxides (e.g., SiO_2, Al_2O_3 and TiO_2), which have tortuous pore channels, zeolites have a well-defined pore system and a crystalline structure. The chemical environment within the zeolite pore channel can be manipulated to influence the molecular transport of diffusing species during separation. When compared with conventional membranes, zeolite membranes possess a higher open area with low aspect ratio providing volumetric efficiency (Jansen et al., 1994).

Zeolite membranes serve as an excellent choice for application in chemical synthesis, product separation, solvent recovery, liquid/liquid extraction and waste minimisation. (van Bekkum et al., 1994; Jansen et al., 1994; Tsapatsis et al., 1999; Chau et al., 2000). They can be used for separation of close boiling compounds and isomers (Funke et al., 1996a, 1996b) or pervaporation of organic solutions at high temperature (Nomura et al., 1998). Permeation studies have been carried out on MFI-type membranes showing remarkable selectivity for different gas pairs (Lovallo et al., 1998). They are also suitable for gas sensor applications (Koegler et al., 1994).

In recent progress of zeolite membrane development, synthesis approaches have been reported for the preparation of zeolite film with different structure types, silicalite-1 (Cheng et al., 1997), ZSM-5 (Sano et al., 1992), TS-1 (Jung and Shul, 1997), Y-type zeolites (Kusakabe et al., 1997), zeolite LTA (Hedlund et al, 1997), zeolite A (Boudreau et al., 1999) and CaA (Yan and Bein, 1995). Zeolites have been successfully grown as free-standing membranes or onto support materials such as glass, ceramics, porous stainless steel, silicon and alumina tube (van Bekkum et al., 1994, den Exter et al., 1997, Xomeritakis et al., 1999, Chau et al., 2000).

Supported zeolites have been considered for many industrial applications such as membranes, adsorbents, catalyst components and in electronic devices (van Bekkum et al, 1994). Because of their greater mechanical strength and thermal stability provided by the support material, handling and implementation is easier. Zeolite based membranes require a continuous layer of zeolite crystals with properly aligned zeolite channels. They should be supported on a porous carrier material. They are best prepared on an existing support by hydrothermal treatment. Two synthesis methods are described in the following.

2.4.1 *In-situ* synthesis

The support material is immersed in zeolite precursor gel. The seed-free substrate is in direct contact with the synthesis mixtures and hydrothermal treatment takes place at autogenous pressure. Koegler et al. (1997) has proposed a model for

the *in-situ* growth of Si-ZSM-5 (silicalite-1) where the precursor gel layer acts as an anchoring site for template molecules. Nucleation and crystal growth take place at the interface of the gel and the synthesis solution where both silicon source and template are abundant. Large non-intergrown crystals were observed over the uncoated substrate and the film obtained by *in-situ* growth exhibits [0k0] or [h00] out-of-plane preferred orientation (Xomeritakis et al., 1999; Koegler et al., 1997). The thin-film model for zeolite Si-ZSM-5 is illustrated in figure 2.11.
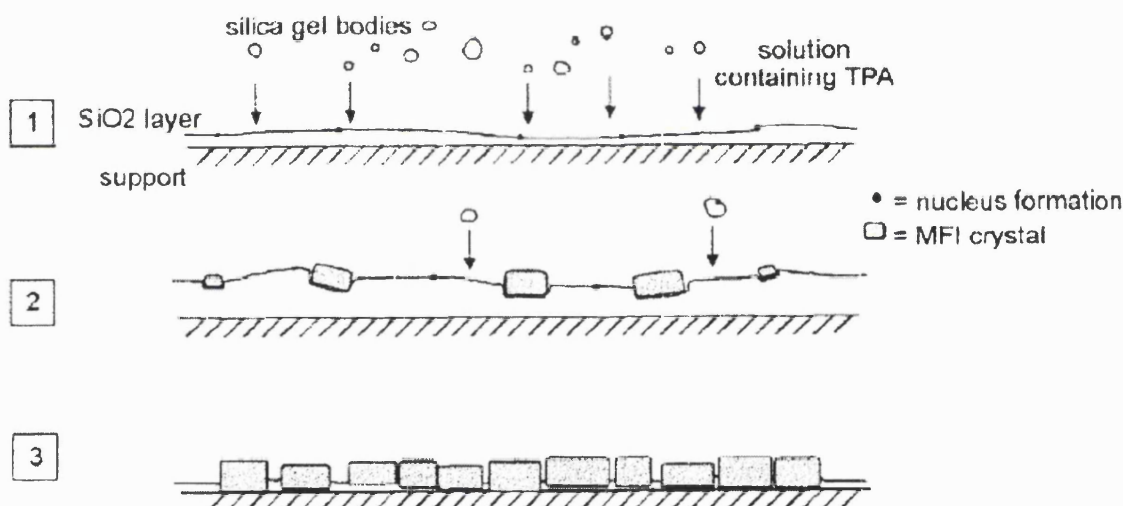
Figure 2.11 **A Si-ZSM-5 thin-film growth model on a support. The silica gel (Step 1) is first deposited on the support, forming a thin, low-density silica surface. TPA from the solution will be attracted to the surface where nucleation will take place (Step 2 and 3). Crystals will grow by consuming the gel (Koegler et al, 1997).**

58

2.4.2 *Ex-situ* synthesis

Zeolite film can be prepared by preseeding the support layer with nanocrystalline zeolite particles prior to hydrothermal treatment. MFI films prepared by *ex-situ* (secondary) and *in-situ* growth will exhibit different microstructures (Lovallo et al., 1998; Xomeritakis et al., 1999). During secondary growth, the nucleation stage is bypassed where growth of seed particles starts directly on the seeded-coated substrate once they are in contact with the synthesis solution (Gouzinis and Tsapatsis, 1998). Gel formation is not observed and the precursor layer also prohibits further nucleation or incorporation of newly formed crystal, leading to a continuous polycrystalline film with columnar grains. The film is well intergrown with small surface roughness. However, defects will be developed throughout the area in the absence of close-packed precursor seeds. The precursor layer is important to ensure the final film quality.

The orientation of zeolite films can be manipulated by secondary growth conditions. Tsapatsis and co-workers (1999) have prepared the c-oriented [001] and the [h0h]-oriented films on alumina support by changing the synthesis temperature as shown in figure 2.12.
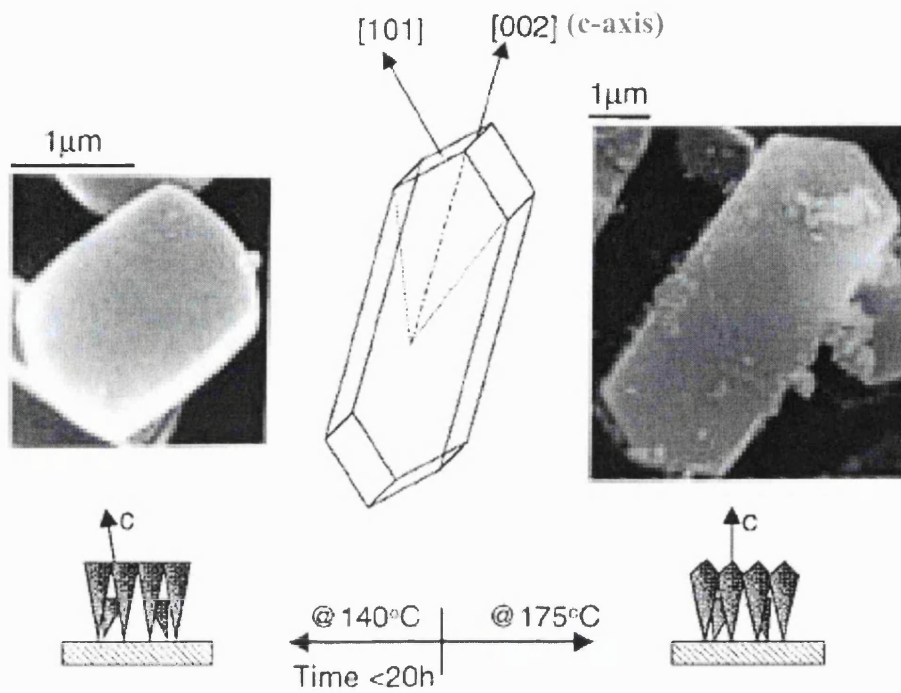
Figure 2.12 SEM images of MFI crystal grains in solution under conditions of secondary growth at 140°C and 175°C (Gouzinis and Tsapatsis, 1998)

2.5   Introduction to microreactors

The small dimensions of microreactors open up innovative pathways for many reactions. Many research institutes and companies are developing microchemical systems, as they are potentially beneficial to the environment. It is believed that microfabrication chemical systems with integrated sensors and actuators will revolutionize chemical research and development (Jensen, 2001). Figure 2.13 illustrates the scale of Microelectromechanical (MEMS) when compared with different components in conventional systems. The drawback is that submillimeter channels may sometimes be blocked by particulates.
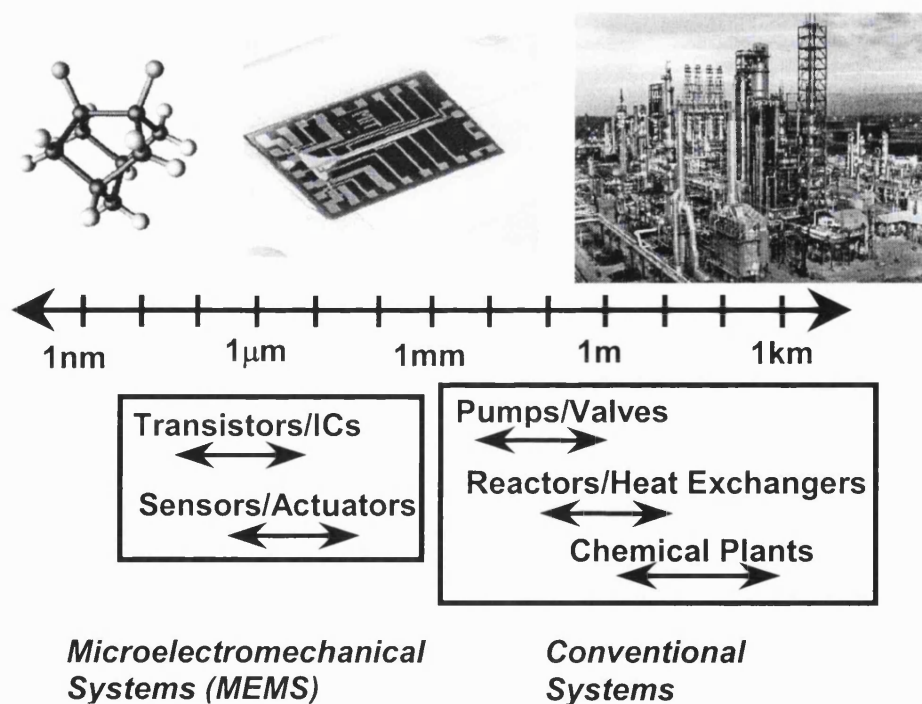
Figure 2.13   Scale of microelectromechanical systems in comparison with conventional systems

2.5.1 Definition of microreactors

Microreactors are defined as miniaturized reaction systems fabricated by using, at least partially, methods of microtechnology and precision engineering (Ehrfeld et al, 2000). They are usually micromachined on silicon, stainless steel, glass, etc. with characteristic dimensions in the micrometer to millimeter range. They contain submillimeter internal structures like fluid channels integrated with heaters, temperature and flow sensors.

2.5.2 Advantages of microreactors

Fast screening of materials

Microreactors have the properties of short response times and small volumes for reducing the inertia of the whole system (Zech et al., 2000). Miniaturization enables a flexible, robust on-line screening system for use in catalysed reactions under harsh processing conditions (Zech et al., 2000). Actual catalytic performance can be detected based on fast screening processes offered in microreactors (Védrine, 2000).

Well-defined flow characteristics

Laminar fluid flow within the microsystem results in a more uniform velocity distribution inside the microchannels. This provides benefits for reaction kinetics and mechanism studies. Flow visualization using computer fluid dynamics can be

employed to further understand the behaviour of microfluidic reactions. Detailed simulation can be served as the best tool for design and data interpretation. Optimum design and operating parameters can be located (Hsing et al., 2000).

Easier scale-up through replication

Microreactors have the ability to integrate different microdevices for better control and easier scale-up. Multiple repetition of basic units can be operated in parallel to cope with the annual production of high value added chemicals (Gavriilidis et al., 2002).

High surface area to volume ratio

The large surface area to volume ratio in a microreactor gives excellent heat and mass transfer properties (Drost et al., 1997; Losey et al., 2000), which provides effective heat management for isothermal processing even in fast and explosive reactions (Richter et al., 2000). They are also an excellent choice for use in multiphase reactions as the mass transfer path is minimal. Explosion proof oxidation, which cannot be carried out utilizing conventional reactors, can now be safely operated using microreactors (Jensen, 2001).

Improved safety

Microreactors enable safer handling of explosive and hazardous chemicals. The basic idea of having small units would help to prevent any major safety hazards from occurring within the system. Smaller chemical plants can be located near the

63

intended point of application to eliminate storage and shipping constraints (Ajmera et al., 2001).

Efficient chemical production

It is recognized that microreactors can provide better energy and material utilization leading to more efficient chemical production and less pollution (Quiram et al, 2000). Microreactors can achieve small sizes, affordability and low levels of emission by relying on high rates of heat and mass transfer through specially fabricated microchannels (Drost et al, 2000). As a result, operational and capital cost for the process can be greatly reduced.

Production flexibility

Repetition of basic units of microreactors provides the ability to increase product output by scaling out (numbering up) instead of scale up of the whole systems. This results in higher flexibility in adapting production rate. A broader range of operating conditions can be supported in comparison to the conventional system (Ehrfeld et al., 2000)

2.5.3 Micromachining techniques

Most of the fabrication methods for MEMS are adapted from technology used in the integrated circuit industry where materials are restricted to silicon and its related compounds. Other micromachining methods have been developed for other materials like glass, stainless steel, ceramic, etc. The following shortlists some of the developed fabrication procedures used for microchemical devices:

<u>Photolithography and wet etching</u>

Silicon possesses excellent mechanical strength, chemical resistance and thermal stability, which is an ideal material for semiconductor manufacturing. The perfect single crystal structure is great for chemical functionalisation and material deposition. Nowadays, silicon and its compounds are widely employed to produce complimentary metal-oxide semiconductor (CMOS) in integrated circuit (IC) technology.

The basic techniques for microfabrication involve delineating a pattern image in a photosensitive polymer followed by wet anisotropic etching (Madou, 1997) as shown in figure 2.14. A photoresist is spun onto a clean silicon wafer, previously deposited with silicon nitride as a masking layer. The patterns on a chromium plated glass mask are transferred onto the wafer following exposure to UV light. The patterns on the wafer are developed and the exposed silicon nitride layer will be removed using dry plasma etching, followed by silicon wet etching. There are two types of silicon wet etchants. Isotropic etchants etch silicon at equal rates in all

directions. They are easily used but are difficult to control for high precision. Wet etchants, like potassium hydroxide (KOH), ethylene diamine pyrocatechnol (EDP) and hydrazine, etch silicon [100] crystallographic plane faster than [111] plane. This process is very reproducible allowing precise etching (Wise and Najafi, 1991).
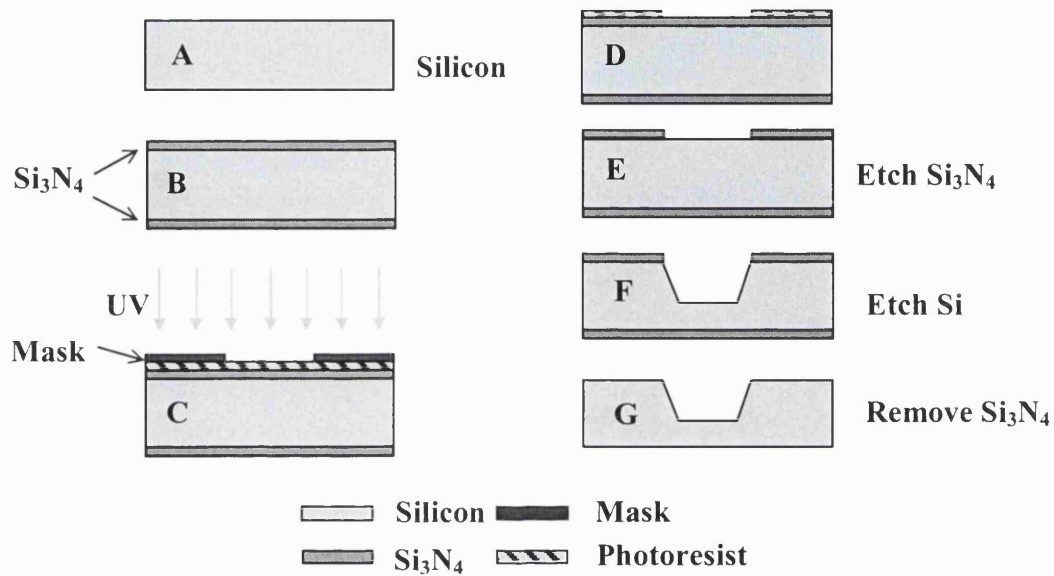
Figure 2.14   Microfabrication of silicon structure

<u>Dry etching</u>

Dry etching involves various methods in which a solid state surface is etched in the gas phase, through chemical or physical interaction between the ions in gas and the atoms of the substrate. The most often applied technique can divided into three groups (Fatikow and Rembold, 1997):

- physical sputter etching or ion beam etching
- chemical plasma etching

- combined physical/chemical etching

Sputter etching and ion beam etching are both physical processes, which employ the concept of elctrostatically accelerating chemical inert ions. These methods are anisotropic, allowing a precise structure of smooth walls, but they are unselective and slow.

Reactive gases (chlorine or fluorine) are used in chemical plasma etching, which decompose in the plasma to create active radicals. These particles then diffuse into the surface of the substrate to initiate the etching process (figure 2.15). Another method is the combination of both physical and chemical energy of reactive particles, resulting in high selectivity and anisotropy. Reactive ion etching (RIE) accelerates reactive ions and radicals in an electric field in the direction of the surface to be etched whereas inert gas can be added to reinforce the physical etching process (Fatikow and Rembold, 1997).
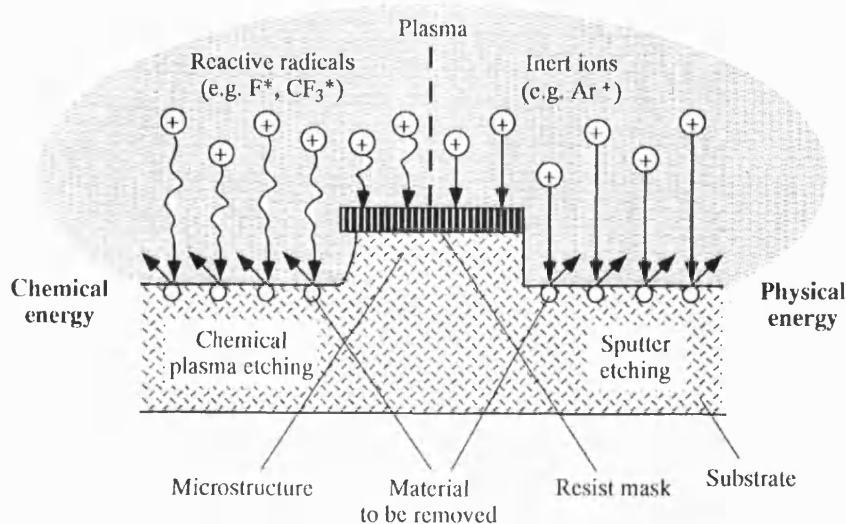
Figure 2.15   Basic dry etching methods (Krull and Endres, 1993)

67

LIGA

LIGA is a German acronym for **LI**thographie, **G**alvanoformung, **A**bformung (lithography, galvanoforming, moulding), which is used for high aspect ratio micromachining (HARM) (Lehr and Ehrfeld, 1994; Ehrfeld et al, 1999). This technology employs x-ray lithography for mask exposure, moulding and electroforming for making the parts. The first step is (1) x-ray lithography using synchrotron radiation, (2) metal deposition to form the mould, (3) injection moulding of plastics and (4) electroforming with the desired metal. Complex microstructures up to the dimension of $0.2\mu m$ can be fabricated. The disadvantage of this process is its high production costs (Fatikow and Rembold, 1997).
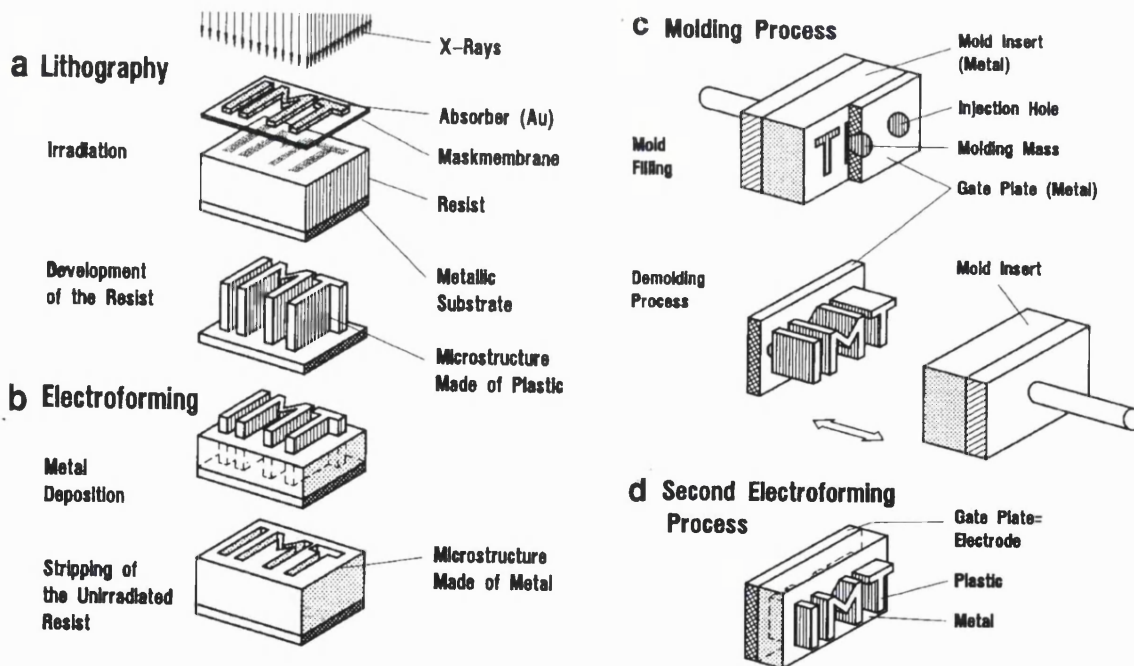
Figure 2.16   The basic process steps of the LIGA technology (Menz et al., 2001)

68

Laser machining

Fabrication of miniaturized reactor parts and components using lasers is becoming more popular (Johansson et al, 1992; Arnold et al, 1995). Laser micromachining can be employed in almost any material, silicon, diamond, quartz, glasses and even soft polymers. 3-dimensional structure can be fabricated by using a laser to remove material without the need of masks. It operates by thermally ablating material from the workpiece surface. A laser beam is focused into a spot with diameters from microns to a few tens of microns using an optical system. Material is locally melted and vaporized due to the absorption of the laser power at the surface, which is then dissipated as a plume of ionised and neutral atoms. The schematic view of a laser micromachining setup is illustrated in figure 2.17.
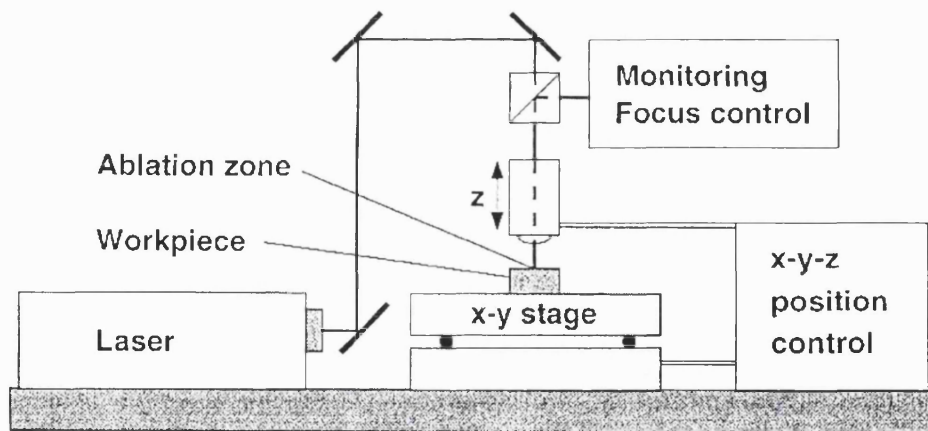
Figure 2.17   **Schematic view of a laser micromachining setup (Menz et al., 2001)**

Multi-lamination technique

Microlamination can be used to fabricate a complex microreactor design in which metals or polymer layers are patterned separately to assemble the desired architecture with features as small as tens of micrometers (Martin et al., 1999; Matson et al., 1999). The method involves the patterning and bonding of thin layers of material, called laminae. The procedure can be divided in three steps (1) lamina patterning (usually via laser ablation), (2) laminae registration (alignment) and (3) laminae bonding by diffusion bonding technique. One drawback of this technique is the requirement of high precision micromachining and an alignment tool.
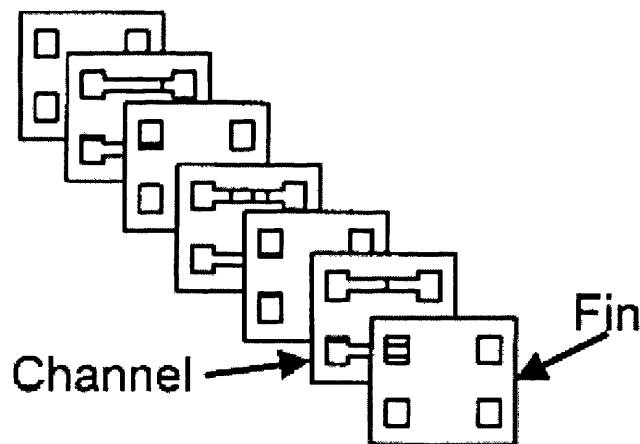
Figure 2.18   Schematic of the microlamination procedure used to produce a dual microchannel array (Paul et al, 2000)

<u>Microelectro-discharge machining (μEDM)</u>

This method is based on the erosion of the substrate using a controlled electric discharge between an electrode and the substrate, which can be utilized to shape 3-dimensional microstructures out of electrical conductive material. It is a process in which a tool is imaged onto a workpiece. Metal is removed by high-frequency electric sparks generated by pulsating a high voltage between the cathode tool, shaped in the form of desired cavity, with a conductive workpiece, acting as the anode (Madou, 1997). Material of the electrodes is evaporated when the breakdown voltage is exceeded (Reynaerts et al., 1997).
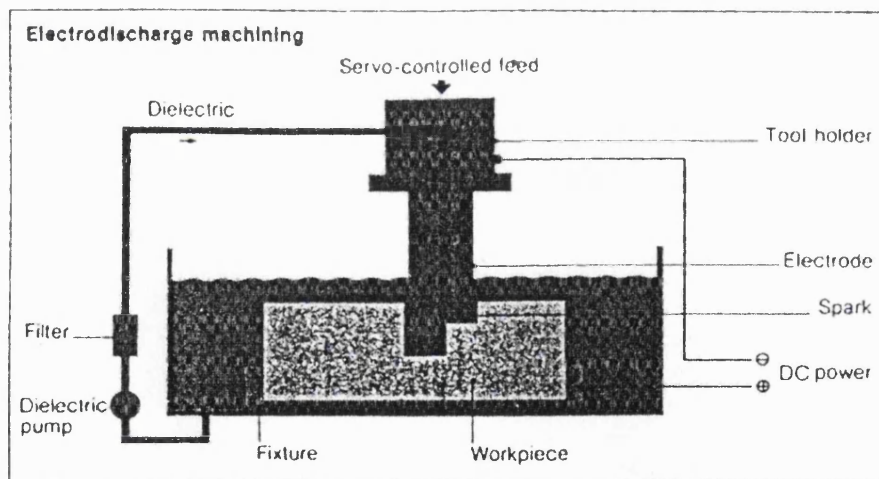
Figure 2.19   **Schematic view of the setup of microelectrodischarge machining (Madou, 1997)**

71

Dip pen nanolithography

Direct-write "dip-pen" nanolithography (DPN) has been developed by Piner and co-workers (1999) to deliver collections of molecules in a positive printing mode. DPN employs scanning tunneling and atomic force microprobes (AFM) to write alkanethiols with up to 30 nanometers linewidth resolution on a gold thin film (figure 2.20). Molecules are delivered from the AFM tip to the solid substrate through capillary transport. This method can act as a potential tool for creating and functionalising micro devices (Piner et al, 1999).
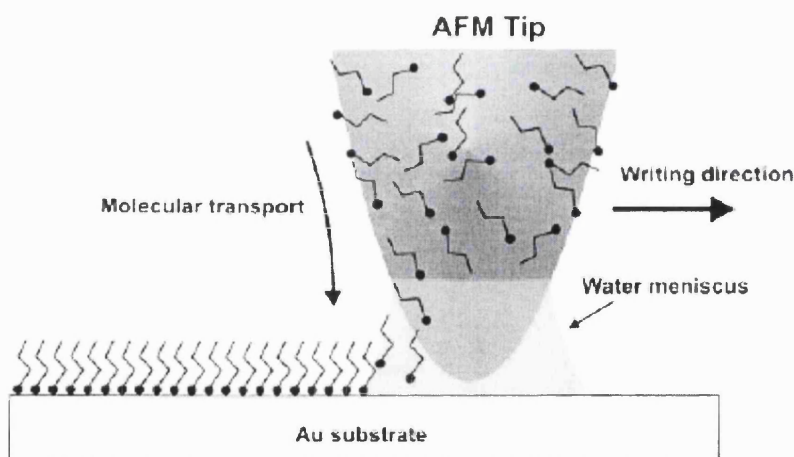
Figure 2.20 **Schematic representation of DPN. A water meniscus forms between the AFM tip coated with 1-octadecanethiol (ODT) and the Au substrate. The size of the meniscus, which is controlled by relative humidity, affects the ODT transport rate, the effective tip-substrate contact area, and DPN resolution.**

2.6 Application of microreactors

2.6.1 Access to new reaction regimes

Microreactors can suppress the formation of hot spot and the problems of thermal runaway for exothermic processes. Aggressive conditions or regimes that are difficult and unsafe in conventional systems can now be carried out with microchemical systems. These features are especially useful for hydrocarbon partial oxidation for producing oxygenates (e.g. alcohols and aldehydes) and nitrogen bearing compounds (e.g. cyanides, nitriles and cyanates). One example is partial oxidation with pure oxygen in a microreactor (Srinivasan et al., 1997). A silicon-based microreactor with integrated heater, flow and temperature sensors was fabricated to study Pt-catalysed ammonia oxidation.

Hazards dealing with storage and shipping of toxic chemicals can also be avoided by shifting plants near the point of application. A microfabricated silicon packed-bed reactor for phosgene synthesis is a potential example for on-site and on-demand production of hazardous and toxic chemicals (Ajmera et al., 2001). The increased surface area attained at the submillimeter channel dimensions enables a larger degree of control and safety in comparison to macroscopic reaction system.

2.6.2 Study of reaction kinetics

Microreactors have the following properties: (a) efficient thermal control; (b) short response time; (c) defined flow characteristics; (d) large surface area to volume ratio and (e) small volumes for reducing the inertia of the whole system (Zech et al, 2000). These features are advantageous for extraction of chemical kinetics from microreactor experiments (Ajmera et al., 2001). Undesirable side effects due to poor heat exchange can be avoided, such as a long time required to heat up the inlet reaction mixture and to quench the outlet product stream (Rebrov et al., 2002). Inaccessible residence time can be achieved due to uniform velocity distribution in microreactor. This opens up new possibilities for investigating fast kinetics of chemical reactions.

The low temperature kinetics of ammonia oxidation on supported polycrystalline platinum catalyst was examined in an aluminium-based microreactor (Rebrov et al., 2002). A silicon cross-flow microreactor with a short pass multiple flow-channel geometry was developed for the testing of catalyst particles for gas phase chemical reactions (Ajmera et al., 2002). The cross flow design minimized pressure drop through the catalyst bed in contrast to typical microfabricated packed-bed configurations, which are susceptible to large pressure drops (figure 2.21). Kinetic studies with carbon monoxide oxidation were performed on the cross-flow microreactor showing absence of transport limitations.

4 thermocouple wells
64 bifurcated inlet channels
Packed-bed:
(400 µm x 25550 µm x 500 µm)
256 pressure drop channels
and catalyst retainers
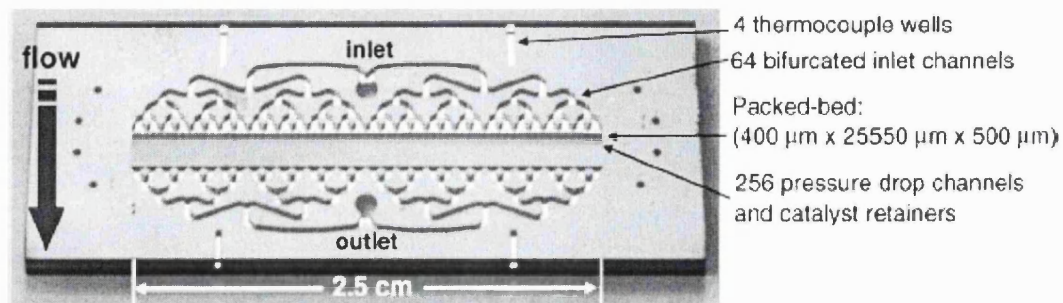
Figure 2.21   **The silicon cross-flow reactor chip. The reactants are bifurcated into 64 inlets that pass over a shallow catalyst bed. Catalyst retainers act as a filter to keep the bed in place while pressure drop channels distribute flow evenly across the bed. (Ajmera et al, 2002)**

2.6.3 High throughput screening

The development of miniaturized analysis systems combining with miniaturized reactions methods has yielded a wide range of novel devices for high throughput screening, catalysts testing and on-line monitoring of production systems (Jakeway et al., 2000). The ability to perform parallel solution-phase reactions with real-time compound analysis and identification has been demonstarted (Mitchell et al., 2001). This facilitates drug discovery via the coupling of compounds library generation with high throughput screening.

75

Greenway et al. (2000) has constructed a flow injection microreactor for high throughput continuous flow organic synthesis. The synthesis of 4-cyanobiphenyl was carried out in micro-channels (300μm wide and 115μm deep) etched onto glass while the yield of the product was analysed by GC-MS. The supported catalyst (1.8% palladium on silica) was immobilised onto the reactor manifold. Another example of heterogeneously catalysed reaction was developed by Zech et al. (2000). The catalyst screening of the oxidation of methane was studied using a reactor module consisting of 35 stainless steel microstructures. Each of these microstructures was used for the insertion of different catalyst wafers made of materials such as metals, silicon, ceramic and glass. The product was analysed using a quadrupole mass spectrometer (QMS) within 60s. The results show good reproducibility and errors below 10%.

Researchers at Institut für Angewandte Chemie Berlin have developed a parallelized catalyst screening unit using conventional mini-scale reactors (Rodemerck et al., 2000). The reaction was oxidation coupling of methane with $Mn/Na_2WO_4/SiO_2$ mixtures of varying composition as a catalyst. The first system consisted of 15 quartz glass reactor tubes, 3.5mm inner diameter connected to an analytical system QMS, providing more accurate results. The second system will be a ceramic monolithic reactor. Up to 250 catalyst compositions can be prepared and tested in parallel.

2.6.4   Process integration

Microreactors have the ability to integrate different microchemical devices for better control and easier scale-up. Prototype microreactors with integrated heaters and sensors for flow, temperature and chemical composition have been fabricated on a silicon wafer as shown in figure 2.22 (Franz et al., 1998; Quiram et al, 2000). Studies using Pt catalyzed NH_3 oxidation was carried out as the model reaction. The heat transport properties were improved by replacing the silicon nitride membrane supporting the catalyst with a more thermally conductive silicon membrane. The heat of reaction was conducted away in order to suppress the typical ignition/extinction behaviour of catalytic oxidation reactions. The small thermal mass of the reactor membranes lead to very fast open-loop thermal response times (<20ms), allowing excellent feedback temperature control.

The idea for combining reaction and separation process in microreaction systems was developed recently. A palladium-based micro-membrane has been fabricated for water gas shift reaction and hydrogen gas separation in catalytic microreactors for methanol fuel reforming (Karnik et al, 2001). The membrane is a composite of four layers, copper, aluminium, spin-on-glass (SOG) and palladium whereas copper, aluminium and SOG layers have an array of patterned holes (perforations) as the structural support for the main element of palladium films. Copper will act as membrane support as well as catalytic material in the water gas shift reaction to convert the unwanted carbon monoxide produced earlier in the

microreaction system into hydrogen, which will then be separated by the membrane. The micromembrane can withstand a pressure gradient of 10 psi. The fabrication process can allow for heaters and temperature sensors integrated into the device.
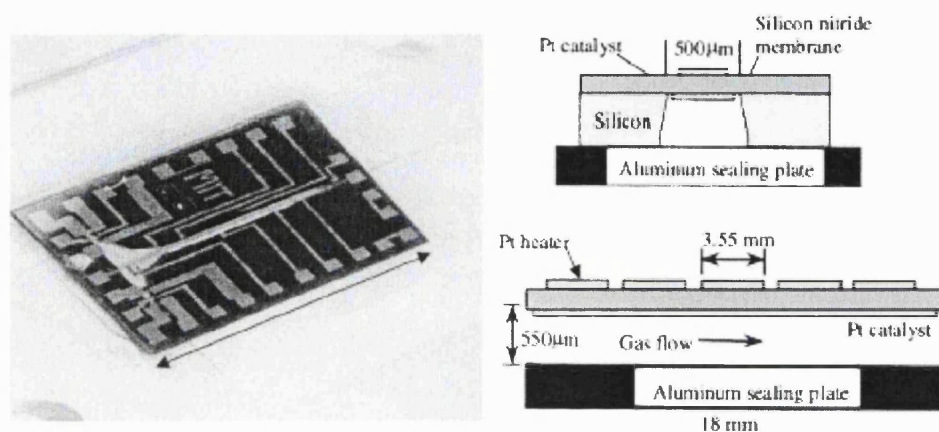
Figure 2.22   Gas-phase microreactor. Photograph of device. Front view and side schematics (Srinivasan et al., 1997; Quiram et al., 2000)

2.6.5   Process development

Microreactors have the ability to accommodate completely new reaction regimes and provide information that is not accessible otherwise (Richter et al., 2000). Reactor performance can be tested quickly. The processing conditions and characteristics can then be successfully used to develop a conventional reactor based on a standardized choice of components. This can all be accomplished by using a minimum amount of chemicals (Ehrfeld et al., 2000, Krummradt et al., 2000; Wörz et al., 2001). Applying microreactors for process development, optimal conditions can be located much quicker compared to conventional means (Wörz et al., 2001).

The process development for the synthesis of vitamin precursors has been studied (Richter et al., 2000; Ehrfeld et al., 2000; Wörz et al., 2001). A microreactor was developed as the reaction is highly exothermic whereas the reactant, intermediate and product will very quickly form a by-product, which reduces the selectivity and yield. The channels are 900μm deep and 60μm wide and surrounded by cooling channels (Richter et al., 2000). The reaction was carried out isothermally with rapid mixing. No hotspot and adiabatic temperature rise were observed. Another example is the oxidative dehydrogenation of alcohol to aldehyde. This is also a highly exothermic reaction. The microreactor is made of silver, the catalytically active material (Wörz et al., 2001).

2.6.6 Extraterrestrial Processing

Micro/nano-technology represents the synthesis and integration of materials, processes and devices ranging from submillimeter to submicrometer size, which is currently an area proceeding at a very fast pace (de Aragón, 1998). The utilization of micro/nano-technologies in the space sector is very promising. Lightweight, compact chemical systems can be applied to reduce total resources required yet providing higher system performance per unit cost and mass (de Aragón, 1998).

Research has been conducted at the Pacific Northwest National Laboratory (PNNL) for NASA In Situ Resource Utilization (ISRU) program planned for future missions to Mars including chemical processes (Wegeng and Drost, 1998). In situ

propellant production (ISPP) is to convert the carbon dioxide from the Martian environment to propellants, oxygen and other useful chemicals to reduce the required launch mass from Earth. The program involves collecting and pressurizing atmospheric carbon dioxide, conversion reactions, chemical separations, heat exchangers and cryogenic storage (TeGrotenhuis et al., 2000). Due to negligible convective heat transfer within the low-pressure environment of space, high energy efficiency is achieved through the extensive recuperation and energy cascading from hot to cold unit operations to minimize thermal and electrical wastage.

Developments in micro chemical and thermal systems (MCTS) have resulted in an improved efficiency, reduction in volume and weight. This technological advancement has fuelled tremendous leaps of faith in the progress of continued space exploration (TeGrotenhuis et al., 2000).

2.7   Incorporation of zeolites within microsystems

2.7.1   Microfabrication of zeolite films

Regrowth of zeolite film using smooth and polished surfaces as on silicon wafers was introduced (Jansen and van Rosmalen, 1993). The growth of a continuous film of MFI-type on silicon [001] wafer platelets was first described by Jansen and van Rosmalen (1993). Schoeman et al. (1997) has reported the direct synthesis of thin silicalite-1 film (180nm to 1μm thick) on silicon wafers at 100°C. This enables the advancement in incorporating MFI zeolites in microchemical systems by employing traditional semiconductor technology.

A recent development of microfabricated zeolite thin film was reported: den Exter (1997) and co-workers have grown free-standing silicalite-1 membranes onto silicon microchannels. Crystal growth was performed over a silicon nitride window inside the wafers. The window-containing wafers were prepared using traditional semiconductor technology. After hydrothermal synthesis, the nitride windows were then removed to form an oriented and locally non-supported layer of MFI (figure 2.23). However, the presence of crack formation was observed during removal of organic templates.
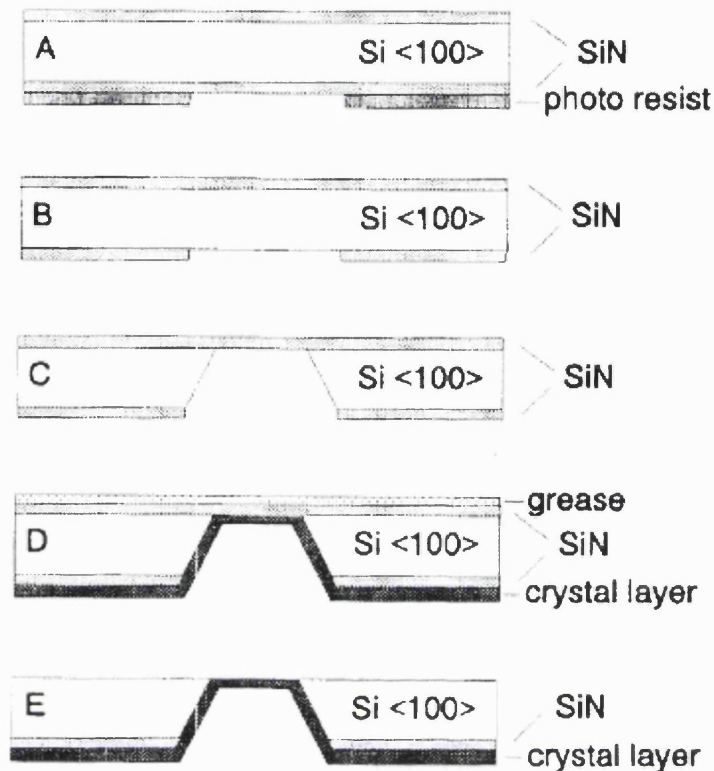
Figure 2.23   Principles of thin-layer preparation in silicon/silicon nitride composites (den Exter et al., 1997)

The production of a coating of zeolite crystals has also been attempted. Rebrov et al. (2001) have grown ZSM-5 zeolite on stainless steel plates with a microchannel structure to test its performance for selective catalytic reduction (SCR) of nitric oxide with ammonia. The schematic diagrams of the stainless steel microchannel structure are illustrated in figure 2.24. As the microchannels are only 0.5mm wide, it is important to obtain a single layer of zeolite crystals to avoid pressure drop across the microreactor. Ce-ZSM-5 zeolite was chosen as the catalyst

due to the improved hydrothermal stability when compared with other ion-exchanged zeolites. Experimental results have revealed the absence of mass transfers limitations and a faster SCR reaction rate was observed in comparison with the result obtained with pelletized Ce-ZSM-5 catalysts.
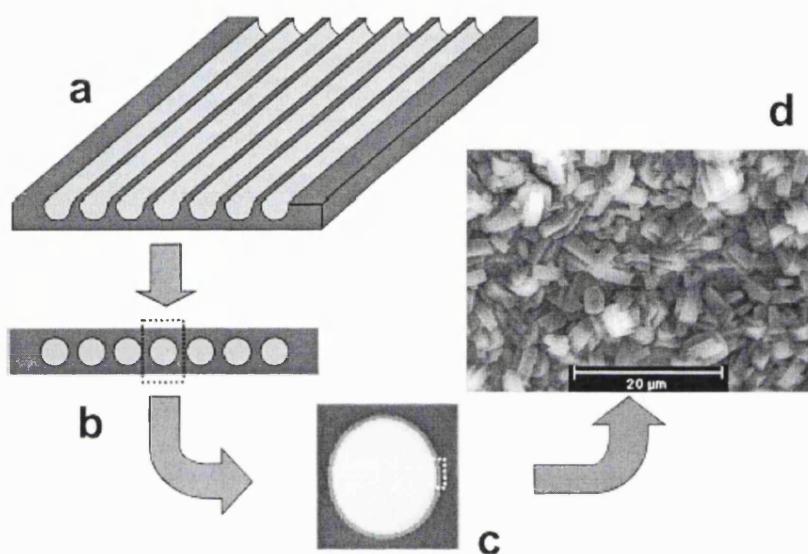
Figure 2.24   **Schematic representation of stainless steel microchannel structure. (a) isometric view of one plate, (b) front view of two plates sealed together, (c) single microchannel with zeolitic coating and (d) scanning electron micrographs of zeolitic coating. (Rebrov et al., 2001)**

2.7.2   Proposed zeolite incorporation techniques

The growth of zeolite crystals onto silicon wafers enables new possibilities to incorporate zeolites in the design architecture of microchemical devices. Zeolites

have the advantages of withstanding high temperature treatment without cracks and delamination. They can provide better adhesion to the silicon substrate and can be microfabricated using standard clean room procedures. Photolithography methods and various etching techniques can be applied to pattern zeolite microstructures.

An elegant way to incorporate zeolite in microreactors is selective deposition of zeolite crystals onto the microchannels. Traditional semiconductor technology can be employed in fabricating silicon microstructures. In this work, zeolite layers are grown selectively onto silicon microstructures by hydrothermal synthesis. It is shown that zeolites can be utilized as catalysts, membrane and structural materials in the design architecture of different micro chemical devices.

Chapter 3

Instrumentation and Methodology

3.1   Introduction

Novel fabrication techniques have been developed to incorporate zeolite in the design architecture of microchemical devices. MFI zeolites were utilized as catalysts, membrane and structural materials in microreactors and microseparators. In this work, traditional semiconductor technology was employed in microfabricating silicon microstructures. Zeolite layers were grown directly on the silicon substrate by applying zeolite thin film technology. Localized zeolite growth was developed which would selectively incorporate a zeolite catalyst layer within the confines of the microchannel. The experimental procedures for microchannel fabrication and the selective incorporation of zeolite materials will be discussed in detail in this chapter.

3.2   Selection of substrate

Silicon possesses a single crystal structure with a well-defined surface. Its flat surface can provide great adhesion to zeolite crystal layers, which are excellent for zeolite thin film application. Photolithography and standard microfabrication procedures can be employed to fabricate a silicon microstructure. These techniques are well developed and commonly available whereas advanced and expensive tools are required for materials like glass, ceramic or other metal substrates. The silicon wafers used in the experiment are purchased from Gritek. The P-type silicon wafers are (100)-oriented with a thickness of 525μm.

3.3   Microchannel fabrication

A T-shaped design pattern was employed for the standard structure of the zeolite microchemical devices, which is based on the design reported by Srinivasan and co-workers (1997). It is a simple and elegant design consisting of two inlets and a single outlet for connection to reactant sources and analyser respectively. It can provide *in-situ* mixing of reactants before entering the microreactor avoiding hazards involved in a pre-mixed feed. Figure 3.1 illustrates the dimensions of the reactor pattern etched onto a chromium mask.
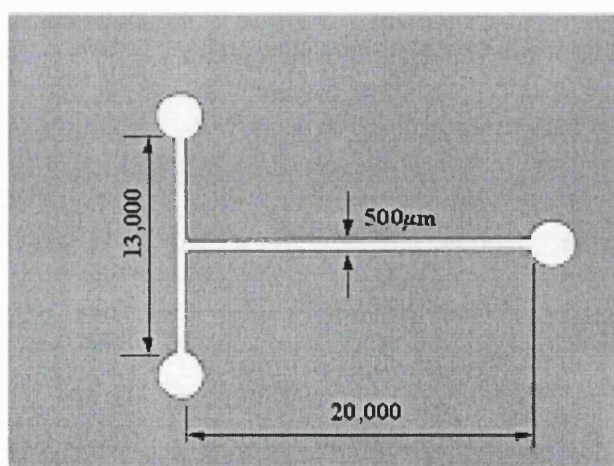
Figure 3.1   A magnified picture of the T-shaped pattern on a chromium glass mask used in lithography process with the dimensions in μm.

By applying standard microfabrication technique, the T-shaped pattern was etched onto the silicon wafer resulting in a trapezoidal channel cross-section with a depth of 250μm. The details of the fabrication procedure are summarized in figure 3.2.

The procedure utilised a P-type (100) silicon wafer (figure A). It was cleaned by immersing in H_2SO_4/H_2O_2 (10:1) for 10 min and HF/H_2O (1: 50) for 1 min to strip off the layer of oxide deposited on the surface. Extra precaution should be taken as HF is an extremely dangerous chemical. The wafer was now free of organic and metal impurities for the next step. A thin layer (500nm) of low stress silicon nitride was deposited onto the wafer at 1113K and 200 mtorr by low pressure chemical vapour deposition (LPCVD) (figure B). The nitride layer was grown from the decomposition reaction of dichlorosilane (64 sccm), ammonia (16 sccm) and nitrogen (100 sccm) at a rate of 40Å/min.

A 1-3 μm thick positive photoresist was then spun on the nitride-coated wafer. The patterns on the mask were transferred onto the wafer by exposure to UV light (figure C). The patterns were developed (figure D) and the exposed silicon nitride layer was removed by dry plasma etching at a rate of 80 nm/min (figure E). The remaining layer of photoresist was stripped off using oxygen plasma.

After that, the wafer was ready for wet etching. The microchannels were etched in a 30wt % KOH solution at 343K for 6 hours (figure F). The anisotropic etching rates along the silicon <111> and <100> directions resulted in a trapezoidal channel cross-section with an angle of 54.7°. Finally, the remaining silicon nitride layer was removed using hot H_3PO_4 solution at 433K and a rate of 40Å/min (figure G).
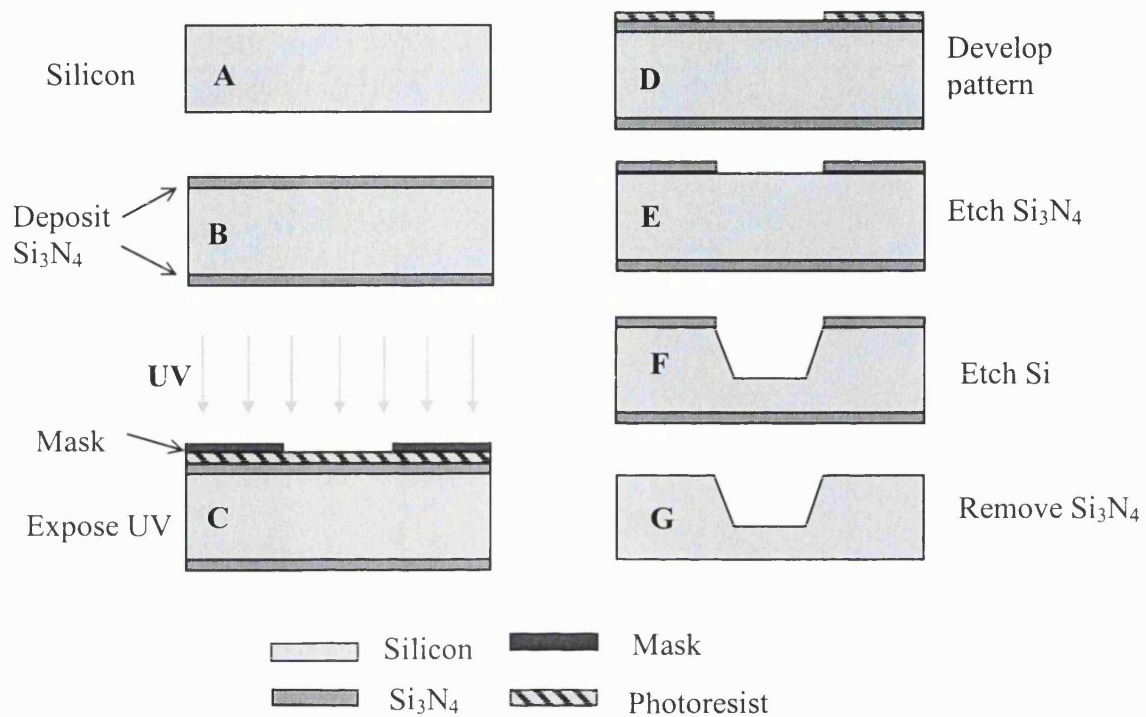
Figure 3.2   Schematic diagram for microchannel fabrication

3.4   Incorporation of zeolite within microreactor

3.4.1   Localized zeolite growth

Direct regrowth of zeolite crystals onto the silicon substrate can provide better adhesion, which can withstand cracks or delamination under high temperature

treatment. Localized zeolite growth was developed to selectively incorporate zeolite catalyst layers within the microchannel.

Using this method, zeolite growth is confined within the microchannel. This was achieved through surface modification using chemical functionalization and seeding to locally promote the growth of the zeolite layer (Chau et al, 2000, Wan et al, 2001). Mercapto-3-propyltrimethoxysilane was introduced in the microchannel, which was then seeded with colloidal zeolite using micropipette (figure A). The seeding procedure was repeated three times to obtain the desired seed population of $(5 \times 10^{13}$ seeds/m$^2)$. The seeds were then calcined in air at 823 K for 6 hours, prior to the hydrothermal growth of the zeolite layer. The etched microreactor pattern was then placed on a specially designed Teflon holder such that the pattern was facing downwards (figure B). The other side facing upwards was wrapped with Teflon tape to shield from the synthesis solution. After the hydrothermal treatment, the silicon sample was rinsed with deionized distilled water and dried overnight. It was then calcined in air at 823K (2K/min ramp) for 24 hours to remove the organic template and activate the catalyst.

A	B	C
Confined seeding	Zeolite growth	Final product

Silicon   Zeolite   Teflon
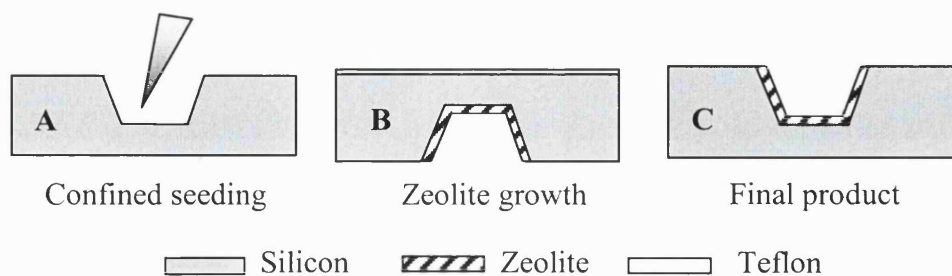
Figure 3.3   Process diagram for zeolite incorporation within microchannel

3.4.2   Preparation of TS-1 synthesis solution

The "Mixed alkoxides" method is adopted to prepare the TS-1 synthesis solution, which is based on the original procedure developed by researchers in Enichem (Taramasso et al., 1983). The schematic diagram in figure 3.4 describes the steps for preparing the synthesis solution. The procedure starts with the hydrolysis of tetraethyl orthotitanate (TEOT) and tetraethyl orthosilicate (TEOS) mixtures. Extra care should be taken to make sure that all apparatus were completely dry as the presence of water would hydrolyse the titanium compounds to form hydrated TiO_2. In step 1, TEOS was first added into a Teflon vessel, which was pre-rinsed with ethanol. Together with the sealed bottle of TEOT, they were placed in the nitrogen hood and purged for an hour to prevent carbon dioxide and water absorption (Step 2). TEOT was then added into the TEOS solution (Step 3). The TEOT/TEOS mixture should change to light yellow to obtain depolymerisation of the titanate oligomers that may be present in TEOT. The yellow colour came from partially hydrolysed TEOT, however, full hydrolysation will result in precipitation of amorphous TiO_2. The above steps should be repeated if a colourless or white mixture was obtained indicating formation of TiO_2 and the synthesis has failed (van der Pol and van Hoff, 1993).

91

Mixture of tetrapropylammonium hydroxide (TPAOH) and deionized water was then added gradually to complete the hydrolysis (Step 4). The mixture should be added dropwise so that a clear solution was formed. This was to ensure that there were enough silanol groups for the condensation reaction to occur with the monomeric hydrolysed titanium species (Perego et al, 1998). After vigorous stirring for another hour, the mixture was heated at 80°C water bath for 3 hours to aid the hydrolysis (Step 5). The volume of the synthesis mixture was maintained by adding deionized water (Step 6). The obtained clear solution was then stirred overnight for hydrothermal treatment. Table 3.1 lists the standard compositions of TS-1 synthesis solutions used for the formation of colloidal seeds and catalyst layer.

It should be noted that the presence of metal ions in the TS-1 synthesis solution would inhibit the incorporation of titanium ions into the zeolite framework (Perego et al, 1998). All the glassware and Teflon vessels should be cleaned with acid solution (HNO_3) and dried completely before preparation.

Synthesis solution	TEOS	TPAOH	TEOT	H_2O
TS-1 colloidal seeds	20	9	0.75	404
TS-1 regrowth solution for catalyst layer	40	10	1.6	10000

Table 3.1   **Composition of TS-1 synthesis solutions**

Step 1 TEOS was added into the Teflon vessel.
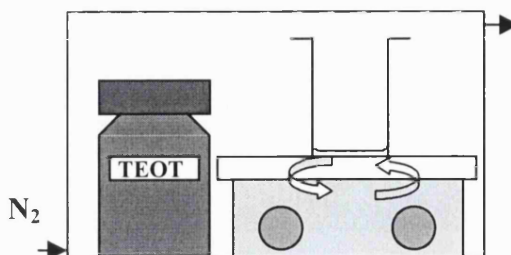
Step 2 The Teflon vessel with TEOS was stirred under nitrogen for at least 1 hour. A sealed bottle of TEOT was kept in the nitrogen hood at the same time.
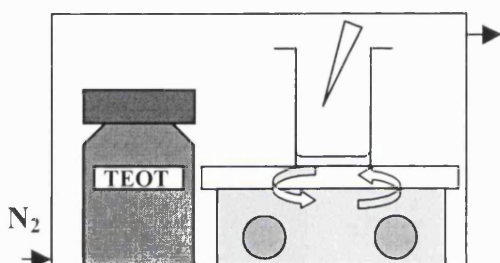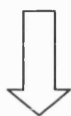
Step 3 TEOT was then added and the mixture continued to be stirred for another hour. The colour should change to light yellow.
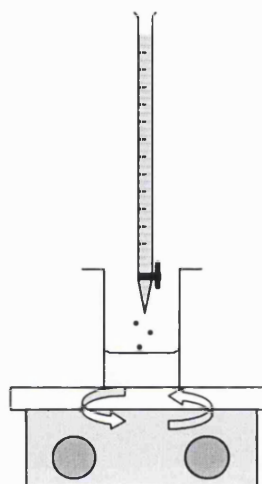
Step 4 Mixture of TPAOH with H_2O_2 was added at 1ml/min into the synthesis solution after removal from the nitrogen hood. It was then stirred for an hour to obtain a clear solution.
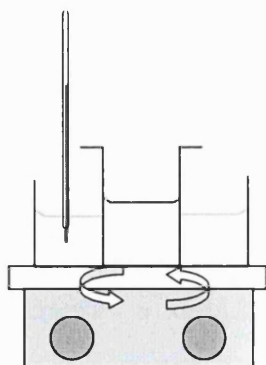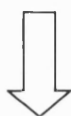
Step 5 The mixture was heated at 80°C in a water bath and stirred continuously for three hours. The water level on the Teflon bomb was marked before heating.
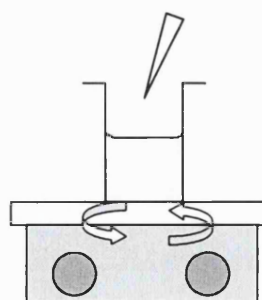
Step 6 Deionized water was then added back to the mark after heating. The synthesis solution was then stirred overnight before hydrothermal treatment.

Figure 3.4   Preparation of TS-1 synthesis solution

3.4.3 Hydrothermal treatment of synthesis mixture

The schematic diagram for zeolite hydrothermal synthesis is illustrated in figure 3.5. The silicon sample was placed in a Teflon holder with the etched pattern facing downwards (figure A) to prevent any powders and precipitates from being incorporated into the growing zeolite film. The sample along with the synthesis solution was transferred into a 125 ml Teflon vessel. The synthesis solution should be 5mm above the sample holder. The Teflon vessel was sealed in a stainless steel digestion bomb where hydrothermal treatment took place at autogenous pressure. The autoclave was placed in a preheated oven at 398K for 24 hours (figure C). After each synthesis, the Teflon vessel was cleaned using 1M HNO_3, which was sealed in the autoclave and heat treated for another 24 hours. This was to remove all the zeolite particles attached on the vessel surface to prevent pre-seeding in the next synthesis.

A   Place silicon sample onto specially designed Teflon holder

B   Place sample holder into synthesis solution

C   Hydrothermal treatment within autoclave
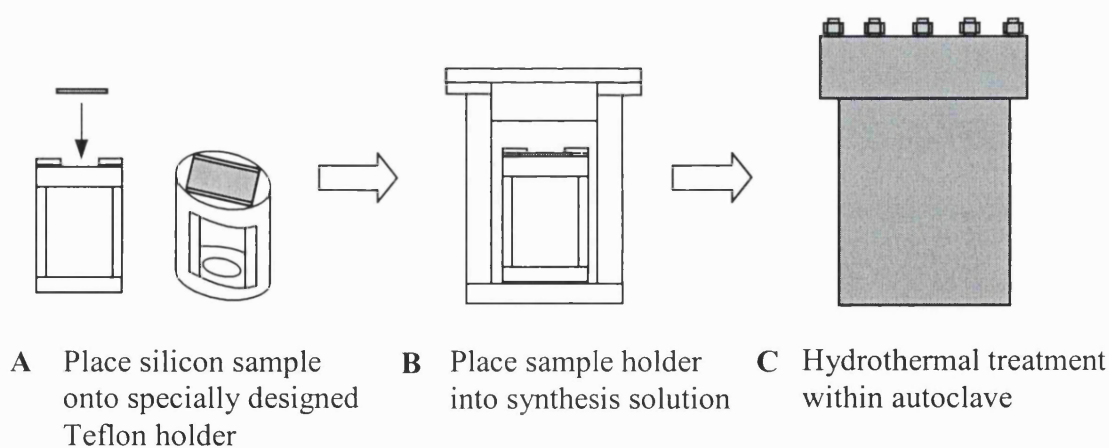
Figure 3.5   Schematic diagram for zeolite synthesis

3.5   Bonding of microreactor

The microreactor was bonded to a clean glass with pre-drilled holes after hydrothermal synthesis. The glass was spread with a thin layer of SU-8 (Sotec Microsystems) and adhered to the etched microreactor. The holes on the glass plate were connected to reactant feedthrough and outlet for sample collection.

The adhesive material employed for reactor bonding is SU-8. It is a positive photoresist that hardens on exposure to UV light. The material can withstand hydrocarbons (i.e., methanol, MTBE and 1-pentene) and temperatures up to 373 K. SU-8 used in the experiment is SM1040, which is suitable for a thinner layer of deposition (1-10μm). Figure 3.6 illustrates the procedure for bonding of the microreactor.

The procedure first starts with a pre-drilled glass (step 1). The glass and microreactor should be cleaned thoroughly with acetone to remove any dirt and oil on the surface. Tapered holes were drilled onto the glass by precision drilling using diamond drill bits (RS) to provide a good fit to the silicone tubing.

A thin layer of SU-8 was brushed on both the surface of glass plate and the silicon sample avoiding the channel (step 2 & 3). A better adhesion could be obtained when bonding the two layers together. Both the glass plates and silicon sample were heated on a hotplate at 95°C for 10mins to evaporate off the liquid and prepare for

adhesion. The hotplate was then lowered to a temperature of 80°C to bond the two pieces together before the SU-8 dried up (step 4). Deadweight can be applied on the microreactor during the cooling process. It was then exposed to UV light for 6-7 minutes for the resist to set. A color change from pale yellow to yellowish brown was observed (step 5).

After exposure to UV light, the bonded reactor was heated at a temperature of 95°C to complete the polymerisation (step 6). A leak-free seal between glass and silicon was thus obtained. Silicone tubing (∅0.5mm) was then squeezed into the holes to act as an interface for reactant feedthrough and sample collection (step 7).

Step 1 Tapered
holes drilled
onto the glass

Cross-section
of the glass
holes

Step 2 SU-8
layer applied
onto the surface

Step 3 SU-8
layer applied
onto the surface

Both heat on hotplate
for 10mins at 95°

Step 4 Lower the
temperature to
80°C then press
the glass to the
sample

Step 5 Illuminate with
UV light (about 400nm)
for 6-7 mins. The colour
will change from pale
yellow to yellowish
brown.

Step 6 Complete
the polymerisation
at 95°C for 15
mins.

Step 7 Squeeze
silicone tube into
glass holes

Figure 3.6   Procedure for microreactor bonding

3.6   Descriptions of microreactor setup

The reactivity of the catalyst was then tested in the microreactor. The setup is shown in figure 3.7 and 3.8. The reaction mixture contained 0.9M 1-pentene (99%, Aldrich), 0.2M hydrogen peroxide (30wt%, BDH) and the solvent used is methanol (99.8%, Fluka). The reactants were fed to the microreactor through a syringe pump (kdScientific) at a rate of 30-120 µl/h. The reaction took place at a temperature of 298K by immersing the microreactor in a thermostated water bath. The sample was collected through the PTFE tubing in a microlitre vial. In order to prevent evaporation, the vial was placed inside an acetone ice bath (183K) during the reaction. The acetone ice was prepared by gradually adding liquid nitrogen into a vacuum flask containing acetone. It was then stirred continuously until a slurry was formed. Samples were withdrawn from vials by precision syringes (1µl) for analysis.
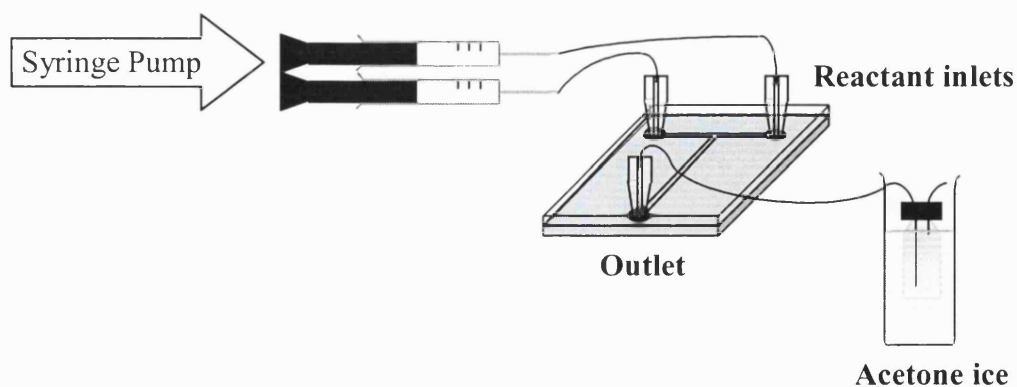
Figure 3.7   Schematic diagram of microreactor setup
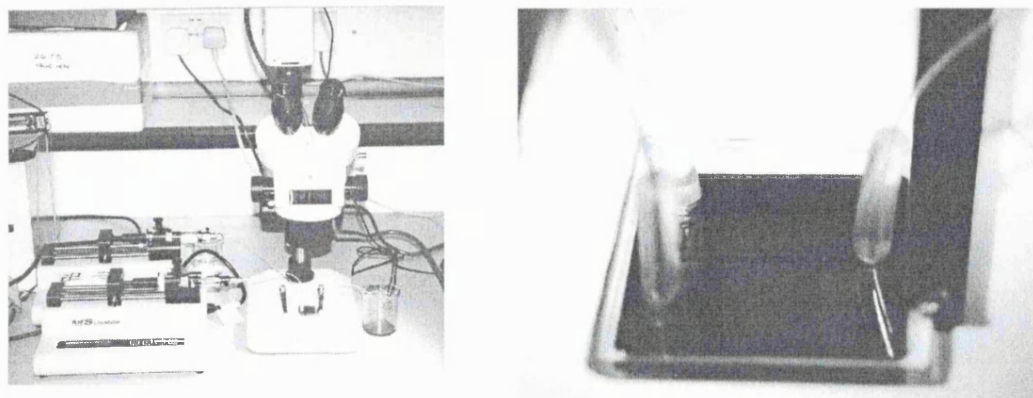
Figure 3.8   Pictures of microreactor setup

3.7   Analysis of reaction samples

3.7.1   Gas chromatography

Gas chromatographic analyses were performed by a PoraPLOT Q column (30m×0.53m) using a flame ionisation detector with tert-butyl methyl ether, MTBE (99.8%, Fluka) as the internal reference. Methanol, 1-pentene and the product 1,2-epoxypentane showed well-resolved chromatographic peaks. The GC conditions used are illustrated in figure 3.9. Figure 3.10 presents the sample chromatography with peaks of methanol, 1-pentene, MTBE and epoxypentane. The byproduct, glycol monoethylether, which appeared at a residence time of 30mins, is not shown here.

FID Temperature Program

Oven Method

Initial Temperature (°C): 200

Final Temperature (°C): 200

Hold Time (mins): 10.00

FID Method

Gas Carrier (ml/min): 5.00

(170kPa)
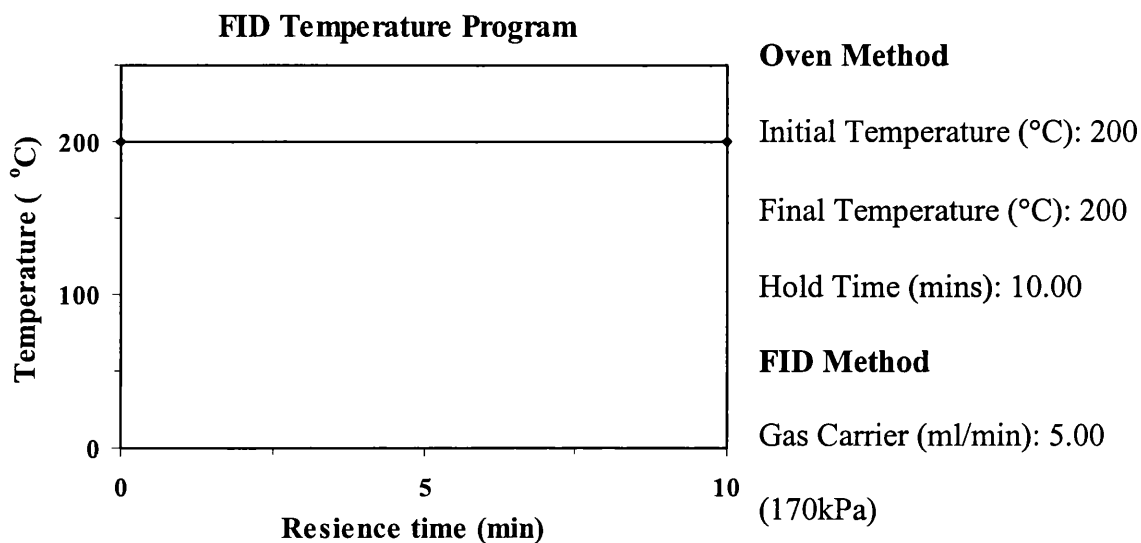
Figure 3.9   GC conditions used for sample analysis in 1-pentene epoxidation

FID Chrom-Card Strip-Chart

Peak

1. 2.16min   Methanol

2. 3.40min   Pentene

3. 4.66min   MTBE

4. 6.77min   Epoxypentane

Split ratio = 25
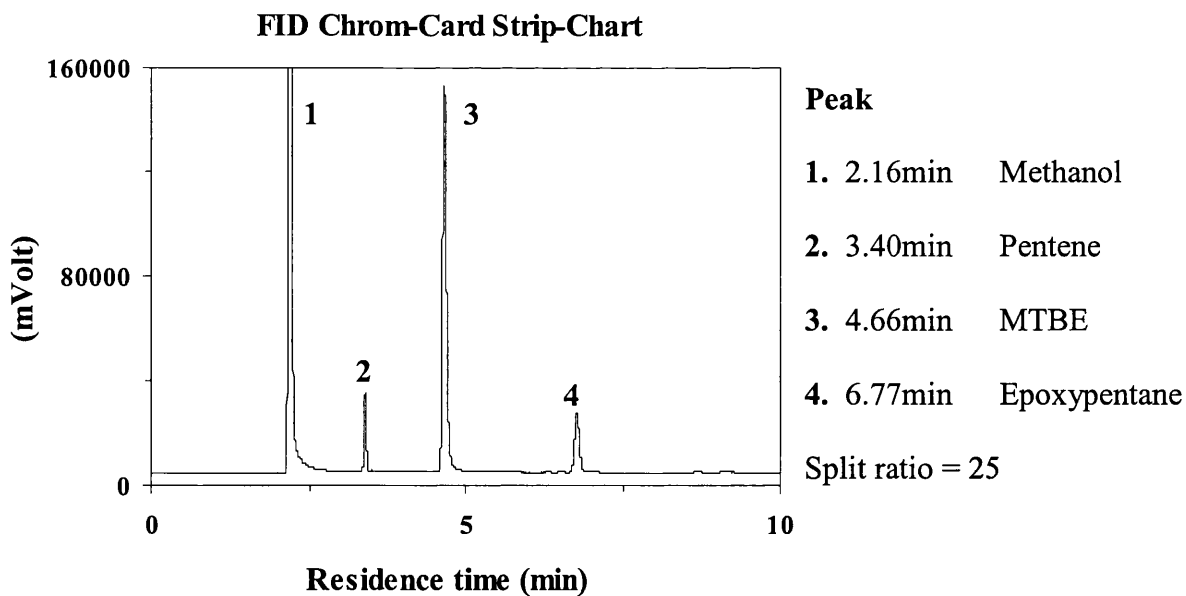
Figure 3.10   Sample gas chromatograph for different components

100

Pentene / MTBE

y = 0.7207x
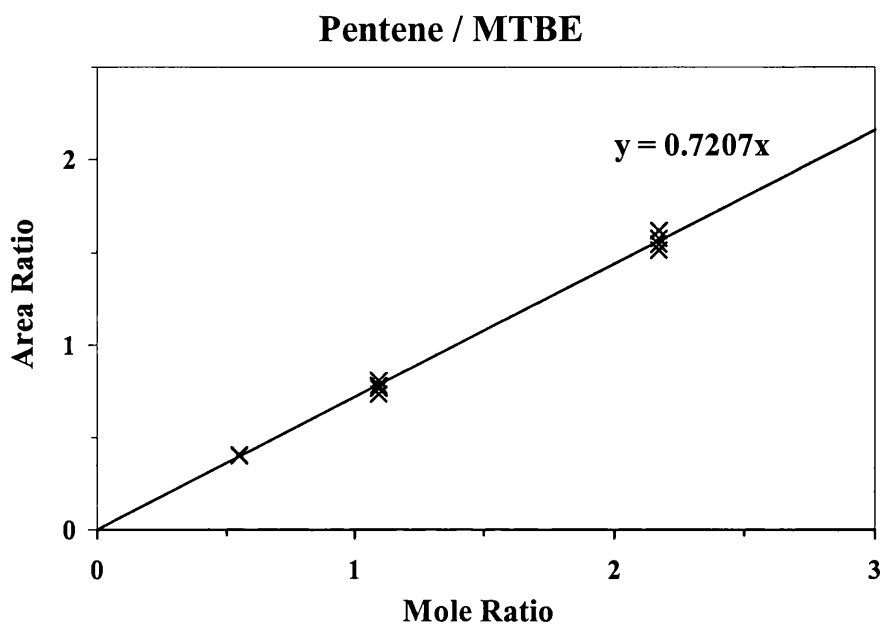
Figure 3.11   Calibration factor of pentene using MTBE as internal standard

From figure 3.11, the slope of the graph obtained is 0.7207, which is the calibration factor of pentene with respect to MTBE. The mole of pentene in the reaction sample can be calculated as below:

$$\frac{Area\ of\ pentene}{Area\ of\ MTBE} = 0.7207 \times \frac{Mole\ of\ pentene}{Mole\ of\ MTBE}$$

$$\therefore Mole\ of\ pentene = \frac{Area\ of\ pentene}{Area\ of\ MTBE} \times \frac{Initial\ mole\ of\ MTBE}{0.7207}$$

Expoxypentane / MTBE

$$y = 0.6964x$$
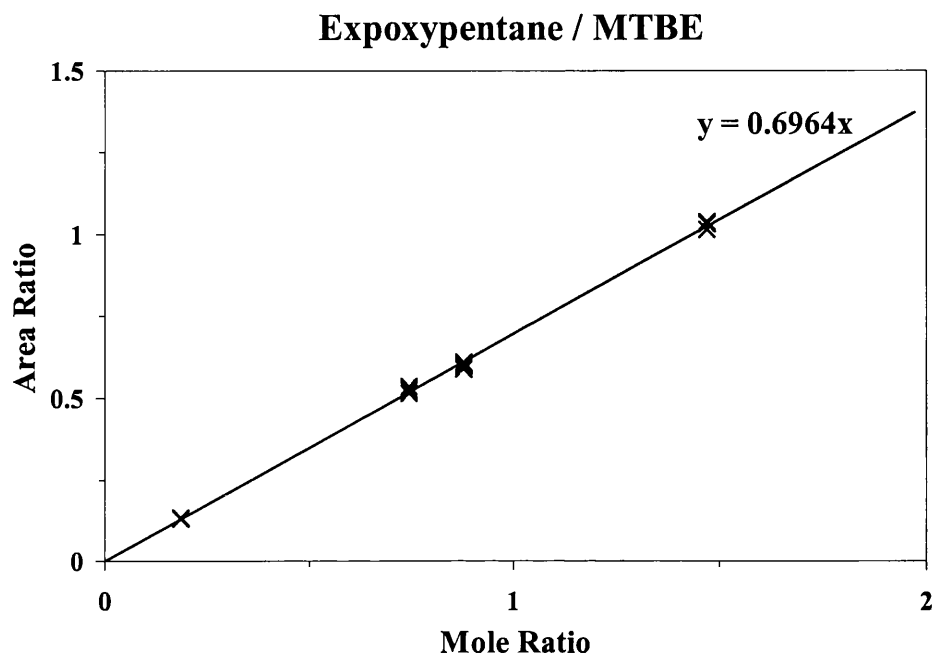
Figure 3.12   Calibration factor of epoxypentane using MTBE as internal standard

The calibration factor of epoxypentane with respect to MTBE is 0.6964. The mole of epoxypentane in the reaction sample is calculated in the following:

$$Mole\ of\ epoxypentane = \frac{Area\ of\ epoxypentane}{Area\ of\ MTBE} \times \frac{Initial\ mole\ of\ MTBE}{0.6964}$$

3.7.2 Iodometric Titration

The concentration of hydrogen peroxide in the reaction sample was determined by iodometric titration. Hydrogen peroxide, which is an oxidizing agent can be treated with excess iodide ions I^- (potassium iodide, KI) to produce I_3^-. Iodometric analysis is completed by titrating the liberated I_3^- with standard thiosulfate. Starch is not added until just before the end point (Harris, 1996).

The chemical reaction is presented in the following equations:

$$H_2O_2 \;+\; 3\,I^- \;+\; 2\,H^+ \;\rightleftharpoons\; I_3^- \;+\; 2\,H_2O \qquad\qquad 3.1$$

$$I_3^- \;+\; 2\,S_2O_3^{2-} \;\rightleftharpoons\; 3\,I^- \;+\; \underset{\underset{O^-}{|}}{\overset{\overset{O}{\|}}{O=S}}-S-S-\underset{\underset{O^-}{|}}{\overset{\overset{O}{\|}}{S}}=O \qquad 3.2$$
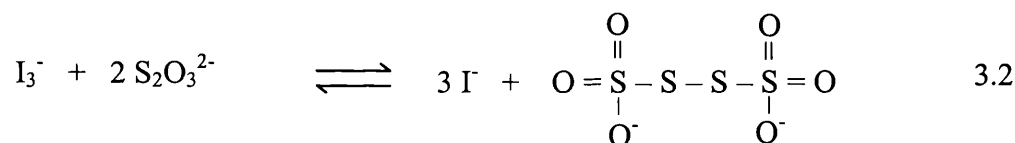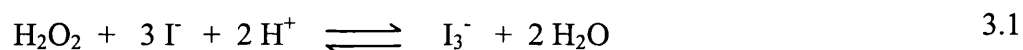
From the above formulae, it shows that 2 moles of sodium thiosulphate are required to titrate against 1 mole of hydrogen peroxide presented in the sample.

Titration amount: $2 \times Na_2S_2O_3 \;\equiv\; H_2O_2 \;\equiv\; I_2 \;\equiv\; 2 \times KI$
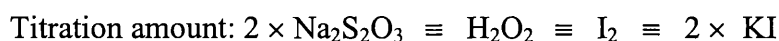
The reagent required are: 3 M H_2SO_4, 20gdm^{-3} KI and 1M $Na_2S_2O_3$.

Preparation Procedure of sodium thiosulfate solution

A stable solution of $Na_2S_2O_3$ was prepared by dissolving the reagent in high-quality, fresh boiled distilled water. Dissolved CO_2 promotes disproportionation of $S_2O_3^{2-}$

$$S_2O_3^{2-} \;+\; H^+ \;\rightleftharpoons\; HSO_3^- \;+\; S(s) \qquad\qquad 3.3$$
$$\text{Bisulfate} \quad \text{Sulfur}$$
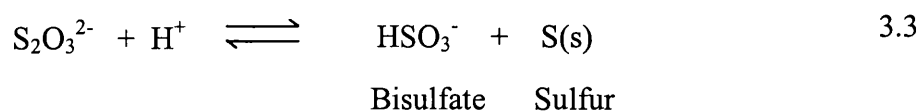
and metal ions catalyse atmospheric oxidation of thiosulfate. Thiosulfate solutions were stored in the dark with 0.1g of Na_2CO_3 per litre to maintain optimum pH. Three drops of chloroform should be added to a thiosulfate solution to prevent bacterial growth. Although an acidic solution of thiosulfate is unstable, the reagent can be used to titrate I^{3-} in acid because reaction 3.2 is faster than reaction 3.3 (Harris, 1996).

Preparation Procedure of starch solution

The starch solution was prepared by rubbing 20g of soluble starch with 50ml of water to form a paste. They were then brought to boil in $1dm^3$ water. The solution should be changed after a few days due to bacterial growth.

Titration procedure

1. The sample containing hydrogen peroxide was collected in a conical flask. Excess potassium iodide was added together with 3M sulphuric acid (about a quarter of the amount of potassium iodide).

2. The mixture was stirred vigorously by shaking the conical flask until oxygen bubbles were formed. The solution would turn from clear to brown colour indicating the formation of iodine.

3. The mixture with iodine formed was titrated against 1M standard sodium thiosulphate solution.

4. A few drops of starch solution were added as indicator at the end of titration.

5. The end point was recorded when the solution suddenly turned from dark blue to clear. Due to oxidation by air, the mixture will turn to dark blue again after the

end point, the volume should be recorded at the instance when the titration mixture changed colour.

3.8 Characterisation of zeolite-based microchemcial devices

X-ray diffraction

The crystal structure, crystallinity and crystallographic orientation of the zeolite film were determined using a Philips PW 1030 X-ray diffractometer equipped with CuKα X-ray source and graphite monochromator. The X-ray line intensity was obtained for $5^{\circ} \leq 2\theta \leq 45^{\circ}$ at a scan rate of 0.02°/min and time constant of 0.02.

X-ray diffraction (XRD) involves the irradiation of a sample with X-rays and collection of the resultant X-rays diffraction pattern. The X-rays are usually CuKα lines with wavelengths in the Å range, which are sufficiently energetic to penetrate solids and are well suited to probe their internal structure. It is used to estimate particle sizes and to identify bulk phases. The position of diffraction peaks carries information on the spacing of the reflecting planes. Diffraction lines from perfect crystals are very narrow. Crystalline patterns will show sharp peaks while amorphous phases and small particles will show broad bands and weak or zero diffraction (Niemantsverdriet, 1993). The following shows the XRD pattern of ZSM-5 extracted from literature (Koningsveld et al., 1987).

Figure 3.13   **XRD patterns of uncalcined ZSM-5 (Database of zeolite structures, 2003)**
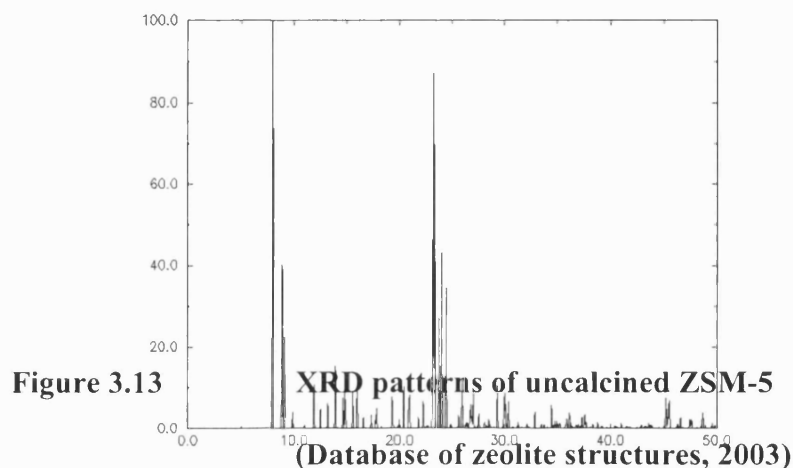
X-ray photoelectron spectroscopy

The bulk and surface compositions of the incorporated zeolites in the microchemical devices were examined by x-ray photoelectron spectroscopy (XPS, Physical Electronics). XPS represents the energy distribution of electrons that are emitted from the catalyst due to the photoelectric effect: an atom absorbs a photon of energy hv (X-ray source), a core or valence electron with binding energy E_b is ejected with kinetic energy E_k. XPS measures binding energies, which contain information on the state of the atom before photoionization (the initial state) and on the core-ionized atom left behind after the emission of an electron (the final state) (Niemantsverdriet, 1993). In XPS, the intensity of photoelectrons $N(E)$ is measured as a function of their

106

kinetic energy, E_k. The XPS spectrum is a plot of $N(E)$ versus E_k, more often, versus binding energy E_b.(figure 3.14). The details of photoemission are illustrated in figure 3.15.

- Kinetic energy, $E_k = hv - E_b$ where E_k– kinetic energy

$$hv\text{- X-ray source}$$

$$E_b - \text{binding energy}$$

- Binding energy increases with oxidation state

- Deexcitation of the excited ion occurs via X-ray fluorescence or via Auger transition
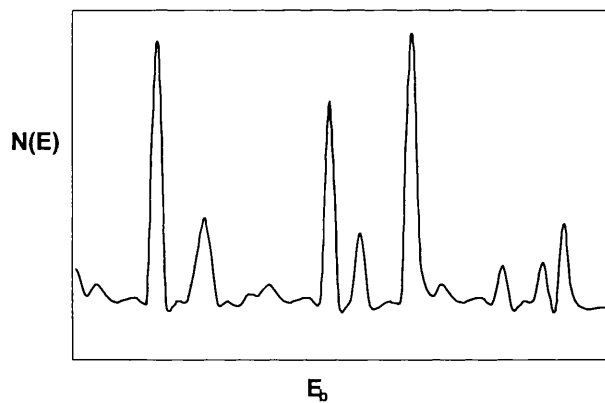
Figure 3.14   Plot of number of emitted electron against binding energy
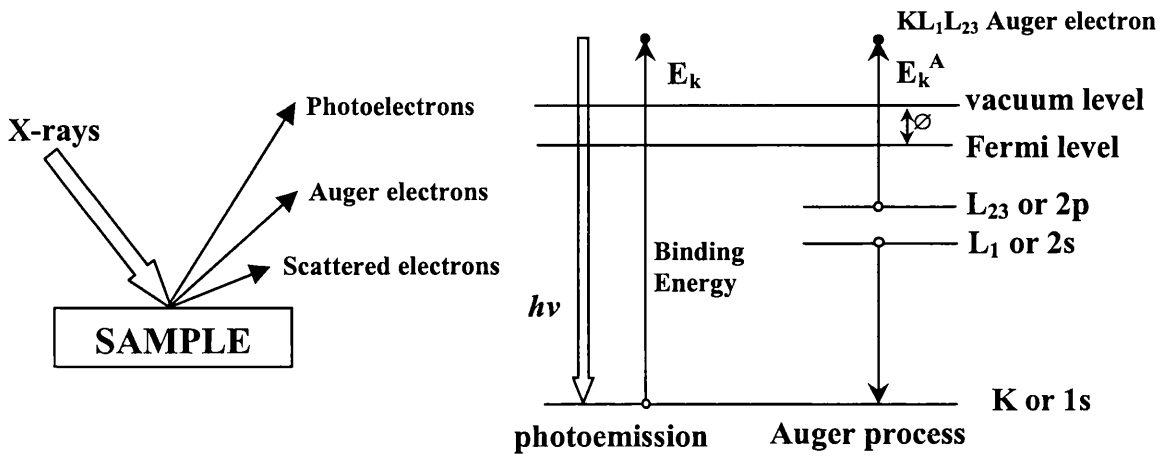
Figure 3.15 **Photoemission and Auger decay: an atom absorbs an incident X-ray photon with energy hv and emits a photoelectron with kinetic energy $E_k=hv-E_b$. The excited ion decays either by the indicated Auger process or by X-ray fluorescence (Niemantsverdriet, 1993).**

Scanning electron microscopy

Structural analyses of the zeolite film and microchannel structure were conducted using scanning electron microscopy (SEM). The film thickness, grain size and zeolite morphology were examined using a JEOL JSM 6300 scanning electron microscope. The samples were mounted onto aluminium specimen stubs with conducting carbon tape and sputter-coated with a 10 nm layer of gold to reduce sample charging.

Electron microscopy is used to determine the size and shape of supported particles. It can also determine the composition of the particles, by detecting the X-rays produced by the interaction of the electrons with the sample, or by analysing how the electrons are diffracted (Delannay, 1984).

Electrons have characteristic wavelengths typically in the range 0.01-0.1Å which is sufficiently small to resolve atomic detail. Figure 3.16 summarizes what happens with high energy (100-400 keV) electrons when the primary beam hits the sample (Niemantsverdriet, 1993).
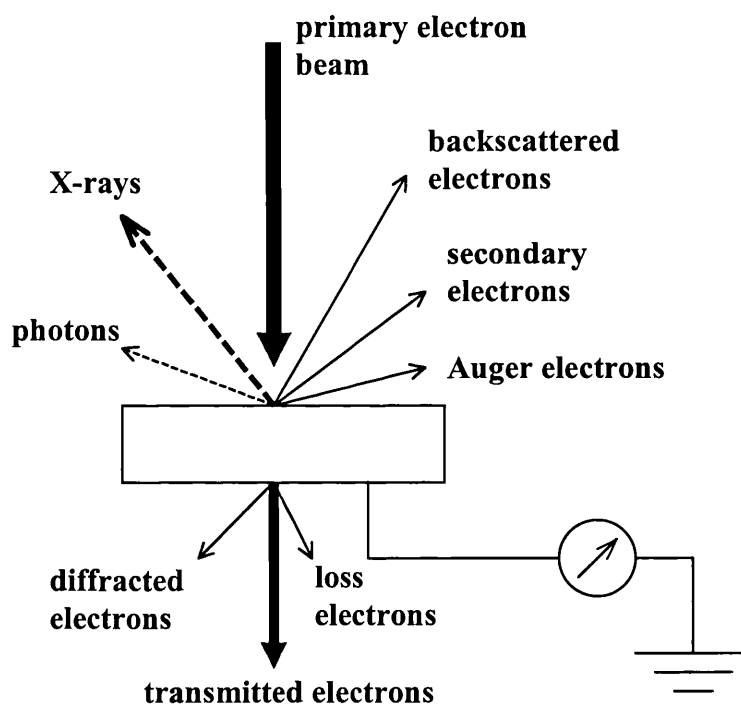
Figure 3.16   The interaction of the primary electron beam with a sample in electron microscopy produces a wealth of detectable signals.

SEM is carried out by rastering a narrow electron beam over the surface and detecting the yield of the secondary or back-scattered electrons as a function of the position of the primary beam (contrast due to the topology and composition of a surface). The secondary electrons have low energies of 10-50eV and originate from the surface region of the sample. Back-scattered electrons come from deeper and carry information on the composition of the sample, because heavy elements are more efficient electron scatterers and appear brighter in the image. SEM instruments produce image with a resolution of 5nm (Niemantsverdriet, 1993).

Transmission electron spectroscopy

Transmission electron microscopy (TEM, JEOL JEM 2010) is used to characterize particle size and morphology of the colloidal zeolite seeds. It uses transmitted and diffracted electrons to project all information in a two-dimensional image. A TEM instrument is very similar to an optical microscope with electromagnetic lenses replacing its optical counter part. The dark field image is obtained from the diffracted electron beams, which are slightly off angle from the transmitted beam. Typical operating conditions of a conventional TEM instrument are 100keV electrons. TEM is different from SEM as SEM sees contrast due to the topology of a surface, and TEM projects all information in a two-dimensional image. However, TEM can reach down to subnanometer resolution (Niemantsverdriet, 1993).

Energy dispersive analysis of X-rays

Another method to examine the bulk and surface compositions of incorporated zeolites is energy dispersive x-ray spectroscopy (EDXS, Oxford Instruments). Characteristic X-rays are emitted from the atoms in the sample when they are ionized by the electron beam. Emitted X-rays are characteristic for an element for determining the chemical composition of a selected part of the sample (0.5-1μm for bulk samples). The X-ray spectrum detected consists of a series of peaks representing the type and relative amounts of each elements in the sample (Wachs, 1992). Unlike XPS, EDX cannot provide information about the chemical state of the elements.

Thermogravimetric and differential thermal analyses

Thermogravimetric and differential thermal analyses (TGA/DTA, Setaram 92-18) were used to determine the amount of water and hydrocarbons adsorbed on the titanium silicalite-1 catalyst. The TS-1 powder sample was placed in a platinium crucible and heated from 298K to 1073K at a rate of 5K/min in air. The reference material for DTA analysis was alpha alumina powder. The sample weight was measured by TGA while DTA recorded the change in temperature for constant heating.

TGA analysis measures the gain or loss in weight of the sample as a function of the composition of the atmosphere and the temperature. A gravimetric thermoanalyzer consists of (1) an automatic magnetic re-equilibrating balance (2) a temperature-programmed furnace and (3) a gas flow circuit to control the gaseous environment. This setup is equipped to allow for other analytical methods such as DTA. The exothermal or endothermal effects accompanied by changes in the physiochemical states of the sample under changing temperature can be measured by DTA (Auroux, 1994).

Chapter 4

Incorporation of Zeolites in the Design Architecture of

Microchemical Systems

4.1   Introduction

Molecular sieve zeolites are microporous tectosilicates with different pore sizes. They can precisely tailored up to the scale of sub-nanometer to create desired arrangement and properties, which are of great interest in the field of catalysis, ion-exchange, separation and extraction (Davis and Lobo, 1992; Davis, 1998, Caro et al., 2000). Zeolites, with their thermal and chemical stability, offer a great choice for integration into microsystems. Their molecular structures can be tuned and engineered precisely for design and application in nano devices (Yan and Bein, 1995).

Recently, zeolites have found applications as catalyst and membranes in microchemical devices. Free-standing silicalite-1 membranes have been grown onto silicon microchannels (den Exter et al., 1997). ZSM-5 zeolites were deposited onto machined stainless steel microchannels for selective catalytic reduction of NO with ammonia (Rebrov et al., 2001). These belong to an emerging new technology: the microchemical systems that also include other microdevices such as micromixers, micro heat-exchangers, micro-actuators and microsensors (Ehrfeld et al., 2000). Ultimately, these discrete components can be assembled to create micro-analytical laboratories, portable manufacturing plants and miniature fuel cells to satisfy the needs of an increasingly mobile society.

Microreactors have great potential as analytical tools for catalytic, chemical and biochemical research. They also represent another method for production of specialty chemicals and biochemicals. Their unique properties, which include high heat and mass transfer rates (Drost et al., 1997, Losey et al., 2000, Ehrfeld et al., 2000) and short residence time (Jensen, 2001, Gavriilidis, et al., 2002) make them an invaluable tool for studying demanding reaction systems. Microreactors can provide important information on reaction mechanisms and intrinsic kinetic rates that are essential for reactor design and scale-up. They can also be used for rapid screening of synthesis pathways to determine the most efficient and environmentally responsible synthesis route. Pioneering work in microreactor has been carried out among others by groups at Institüt für Mikrotechnik Mainz (IMM), Forschungszentrum Karlsruhe GmbH (FK), Massachusetts Institute of Technology (MIT), Pacific Northwest National Laboratory (PNNL), Technische Universität Chemnitz (TUC), etc.

Miniaturization can also benefit membrane separation processes. It enables large membrane areas to be accommodated within a small volume allowing for the design of a compact separation unit. Instead of one continuous membrane surface, a membrane microseparator will consist of an assembly of smaller membranes that provides the same effective separation area. It is expected that by keeping the individual membrane area small, the risk of membrane failure due to accumulated stresses associated can be significantly diminished. This is particularly important for inorganic membranes, where embrittlement, crack-formation and delamination are

some of the leading causes of failure. den Exter et al. (1997) have prepared free-standing zeolite micromembranes on silicon substrates.

In this chapter, traditional semiconductor fabrication methodology along with zeolite thin film technology is employed to create microstructured patterns that can be employed in microchemical systems, such as microreactors, microseparators or microelectrochemical cells.

4.2   Experimental

Figure 4.1 gives the general outline of the procedure for the fabrication of zeolite-based microstructured patterns using standard semiconductor microfabrication technology. First, a zeolite-silicon composite was prepared by growing an oriented polycrystalline zeolite film onto a silicon wafer. The design pattern was then transferred and etched onto the zeolite-silicon composite using conventional photolithography.

A — Silicon

B — Teflon tape on the bottom side prior to zeolite

C — Hydrothermal synthesis

D — Zeolite-silicon composite

E — Resist coating

F — Photolithography

G — Expose zeolite in BOE

H — Photoresist stripping

I — Final product

Silicon   Zeolite   Zeolite Nanocrystals

Mask   Teflon   Photoresist
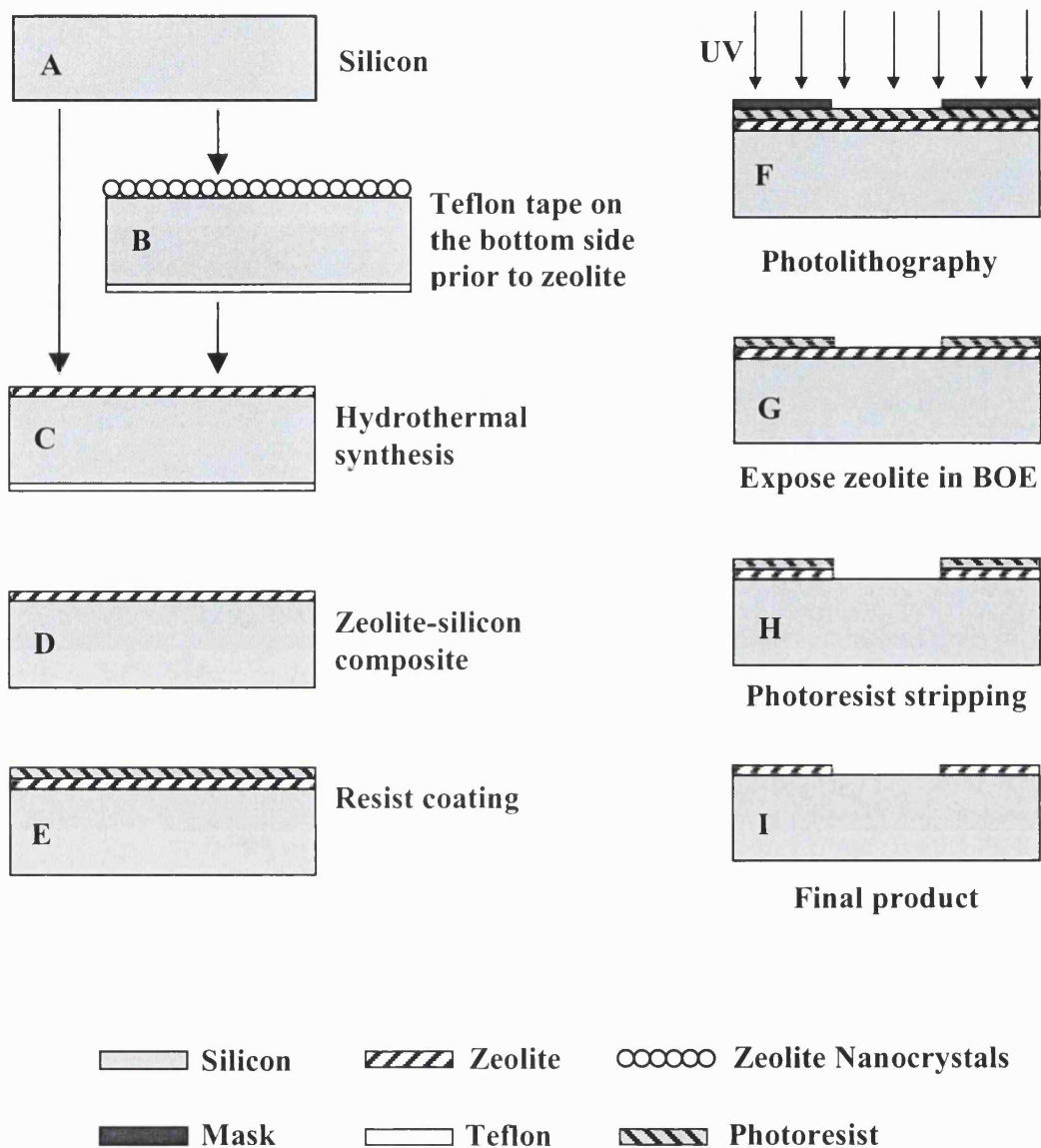
Figure 4.1   Fabrication of zeolite-based microstructured patterns

4.2.1   Preparation of zeolite-silicon composite substrate

Two different approaches were employed in this study to prepare well intergrown, polycrystalline zeolite films onto silicon substrates. In the first method (figure 4.1A, 4.1C), silicalite-1 (Sil-1) films on silicon were prepared from a synthesis

117

mixture containing 6.5 ml of organosilicon precursor, tetraethyl orthosilicate (TEOS) mixed with 65 ml of 0.05 M aqueous solution of the organic template, tetrapropylammonium hydroxide (TPAOH) to give mole ratios of 80 TEOS: 10 TPAOH: 10,000 H_2O. The silicon was held in a horizontal position with the polished surface facing downwards. This decreased the number of growth defects caused by incorporation of zeolite powder from the solution. The backside of the silicon was covered with a layer of Teflon ribbon to prevent zeolite growth. Placed within an autoclave vessel, the completely immersed silicon was hydrothermally treated at 448 K in a preheated oven (Memmert) between 6 to 48 h.

In the second approach (figure 4.1B, 1C), the silicon substrate was pre-seeded with zeolite nanocrystals before hydrothermal synthesis. Schoeman et al. (1997) have shown that submicron MFI zeolite films can be successfully grown onto seeded silicon. The colloidal Sil-1 seeds were prepared from a synthesis mixture containing 15 g of fumed silica, 0.85 g of sodium hydroxide, and 60 ml of 1 M tetrapropyl ammonium hydroxide (TPAOH) solution. The mixture was stirred for 24 h at room temperature to produce a clear and homogeneous solution. This solution was then transferred to a 125 ml Teflon autoclave (Parr Scientific Inc.) and heated in an oven (Memmert GmbH Co.) to a temperature of 398 K. After 8 h of hydrothermal treatment, the colloidal zeolites were recovered and purified using a series of centrifugation and rinsing steps. The Sil-1 seeds were stored as 2 wt.% colloidal suspension in ethanol.

The seeding procedure involved immersion of the silicon in 0.05 M 3-mercaptopropyl trimethoxysilane/ethanol solution in order to functionalize the substrate. The excess surfactants were rinsed off using ethanol. This was followed by immersion in colloidal suspension of Sil-1 seeds. The seeded substrate was then dried in the oven at 333 K for 15 min. This procedure gave uniform seed coverage on the silicon. The seed population on the substrates can be adjusted by repeating the seeding process several times. This way, seed populations up to 95 x 10^{12} crystals per m^2 (i.e., complete surface coverage) were obtained. The seeded silicon was then placed horizontally in a synthesis mixture containing 40 TEOS: 10 TPAOH: 20,000 H_2O, and sealed in an autoclave for hydrothermal regrowth at 398 K. Zeolite films grown for 6, 12, 24 and 48 h were examined to determine layer thickness, surface morphology and film orientation. After the synthesis, the zeolite-silicon composites were rinsed in deionized distilled water, dried overnight in an oven at 333 K and stored in a dry container (figure 4.1D).

Starting with a zeolite-silicon composite substrate, a layer of positive photoresist was next spin-coated onto the substrate (figure 4.1E). The resist was soft baked at 383 K for 1 min. Using contact printing, the micropattern etched on the photomask was transferred onto the polymer resist layer after exposure to UV light (figure 4.1F). The resist irradiated with UV light was washed away to expose the zeolite layer underneath (figure 4.1G). The sample was then hard baked at 393 K for 30 min to harden the photoresist and improve its adhesion. A buffered oxide etching solution (BOE) containing 1 HF: 6 NH_4F was used to isotropically etch the

micropattern onto the zeolite layer. The etched substrate was rinsed with deionized distilled water and dried using clean nitrogen gas. The photoresist was stripped from the surface using acetone or oxidised using oxygen plasma (figure 4.1H). After a final rinsing in deionized distilled water, the patterned substrate was dried overnight at 333 K and calcined in air at 823 K for 6 h (figure 4.1I) to remove the organic templates trapped within the zeolite cages. This final step frees the zeolite pore environment for catalysis and separation.

4.2.2 Characterisation

Structural analyses were conducted using X-ray diffraction (XRD) and scanning electron microscopy (SEM). The crystal structure, crystallinity and crystallographic orientation of the zeolite film were determined using a Philips PW 1030 X-ray diffractometer equipped with CuKα X-ray source and graphite monochromator. The film thickness, grain size and zeolite morphology were examined using a JEOL JSM 6300 scanning electron microscope. The samples at various stages of fabrication were inspected visually using an optical microscope (Olympus, BH-2). The surface roughness of the silicon substrate was examined by atomic force microscopy (Nanoscope IIIα, Digital Instruments). These combined characterisation techniques provide detailed information on the microstructure of the zeolite-silicon composite material used in the preparation of microchemical devices.

4.2.3. Materials

The silicon substrate was a four-inch diameter p-type Si (100) wafer. The silicon was cleaned using a series of sonification and rinsing in ethanol (99.8%) and deionized distilled water. The wafer was then dried overnight in the oven at 333 K and stored in a dry container for later use. Smaller substrates were obtained by sectioning the wafer into 2.5 cm × 3.0 cm rectangular pieces. Chemicals used in zeolite synthesis were tetraethyl orthosilicate (98%, Aldrich), tetrapropylammonium hydroxide (1 M, Aldrich), fumed silica (0.01μm, 99.8%, Aldrich) and sodium hydroxide (98%, BDH). The 3-mercaptopropyl trimethoxysilane (99%) employed in grafting the zeolite seeds onto the silicon substrate was purchased from Aldrich. For microfabrication, the following chemicals were used: HPR-207 positive photoresist (Fuji-Hunt Electronics Technology Co), FHD-5 positive developer (Olin), Superwet BOE Etchant 6-1 (General Chemical) and acetone (Lab Scan).

4.3.   Results and discussion

4.3.1. Synthesis of zeolite-silicon composite

The clean silicon substrate (figure 4.2a) was seeded using the procedure described in the experimental section in order to obtain a complete and uniform seed coverage (i.e., 95 x 10^{12} seeds/m^2) as shown in figure 4.2b. The 120 nm colloidal Sil-1 seeds were roughly ellipsoidal in shape with no apparent crystal facets. XRD

analysis of the zeolite seeds indicated an MFI-type crystalline structure. It was clear from comparing the surface line profiles of the plain (figure 4.2a, Inset) and seeded silicon (figure 4.2b, Inset) obtained by atomic force microscopy that seeding results in an increased surface roughness.
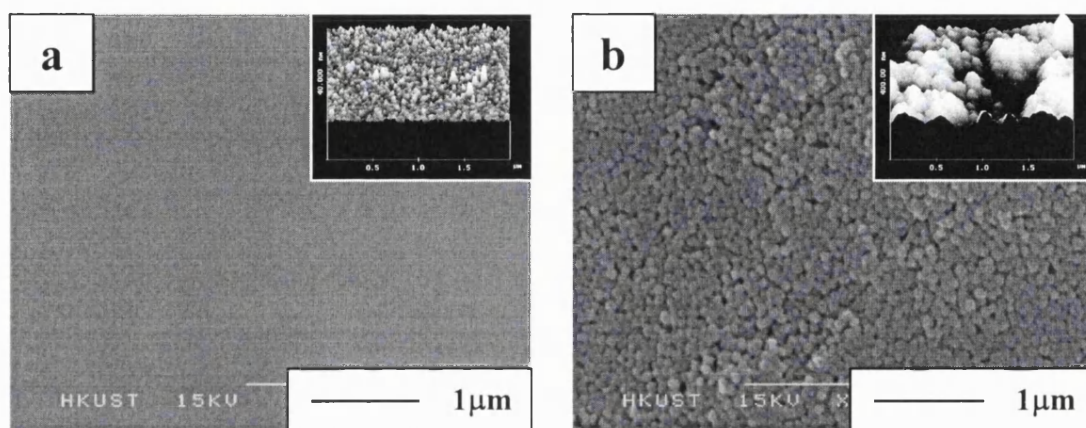
Figure 4.2   Scanning electron and atomic force micrographs of (a) plain silicon and (b) seeded silicon substrates (figure insets are AFM surface profiles of the plain and seeded silicon at the same magnification)

The deposition and growth of Sil-1 zeolite onto clean and seeded silicon substrates are shown in figure 4.3 and 4.5, respectively. Figure 4.3 displays the microstructure of Sil-1 zeolite deposited onto silicon substrate after 6, 12, 24 and 48 h of hydrothermal synthesis. Approximately 4.7×10^9 crystals/m^2 occupied the surface of the sample after 6 h of synthesis (figure 4.3a). The zeolites had a relatively uniform size of 7 μm x 17 μm giving the crystals an average length-to-width ratio of 2.4. The coffin-shaped crystals had a thickness of about 2.3 μm (figure 4.3a, Inset). Intergrowth and coalescence were evident where two neighbouring crystals impinged

122

upon one another, forming larger irregular shaped rafts shown in figure 4.3a. Although the individual zeolites had random placement and alignment on the silicon surface, most of the crystals grew on the silicon with their (020) plane parallel to the surface. This means that the straight zeolite pore channels were aligned perpendicular to the surface. About half of the crystals exhibited secondary growths that emerge from the flat (020) planes. These secondary crystals were oriented with their (200) planes parallel to the silicon surface. The resulting morphology was reminiscent of twinned Sil-1 crystals. The inset in figure 4.3a shows that the surface of the zeolite-silicon composite substrate is rough, mainly because of the non-uniform coating and presence of secondary growths.

Through crystal growth and coalescence, nearly 90% of the surface was covered by zeolite crystals after 12 h of synthesis (figure 4.3b). Further nucleation was not evident and the crystal population per unit area remained unchanged. The crystals were significantly larger (9 μm x 32 μm) with most of the growth along their length (i.e., c-axis). This resulted to an elongated shape with a length-to-width ratio of 3.7. Growth along the zeolite width (i.e., a-axis) and thickness (i.e., b-axis) was small in comparison. Secondary in-plane (figure 4.3b) and off-plane crystal growths (figure 4.3b, Inset) were common. This resulted in an uneven surface as shown in the figure inset. It is interesting to note that cavities formed by dissolution of the silicon substrate were also observed. Usually the cavities were hidden beneath the zeolite layer, and were therefore undetectable from surface inspection. After 24 h of hydrothermal synthesis (figure 4.3c), the crystals nearly doubled in size compared to

those shown in figure 4.3b. These zeolites were roughly 6 μm thick, 16 μm wide and 64 μm long. Nearly all crystals exhibited secondary growth, which was responsible for its rough surface (figure 4.3c, Inset). An additional 24 hours of synthesis allowed the secondary crystals with (200) orientation to grow sufficiently large to coalesce and form an intergrown layer (figure 4.3d). Defects in the form of misaligned crystals interrupted the otherwise smooth surface (figure 4.3d). Unfortunately, defects in the form of large cavities within the silicon were also present (figure 4.3d, Inset). The X-ray diffraction pattern of this zeolite-silicon composite is shown in figure 4.4a.

Without pre-seeding, zeolite nuclei were formed on silicon by heterogeneous nucleation or were incorporated after it had nucleated in the solution (i.e., homogeneous nucleation). It had also been suggested that microcrystals deposited from the solution may act as seeds for zeolite growth (Bein, 1996). The number of nuclei formed was usually less than 1 per micron square, especially in the absence of ageing. This means that the concentration of nutrients immediately surrounding the seeds is uniform. Off-plane crystal growth was observed (figure 4.3b, Inset), but were not as common as the in-plane zeolite growth (figure 4.3a). The latter zeolites were oriented with their (020) plane parallel to the surface. It had been argued that the (020) oriented zeolite crystals have a more stable configuration because of their larger contact area with the support (Jansen and van Rosmalen, 1993).

The Sil-1 displayed anisotropic growth that was typical of MFI-type zeolites (Jansen, 1991; Iwasaki et al., 1997). The growth rate along the c-axis of the zeolite

crystal (i.e., <002>) was the highest at 2.6 μm/h, followed by a-axis (i.e., <200>) at 0.6 μm/h and b-axis (i.e., <020>) at 0.2 μm/h. Figures 4.3a-4.3c show that the zeolites grew rapidly along the c- and a-axis, completely covering the silicon surface in less than 24 h of synthesis. However, the increase in the layer thickness corresponding to the zeolites' b-axis was small. A competing crystal orientation was evident even at the start of film growth (figure 4.3a). The (200)-oriented crystals grew directly from the existing (020) crystals, and predominated once the (020) crystals formed a complete film. This gave the resulting zeolite film (figure 4.3d) two distinct layers of different crystallographic orientations.
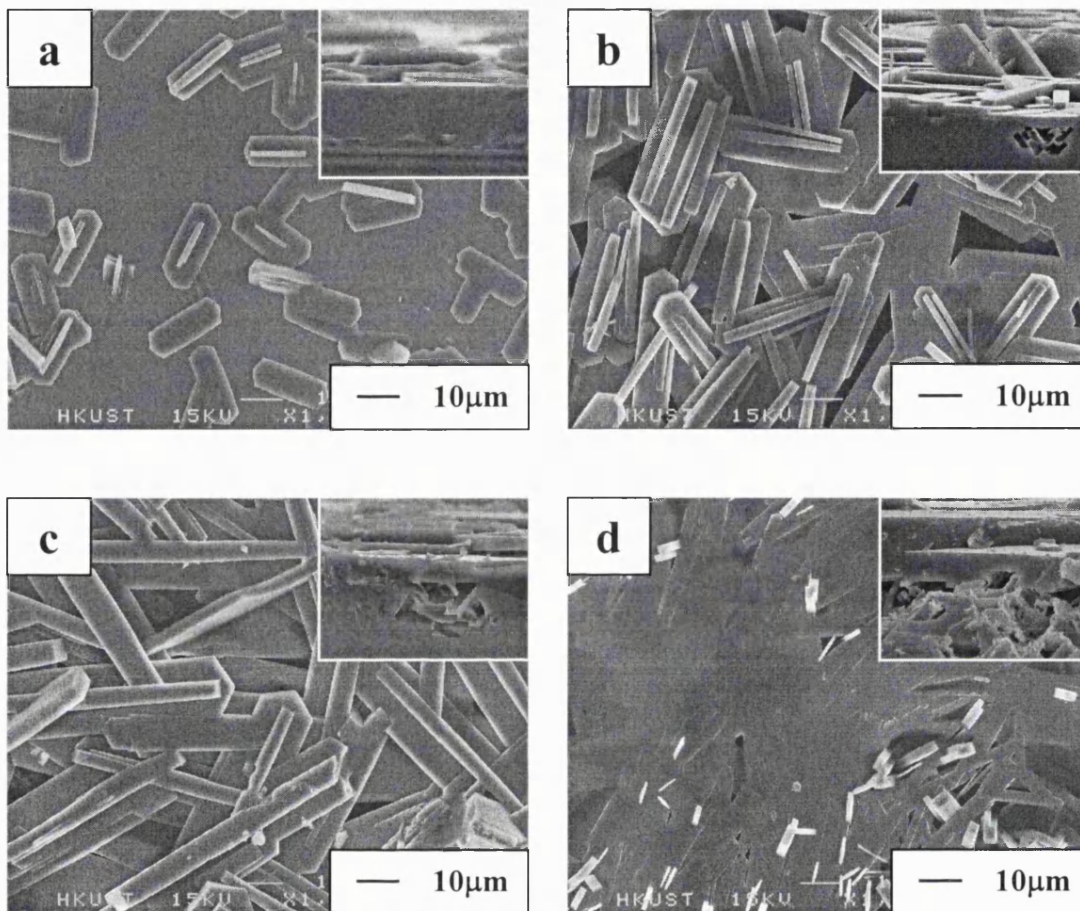
Figure 4.3   Scanning electron micrographs of Sil-1 grown on plain silicon for: (a) 6 h, (b) 12 h, (c) 24 h and (d) 48 h of hydrothermal synthesis (80 TEOS - 10 TPAOH - 10000 H_2O, 448 K) (figure insets are the cross-sectional views at 2.5× higher magnification)
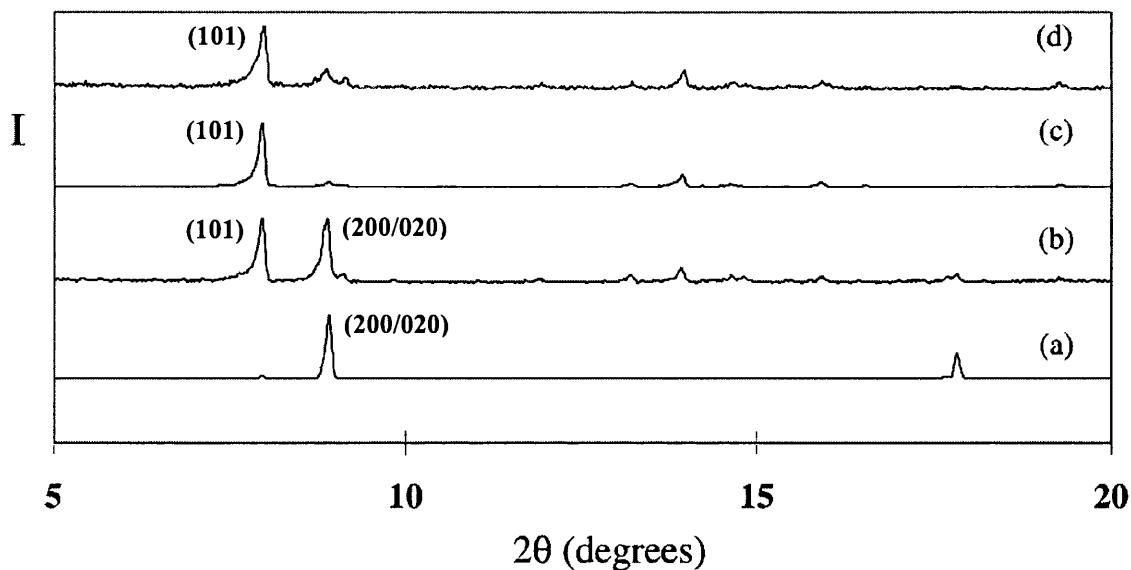
Figure 4.4   XRD patterns of samples shown in (a) figure 4.3d, (b) figure 4.6a, (c) figure 4.6b and (d) figure 4.5c.

It is well known that zeolite growth and morphology are strongly dependent on the synthesis parameters (Persson et al., 1994). Using a different synthesis composition and conditions, den Exter et al. (1997) obtained a zeolite film on silicon that displayed a mixture of (020) and (200) orientations. Although it has not been reported before, the presence of microcavities is not unexpected since silicon is known to dissolve in the alkaline synthesis solution. These defects can be prevented by using less alkaline solution, but at the expense of a longer induction time for zeolite nucleation. An (020)-oriented Sil-1 film, with its straight pore channels, is of great interest in membrane separation. In addition, the slow crystal growth along the b-axis is ideal for the preparation of ultrathin zeolite membranes. However, most microchemical systems will require high-aspect ratio patterns that demand a thick

zeolite layer. In these circumstances, a film consisting of zeolites oriented along its c- or a-axis (i.e., faster growth rate) are more appropriate.

Figure 4.5 shows the zeolite microstructure grown on seeded silicon for 12, 24, 48 and 72 h. Unlike the zeolites grown on plain silicon, a complete film was obtained after 12 h of hydrothermal synthesis (figure 4.5a). The 1.1 μm thick zeolite layer consisted of intergrown crystals (figure 4.5a, Inset). The zeolites were aligned with their c-axis nearly normal to the surface. X-ray diffraction analysis indicated that the zeolites grew with a preferred orientation of (101) on seeded silicon (figure 4.4d). The film had a (101) orientation with the zigzag pore channels normal to the substrate. Analysis of the SEM images indicated that the grains had an average size of 0.6 μm and a length-to-width ratio of 1.4. These gave the grains a rectangular shape as shown in figure 4.5a. Zeolite films grown for longer time (i.e., 24 to 72 h) had larger crystal grain size, better intergrowth and smoother film surfaces as shown in figure 4.5b-4.5d. Through growth and coalescence with neighbouring crystals, the grain size increases from 0.6 to 1, 1.3 and 2.3 microns, whereas the film thickness increases from 1.1 to 2.2, 2.9 and 4.1 μm after 12, 24, 48 and 72 h of synthesis, respectively. As a result, the individual zeolite crystals had a wedge-like shape (cf. figure 4.5c, Inset). Due to the extensive coalescence and intergrowth between the crystals, it was difficult to ascertain the grain morphology from the SEM images. However, it is clear from the figures that the inter-crystal grain boundary decreases with the synthesis time. X-ray diffraction analysis indicated that these zeolite films also have a (101)-preferred orientation.
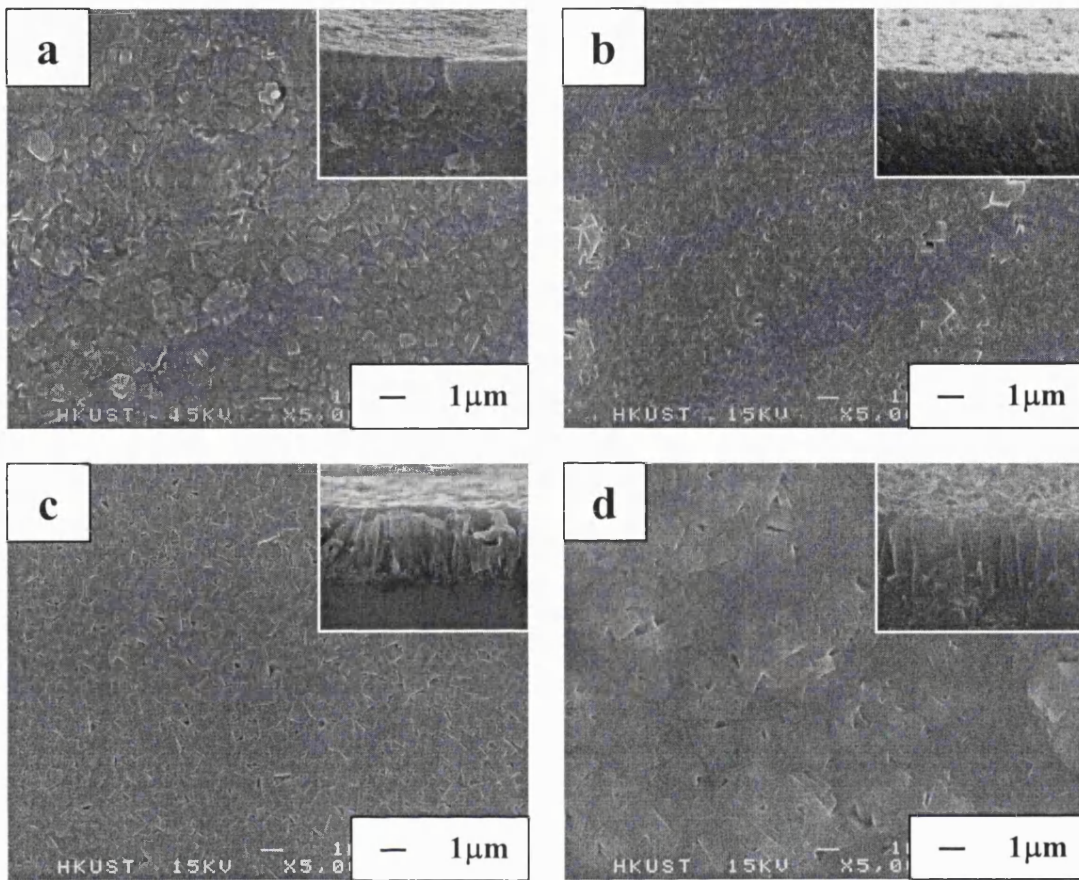
Figure 4.5   Scanning electron micrographs of Sil-1 grown on silicon with 95×10^{12} seeds/m^2 for: (a) 12 h, (b) 24 h, (c) 48 h and (d) 72 h of hydrothermal synthesis (40 TEOS - 10 TPAOH - 20000 H_2O, 398 K) (figure insets are the cross-sectional views at 2× higher magnification)

129

The zeolite nanocrystals on the seeded silicon acted as nuclei for zeolite crystal growth. From the seed layer, the zeolites grew towards the solution where the concentration of the nutrient is high. Coalescence and growth termination were the results of the intense competition between neighbouring growing crystals, and helped shape the film microstructure. The dense crystal population and the relatively uniform concentration gradient of nutrient above the growing zeolite layer favoured the growth of the crystal along the c-axis. This gave the MFI zeolite film a preferred (101) orientation. The intergrowths between neighbouring crystals provided the polycrystalline film its mechanical strength and stability. The zeolite films (figure 4.5) grown from a thick seed layer and dilute synthesis solution do not display any abscess or microcavity defects as observed in figure 4.3b-4.3d. However, the growth rate was slow with the growth along the c-axis being only about 0.14 μm/h, while the b- and c-axis growths were approximately 0.05 μm/h. Higher growth rates can be obtained by using more concentrated synthesis mixtures and higher hydrothermal treatment temperatures.

Figure 4.6 shows the Sil-1 film microstructures obtained from two different seed concentrations. Figure 4.6a displays the zeolite film grown on silicon with seed population of about 1.5×10^{12} seeds/m^2 (i.e., 1.5 seed/μm^2), which is about 1.6 % of complete seed coverage. The 2 μm thick polycrystalline film was made of randomly oriented intergrown zeolite crystals as shown in the figure. This was confirmed by the X-ray diffraction pattern in figure 4.4b. Diffraction peaks corresponding to (101) and (200)/(020) crystallographic orientations were evident in the figure. Zeolites grown

on silicon wafer with a partial seed coverage ($\sim$ 26 %) of 25 x 10^{12} seeds/m^2 formed a polycrystalline film (figure 4.6b) with (101) orientation (figure 4.4c). Figure 4.6b shows that the zeolite film was 4 μm thick with an average grain size of 1.4 μm. Examination of the X-ray diffraction patterns shown in figure 4.4a-4.4d indicates that zeolite film orientation is influenced by the initial seed population present on silicon. Zeolite growth on an unseeded substrate had predominantly (020) and (200) orientations (figure 4.4a). The addition of zeolite seeds favoured the growth of films with (101) orientations (figure 4.4b-4.4d). As the seed population increases to full coverage, a well-oriented (101) zeolite film was obtained (figure 4d). Intermediate seed coverages led to films with mixed (101) and (200) orientations. This suggests that the zeolite film orientation can be manipulated through seeding. Changing the seed population alters the immediate environment of the growing zeolite. Growth competition between neighbours can significantly change the concentration gradient of nutrients around the growing crystal and can affect the growth of the zeolite (Iwasaki et al., 1997). Figure 4.7 displays the schematic drawing of the zeolite pore structure viewed along the <101>, <200> and <020> axes, respectively. Only the (020)-oriented film has the straight channel pores aligned normal to the silicon substrates, whereas in the other two orientations, the zigzag channel is normal to the support.
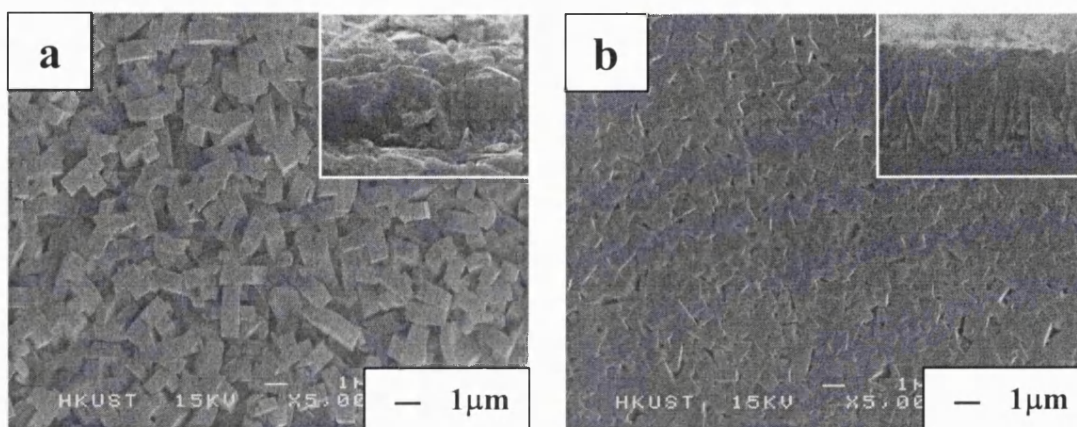
Figure 4.6   MFI zeolites grown on silicon with seed populations of (a) 1.5×10^{12}

seeds/m^2 (40 TEOS – 10 TPAOH – 20000H$_2$O, 398K) and (b)

25×10^{12} seeds/m^2 (40 TEOS – 10 TPAOH – 20000H$_2$O, 398K)

(figure insets are the cross-sectional views at 2× higher

magnification)

(101)   (200)   (020)
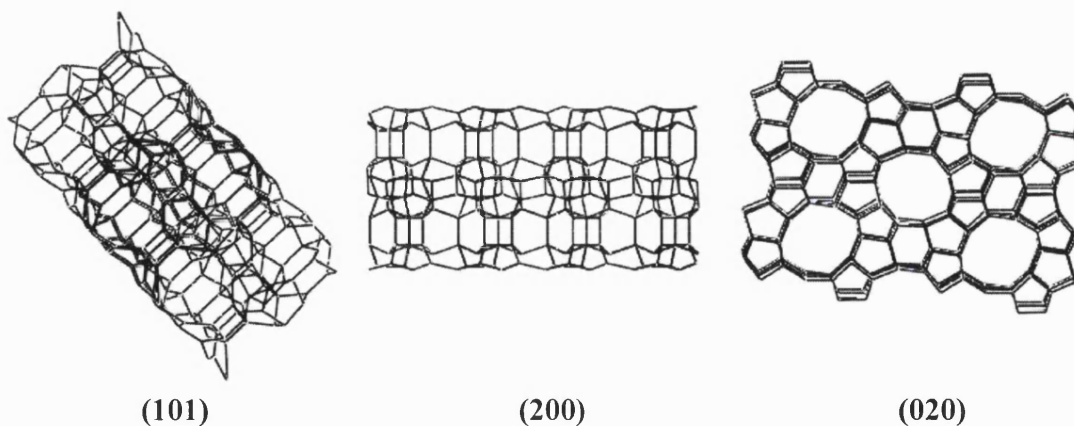
Figure 4.7   Schematic drawing of the zeolite pore structure viewed along

<101>, <200> and <020> axes

4.3.2. Fabrication of zeolite micropatterns and their stability

The previous section showed that zeolite films of controlled orientations and thickness could be grown on a silicon wafer to serve as substrate for the fabrication of microchemical devices. The ability to engineer and tailor the zeolite microstructure and chemistry is very important for the effective incorporation of zeolites as catalyst, membrane and structural materials in microchemical systems. The zeolite-silicon composite substrates were thermally stable, as they were able to withstand temperatures up to 873 K in both oxidising and reducing atmospheres for extended periods of time without crack formation or film delamination. The zeolite film was also stable in low to moderate concentrations of acids and bases, except in the presence of fluoride containing acids and salts. However, corrosion of the silicon was evident in alkaline solution. The composite substrate was also stable in alcohol, acetone and aromatic solutions (e.g., xylene). However, this does not necessarily mean that the fabricated zeolite *micropatterns* are stable under similar conditions.

Zeolite microchannels

Figure 4.8 displays three test patterns etched onto the zeolite-silicon composite substrate using the procedure discussed in the experimental section. These images were taken after the microfabricated patterns had been subjected to 2 weeks of thermal cycling between 303 K and 873 K in a furnace. Figure 4.8a displays a series of microchannels etched onto a 10 µm thick silicalite-1 (101) film grown on seeded

silicon. The cross-section of the channels was rectangular with width of 5 microns. The shape of the serpentine channels was based on a cosine function with a periodicity defined by the peak-to-peak distance (L) of 15 μm. The shape of the channels was varied by changing the amplitude (A) of the cosine function. Starting from the left of the figure, the value of A for the first channel was 5 μm, the next two were 6 μm and the following 2 were 6.5 μm. The last two patterns consisted of staggered lines of 6 μm holes. It is clear from the results that complex microchannel geometries can be faithfully reproduced from the mask onto the zeolite-silicon composite substrate using the new fabrication technique. The pattern shown in figure 4.8b simulates a complex channel network that can exist in a microfluidic device. The figure shows a central distribution hub from which a network of microchannels radiates. Abrupt changes in channel width and direction were also incorporated to further test the precision of the new fabrication technique. The narrowest channel had a width of 3 μm and height of 10 μm, giving the channel an aspect ratio of about 3. There was no serious degradation in the microfabricated patterns (cf. figure 4.8a and 4.8b) even after prolonged exposure to harsh thermal conditions. Although microchannels narrower than 30 μm are rarely used in microchemical and microfluidic devices, the ability to fabricate high-resolution features is useful for incorporating microfabricated zeolite catalysts within microreactor channels.
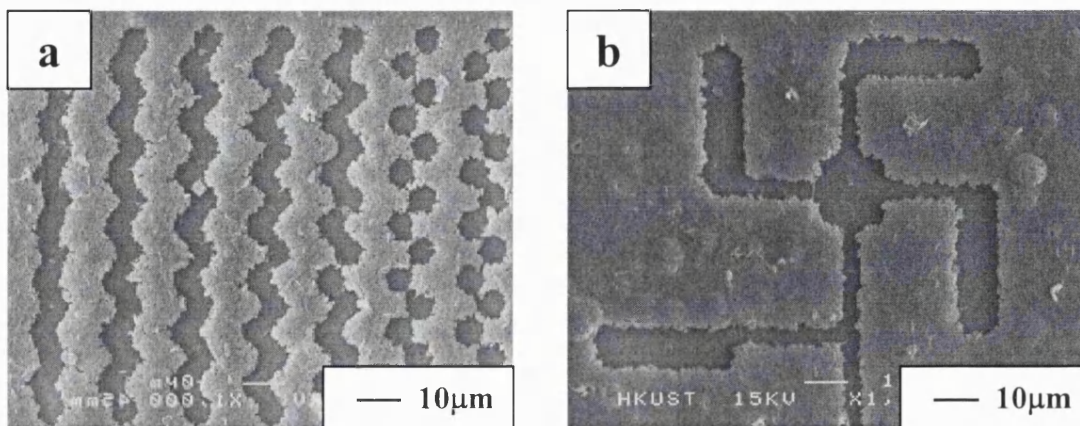
Figure 4.8   **Examples of zeolite micropattern (a) microchannels and (b) fluid distribution hub**

Zeolite micropatterns

The microstructure of the catalyst coating could be engineered during the synthesis to introduce surface roughness and create intercrystalline porosity to promote fluid mixing and enhance mass transfer. Access to the zeolite can also be manipulated by changing the zeolite orientation (cf. figure 4.7). The zeolite deposited within the microchannels can be further micropatterned to create regular array of microfabricated catalysts with exact size, geometry and spacing. Figure 4.9 shows an example of a microfabricated zeolite grid. Each zeolitic line forming the 8 x 16 μm rectangular grids was 5 μm wide and 10 μm high. The zeolite grid was stable during thermal treatment, and the occasional breaks in the zeolite lines were created during the etching process. Unlike a fixed bed catalytic reactor, a microfabricated catalyst laid out in a regular pattern can be easier to simulate. Thus, an optimum catalyst array can be pre-designed to the specifications demanded by the application. Complex

catalyst arrays can be fabricated with features as small as 3 μm using the new technique. Further improvement in the fabrication procedure is underway to reach the target size of 1.25 μm, which is the current limit for photolithography. Electron beam lithography can create submicron features of about 0.1 μm (Madou, 1997), but the process is expensive and time consuming.
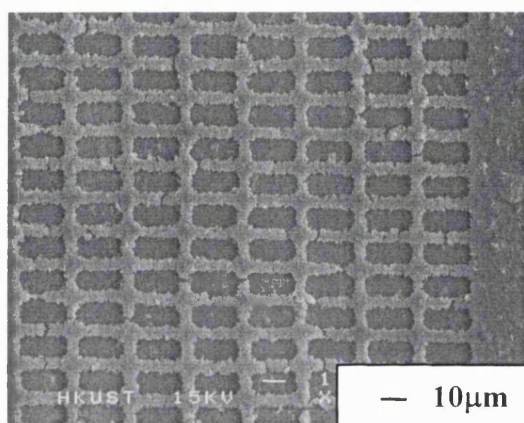
Figure 4.9   Example of a microfabricated zeolite grid

4.3.3   Incorporation of zeolites in microchemical devices

Zeolite-based microreactors

A variety of designs for microreactors have been suggested so far, but in all cases the microchannel is the central structural element in the reactor architecture. The T-shaped microreactor used by Srinivasan et al. (1997) is a simple yet elegant design. Based on a T-mixer, it allows in-situ mixing of reactant streams (at a T-junction) before entering the reactor channel. Hsing et al. (2000) have conducted both mathematical modelling and reaction experiments on the T-shaped microreactor,

clearly demonstrating the effectiveness of the reactor design for many partial oxidation reactions. Figure 4.10a displays a T-shaped microchannel etched onto a layer of (101)-oriented zeolite film supported on seeded silicon. The width of the reactor microchannel was 500 μm and its length was 20 mm. The height of the channel is defined by the thickness of the zeolite film that forms the walls of the channel. Zeolite films with less than a micron to more than 100 μm thick can be prepared by varying the synthesis parameters. A portion of the microchannel is magnified in figure 4.10b and 4.10c. From the figure, it is clear that the bottom of the microchannel is zeolite-free and the catalysis can take place mainly on the zeolite walls. Besides its role as a catalyst, the zeolite also functions as the main structural material for the microreactor. One possible drawback in this reactor design is molecular diffusion into the bulk of the zeolite. This can pose a problem in various cases, such as in reaction rate determination. However, most molecules diffuse slowly in zeolite and for pentene and hexene, it will require a residence time greater than an hour to result in a 0.001 % reactant loss in this type of microreactor design. A variation of the T-shaped microreactor design is shown in figure 4.10d. The main purpose of the serpentine structure is to provide longer residence time to accommodate reactions with slow kinetics.
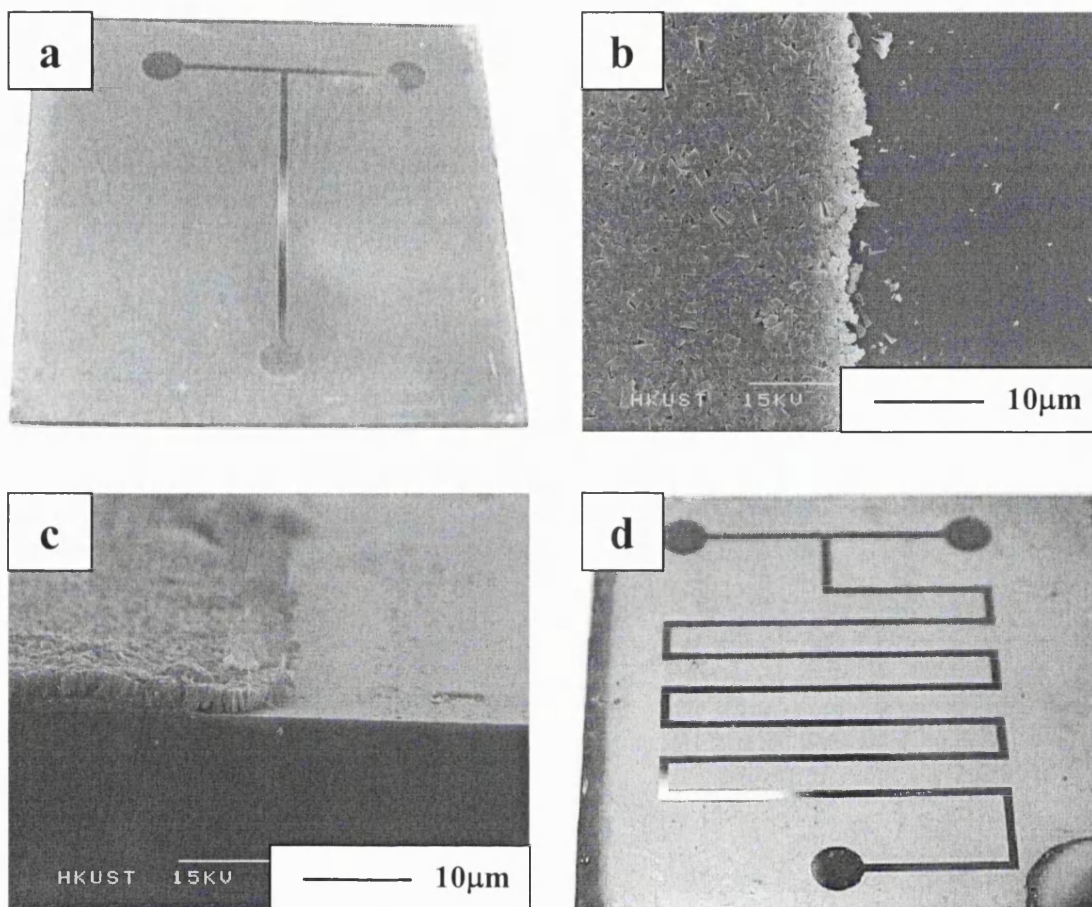
Figure 4.10 **(a) T-shaped microchannel etched onto 1 (101)-oriented Sil-1-silicon composite, (b) magnified of the zeolite microchannel, (c) cross-sectional view of the zeolite microchannel and (d) an example of serpentine-shape zeolite-based microreactor**

Zeolite Micromembranes

Zeolite with its uniform nanometer-sized pores and molecular sieving properties are ideal material for micromembranes. An zeolite membrane microseparator can serve many separation functions envisaged in a micro-analytical

laboratory and miniature plant, from sample purification to product isolation. Figure 4.11a displays a simple design for a miniature membrane contactor. The zeolite membrane between the two microchannels (figure 4.11b) allows the selective exchange of components between two passing streams of liquid or gas. Using Sil-1 zeolite as the membrane barrier, hydrophobic compounds can be transferred across the membrane from an aqueous to an organic solution (Wu et al., 1998). Molecular sieving separation of isomers and close-boiling compounds has been demonstrated in a Sil-1 membrane (Funke et al., 1996a and 1996b). A similar separation performance is expected in a zeolite membrane microseparator. Unlike other chemical engineering unit operations, membrane scale down is straightforward and beneficial. It reduces the risks of failure in brittle inorganic membranes such as zeolites.
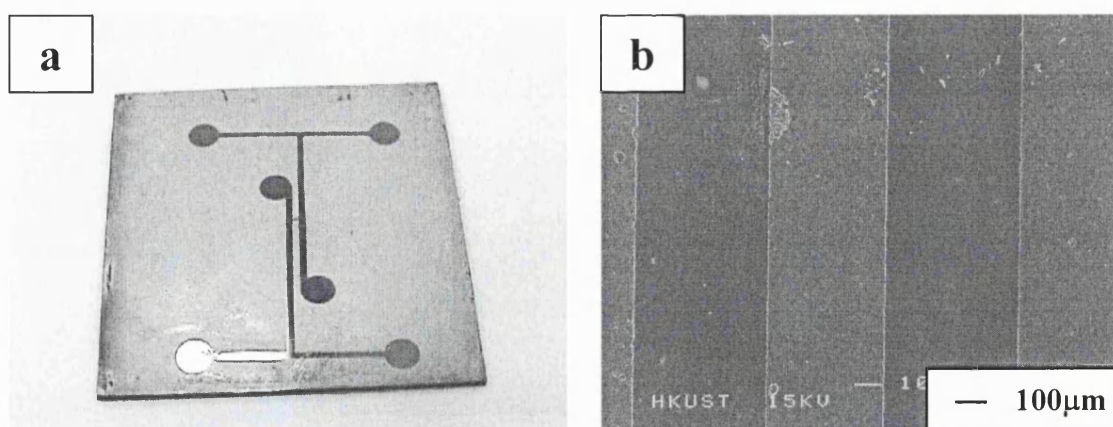
Figure 4.11   **(a) An I-shaped pattern fabricated onto Sil-1-silicon composite and (b) magnified view of the membrane layer between the two microchannel**

4.4   Concluding remarks

A new fabrication procedure for incorporating zeolite catalysts, membranes and structural materials within the architecture of microchemical devices was developed based on microelectronic fabrication and zeolite thin film technologies. The ability to engineer and tailor the zeolite structure is essential for the incorporated zeolites to effectively perform its various tasks. Zeolite films with preferred orientation and engineered microstructure were successfully grown on a silicon substrate. Direct manipulation of the film microstructure (i.e., thickness, orientation etc.) was achieved by controlling the seed population, synthesis composition and hydrothermal treatment conditions. High-resolution micropatterns of complex microchannel networks and geometry, as well as particle arrays as small as 3 μm, were successfully fabricated from zeolite. These zeolite patterns survived prolonged thermal treatment under harsh conditions (i.e., temperature oscillations between 303 to 873 K) demonstrating their excellent thermal stability. Design blueprints for the incorporation of zeolites in microreactors and membrane microseparators were illustrated. Working models were built using the new fabrication technique, and the structural details of the microsystem architecture were examined. Studies are now underway to test the performance of the zeolite-based microchemical devices for chemical reactions and separations.

Chapter 5

Design and fabrication of zeolite-based microreactors

and membrane microseparators

5.1   Introduction

Microtechnology researchers envisage that desktop miniature factories and micro-pharmacies can be developed through the advances in the fabrication of micromixers, reactors and separators (Kawahara et al., 1997). Microreactors have the advantages of better energy and material utilization, and result in more efficient chemical production and less pollution. The large surface area-to-volume ratio that can be attained in a microreactor enhances heat and mass transfer rates (Drost et al., 1997). Higher chemical conversions were also obtained from such devices (Hardt et al., 2000). In addition, the integration of microsensors and actuators enables rapid and precise control of the reactor operation (Srinivasan et al., 1997). Other advantages include simpler process optimization (Jensen, 2001), rapid design implementation (Ehrfeld et al., 2000), easier scale-up through replication and better safety (Lerou and Ng, 1996; Jensen, 1999). At the same time, separation processes can benefit from the large surface area-to-volume ratio obtained in a microseparator. Chemical engineering separation processes, such as extraction and membrane separation have been successfully miniaturized (TeGrotenhuis et al., 1999; Turner et al., 2000a, 2000b).

In microreactors, an important task is to incorporate an active catalyst within the microchannels. Metal catalysts (e.g., Pd, Pt, Ag) can be coated as a thin layer using sputter coating, thermal deposition or chemical vapour deposition (Thomas and Thomas, 1997; Kursawe and Hönicke, 2000). An alternative method is to form a porous oxide layer by anodization, and impregnate it with a solution of the metal precursor (Wießmeier

and Hönicke., 1996a and 1996b). However, deposition of zeolites requires a different strategy. Zeolite films can be grown directly on microstructured supports by *in-situ* synthesis. Free-standing silicalite-1 membranes have been grown onto silicon microchannels (den Exter et al., 1997). ZSM-5 zeolite has also been grown on machined stainless steel microchannels for selective catalytic reduction of NO with ammonia (Rebrov et al., 2001).

Zeolites are important catalysts in many chemical and petrochemical processes, such as production of fuels, pollution abatement and more recently, clean fine chemicals production (Hölderich and van Bekkum, 1991; Maxwell and Stork, 1991; van Bekkum et al., 1994; Armor, 1999). The aluminum containing MFI zeolite, Al-ZSM-5 is an important catalyst for many hydrogenation, disproportionation, isomerization and alkylation reactions (Maxwell and Stork, 1991; Jacobs and Martens, 1991). It finds uses in petroleum refining, petrochemical production and more recently, it is being considered as an alternative catalyst for synthesis of fine chemicals (Feast and Lercher, 1996; van Bekkum, 1998). Metal-exchanged ZSM-5 zeolites such as Cu-ZSM-5 are potential environmental catalysts since they exhibit high activity for NOx reduction (Amiridis et al., 1996). TS-1 zeolite is known to be an efficient catalyst for selective oxidation of alcohols (Maspero and Romano, 1994), epoxidation of alkenes (Clerici et al., 1991) and hydroxylation of aromatics (van der Pol et al., 1992)

Zeolites with their molecular sieving properties (Jansen et al., 1994; Coronas and Santamaria, 1999a) and tunable pore structure (Yan and Bein, 1995) are strong

143

candidates for membrane separation in miniature devices. Separation efficiency can be increased by the large surface area-to-volume ratio that can be achieved in such microsystems. High permselectivity has been observed in separation of azeotropic mixtures (Sano et al., 1994), permanent gases (Kusakabe et al., 1998), close-boiling hydrocarbon compounds (Funke et al., 1996a) and isomers (Funke et al., 1996b; Xomeritakis et al., 1999) using zeolite membranes. The zeolite pores can host different ions, atoms, molecules and clusters that can be used to modify its structural, chemical, catalytic, separation, electronic and optical properties. Zeolite membranes can also be utilized in membrane reactors. Their excellent permselectivity and molecular sieving properties can benefit many reaction systems that are constrained by unfavorable thermodynamics. Membrane reactors can exhibit better yield and higher selectivity than fixed bed reactors (Armor, 1989; Hsieh, 1991; Zaman and Chakma, 1994; Saracoo and Specchia, 1994). The ability of a membrane reactor to control the addition and mixing of reactants and the selective removal of products result in better material utilization, less waste and pollution, and safer operation. Other application includes miniature electrochemical cells and sensors. In this case, zeolite films can act as membrane barriers for creating microcompartments for storage of chemicals, catalysts and enzymes.

This chapter is to investigate the different designs and fabrication strategies for zeolite catalytic microreactors and membrane microseparators. MFI-type zeolites including silicalite-1 (Sil-1), aluminum ZSM-5 and titanium silicalite-1 (TS-1) were incorporated into the microreactor design as a structural material, catalyst or membrane. The microstructure of these zeolites was manipulated in terms of thickness, orientation

and intergrowth. These zeolite-based microdevices have potential applications as catalytic reactors, separators, molecular filters, sensors, membrane reactors and electrochemical cells.

5.2   Experimental

5.2.1   Microchannel design and fabrication

A T-shaped design pattern was chosen for the microchannel reactor and separator. The design is similar to that reported by Srinivasan et al. (1997). It consists of two inlets and a single outlet that can be connected to reactant sources and analyzer, respectively, through the round docking pads. This reactor design has the advantage of independent control and monitoring of the reactant and product streams. It also provides in situ mixing of reactants, thus avoiding some of the hazards associated with a premixed feed. The mixing efficiency of the T-junction depends on flow rates, nature of the reactant molecules and channel aspect ratio (width/height). This means that the mixing length can vary depending on reaction and operating conditions, but it is generally small (Gobby et al., 2001).

The schematic diagram shown in figure 5.1 displays the dimensions of the reactor pattern etched onto a chromium mask. Patterns with three different channel widths of 200, 500 and 1000 μm were prepared. The microchannels were fabricated using a standard photolithography technique onto silicon wafer (Madou, 1997). The details of the

145

fabrication procedure are described in chapter 3.3. The anisotropic etching rates along the silicon <111> and <100> directions result in a trapezoidal channel cross-section with an angle of 54.7° (figure 5.2a-d). The depth of the microchannels used for zeolite growth was 250 μm (figure 5.2b). The wafers containing the etched microreactor patterns were then cleaned thoroughly to remove dirt and contaminants from the surface. The wafers were sonified for 15 min each, in ethanol and deionized distilled water. They were blown dry to remove excess water from rinsing, dried in an oven at 333 K for overnight, and stored in a container for later use.
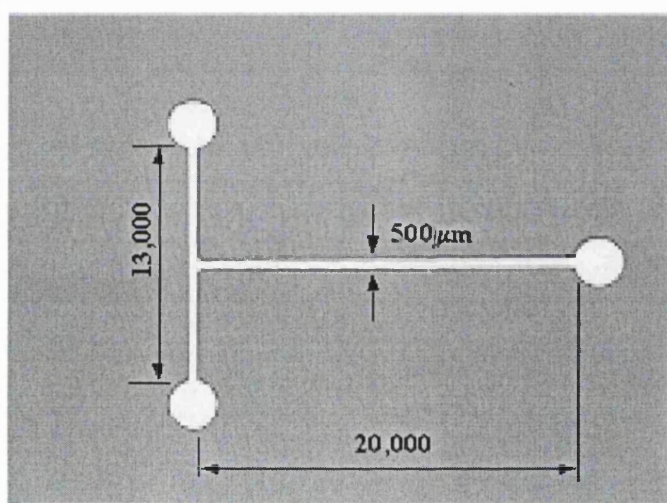
Figure 5.1 A magnified picture of the T-shaped pattern on a chromium glass mask used in lithography process with the dimensions in μm.
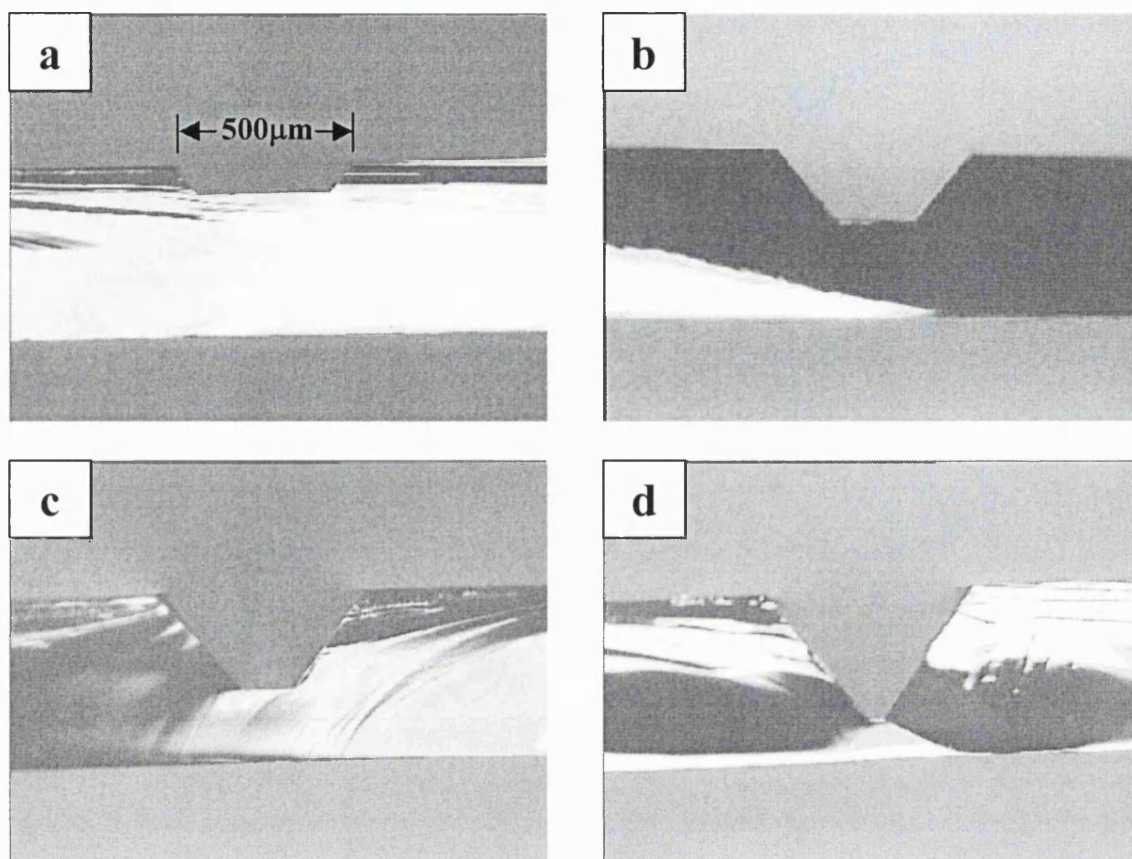
Figure 5.2   **Cross-sectional views of the T-reactor channel after wet etching for**

(a) 4 h, (b) 6 h, (c) 8 h and (d) 10 h in 30 wt.% KOH solution at 353 K

5.2.2   Zeolite synthesis

Preparation of zeolite seeds and powders

The colloidal Sil-1 seeds were prepared from a synthesis mixture containing 15 g of fumed silica, 0.85 g of sodium hydroxide, and 60 ml of 1 M tetrapropyl ammonium hydroxide (TPAOH) solution. The details are described in chapter 4.2.1. The transmission electron micrograph in figure 5.3a shows that the Sil-1 seeds have a spherical shape and an average particle size of 120 nm. X-ray diffraction analysis

indicates that the colloidal zeolites are crystalline and have a MFI type structure (figure 5.3). The zeolite has a BET surface area of 420 m^2/g as measured by N_2 physisorption (Coulter, SA3100).
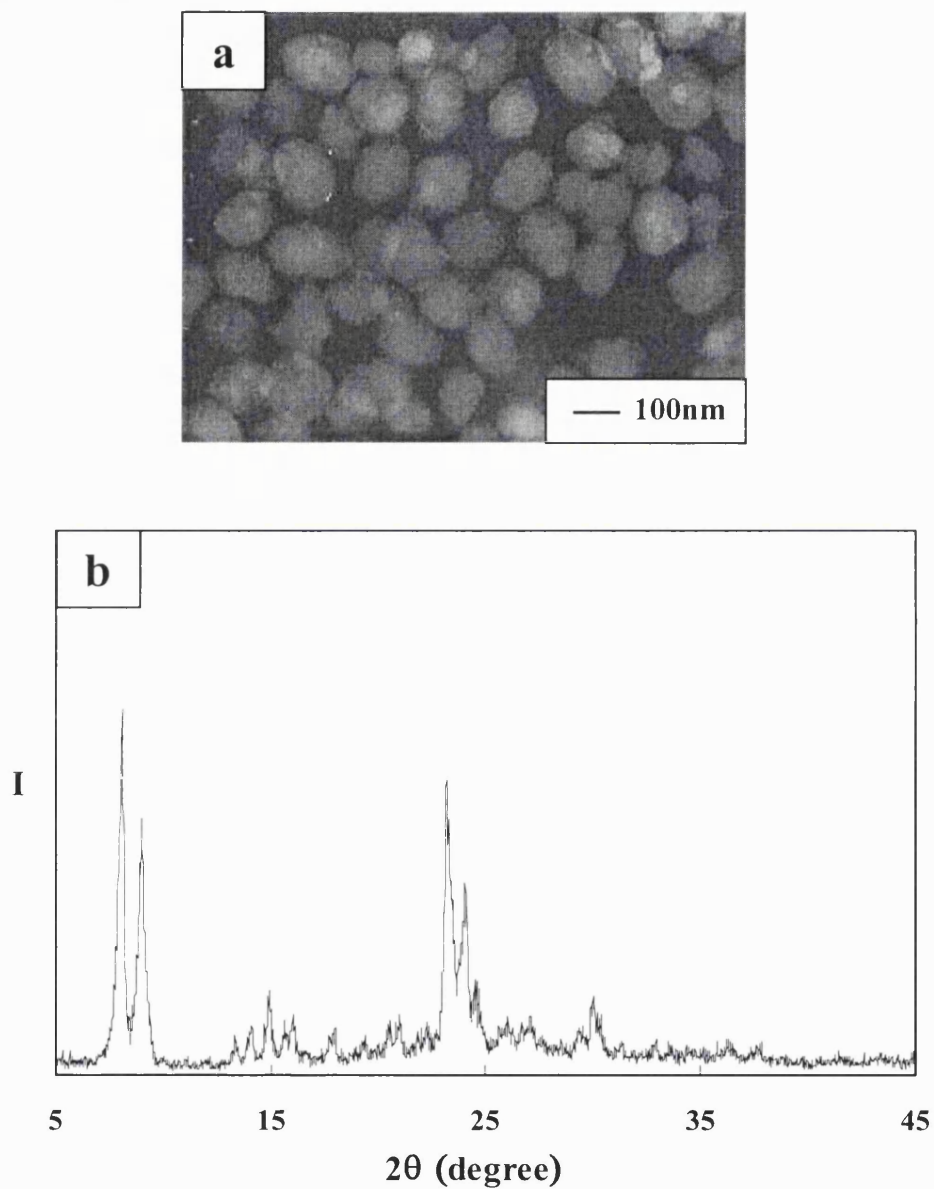
Figure 5.3   **(a) Transmission electron micrograph and**

                        (b) X-ray diffraction pattern of colloidal Sil-1 zeolite

A similar preparation procedure was used for making colloidal Al-ZSM-5 and TS-1 zeolite seeds. The synthesis solution for colloidal Al-ZSM-5 contained $10SiO_2$: $0.2AlOOH$: $2.4TPAOH$: $1NaOH$: $110H_2O$. The 120 nm Al-ZSM-5 zeolites (XPS Si/Al = 18, BET surface area = 400 m^2/g) were obtained after 8 h of hydrothermal treatment at 398 K. The 120 nm TS-1 was prepared from a solution with the composition of $20TEOS$: $0.75TEOT$: $9TPAOH$: $404H_2O$. Chemical analyses using EDXS, XPS and micro-Raman indicated that the colloidal TS-1 has a spatially uniform Si/Ti content of 20, with most of the Ti ions incorporated within the zeolite framework. The BET surface area of the TS-1 seeds (425 m^2/g) is comparable to that of Sil-1 and Al-ZSM-5. The Sil-1, Al-ZSM-5, TS-1 seeds were stored as 2 wt.% colloidal suspension in ethanol.

NaZSM-5 powder was used for zeolite incorporation within the reactor microchannel. It was prepared by pre-seeding a synthesis solution containing $40SiO_2$:$0.8AlOOH$: $0.4NaOH$: $10TPAOH$: $20,000H_2O$ with 20 mg of colloidal zeolite seeds. After hydrothermal treatment at 398 K and 48 h, NaZSM-5 powders with a uniform crystal size of 0.5 μm and a Si/Al ratio of 16 (i.e., XPS analysis) were obtained.

5.2.3   Fabrication of zeolite-based microreactors

Four methods were examined for preparing zeolite-based microreactors. The first three methods were based on incorporating zeolites onto prefabricated microchannels

(figure 5.4a-c), while in Method 4, the microchannel was fabricated onto a zeolite-silicon composite wafer (figure 5.4d).

Method 1   Zeolite powder coating

The zeolite powder coating method simply deposits the zeolite powder onto the microreactor channel (figure 5.4a). The zeolite was suspended in liquid and introduced into the microreactor channel using a micropipette. A light sonification ensures that the channel is evenly filled with zeolite slurry. The microreactor was subsequently dried at 333 K and calcined in air at 823 K. The amount of zeolite added was determined from the weight gain measured after the calcination. The desired zeolite loading was obtained by repeated coating with the zeolite slurry.

Method 2   Uniform zeolite film growth

Uniform zeolite film growth has been obtained by den Exter et al. (1997) and Schoeman et al. (1997) on plain and seeded silicon wafers, respectively. Figure 5.4b illustrates the procedure used for zeolite growth onto prestructured silicon wafer. The zeolite was grown onto the silicon wafer by immersing it in zeolite synthesis solution, either immediately after the fabrication of the microreactor pattern or following pre-

a

Apply zeolite powder

Final Product

b

With or without seeding

Hydrothermal synthesis

Final Product

c

Confined seeding

Final Product

d

Zeolite-silicon composite

UV

Photolithography

Zeolite etching

Final Product

Silicon

Mask

Zeolite

Photoresist
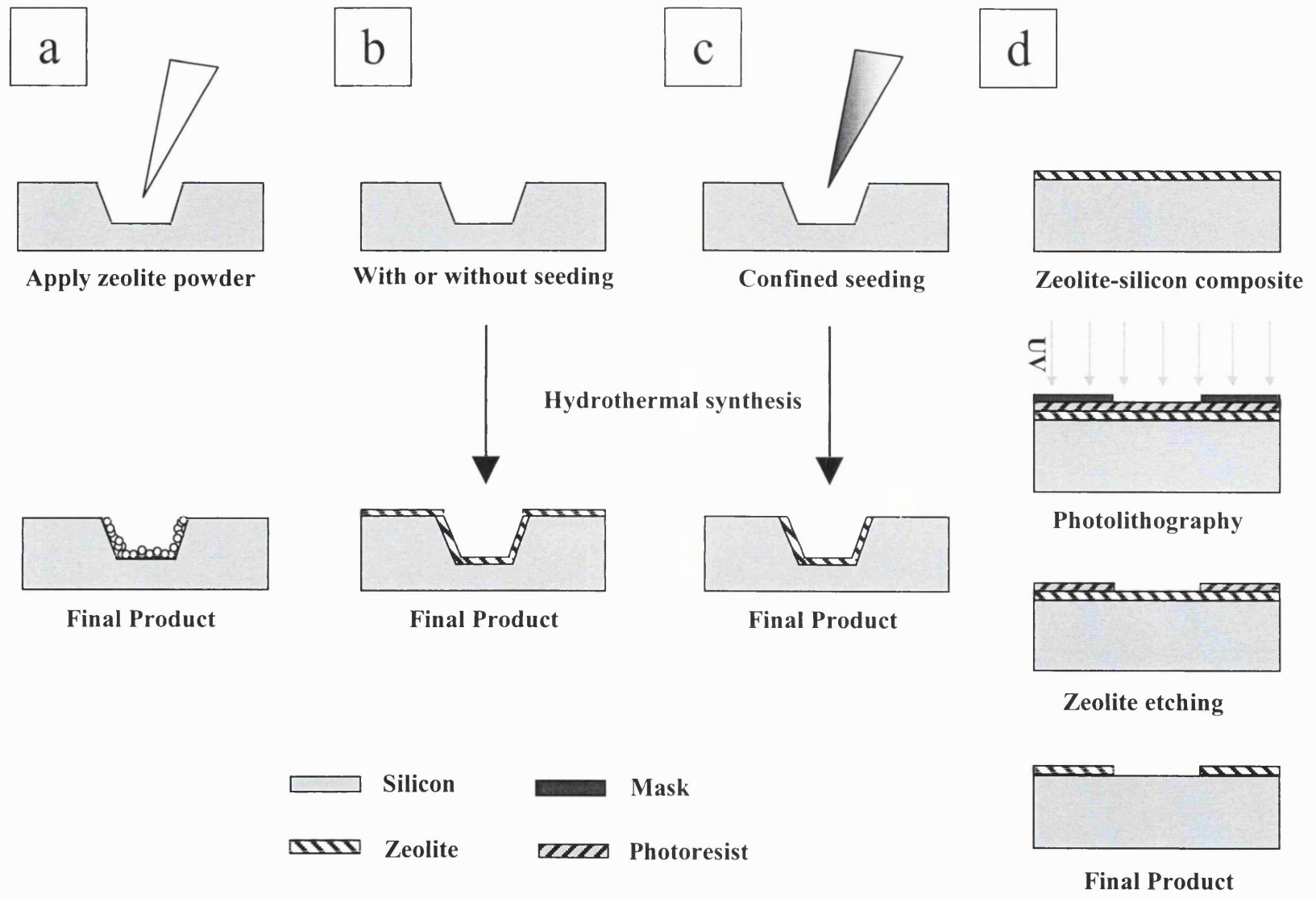
Figure 5.4   **Process diagram for zeolite incorporation using (a) Method 1, (b) Method 2, (c) Method 3 and (d) Method 4**

seeding with colloidal zeolites. The latter entailed functionalization of the silicon wafer with mercapto-3-propyltrimethoxysilane (50 mM in ethanol), followed by immersion in colloidal suspension of zeolite seeds and finally drying at 333 K. The seeding procedure was repeated three times to obtain the desired seed population of (5×10^{13} seeds/m^2). The seeds were then calcined in air at 823 K for 6 h, prior to the hydrothermal growth of the zeolite layer.

Sil-1 film was grown from solution with the composition of 40TEOS: 10TPAOH: 20,000H_2O prepared by adding 1.65 ml of tetraethyl orthosilicate (TEOS) drop-by-drop to 70.4 ml of 0.027 M TPAOH solution. The mixture was stirred at room temperature for 24 h to produce a clear and homogeneous solution. Aluminum, titanium and other metal ions can be added to impart the zeolite with the desired catalytic activity. The wafer containing the etched microreactor pattern was then placed in a Teflon holder such that the pattern was facing downwards. This was to prevent powders and precipitates from being incorporated into the growing zeolite film. The wafer can also be placed vertically in the Teflon holder. The sample and solution were transferred into a 125 ml Teflon vessel and sealed within a stainless steel sleeve. The autoclave was placed in a preheated oven (T = 398 K) and allowed to react for 24 h. At this temperature, the solution generates an autogenous pressure of about 230 kPa. It was ensured that the liquid level was always more than 5 mm above the sample surface. After the hydrothermal treatment, the reaction was quenched to room temperature, and the silicon sample was rinsed with deionized distilled water and dried overnight at an oven temperature of 333 K.

Method 3 Localized zeolite growth

Localized zeolite growth was achieved through selective seeding. In order to confine zeolite growth only within the microchannel, the microchannel was first functionalized with mercapto-3-propyltrimethoxysilane and then seeded with colloidal zeolite using a micropipette (figure 5.4c). In some experiments, the microchannel was seeded more than once to obtain the desired seed population. The wafer was calcined in air at 823 K for 6 h. Sil-1 was then grown in the microchannel following the same hydrothermal synthesis procedure described in Method 2. Al-ZSM-5 and TS-1 zeolites were also deposited within the microchannel. For the former, colloidal Al-ZSM-5 was used for seeding the microchannel and the Al- ZSM-5 layer was grown from a hydrothermal synthesis solution containing 40TEOS: 4AlOOH: 10TPAOH: 4NaOH: $20,000H_2O$ at a temperature of 398 K and for 24 h. TS-1 zeolite was grown within the confines of the microchannel by preseeding with colloidal TS-1 followed by hydrothermal treatment in a solution with a composition of 40TEOS: 1.6TEOT: 10TPAOH: 10,000H2O at 448 K and 24 h.

Method 4 Etching of zeolite-silicon composite

Etching of zeolite-silicon composite wafer is an alternative method for fabricating zeolite-based microreactors. A uniform layer of zeolite film was first grown onto a 4-in. diameter silicon wafer using hydrothermal synthesis method. 1-20 μm thick MFI-type zeolite films with (101) and (200) orientations had been prepared. The details of their synthesis were discussed in chapter 4. In this study, a 5 μm thick, highly oriented (101) Sil-1 on silicon composite wafer was used as the substrate material for the T-

microreactor. A 3 μm layer of HPR-207 photoresist was coated onto the 4-in. composite

wafer, and the T-reactor pattern was transferred onto the wafer using standard

photolithography (figure 5.4d). The reactor channel was then etched by BOE solution

(1HF:6NH$_4$F, Olin) and the remaining photoresist was stripped using acetone (Lab-scan).

5.2.4   Fabrication of zeolite membrane microseparators

The membrane microseparator consists of a T-shaped channel on the front and a

rectangular recess at the back. The fabrication procedure used is illustrated in figure 5.5.

Using standard microfabrication technology, the T-microchannel and the rectangular

recess were etched onto the silicon wafer (figure 5.5, steps A-E). The etching rate and

time were used to control the depths of the microchannel and the recess. Etching was

allowed to continue until less than 50 μm of silicon separates the microchannel and the

recess. The Sil-1 membrane was then deposited onto the microchannel (figure 5.5, steps F

and G) following seeding with colloidal Sil-1 and hydrothermal treatment in a synthesis

solution containing 40TEOS: 10TPAOH: 20,000H$_2$O. The remaining 50 μm thick silicon

was then etched using TMAOH solution to expose the zeolite membrane.

T-reactor pattern transfer at the frontside

A

Membrane pattern mask

B

UV

Front

Back

C

D

Etch Si_3N_4

E

Etch Si in KOH

F

Zeolite growth at the front

G

Etch Si in TMAOH

Silicon   Mask Si_3N_4

Zeolite   Photoresist   Teflon Tape
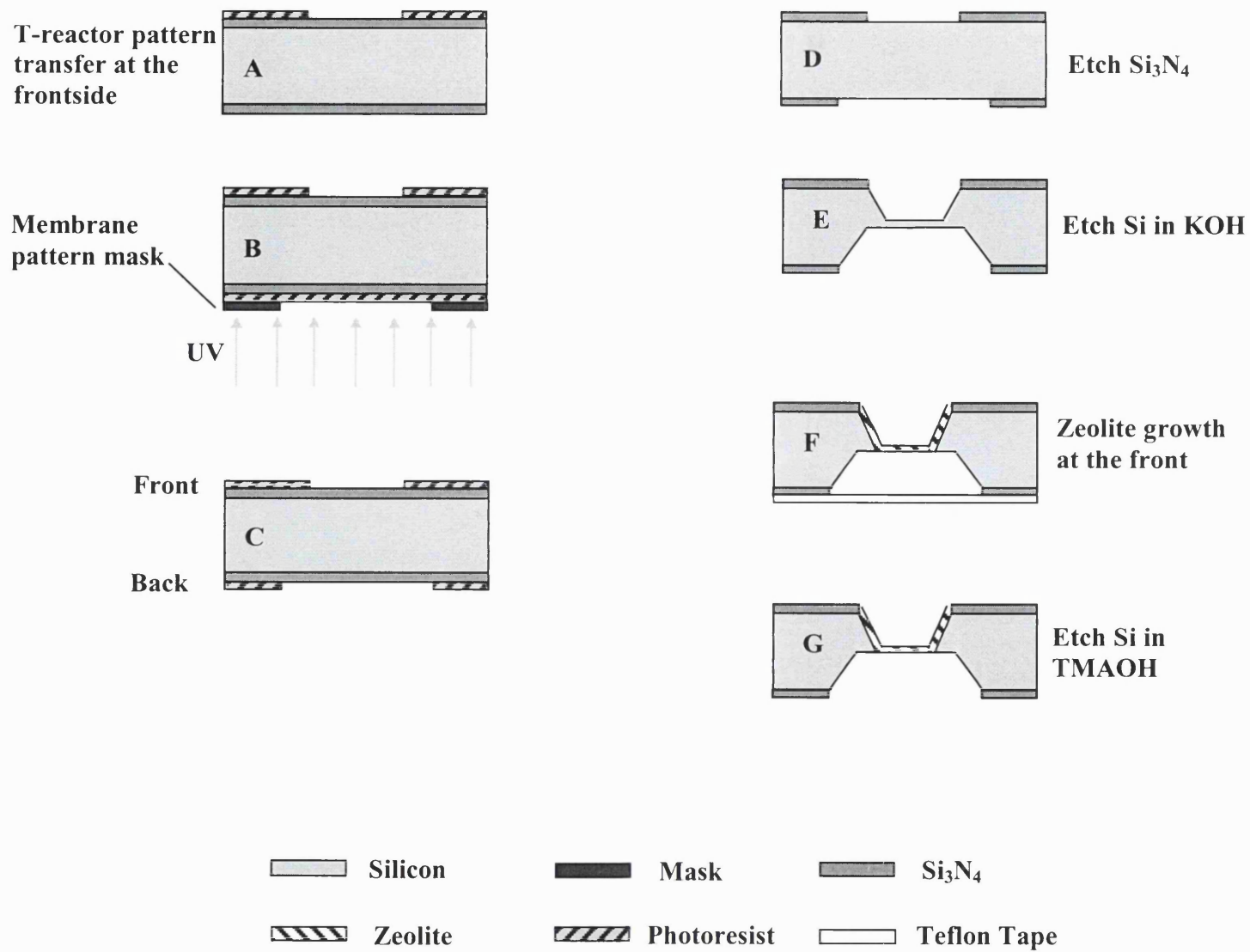
Figure 5.5   Process diagram for the fabrication of zeolite membrane microseparator

5.2.5 Characterization

The fabricated units were analyzed by optical microscopy (Olympus BH-2) and scanning electron microscopy (SEM, JEOL JSM 6300) before and after the incorporation of the zeolites. The optical microscope was used mainly for quality control at each stage of the fabrication. The SEM was employed to determine the exact shape and dimensions of the microchannels, and to measure the thickness of the zeolite layer deposited onto the channel. The zeolite crystal size, shape and intergrowth were also determined from analysis of the SEM micrographs. The structure, crystallinity and orientation of the deposited zeolites were analyzed by an X-ray diffractometer (XRD, Philips PW 1030). Bulk and surface compositions of the incorporated zeolites were examined by energy dispersive X-ray spectroscopy (EDXS, Philips PW 1830) and X-ray photoelectron spectroscopy (XPS, Physical Electronics PHI 5600).

5.2.6 Materials

Potassium hydroxide (85%, BDH Lab.), tetramethylammonium hydroxide (25% Moses Lake Ind.) and phosphoric acid (85%, Olin) were used to wet-etch the miniature reactor and membrane patterns onto the silicon wafer and to strip the protective silicon nitride layer. Ethanol (99.9%, Fisher) was used in degreasing and cleaning the wafer at various stages of the device fabrication and zeolite incorporation. Mercapto-3-propyltrimethoxysilane (99%, Aldrich) was employed in grafting the zeolite seeds onto the microchannels. For the zeolite synthesis, the chemicals used were fumed silica (0.01

μm, 99.8%, Aldrich), TEOS (98%, Aldrich), alumina sol (Vista), tetraethyl orthotitanate (95%, MERCK-Schuchardt), TPAOH (1 M, Aldrich), triethoxymethylsilane (TEMS) (99%, Aldrich) and sodium hydroxide (98%, BDH). After hydrothermal synthesis, the Teflon containers and sample holders were cleaned using 1 M NaOH solution under hydrothermal conditions at 423 K overnight. These accessories were then carefully rinsed in distilled water. This cleaning procedure was necessary to remove zeolite particles that may have formed on the walls of the containers and holders.

5.3   Results and discussion

The main goal of this chapter is to illustrate different strategies for incorporating zeolites as catalyst, membrane or structural material into the architecture of miniature chemical devices such as microreactor and microseparator.

5.3.1   Zeolite-based microreactors

<u>Method 1   Zeolite powder coating</u>

Zeolite powder can be incorporated directly onto the prefabricated microreactor channel using Method 1. Figure 5.6a shows a microchannel coated with monodispersed NaZSM-5 crystals (0.5 ± 005 μm) grown from seeded synthesis solution. The zeolite crystals uniformly coated the surface of the microchannel forming a zeolite layer 7 ± 1.2 μm thick and a loading of 0.3 mg (figure 5.6b).

This technique is relatively simple and straightforward, and can be easily used to incorporate other types of catalyst in addition to zeolites. The zeolite loading can be controlled by changing the concentration of zeolite in the slurry and through repeated coating of the microchannel. However, the powder adhesion was poor and the zeolites were easily removed. Using chemical grafting and polymer adhesives can significantly improve powder adhesion, but they can also interfere with the function of the catalyst and the operation of the reactor. An alternative method is to grow the zeolite layer onto the microchannel using the other methods described in this chapter (i.e., Methods 2 and 3).
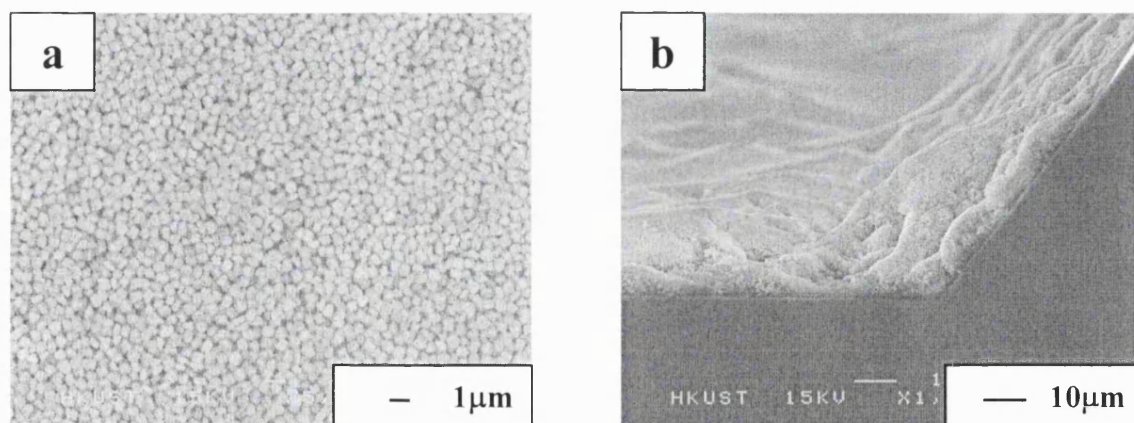
Figure 5.6 **Scanning electron micrographs of NaZSM-5 zeolite powders deposited onto the T-reactor microchannel using Method 1**

Method 2   Uniform zeolite film growth

In this method, a uniform zeolite film was grown onto the etched T-microreactor pattern as shown in figure 5.7a. The figure shows that the MFI zeolite film uniformly covers the wafer (figure 5.7b), including the etched microchannel (figure 5.7c). The film

was made of well-intergrown zeolite crystals that were oriented with their <101> crystallographic axis perpendicular to the silicon surface. From the channel cross-section, the zeolite film was measured to be about 3 μm thick along the wafer surface but was slightly thinner (2.5 μm) at the floor of the channel (figure 5.7d). This indicates that mass transfer resistance is present during the zeolite growth, or a different nucleation/growth mechanism may be dominant on the wafer surface and the microchannel floor. Figure 5.7d inset shows that the film is smooth with a surface roughness (peak-to-valley) less than 0.3 μm.

Method 2 may present some difficulty in reactor sealing if smooth surfaces are required, as in the case of thermal and anodic bonding (Madou, 1997). Although adhesives and cements may be employed for sealing, they can introduce other complication such as low thermal resistance, contamination and incompatibility with reactants.
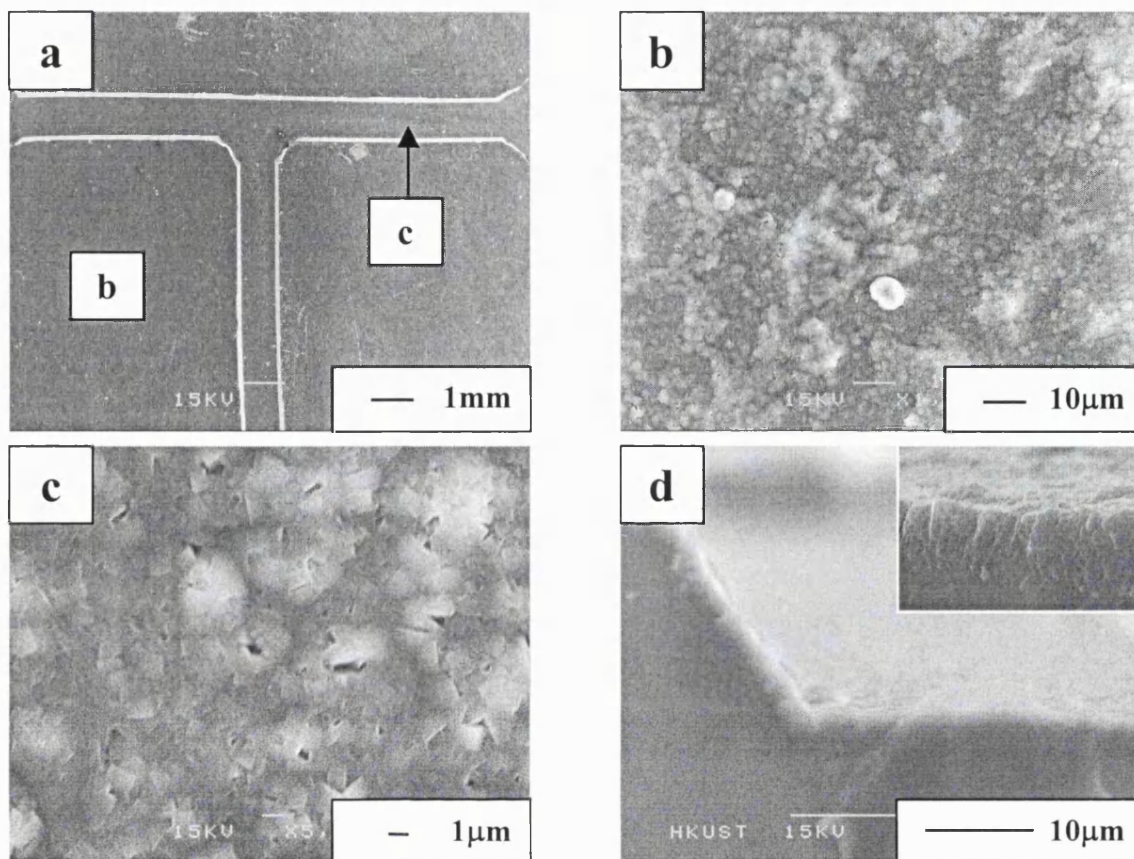
Figure 5.7   (a) Scanning electron micrograph of the zeolite-based miniature T-reactor prepared by Method 2 (b) Top-view of a well oriented (101) zeolite film grown on the surface of the silicon wafer (c) Top-view of the well-oriented (101) zeolite film grown within the reactor microchannel (d) A cross-sectional view of the well-oriented (101) zeolite film within the reactor microchannel (The figure inset is at 2× higher magnification.)

Method 3   Localized zeolite growth

Method 3 differs from Method 2 in that the zeolite is incorporated only within the confines of the microchannel. This was achieved through surface modification using

chemical functionalization and seeding to locally promote the growth of the zeolite layer. A zeolite-based T-microreactor prepared by Method 3 is shown in figure 5.8a. Figure 5.8b and 5.8c show that the zeolite growth is confined within the microchannel and that the Sil-1 film is well-intergrown and uniform along the length of the channel (figure 5.8c). Outside the microchannel, a few zeolite crystals (one zeolite per 100 μm^2) precipitated from the solution decorates the surface of the wafer (figure 5.8b).
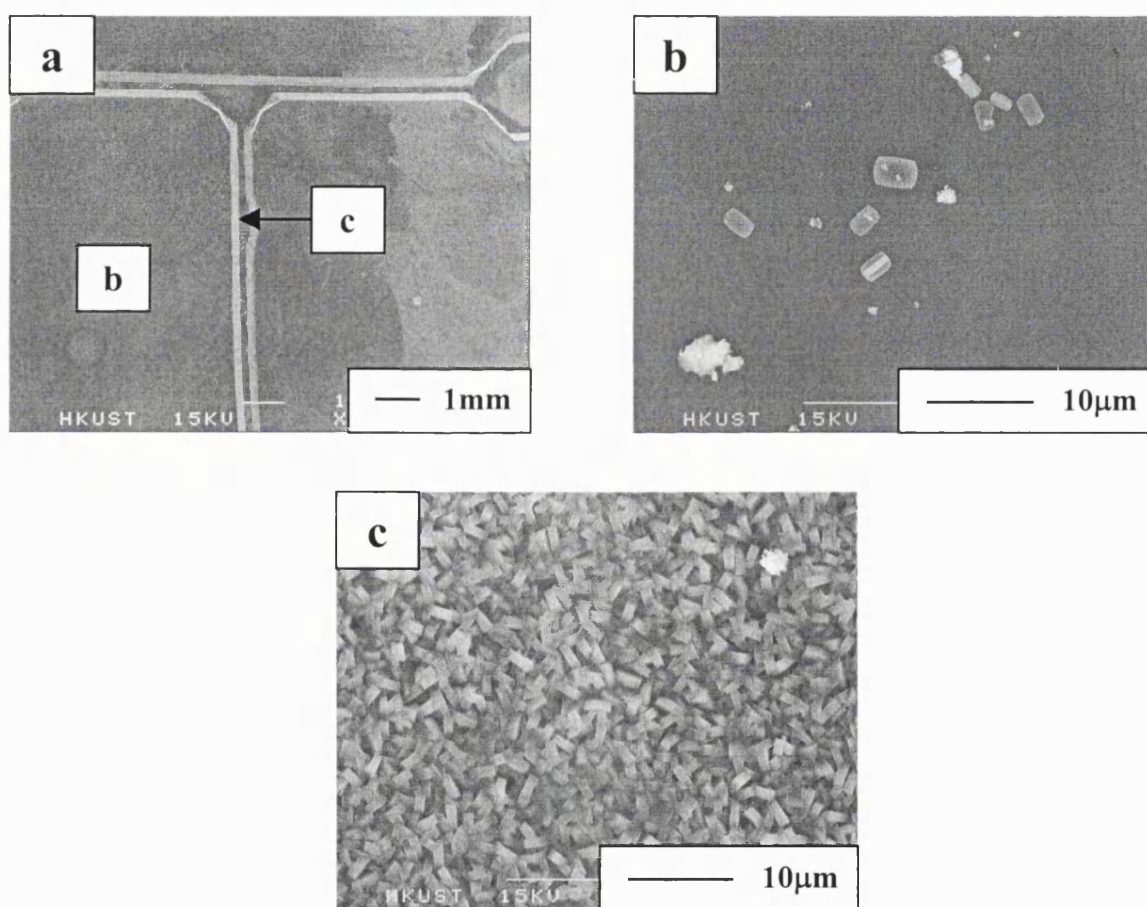
Figure 5.8   **(a) Scanning electron micrograph of the zeolite-based miniature T-reactor prepared by Method 3 (b) Image of the wafer surface outside of the T-reactor channel (c) Microstructure of the zeolite layer grown within the confines of the microchannel**

Figure 5.9a displays a T-microreactor (1000 µm) with a deposited layer of ZSM-5

catalyst within its channel. The intergrown zeolite film (figure 5.9b) was 4.7 µm thick

which gave a catalyst loading of about 0.5 mg. From XPS analysis, the Si/Al ratio of the

deposited zeolite catalyst was determined to be 27. The ZSM-5 can be readily

transformed into a protonated HZSM-5 acid catalyst using well-established treatment

procedure (Biscardi and Iglesia, 1998). Method 3 was also used to prepare the TS-1

zeolite microreactor shown in figure 5.9c and d. In this case, the TS-1 zeolites were

grown on a 500 µm T-microreactor (figure 5.9c). Using isomorphous substitution of

titanium ions into the MFI zeolite framework (Taramasso et al., 1983; Tuel et al., 1990),

a Si/Ti ratio of 17 was obtained for the zeolite film shown in figure 5.9d. The film is well

intergrown but exhibits a smaller crystal size than the ZSM-5.
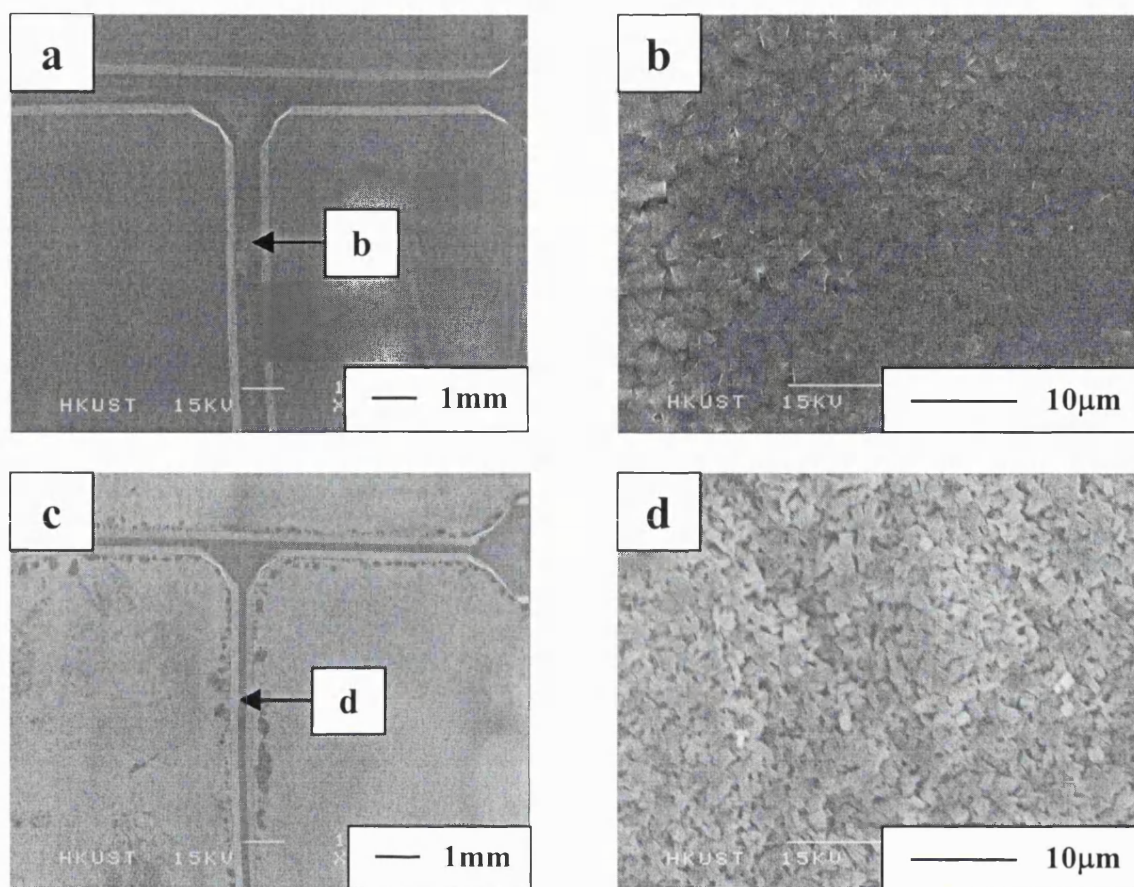
Figure 5.9   SEM images of the zeolite-based microreactor and zeolite catalyst

layer prepared by Method 3 (a) and (b) Al-ZSM-5 with Si/Al ratio of

27 (c) and (d) TS-1 with Si/Ti ratio of 17

Method 4   Etching of zeolite-silicon composite wafer

In Method 4, the T-reactor pattern was etched onto a highly oriented (101) zeolite film grown onto 4-in. silicon wafer (figure 5.10a). This zeolite-silicon composite wafer was obtained by seeding the wafer five times with colloidal zeolites followed by 48 h hydrothermal synthesis at 398 K in a solution containing 40TEOS: 10TPAOH: 20,000H_2O. A clean pattern was obtained (figure 5.10a and 5.10b) where the 5 μm thick interlocking Sil-1 crystals form the wall that defines the reactor channel (figure 5.10c). The good precision that can be attained using this method is apparent in figure 5.10b. The channel was etched all the way through the zeolite layer to expose the silicon underneath which forms the floor of the channel (figure 5.10d). There are several advantages in using this fabrication methodology. Microfabricated catalysts can also be realized using this method. Here, the shape, morphology, quantity and individual locations of the zeolite catalysts can be precisely engineered to optimize the microreactor performance. Miniature electrochemical cells and sensors, in which membrane barriers are an integral part of the design, can also be made using this procedure. The details are illustrated in chapter 4.
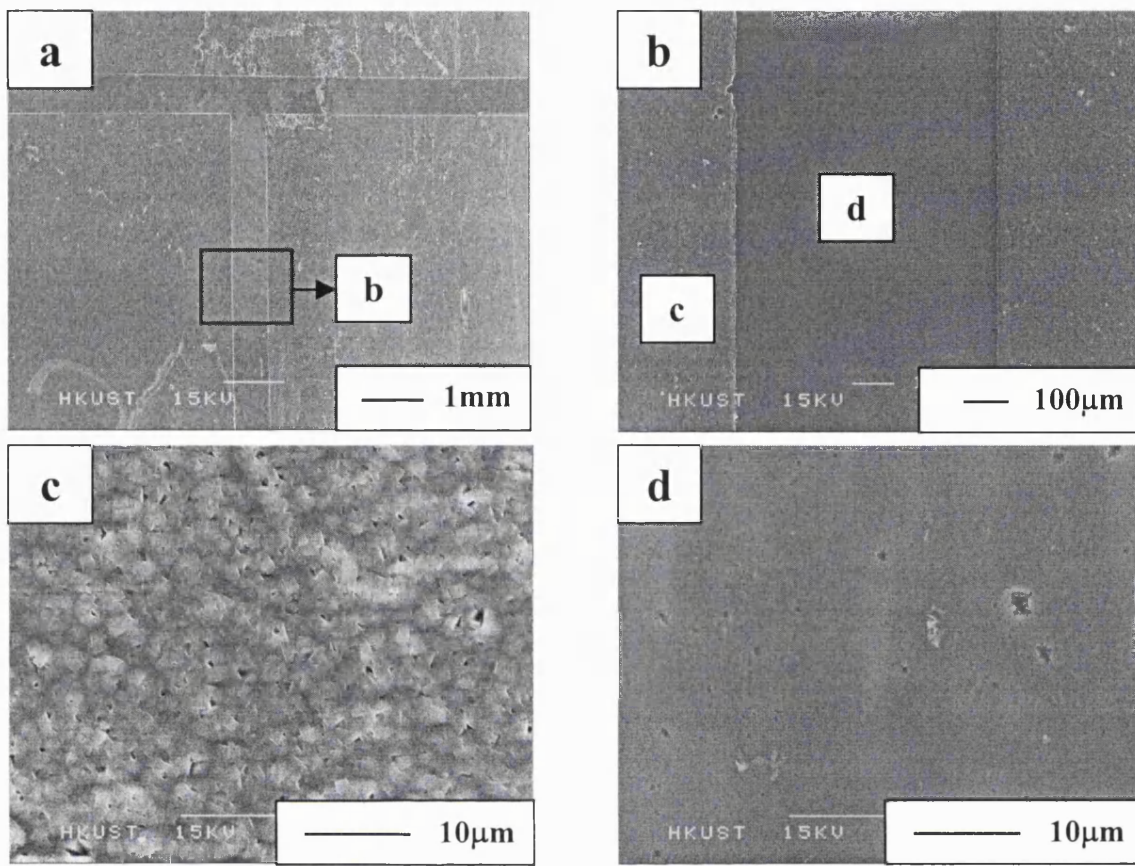
Figure 5.10 (a) Scanning electron micrograph of the zeolite-based miniature T-reactor prepared by Method 4 (b) Top-view of the reactor microchannel etched through the zeolite film layer (c) Microstructure of the deposited zeolite film layer that made up the wall of the reactor channel (d) Microstructure of the etched silicon wafer, which formed the base of the microchannel

5.3.2 Zeolite membrane microseparator

For commercial application, a large membrane area is usually needed to provide the required separation or production throughput. However, the scale-up of zeolite

membranes is difficult. Made of inorganic crystals, the zeolite membrane accumulates stress during thermal treatment and high-temperature operations that can lead to mechanical failure. The mechanical stress increases in proportion to the membrane area, making large membranes more susceptible to cracks and defects. Using miniaturization technology developed for microchemical devices, one can achieve membrane scale-up through replication while maintaining the individual membrane area small to prevent stress related failure. In addition, the large surface area-to-volume ratio that can be obtained in these microsystems is expected to enhance the membrane separation performance.

Following the procedure described earlier in the experimental section (figure 5.5), zeolite membrane microseparator was fabricated. The free-standing zeolite membrane was deposited on the microchannel (figure 5.11). The picture shown in figure 5.11a was taken with a light shining from the back of the fabricated pattern. The free-standing membrane is easily distinguished by its lighter color. Figure 5.11b is a higher magnification image of the deposited zeolite membrane. It is clear from the figure that the zeolite growth was confined within the microreactor channel. The 16μm thick zeolite film was uniformly deposited along the length and width of the microchannel. A portion of this film formed the free-standing zeolite membrane as shown in figure 5.11a. SEM characterization showed that the film was made of intergrown Sil-1 crystals that have an average size of about 7 μm (figure 5.11c). An image of the recess etched onto the back of the silicon wafer is shown in figure 5.11d. The zeolite membrane is clearly evident in the

figure. It has dimensions of 0.7 × 4.8 mm² as defined by the width of the microchannel and the length of the recess.
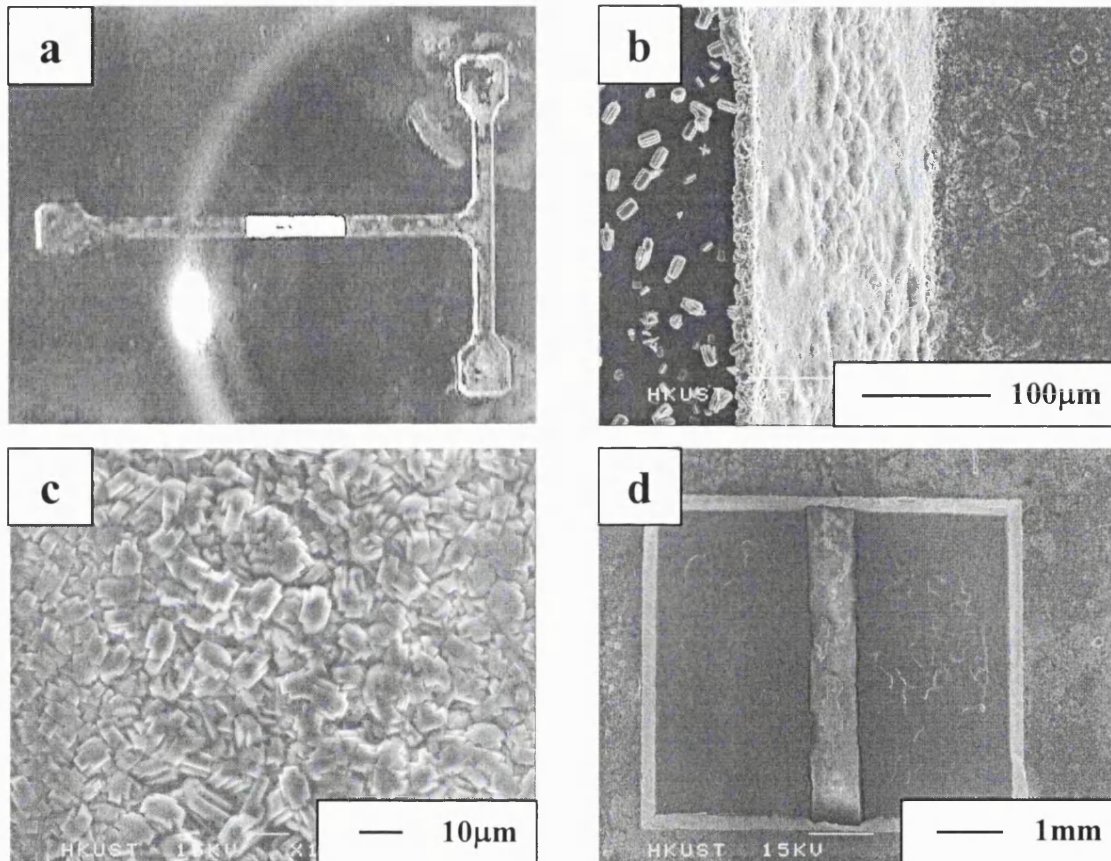
Figure 5.11 (a) A SEM picture of the T-microchannel coated with a layer of Sil-1 membrane (the light rectangular area is the free-standing zeolite membrane) (b) A higher magnification image showing that the zeolite membrane was confined within the microchannel (c) A higher magnification image of the zeolite membrane grown within the T-reactor channel (d) A picture of the recess fabricated at the back of wafer with the exposed zeolite membrane

5.4   Concluding remarks

The ability to engineer the zeolite film microstructure and tailor its chemical and catalytic properties is important for the successful incorporation of zeolites as catalyst, membrane or structural materials in microchemical devices that include microreactors and microseparators. Different fabrication strategies were adopted to incorporate zeolites as powder catalysts (Method 1) or film within the reactor microchannel (Method 3). Alternatively, a uniform zeolite film was deposited onto a prefabricated silicon wafer (Method 2) or plain silicon to form a zeolite-silicon composite onto which the reactor pattern was etched using traditional semiconductor fabrication techniques (Method 4). Using these methods, Sil-1, ZSM-5 and TS-1 zeolites were successfully integrated into microreactors either as catalyst or part of the reactor's architecture. A zeolite membrane microseparator was made using this new fabrication technology. The zeolite membrane layer was deposited within a T-microchannel. This design promises many potential applications as membrane devices, membrane microreactors, electrochemical cells and sensors. Studies are now underway to test the performance of zeolite catalytic microreactors and membrane microseparators for chemical reactions and separations.

Chapter 6

1-Pentene Epoxidation in Titanium Silicalite-1

Microchannel Reactor:

Experiments and Modelling

6.1   Introduction

There is a growing interest in the use of zeolite and molecular sieve materials as active components of miniature chemical devices such as chemical sensors, microreactors, microseparators and lab-on-a-Chip devices. Zeolite catalysts have been used in microreactors for catalytic reduction of NO with ammonia (Rebrov et al., 2001), alkene epoxidation (Wan et al., 2002) and Knoevenagel condensation of benzaldehyde and ethyl cyanoacetate (Lai et al., 2003). Zeolite micromembranes exhibit excellent permselectivity for gases and hydrocarbon vapors (Chau et al., 2003a). Zeolite micromembranes display excellent proton flux while selectively rejecting methanol, making it an attractive material for the construction of a micro fuel cell device (Chau et al., 2002a). Robertson (2001) employed zeolite adsorbents in a miniature column for gas separation. Further studies of zeolite as structural material in microsystem architecture have been reported (Wan et al., 2001, Chau et al., 2002b, Chau et al., 2003b, Chau and Yeung 2002).

Zeolites can be deposited and grown on silicon and glass substrates by hydrothermal synthesis method. Jansen and Rosmalen (1993) were among the first to describe the growth of continuous zeolite film on silicon wafer. Schoeman et al. (1997) reported an improved method to synthesize ultra-thin silicalite-1 films on a silicon wafer. den Exter and coworkers (1997) prepared a freestanding silicalite-1 (Sil-1) membrane from the deposited Sil-1 film by selective etching of the silicon

substrate. It was demonstrated that Sil-1 films of different orientations and surface morphologies can be grown on silicon by controlled seeding (Hedlund et al., 1999; Lai et al. 2002). This method afforded a convenient way for manipulating the deposited zeolite film microstructure. Several strategies for incorporating zeolites in chemical microsystems have been described in chapter 5.

Microreactors are becoming a crucial component in lab-on-a-chip microdevices (Greenway et al., 2000, Jakeway et al., 2000; Jensen, 2001, Mitchell et al., 2001). Well-defined flow characteristics, rapid transport properties, high precision, spatial and temporal control over temperature, mixing and residence time provide ideal conditions for studying reaction mechanisms and kinetics (Gavriilidis et al., 2002). Microreactors can be operated under conditions that cannot be easily attained in a conventional reactor system, providing much-needed kinetic information in these operating regions (Wörz et al., 2001). Computational modelling and simulation are important tools for the design of microreactor systems (Quiram et al., 2000). Microfluidic calculations provide invaluable information on fluid flow, component mixing and mechanical friction and stress that are important in designing the architectural blueprint of the microreactor (Commenge et al., 2002). Detailed simulation and modelling studies conducted by various researchers have provided important insights to the reaction behaviour in the microsystem environment (Hsing et al., 2000; Rebrov et al., 2002).

Titanium silicalite-1 (TS-1) prepared by isomorphous substitution of titanium ions into the MFI zeolite framework, is an excellent selective oxidation catalyst (Notari, 1996; Clerici et al., 1991, 1993). TS-1 can catalyse many reactions including the conversion of alkenes to epoxides (Clerici and Ingallina, 1993; Langhendries et al., 1999; Schmidt et al., 2000), alcohols to aldehydes (Maspero and Romano, 1994), alkanes to secondary alcohols and ketones (Ingallina et al., 1995), phenol to hydroquinone and catechol (Atoguchi and Yao, 2001) and amines to hydroxylamines (Gontier and Tuel, 1994) using hydrogen peroxide under mild reaction conditions. Such catalyzed processes are environmentally friendly, as the oxidant, aqueous hydrogen peroxide will turn into water whereas the reactions show very high product yields and selectivity.

Exothermic oxidation reactions can benefit from the use of microreactors due to their excellent heat transfer properties. Deubel et al. (2000) has reported that olefin epoxidation is a highly exothermic process (e.g. bond dissociation energy of C_2H_2 is $-5.2kcal/mol$). By confining the explosive and hazardous chemicals within small units, the risk of dealing with strong oxidizing agent like hydrogen peroxide can be minimized.

In this chapter, a detailed study of titanium silicalite-1 microreactor for 1-pentene epoxidation was performed. A novel procedure for the fabrication of a TS-1 microreactor was described where the TS-1 catalysts were confined within the microchannel only. The influence of zeolite structure and chemistry for TS-1 catalysts

was studied by varying the synthesis conditions. A simple reactor model for predicting the behaviour of 1-pentene epoxidation in a titanium silicalite-1 (TS-1)-coated, single-channel microreactor was also presented. The kinetic data for the model were obtained from a separate batch experiment, while the transport data were taken from literature. The influence of reactor geometry, catalyst properties and reaction conditions were evaluated and the results compared with experimental data. It was found that crystal size and titanium incorporation into the zeolite framework exerted a great effect on the catalyst performance. The information provided by the model suggests several ways of improving microreactor performance. Catalyst reactivity was investigated over time to examine catalyst deactivation observed in TS-1.

6.2   Experimental

6.2.1   Zeolite catalyst incorporation in microchannel reactor

The reaction occurs along a 20 mm long catalyst-coated channel. Microreactors with a channel width of 500 μm were prepared by anisotropic etching using KOH solution (30wt%). Precise and localized addition of zeolite materials was obtained using the techniques of chapter 3.4.1. Zeolite growth was confined within the wall of the main channel by selective seeding with TS-1 zeolite nanocrystals. This was accomplished by grafting mercapto-3-propyltrimethoxysilane onto the freshly etched microchannel to provide better adhesion for zeolite seeds. A colloidal

suspension of zeolite nanocrystals was then added, depositing a layer of seeds onto the functionalized surface of the microchannel. The seeded sample was dried in oven at 333 K overnight before calcining in air at 923 K for 6 h.

The colloidal TS-1 seeds were prepared from a clear synthesis solution containing 20 tetraethyl orthosilicate (TEOS): 0.75 tetraethyl orthotitanate (TEOT): 9 tetrapropylammonium hydroxide (TPAOH): 404 H_2O (mole ratio) at 398 K for 50 h. The zeolite seeds were recovered by a series of washing and separation steps to obtain a stable, 2 wt.% colloidal suspension in ethanol. X-ray diffraction confirms that the seeds were MFI-type, TS-1 zeolite. An average particle size of 100nm was determined by scanning electron microscopy (SEM, JEOL JSM 6300). Chemical analyses by X-ray photoelectron spectroscopy (XPS, Physical Electronics PHI 5600), energy dispersive X-ray spectroscopy (EDXS, Oxford Instruments) and micro-Raman (Renishaw 3000) indicated that the colloidal TS-1 has a spatially uniform Si/Ti content of 20, with most of the titanium atoms incorporated within the zeolite framework. A BET surface area of 425 m^2/g was measured by N_2 physisorption (Coulter, SA3100).

The calcination step removed the organic template molecule (i.e., TPA^+) from the deposited TS-1 seeds. It also sintered the seeds into a stable layer and improved their adhesion on the channel wall. A layer of TS-1 catalyst was grown onto the seeded channel from a hydrothermal synthesis solution containing silicon and titanium precursors, as well as the TPA^+ organic template. The synthesis composition

174

was adjusted to control the microstructure and titanium content of the catalyst layer. Triethoxymethylsilane (TEMS) was added to provide an independent control over the zeolite grain size and intergrowth. Synthesis mixtures with composition of 40 TEOS: 1.6 TEOT: 10-14 TPAOH: 0-0.4 TEMS: 10,000 H_2O were found to be optimal in terms of titanium incorporation, crystal size and crystal intergrowth (Table 6.1). The sample and the solution were placed in a Teflon vessel and sealed within a stainless steel autoclave. The synthesis was conducted in an oven at 448 K for 24 h. The TS-1 catalyst was calcined in air at 823 K for 24h to remove the organic template molecules from the zeolite pores.

Sample	Mole Ratio					Time	Temperature	Seeding
	TEOS	TPAOH	TEOT	TEMS	H_2O	(h)	(K)	
1	40	10	1.6	0	10000	24	448	unseeded
2	40	10	1.6	0	10000	24	448	3 times
3	40	14	1.6	0	10000	24	448	3 times
4	40	14	1.6	0.2	10000	24	448	3 times
5	40	14	1.6	0.4	10000	24	448	3 times

Table 6.1   Synthesis conditions for TS-1 catalysts

The microchannel reactors were inspected by optical microscopy (Olympus BH-2) after each fabrication step to ensure high quality standards. The dimensions of the microchannel (i.e., width and depth), the uniformity and precision of the zeolite incorporation, the thickness and microstructure of the catalyst layer as well as its elemental composition were determined by a scanning electron microscope (SEM,

JEOL JSM 6300) equipped with an energy dispersive X-ray spectrometer (EDXS, Philips PW 1830). The structure, crystallinity and orientation of the deposited zeolites were analyzed by an X-ray diffractometer (XRD, Philips PW 1030). The titanium content was examined by X-ray photoelectron spectroscopy (XPS, Physical Electronics PHI 5600) before and after the reaction.

6.2.2   1-pentene epoxidation reaction

Batch reactor

The kinetics of 1-pentene epoxidation reaction were determined using a batch reactor. The catalyst was TS-1 zeolite grown onto a seeded silicon wafer prepared following the synthesis procedure described previously. The 5μm-thick TS-1 film contained 2.5 at.% titanium and consisted of intergrown 2μm zeolite crystals. The wafer was crushed into 5μm powder and added to the reaction mixture containing 3g of 1-pentene and 1 ml of hydrogen peroxide dissolved in 50ml of methanol. This gives an initial 1-pentene and hydrogen peroxide concentration of 1.49M (i.e., 1490 molm^{-3}) and 0.33M (i.e., 330molm^{-3}), respectively. 1g of methyl tert-butyl ether (MTBE) was added as internal standard. The reaction was conducted under well-mixed and isothermal conditions using a mechanical stirrer and a constant temperature water bath (298 K). Samples were taken using a syringe at fixed time intervals for analysis. 1ml of sample was used for iodometric titration to determine hydrogen peroxide concentration and the rest was analyzed by gas chromatography

(HP 6890) to obtain the concentration of the hydrocarbons in the sample. The gas chromatograph was equipped with a 30 m PoraPLOT Q column (Chrompack) and a flame ionization detector. Three GC measurements were made for each sample and the concentration of the reactants and products were determined using a calibration curve prepared from standard solutions (chapter 3.7.1).

TS-1 coated microreactor

A clean Pyrex glass cover was bonded onto the zeolite microreactor to complete the reactor assembly. A positive resist (SU-8) was coated onto the glass cover to serve as an adhesion layer. A leak-free seal was obtained after UV-exposure. Tests showed that the seal was able to withstand hydrocarbon solvents (i.e., methanol, MTBE and 1-pentene) and reaction temperatures of up to 373 K. Pre-drilled holes on the glass cover served as inlets and outlets for reactants and products. The microreactor experiments were conducted using a reaction mixture containing 0.9 M 1-pentene and 0.2 M hydrogen peroxide in methanol/water (volume ratio 50/1). The reaction temperature was kept at 298 K by a temperature-controlled water bath. A syringe pump (kdScientific) delivered the reactants to the microreactor at a constant rate (i.e., 30-120 μl/h) and the product mixture was collected from the outlet using a sample vial cooled in acetone ice. The vials were replaced at fixed intervals. 1 microliter of the reaction solution was injected in a gas chromatograph (HP 6890) equipped with a Poraplot Q column (30 m, Chrompack) and a flame ionisation detector. Three GC measurements were made for each sample and the concentration of the reactants and products were determined using a calibration curve prepared from

standard solutions containing known quantities of reactant (1-pentene), product (1,2-epoxypentane) and internal standard (tert-butyl methyl ether, MTBE).

Catalyst deactivation was investigated by measuring the reaction conversion as a function of time. A 500 μm-wide, microchannel reactor coated with 5μm thick, TS-1 zeolite film (Si/Ti = 30- ∞, 2-4μm crystal grain) was selected for the study. The reaction was conducted at a temperature of 298 K and residence time (τ) of 100s. Samples were collected and analyzed at fixed time interval during the entire 5 hours experiment. Post-reaction analysis of the catalyst was conducted using XPS, thermogravimetric and differential thermal analyses (TGA/DTA, Setaram 92-18) to determine possible causes of deactivation. Catalyst reactivation was conducted at 823K in air. Weakly adsorbed molecules were desorbed at low temperature, while strongly adsorbed organics were removed by oxidation at high temperature. Analyses with XPS were performed after catalyst reactivation.

6.2.3   Materials

Chemicals used for zeolite synthesis include TEOS (98%, Aldrich), TEOT (95%, MERCK-Schuchardt), TPAOH (1 M, Aldrich), TEMS (99%, Aldrich). Mercapto-3-propyltrimethoxysilane (99%) employed for seeding was purchased from Aldrich Chemicals. After hydrothermal synthesis, the Teflon containers and sample holders were cleaned using 1 M HNO_3 (69%, BDH) solution under hydrothermal conditions at 423 K overnight. They were then carefully rinsed in distilled water.

For microreaction experiments, the chemicals used were 1-pentene (99%, Aldrich), hydrogen peroxide (30 wt %, BDH), tert-butyl methyl ether (MTBE, 99.8% Fluka) and methanol (99.8%, Fluka).

6.3   Microreactor Model

A simple two-dimensional axis-symmetrical reactor model was employed to predict the reactant and product concentration profiles within the TS-1 coated microreactor. The model assumes isothermal, steady state operating condition. Equations 6.1 & 6.2 are the differential material balance equations for the bulk fluid in the channel and across the catalyst layer, respectively.

$$U_y \frac{\partial C}{\partial y} = \frac{1}{x}\frac{\partial}{\partial x} x\left(D \frac{\partial C}{\partial x} \right) \qquad 6.1$$

$$\frac{1}{x}\frac{\partial}{\partial x} x\left(D_{eff(int er)} \frac{\partial C}{\partial x} \right) + r = 0 \qquad 6.2$$

$$r = -k_2 \left[H_2 O_2 \right]\left[C_5 \right]$$

where C is the concentration of hydrogen peroxide (molm^{-3}), D is the diffusivity of the bulk fluid in the channel (m^{2}s^{-1}), $D_{eff(inter)}$ is the inter effective diffusivity in the catalyst layer (m^{2}s^{-1}), y is the dimension along the length of the channel (m), x is the radial dimension of the channel, r is the rate of disappearance of hydrogen peroxide

per unit area of catalytic surface (mols^{-1}m^{-2}) and U_y is the fluid velocity along the y

axis (ms^{-1}).

The transport mechanisms are considered to be convection along the flow

direction and diffusion along the traverse directions. The inter-particle diffusion,

$D_{eff(inter)}$ was calculated to be 8×10^{-11} m^{2}s^{-1} based on the bulk diffusitivity taking into

account crystal porosity, constriction factor and tortuosity (Wakao and Kaguei, 1982;

Fogler, 1992). The fluid enters the microreactor from a channel of similar width. It

has uniform concentration and fully developed flow where the velocity profile is

invariant along the flow. The parabolic flow is described by the Hagen-Poiseuille

equation:

$$where \quad U_y = 2U_m \left(1 - x^2 \right) \qquad\qquad 6.3$$

where U_y is the velocity along the y axis (ms^{-1}), U_m is the mean velocity (ms^{-1}), x is

the radial coordinate (m). In the model, the trapezoidal channel was approximated by

a cylindrical channel having the same surface to volume ratio. The external perimeter

of the catalyst layer is 785 μm and for the trapezoidal cross-section is 759 μm. It was

also assumed that the fluid is incompressible, that its properties remain unchanged

during the reaction and the pressure drop along the channel is negligible (Ajmera et

al., 2001).

180

The partial differential equations (Eqns. 6.1 & 6.2) were integrated along the y-axis to calculate the hydrogen peroxide concentration profile in the microreactor. The concentrations profiles of 1-pentene and 1,2-epoxypentane were calculated from the mass balance. The governing equations were solved using Femlab^{TM}. The dimensionless model equations used in the Femlab model are listed in table 6.2. For the computation, the microchannel was partitioned into approximately 8000 finite element cells using an adaptive mesh. The mesh is smaller and denser at the proximity of the catalyst layer where the reaction takes place in order to ensure a more accurate calculation of the concentration profile along the microchannel. The model is a useful and convenient tool for studying the effects of reactor geometry, catalyst properties and reaction conditions on the microreactor performance. Comparisons with experimental data provide an assessment of its predictive capacity. The experimental and model values of microreactor parameters are shown in table 6.3.

Dimensionless model equations	Dimensionless co-ordinates
Mass balance	**for asymmetric model**
Subdomain 1 (bulk channel)	Radial for channel: $x' = \dfrac{x}{R}$
$u(x)Pe\dfrac{R}{l}\dfrac{\partial c}{\partial y'} = \dfrac{1}{x'}\dfrac{\partial}{\partial x'}x'\dfrac{\partial c}{\partial x'}$	Reactor length: $y' = \dfrac{y}{l}$
where $Pe = \dfrac{U_m R}{D_{bulk}}$	**Dimensionless concentration**
Subdomain 2 (catalyst layer)	$c = \dfrac{[H_2O_2]}{[H_2O_2]_0}$
$\dfrac{1}{x'}\dfrac{\partial}{\partial x'}x'\dfrac{\partial c}{\partial x'} + r'' = 0$	**Fully developed velocity**
For second order reaction with respect to	**profile**
hydrogen peroxide and 1-pentene,	$u(x) = 2(1 - x'^2)$
$r'' = -\phi_2^{\,2} \cdot c \cdot (\theta_0 - 1 + c)$	**Ratio of reactant components**
where $\phi_2^{\,2} = \dfrac{k_2\rho\; S_a R^2 [H_2O_2]_0}{D_{eff\,(int\,er)}}$	$\theta_0 = \dfrac{[C_5]_0}{[H_2O_2]_0}$
	Initial conditions
	$c_0\ (subdomain\ 1) = 1$
	$c_0\ (subdomain\ 2) = 0$
	Boundary conditions
	$\dfrac{\partial^2 c}{\partial x'^2} = 0$ at $y = 0$

Table 6.2   Microreactor model equations used in Femlab model

Parameter	Units	Experimental value	Modelling value
Channel length, l	(mm)	20	20
Channel width, w	(μm)	500, 1000	100 - 1000
Channel depth, d	(μm)	250	250
Catalyst layer thickness, δ	(μm)	5	5
Catalyst density, ρ	(g m^{-3})	1.6×10^6	1.6×10^6
Catalyst crystal size, ε	(μm)	2 - 4	2 – 5
Surface area per unit mass of catalyst, S_a	(m^{2}g^{-1})	1.5 – 3.0	1.5 – 3.0
Titanium content of TS-1, β	(at. %)	0 - 3.5	0 – 5
Residence time, τ	(s)	0 - 300	0 – 1000
$[H_2O_2]_0$	(molm^{-3})	200	100 – 1000
Stoichiometric ratio of 1-pentene to H_2O_2, θ	-	4.5	1- 8
Diffusion coefficient			
Bulk channel, D_{bulk}	(m^{2}s^{-1})	-	2×10^{-9}
Catalyst layer, $D_{eff(inter)}$	(m^{2}s^{-1})	-	8×10^{-11}
Kinetic constants			
Second order reaction, k_2	(m^{4}mol^{-1}s^{-1})	-	7.643×10^{-12}

Table 6.3   Experimental and model values of microreactor parameters

6.4   Results and discussion

6.4.1   Batch reactor

Reaction kinetics and its corresponding rate constant were calculated from the reaction data obtained from the batch reactor experiment using TS-1 zeolite grown on silicon wafer as a catalyst. The upper range of Weisz-Prater parameter for the batch reaction is 82 (appendix A4) indicating that the intra-particle diffusion resistance is large and most of the reaction occurs at the external surface of the zeolite crystal. Therefore the reaction rate is expressed per external surface area of the zeolite crystals. Figure 6.1 plots the amounts of hydrogen peroxide consumed and 1,2-epoxypentane produced in the batch reactor as a function of reaction time. A 90% selectivity of 1,2-epoxypentane on hydrogen peroxide conversion was obtained. The experimental data were fitted to first- and second-order reaction models (i.e., $r = -k_1[H_2O_2]$ and $r = -k_2[H_2O_2][C_5]$) giving rate constants, k_1 of $9.443 \times 10^{-9} ms^{-1}$ and k_2 of $7.643 \times 10^{-12} m^4 mol^{-1} s^{-1}$. From the figure it shows that the second-order reaction model fits the data better. Shea and Kim (1992) and Arasasingham et al. (1993) have also indicated that the oxidation of alkene to epoxide is a second order reaction. The details of the calculation can be found in appendix A1.
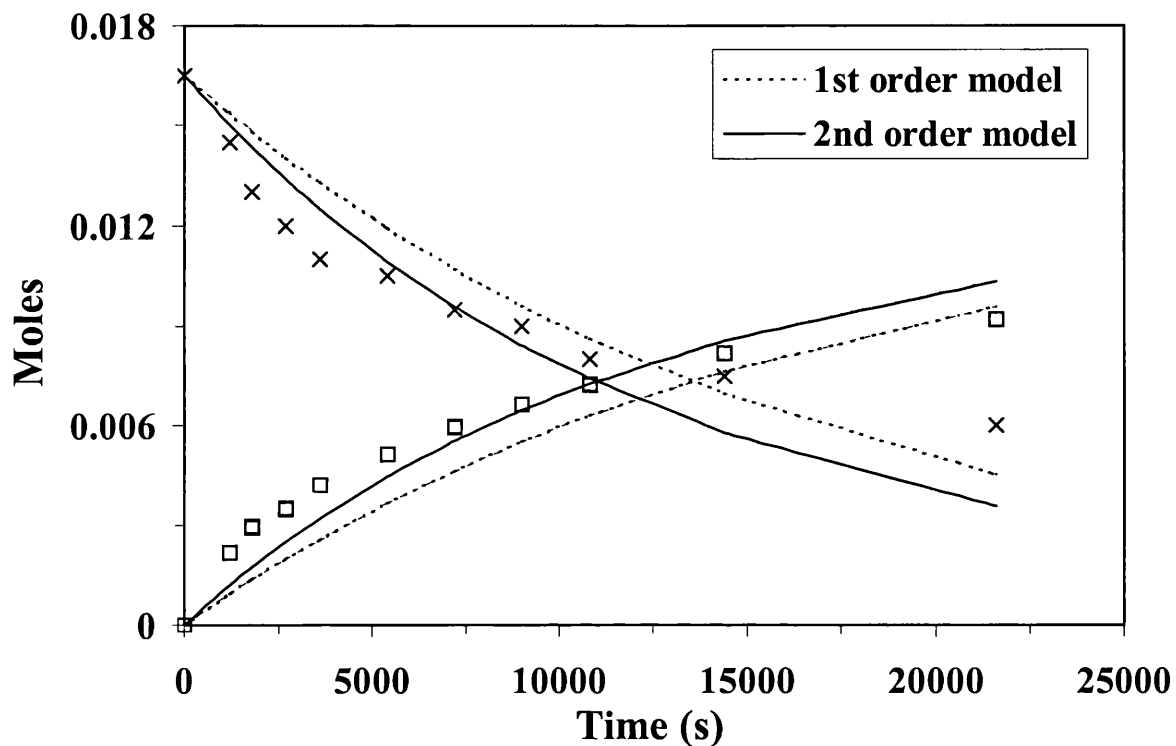
Figure 6.1 Moles of hydrogen peroxide reactant and 1,2-epoxypentane product in the batch reactor as a function of reaction time ($[H_2O_2]_0$ = 0.33 M, $[C_5]_0$ = 1.49 M, catalyst loading = 2g/L, δ = 5 μm, ε = 2 μm, β = 2.5 at.%, T = 298 K, x – hydrogen peroxide, □ - 1,2-epoxypentane)

6.4.2 Zeolite microreactor

A cross-section of the microchannel (figure 6.2) shows that the deposition of TS-1 zeolite (2 at.% Ti) was restricted to the microchannel. Zeolite growth is absent

outside of the seeded microchannel. The zeolite was uniformly deposited along the wall of the channel forming a 5 ± 0.8 µm thick film made up of intergrown 3 µm, zeolite crystal grains (figure 6.2 insets). The zeolite film displayed excellent adhesion to the channel and was able to withstand high temperature treatments (823K) without forming cracks or delaminating from the silicon substrate. Several TS-1 microreactors were prepared and tested in this study. Among the variables investigated were Ti-content of the catalyst (i.e., 0-3.5 at.%), zeolite film morphology and orientation (i.e., (101) and (020/200)-orientations), and zeolite crystal grain size (i.e., 2-5 µm).
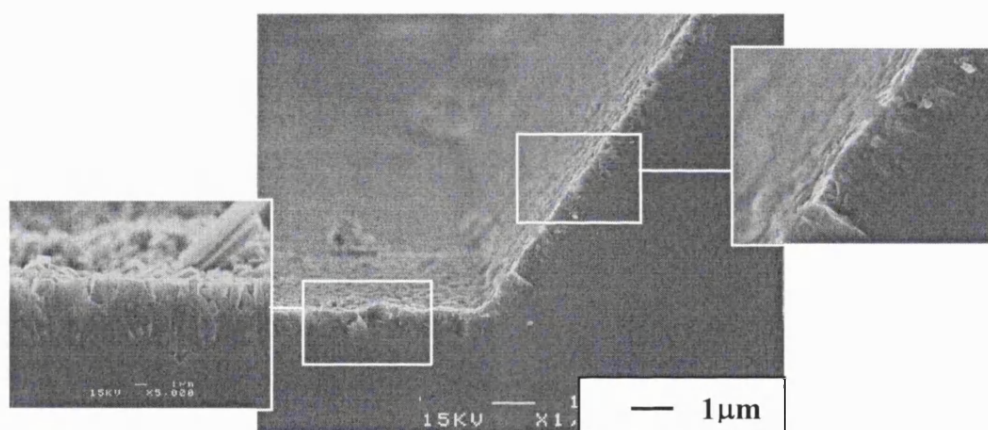
Figure 6.2   SEM picture of TS-1 zeolite layer and its cross-section (insert is 2×

magnification of the figure)

Titanium silcalite-1 has an average pore diameter of 0.55nm where the active site is situated inside the channel system. Internal mass transfer resistance is likely to occur across the catalyst layer. Therefore, branched and cyclic alkenes tend to react more slowly than straight chain alkenes (Clerici and Ingallina, 1993). 1-pentene

186

epoxidation is chosen for the preliminary study of the microreactor due to its faster reaction rate among TS-1 catalysed epoxidations.

The epoxidation of 1-pentene with hydrogen peroxide as the oxidizing agent is shown below yielding 1,2-epoxypentane (scheme 1). The stoichiometry of pentene, hydrogen peroxide to epoxide is 1. The principal by-products are glycols and glycol monoethylethers (Clerici and Ingallina, 1993).

$$CH_3CH_2CH_2CH{=}CH_2 \quad + \quad H_2O_2 \quad \longrightarrow \quad \underset{O}{CH_2\text{---}CHCH_2CH_2CH_3}$$
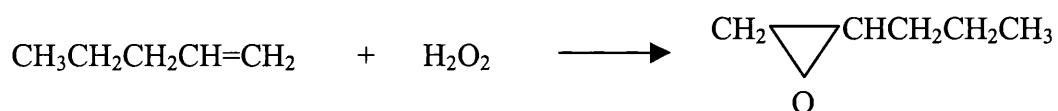
Scheme 1

Reaction tests conducted on a bare silicon microreactor, TiO_2-coated (P25, Degussa) microreactor and anatase TiO_2-coated (Hombikat UV100, Sachtleben) microreactor showed that these materials are inactive for 1-pentene epoxidation. A TS-1 coated microreactor displayed good conversion and selectivity for the epoxidation reaction. Five 500-μm single-channel microreactors (S1a-S1e) were prepared and coated with TS-1 zeolite film grown from standard synthesis solution and conditions (40 TEOS: 1.6 TEOT: 0.4 TEMS: 14 TPAOH: 10,000 H_2O, T = 448 K, t = 24 h) to test reproducibility. Analyses showed that deposited zeolite catalysts had an average titanium-content of 2 ± 0.5 at.%. They also displayed similar film morphology and had an average film thickness of 5 ± 0.2 μm and an average crystal size of 2 ± 0.5 μm. These microreactors were tested for 1-pentene epoxidation reaction at a residence time (τ) of 100s. A 1,2-epoxypentane yield of 10 ± 2 % was

187

obtained. The yield was defined as the ratio of the amount of 1,2-epoxypentane produced to the initial amount of hydrogen peroxide, which is the limiting reagent. Reproducibility was further ensured, by preparing more than one sample for each test microreactor listed in table 6.4, and by repeating some of the reaction experiments more than once. In general, the reproducibility of the reaction results for the same sample was better than ± 5 % and for different samples of the same test microreactor was ± 10%.

Sample	Channel width (μm)	Titanium content (atom %)	Crystal size (μm)	Residence Time (s)
S1a	500	2.02	2 - 2.5	40 – 100
S1b	500	2.04	2 - 2.5	40 – 100
S1c	500	1.89	2 - 2.5	40 – 100
S1d	500	1.72	2 - 2.5	40 – 100
S1e	500	2.42	2 - 2.5	40 – 100
S2	500	3.48	2 - 2.5	40 – 100
S3	500	1.52	2 - 2.5	40 – 100
S4a	500	0.73	2 - 2.5	40 – 100
S4b	500	0.88	2 - 2.5	40 – 240
S5	500	1.0-1.5	2	40 – 100
S6	500	1.0-1.5	3	40 – 100
S7a	500	1.0-1.5	4	40 – 100
S7b	500	1.0-1.5	4	40 – 100
S8	500	1.0-1.5	4.5	40 – 100
S9a	1000	1.74	2 - 2.5	90 - 180
S9b	1000	1.95	2 - 2.5	90 - 180
S9c	1000	2.13	2 - 2.5	90 - 180

Table 6.4   List of fabricated microreactors

6.4.3 Modelling results

<u>Influence of reactor geometry</u>

The microchannel geometry is defined by the width (w) and depth (d) of its cross-section and by the length (l) of the channel. In this study, the depth of the microchannel was fixed at 250 µm and the channel length at 20 mm. Figure 6.3 shows the 1,2-epoxypentane yield as a function of residence time for different channel widths. The experimental data for two channel widths 500 µm (S1a-S1e) and 1000 µm (S9a-S9c) are included in the plots for comparison. It can be seen that there is a good agreement between the model prediction and experimental data, considering the various simplifications made during the model derivation. However, the experimental yield obtained at higher residence time was lower than predicted. It may be due to catalyst deactivation by titanium leaching, which will be discussed later. The narrower channels give higher conversion because the catalyst loading per unit reactor volume is higher, even though the actual amount of catalyst is less due to fixed thickness of zeolite catalyst layer (i.e., 5 µm). However, a narrower channel will experience more severe pressure drop (ΔP), which increases in inverse proportion to the cube of the channel width (appendix A5). Calculations show that pressure drop will be a major problem for channel widths narrower than 100 µm, posing a severe limitation on the microreactor operation. This experimental study has shown that because of the relatively high volatility of 1-pentene, bubbles of hydrocarbon vapor were formed during the reaction. Problems from bubble formation can become severe

189

at low channel diameter, since bubble dislocation would require the use of excess pressures.
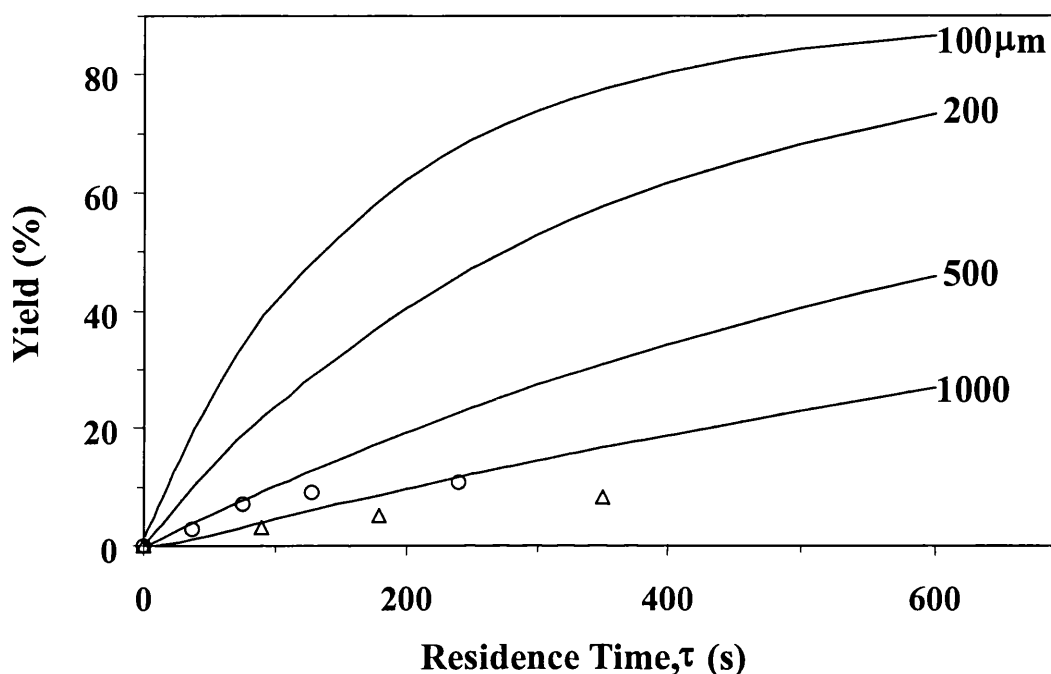
Figure 6.3   1,2-epoxypentane yield as a function of residence time for different channel widths; (O) – 500 μm, (Δ) – 1000 μm (δ = 5 μm, ε = 2-2.5 μm, β = 2.5 at. %, $[H_2O_2]_0$ = 0.2 M, θ = 4.5 and T = 298 K)

Influence of reaction conditions

The reactant concentration, residence time and reaction temperature are parameters that affect the reaction rate. The reaction temperature for 1-pentene epoxidation in the microreactor was kept constant at 298 K. A lower temperature means less reactivity, but a higher temperature leads to vaporization of 1-pentene resulting in bubble formation in the microchannel reactor and ultimately to cavitation. For the same reason, the concentration of 1-pentene in the reaction mixture has to be kept low. To prevent side reactions between the oxidizing agent, hydrogen peroxide

and the methanol solvent, a 1-pentene-to-hydrogen peroxide ratio (θ) greater than the stoichiometric value was used. These practical considerations constrained the operation of the microreactor for 1-pentene epoxidation. Figures 6.4 and 6.5 plot 1,2-epoxypentane yield as a function of residence time for different initial concentrations of hydrogen peroxide reactant and 1-pentene-to-hydrogen peroxide mole ratios. The agreement between the model and experimental data is good. The model indicates that increasing the amount of hydrogen peroxide can improve the yield in the microreactor.
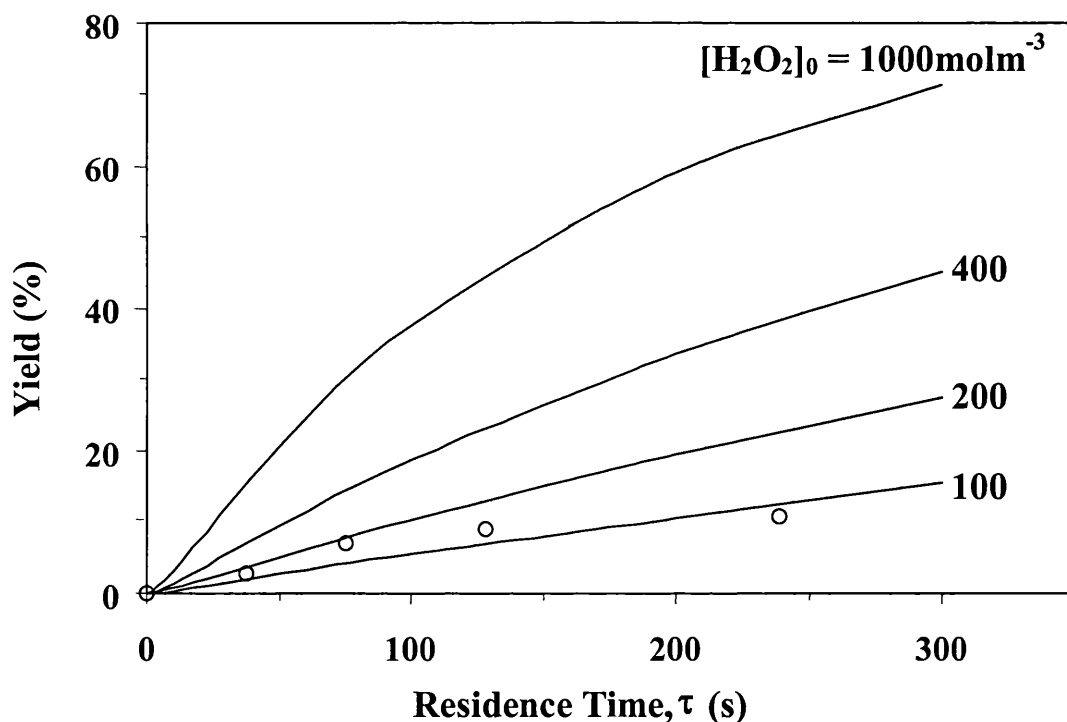
Figure 6.4 **1,2-epoxypentane yield as a function of residence time for different**
$[H_2O_2]_0$ concentrations (w = 500 μm, δ = 5 μm, ε = 2-2.5 μm, β =
2.5 at. %, θ = 4.5 and T = 298 K). Experimental $[H_2O_2]_0$
=200molm^{-3} (symbols – experimental data, lines – model data)
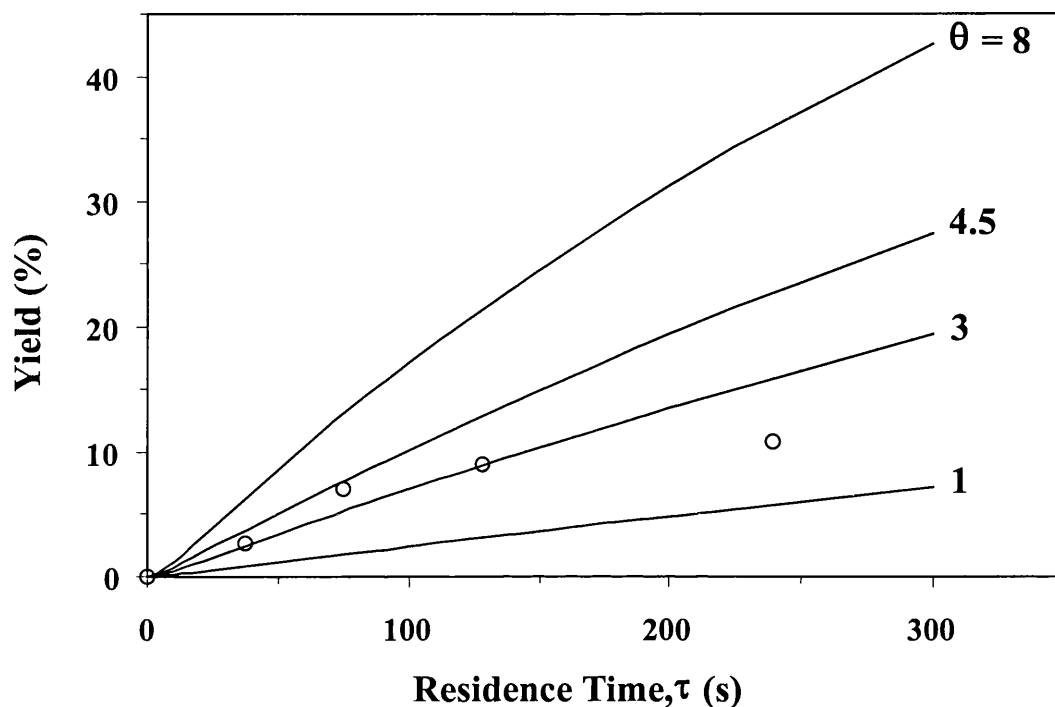
Figure 6.5 1,2-epoxypentane yield as a function of residence time for different θ values ($w = 500$ μm, $\delta = 5$ μm, $\varepsilon = 2$-2.5 μm, $\beta = 2.5$ at. %, $[H_2O_2]_0 = 0.2$ M and T = 298 K). Experimental $\theta = 4.5$ (symbols – experimental data, lines – model data)

6.4.4 Effect of catalyst coating

<u>Film morphology and orientation</u>

It had been described in chapter 4 how seed concentration can affect the morphology and orientation of deposited zeolite film. Figures 6.6a and 6.6b display the microstructures of two TS-1 films grown from the same synthesis solution onto a clean and seeded microchannels. It can be seen from the SEM micrographs in figure 6.6a that on the unseeded substrate the prismatic TS-1 zeolites were deposited with

their (020) crystal plane parallel to the channel wall. Secondary growth crystals were oriented with their (200) planes parallel to the silicon surface. This means that the straight MFI zeolite pore channels were aligned normal to the substrate, while the zigzag channels ran parallel to the channel surface. Indeed, X-ray diffraction analysis confirmed that the film possessed a (020/200) preferred orientation. The microchannel was covered with approximately 3.8×10^{10} zeolite crystals/m^2 that had an average size of 6 μm × 8 μm. Neighboring crystals merged to form an intergrown layer that was occasionally interrupted by defects caused by mismatched growth. Secondary growth is evident from the presence of multi-layered deposit (figure 6.6a) that consisted of smaller zeolite crystals.

TS-1 zeolites grown on seeded microchannel display a different morphology and crystal habit as shown in figure 6.6b. An inverted pyramidal shape evolved as the zeolite grew from the individual seeds. The seed resided at the apex of the pyramidal zeolite grain that terminated on a (101)-crystallographic plane. The XRD pattern displayed predominantly the (101) diffraction line. In this orientation, molecules must diffuse through the zeolite by hopping between the intersecting straight and zigzag zeolite pore channels. The film consisted of 5.5×10^{11} zeolite crystals/m^2 that has an average grain size of 2 μm × 4 μm.

The microreactor coated with a TS-1(020) film displayed low activity for 1-pentene epoxidation. The overall reaction rate at 100s residence time is 9.0×10^{-4} molm^{-3}s^{-1} despite having more accessible pore channels (i.e., straight pores). The

(101) zeolite-coated microreactors exhibit higher reaction rate ($6.3 \times 10^{-3} \text{molm}^{-3}\text{s}^{-1}$), even though the reacting molecules are expected to hop between the straight and zigzag pore channels due to the increased surface roughness and smaller crystal size. The observed behavior can be due to a larger contact area between reactants and catalyst for TS-1 (101) vs. TS-1 (200/020) (i.e., 37.4 m^2/m^2 versus 4.0m^2/m^2). This larger surface area is a result not only of smaller crystal size but also of larger film thickness (5 μm for TS-1 (101) and 2 μm for TS-1 (200/020)).
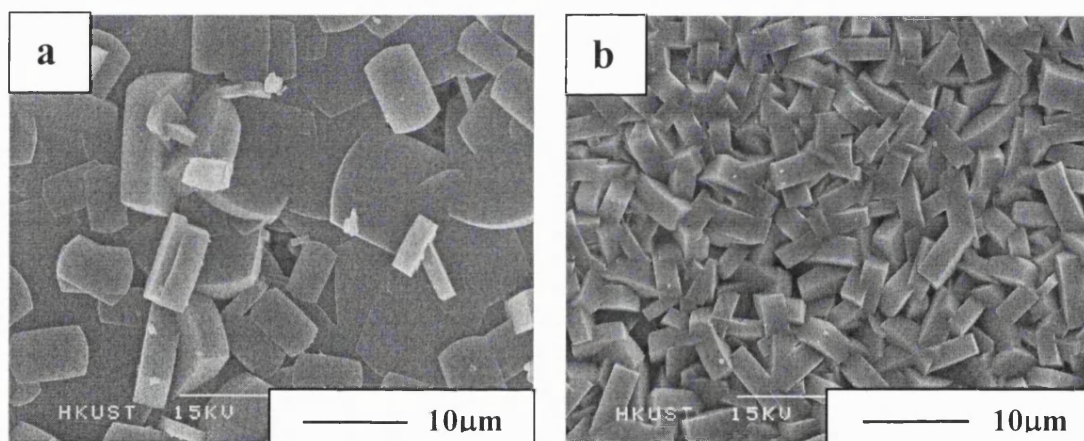
Figure 6.6   (a) SEM picture of zeolite film grown onto silicon support, on unseeded silicon wafer. (b) SEM picture of zeolite film grown on seeded silicon wafer. Regrowth condition: 40TEOS - 10TPAOH - 1.6TEOT - 10000H$_2$O, 175°C, 24hours
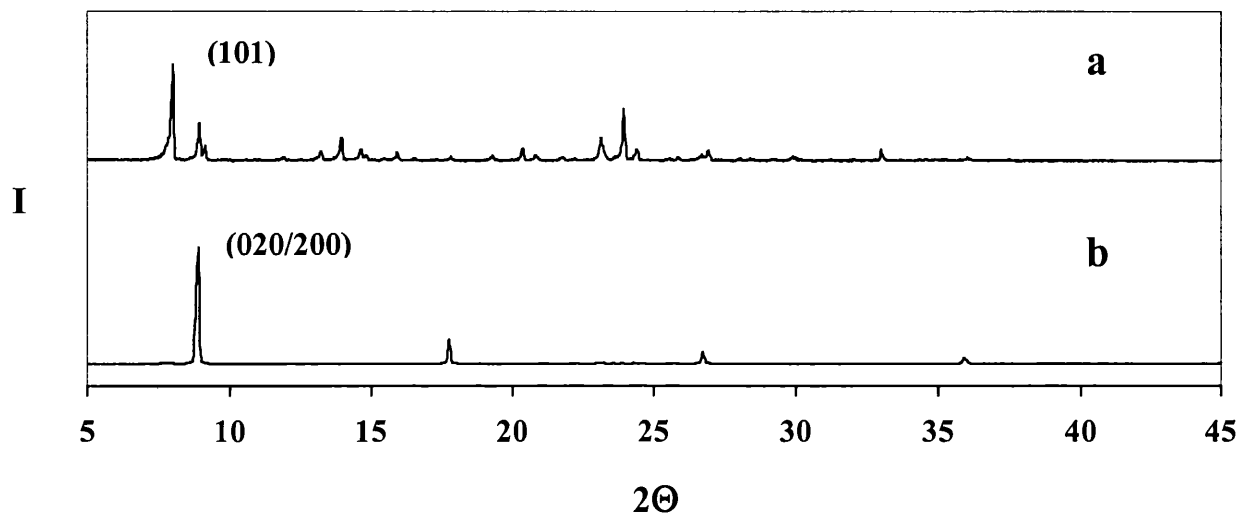
Figure 6.7   Corresponding X-ray diffraction diagram

Zeolite crystal size

   Thin film of TS-1 crystals were regrown from the standard synthesis solution

of 40 TEOS: 1.6 TEOT: 10 TPAOH: 10,000 H_2O. The result illustrated in figure 6.8a

demonstrates an average crystal size of 4μm. The catalyst efficiency is highly

dependent on particle size due to the presence of pore diffusion limitations (van der

Pol et al., 1992). Smaller crystal size with uniform crystal coverage is desired for

better reactor performance. A study of different synthesis conditions has been carried

out to investigate the influence on crystal sizes. It is found that OH^-/Si ratio of 0.35 is

the optimum to reduce the size of titanium siliclate-1 crystallites (Fig. 6.8b). In some

studies, triethoxymethylsilane (TEMS) was added in the synthesis solution to inhibit

the crystal growth of zeolite, thus resulting in a smaller crystal size. By varying the

composition of regrowth solution, crystal sizes, ranging from 2μm to 4μm, were studied (Fig. 6.8a-d). However, a TEMS mole ratio more than 0.4 will inhibit most crystal growth and affect the crystal coverage on the channel wall.

A set of TS-1 test microreactors (S5-S8) was prepared to study the effect of crystal size with product yield. The catalyst coatings of the microreactors have a titanium content of 1.0-1.5 at.% and thickness of 5 μm. They differ in the size of the zeolite crystal grains (figure 6.8). The reaction in the zeolite layer is pore diffusion controlled and most of the reaction occurred at the surface of the catalyst layer with very little reactant diffusing into the zeolite film. A more accurate relationship requires experimental data on the transport properties of the reactants and products in TS-1 zeolite, which are not available. Despite these shortcomings, Figure 6.9 shows that there is good agreement between the simulation results and experimental data.

It can be seen that a catalyst with 2μm crystal size can result in a six times higher product yield than the catalyst of 3μm crystal size. This is due to the increase in surface area and the fact that smaller crystals will facilitate titanium loading within the zeolite framework. Improvement in the catalyst performance can be achieved by increasing the external surface area of the zeolite layers, such as micropattterning the catalyst, increasing the surface roughness or random and irregular deposition of the zeolite crystal onto the catalyst layer.

4μm crystal size

3μm crystal size

2.5μm crystal size

2μm crystal size
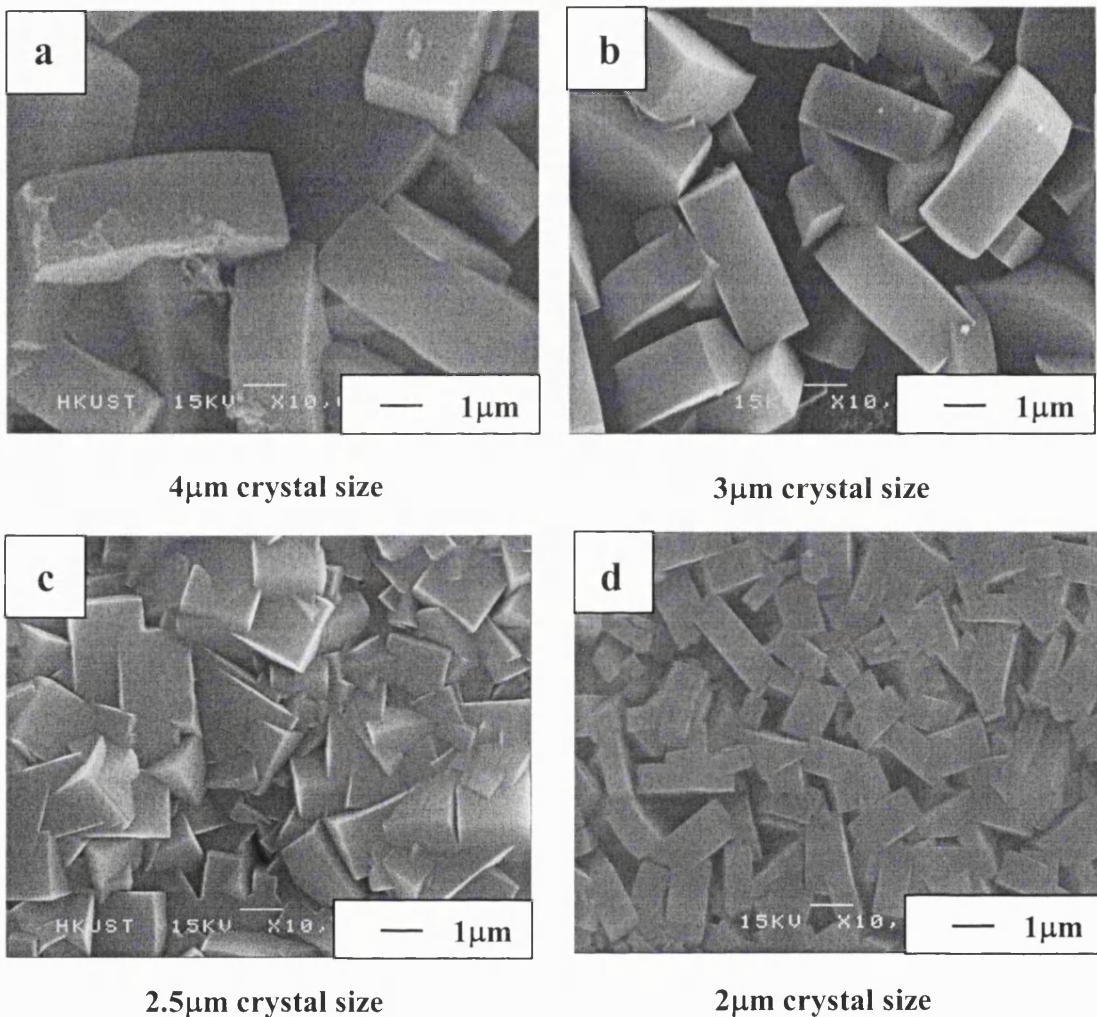
Figure 6.8   SEM picture of zeolite crystal with different sizes with synthesis
solution:

(a) 40TEOS – 10TPAOH – 1.6TEOT – 10000H$_2$O

(b) 40TEOS – 14TPAOH – 1.6TEOT – 10000H$_2$O

(c) 40TEOS – 14TPAOH – 1.6TEOT – 0.2 TEMS – 10000H$_2$O

(d) 40TEOS – 14TPAOH – 1.6TEOT – 0.4 TEMS – 10000H$_2$O

All the samples were prepared with seeded silicon support at a regrowth
temperature of 448K for 24h.

197
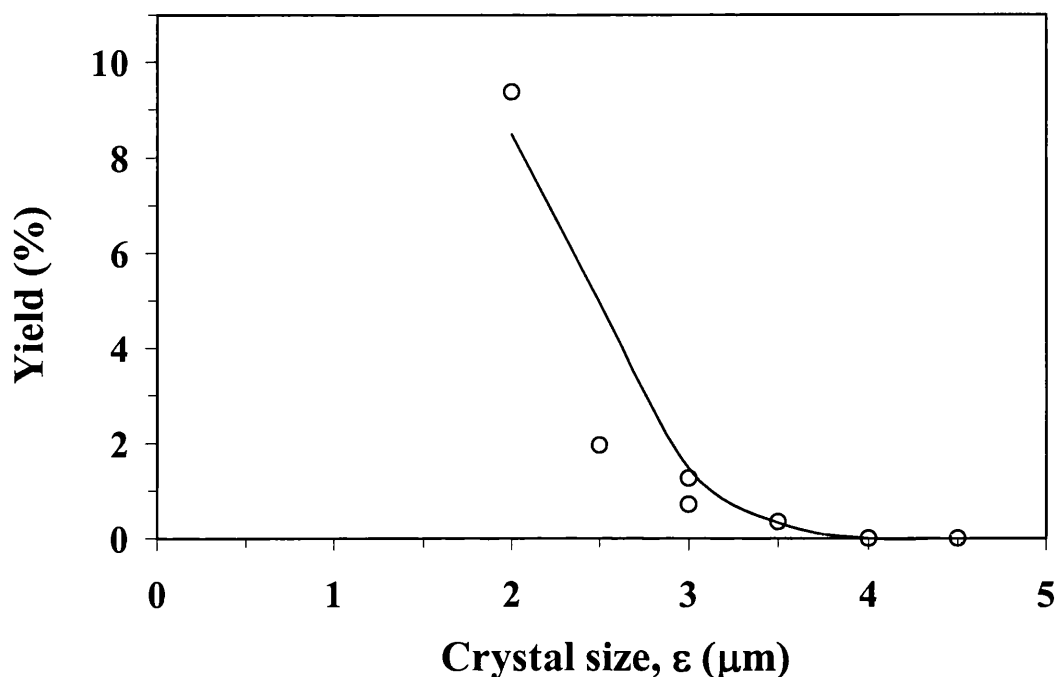
Figure 6.9   1,2-epoxypentane yield as a function of crystal grain size at a fixed residence time of 100s (w = 500 μm, δ = 5 μm, β = 1-2 at. %, $[H_2O_2]_0$ = 0.2 M, θ = 4.5 and T = 298 K)

(symbols – experimental data, lines – model data)

Framework Titanium Content

Synthesis of TS-1 zeolite is difficult to control resulting in poor reproducibility (Notari, 1996). Even under optimum synthesis conditions, the titanium content of the zeolite samples can vary significantly leading to a large difference in their catalytic activity. The insertion of titanium atoms in the zeolite framework is strongly affected by the chemical nature of the titanium and silica precursors, solution pH and synthesis temperature (Carati et al., 1999). The typical TS-1 synthesis composition (e.g.30TEOS: 1.5TEOT: 7TPAOH: 1,200H₂O) is not conducive to film formation. The strong alkaline mixture was observed to etch and dissolve the silicon

substrate. A considerable amount of effort was spent to identify the optimum synthesis composition and condition for the deposition of TS-1 zeolites in microchannels (40 TEOS: 1.6 TEOT: 0.4 TEMS: 14 TPAOH: 10,000 H_2O).

Early efforts led to poor titanium insertion in the zeolite framework as indicated by the XPS data shown in figure 6.10a and 6.10b. Titanium (IV) ions located at the tetrahedral position of the silicalite framework have Ti $2p_{3/2}$ and Ti $2p_{1/2}$ binding energies of 460 eV and 466 eV, respectively. The octahedrally-coordinated Ti(IV) attributed to extra-framework titanium atoms have a Ti $2p_{3/2}$ binding energy of 458 eV and Ti $2p_{1/2}$ of 464 eV (On et al, 1992, Mukhopadhay & Garofalini, 1990, Vayssilov 1997). Figure 6.10a represents a sample prepared by a TS-1 synthesis mixture with a Si/Ti ratio of 1 (40TEOS: 10TPAOH: 40TEOT: 10,000H_2O). Very little titanium is present in the sample. It may be due to the fact that an excess amount of TEOT is used and the hydrolysis of TEOT is not complete when preparing the synthesis solution. Catalysts prepared by this method were inactive for the epoxidation reaction. Using the optimal synthesis mixture composition with a higher ratio of Si/Ti (40 TEOS: 1.6 TEOT: 0.4 TEMS: 10 TPAOH: 10,000 H_2O), better titanium incorporation was observed (figure 6.10b). However, only a portion of the total titanium calculated from peak area at 460.81 eV and 466.56 eV (i.e., up to 48%) was present in the zeolite framework. There was considerable amount of extra-framework titanium in these samples. Although they were active for the epoxidation reaction, the results showed poor reproducibility since the amount of framework titanium varied significantly even for samples made from the same synthesis recipe.
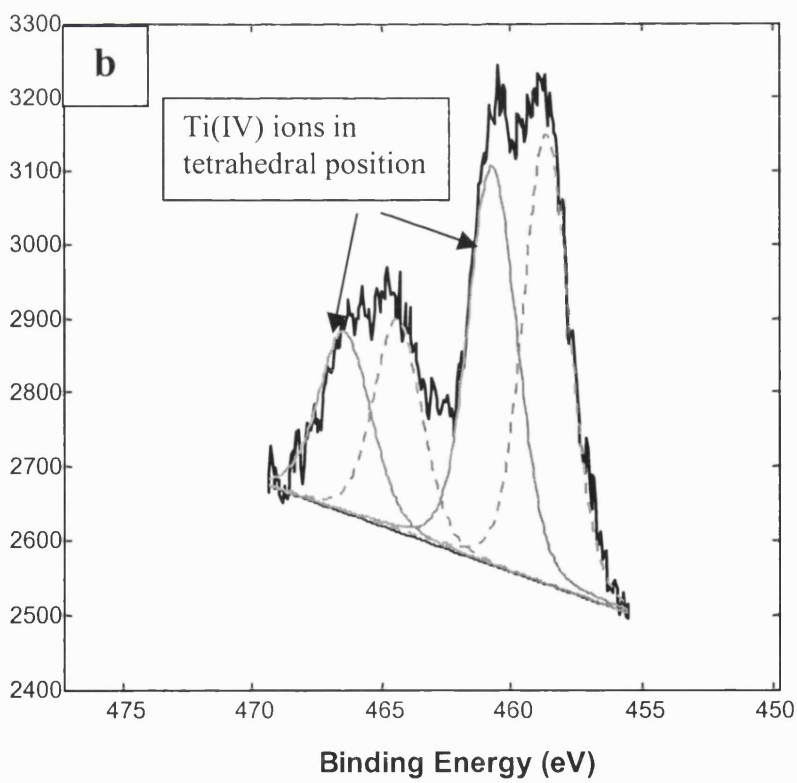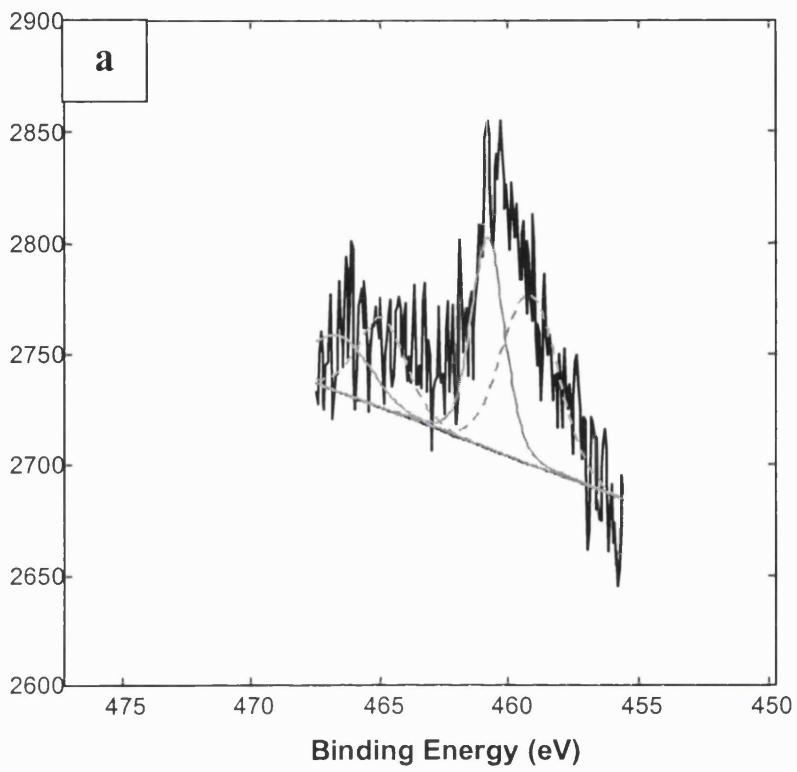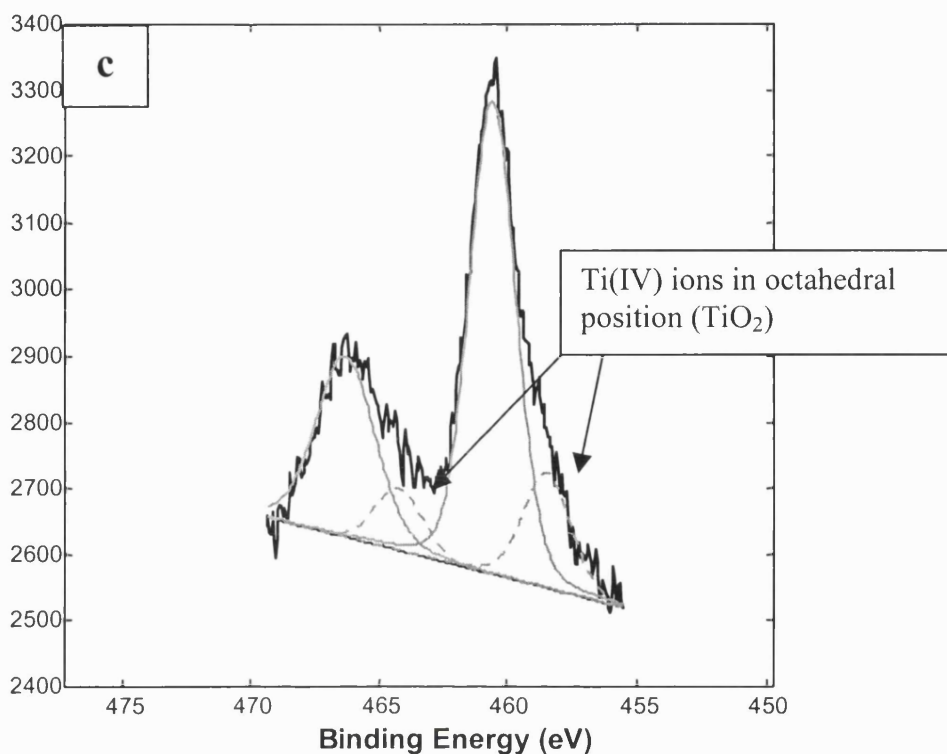
Figure 6.10   XPS spectrum showing

> **(a)   no insertion of Titanium into zeolite framework**
>
> **(b)   partial insertion of Titanium into zeolite framework**
>
> **(c)   full insertion of Titanium into zeolite framework**
>
> **solid line corresponds to tetrahedrally-coordinated Ti(IV)**
>
> **broken line corresponds to octahedrally-coordinated Ti(IV)**

The problem was traced to the alkalis present in the TEOS reagent. The present of alkali was reported to inhibit titanium substitution in TS-1 zeolite (Perego et al, 1998). Complete insertion of titanium into the zeolite framework was obtained after replacing the TEOS reagent with one containing less alkali impurities (figure 6.10c). Extra care was also taken to make sure that all apparatus were completely dry

as the presence of water would hydrolyse the titanium compounds to form hydrated TiO_2 in the synthesis solutions (see chapter 3.4.2). Using the new recipe, TS-1 zeolites with up to 3 at.% titanium were successfully prepared in the microchannel reactor.

Figure 6.11 plots 1,2-epoxypentane yield as a function of titanium content and the results are compared with the model data. The deposited zeolite formed an intergrown TS-1 (101) film on the wall of the 500 μm-wide main microreactor channel. An average crystal size of 2-2.5 μm and a thickness of 5 μm were maintained by adjusting the synthesis conditions. The 1-pentene epoxidation reaction was conducted at room temperature at a fixed residence time of 100s. Vayssilov and co-workers (1997) have reported that for TS-1 catalysed oxidation of anisole, catalyst activity is directly proportional to the titanium-content of the catalyst. Therefore, a simple linear relationship between titanium content and kinetic constant was assumed in the computational model taking into account that TS-1 catalysts with less than 1 at.% titanium content are inactive for the epoxidation reaction. The details of the calculation can be found in appendix A3. The experimental data show a monotonic increase in reaction yield with titanium content of TS-1 catalyst. Furthermore, there is a good fit between the model and experiment data. Although a higher titanium-content should lead to better conversions, the maximum concentration of titanium that could be inserted reproducibly into the zeolite framework is about 3 at.% (Bellussi and Rigutto, 1994).
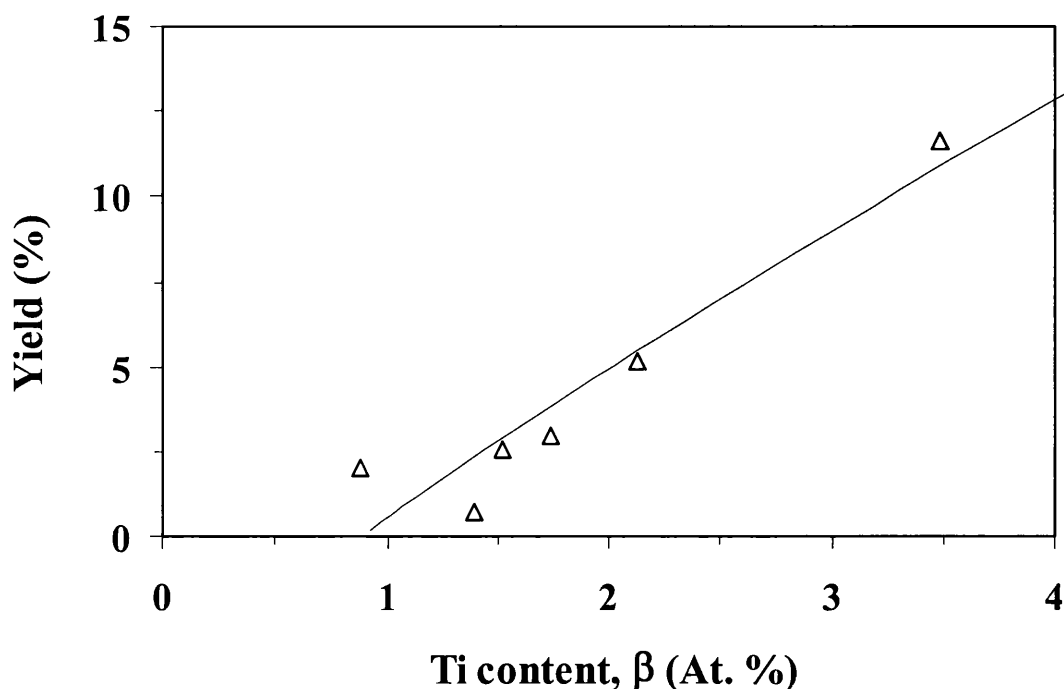
Figure 6.11   1,2-epoxypentane yield as a function of titanium-content at a fixed

residence time of 100s (w = 500 μm, δ = 5 μm, ε = 2-2.5 μm,

$[H_2O_2]_0$ = 0.2 M, θ = 4.5 and T = 298 K)

(symbols – experimental data, lines – model data)

It has been reported that the isolated, tetrahedral Ti(IV) ions in the –Si-O-Ti-

O-Si- zeolite matrix are the active sites for the reaction (Bellussi et al., 1992). Indeed,

zeolite catalysts containing mostly extra-framework titanium (figure 6.10b) displayed

low catalyst activity. The mechanism of 1-pentene epoxidation involves the formation

of an active titanium (IV) hydroperoxide intermediate by hydrogen peroxide

solvolysis (Drago et al., 1998). During the reaction the oxygen atom located next to

the metal centre initiates the reaction by attacking the carbon-carbon double bond of

the alkene molecule (Tantank, et al., 1998).

6.4.5 Catalyst deactivation

A series of experiments were conducted to investigate the deactivation of TS-

1 catalyst in the microreactor. Each experiment (set of five) was around five hours

prior to characterization and reactivation (figure 6.12). Two types of deactivation

were observed. A short-term deactivation at the beginning of each 5 hour experiment

and an overall long-term deactivation. It was suspected that the short-term

deactivation was due to the presence of organic compounds blocking the active sites

and pores of TS-1.

To further understand the catalyst deactivation, TGA was carried out on TS-1

powder sample synthesised under the same synthesis condition as the zeolite film (40

TEOS: 1.6 TEOT: 10 TPAOH: 10,000 H_2O). 100mg of the catalyst was used for

epoxidation (0.9M 1-pentene and 0.2M H_2O_2 in methanol) and the catalyst was

heated in an oven at 333K before the TGA experiment. A mass loss of 35% at 373K

was observed while the total mass loss up to 1073K was 38%. The mass loss at 373K

is attributed to the endothermic desorption of water (enthalpy 638J/g) while the

additional 3% mass loss is attributed to desorption/decomposition of organic

compounds. It can be concluded that water, as one of the by-products, would poison

the catalyst.

In propylene epoxidation, TS-1 deactivated when propylene oxide oligomers deposited inside the zeolite pores. The oligomers could be removed by calcination in air at 773K (Chen et al., 1998) or refluxing with dilute hydrogen peroxide (Thiele and Roland, 1997). Unguina et al. (2000) have studied the deactivation of TS-1 for styrene oxidation with hydrogen peroxide and observed a decline in the catalyst reactivity with time. The presence of diffusional limitations arising high degree of occupancy of the TS-1 pores and strong adsorption of styrene, phenylacetaldehyde and benzaldehyde on the Ti sites were proposed as the main reasons of deactivation. Thiele and Roland (1997) further argue that water co-ordinates to the active site increases acidity and hence the propensity for byproduct formation by acid catalysed reactions. These deactivation mechanisms are consistent with this work. However, the large amount of water observed in TGA experiments may indicate an additional deactivation mechanism (e.g. pore size restriction).
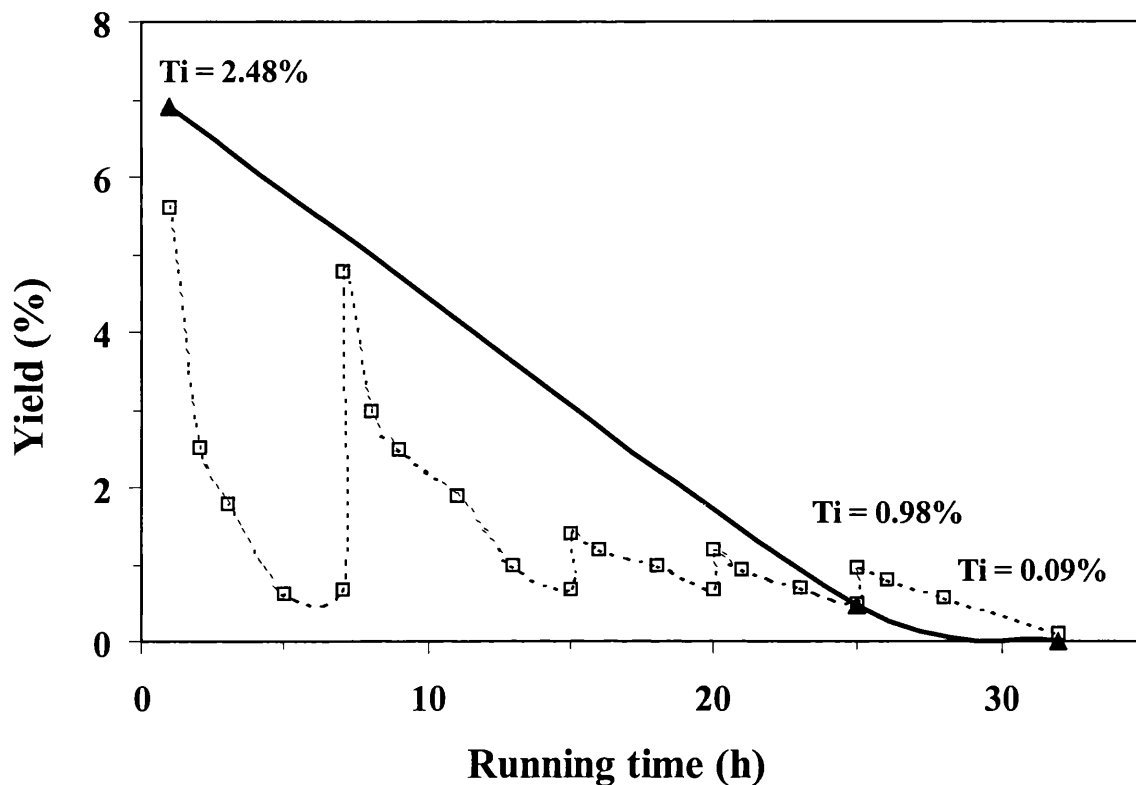
Figure 6.12   1,2-epoxypentane yield as a function of running time at a fixed

residence time of 100s (w = 500 μm, δ = 5 μm, ε = 2μm, $[H_2O_2]_0$ =

0.2 M, θ = 4.5 and T = 298 K)

dotted line – experimental data

solid line – model data

The long-term deactivation can be attributed to titanium leaching (Sheldon et

al., 1998). XPS analysis showed that the amount of tetrahedrally coordinated titanium

present in the catalyst at 1, 25, 32 hours was 2.48, 0.98 and 0.09% respectively

(figure 6.12). The model line obtained from Femlab model with the corresponding

titanium loading displays a good fit to the experimental data. Leaching is caused by

solvolysis by polar molecules reacting with the metal-oxygen framework bonds, resulting in the removal of the metal into solution. The titanium removed from TS-1 during reaction originates from defect sites in the framework where Ti is not perfectly coordinated to the four O-Si groups (Davies et al., 2001a, 2001b). Such defect sites have been proposed by Lamberti et al. (1998) who observed that TS-1 can be highly defective. There is a possibility that TS-1 prepared using a short crystallization period may have an increased concentration of these defect sites (Davies et al., 2001a). Furthermore, it has observed that (Davies, 2001b) titanium leaching is more prevalent under continuous flow conditions. It is possible that the equilibrium established between the solution Ti species and Ti on the catalyst surface is perturbed under such conditions. A similar leaching mechanism may be taking place in this work.

6.5   Concluding remarks

The novel procedure of selective seeding and regrowth techniques enables the selective incorporation of TS-1 catalysts within the microreactor channel. The technique's ability to engineer the zeolite film microstructure and chemistry is invaluable for optimizing the catalytic and transport properties of the incorporated catalyst layer. The deposited TS-1 films were active for catalyzing 1-pentene epoxidation reaction to produce 1,2-epoxypentane. A computational model based on established chemical engineering principles gave accurate prediction of the microreactor behavior and performance. The best operating conditions are to use stoichiometric amount of reactants and high concentration of hydrogen peroxide.

Practical limitations to the microreactor design and operations were imposed primarily by the thermodynamics and fluid properties of the reaction mixture. The high volatility of 1-pentene results to bubble formation in the microchannel.

A 500 μm width microreactor was employed in the study of catalyst performance and its relation to different synthesis conditions. The crystal orientation of (101) prepared with a seeded support displayed a better reactivity than crystals grown on the unseeded silicon wafer with (020/200) orientation. As the reactivity of the catalyst is dependent on the external surface area of the TS-1 crystal, a decrease in crystal size results in higher reaction rates. It is found that a OH^-/Si ratio of 0.35 in the synthesis solution is optimum for small crystals. The addition of TEMS, which acts as crystal growth inhibitor, further improves the catalyst performance by reducing crystal size. Catalysts with different titanium loadings were studied. It is found that the reactivity increases linearly with the TS-1 titanium content. Short-term deactivation was observed and attributed to the formation of organic compounds and presence of water. Catalyst activity could be recovered by calcination. Long-term deactivation by titanium leaching was irreversible.

Chapter 7

Zeolite membrane microreactor for selective oxidation of aniline

7.1 Introduction

Zeolites are microporous crystalline alumino-silcalites in which the microstructure and chemistry can be precisely tailored (Davies and Lobo, 1992). They are widely employed in the fields of catalysis, ion-exchange, separation and extraction. Their selective adsorption and molecular sieving properties make them an ideal candidate as membrane material to integrate reaction and separation processes (Caro et al., 2000; Chau et al., 2000). Zeolites possess fascinating gas permeation and separation properties with oriented pores and uniform pore size, which are most suitable for separation and membrane reactor applications (Lin et al., 2001; Bernal et al., 2002).

The application of membrane in chemical reactors involves the selective removal of one or more of the reaction products through the membrane from the reactors, thus combining reaction and separation in one single unit. Such a system is advantageous for equilibrium-limited reactions, which can increase the product yield and reaction conversion above the equilibrium point (Lai et al., 2003). A membrane reactor can also help to prevent catalyst poisoning and reduce catalyst deactivation by removing the unavoidable by-products in the reaction system (Salomón et al., 2000).

There are a number of examples on the use of zeolite membranes to integrate reaction and separation processes. Zeolites, with their great thermal and mechanical stability, are able to withstand harsh operation conditions. Besides hydrogen

separation, which can be achieved in Pd-based membrane systems, they can be employed in a much broader range of selective separations (Yan and Bein, 1995; Bein, 1996). Illgen and co-workers (2001) have reported the use of hydrogen selective zeolite membranes for hydrogen removal in iso-butane dehydrogenation. MFI type membranes were prepared *in-situ* on tubular α-Al_2O_3 supports with Cr_2O_3 as the catalyst. The membrane supported packed bed displayed a 1/3 improvement in the conversion of iso-butane. Unlike Pd membranes, which will degrade in the presence of hydrocarbons, low cost zeolite membranes offer great selectivity permeance and long time stability for hydrogen removal.

Zeolite membranes can also be employed in the separation of water from hydrocarbons. Espinoza and co-workers (1998) have displayed the use of hydrophilic zeolite for water removal in Fischer-Tropsch synthesis. This resulted in an increase in the reaction rate and catalyst deactivation was reduced. A further example was the synthesis of methyl-*tert*-butyl ether (MTBE) from *tert*-butanol and methanol in zeolite membrane reactors. The hydrophilic membranes used were mordenite and NaA zeolite. MTBE yields were 10% above the equilibrium value obtained without product removal (Salomón et al., 2000). Recently, the coupling of reaction and separation processes was reported (Bernal et al., 2002). A catalytically active zeolite membrane was employed for selective water permeation during ethanol esterification with acetic acid. The use of H-ZSM-5 membrane was able to show efficient integration of reaction and separation. The conversion obtained was greater than in

conventional fixed bed reactors, or in reactors where the zeolite membrane was kept separated from the catalyst.

The oxidation of aniline is an important reaction for the synthesis of its O-containing derivatives (figure 7.1). Hydroxylamines can be employed as reducing agents, stabilizers and polymerisation inhibitors (Tonti et al., 1988) whereas azoxy compounds are of great interest due to their physiological activity and their ubiquitous utilization in liquid crystals (Sakaue et al., 1993). Titanium silicalite-1 zeolites (TS-1) are known for their remarkable properties in the oxidation of organic compounds with hydrogen peroxide under mild reaction conditions (Clerici, 1993; Sheldon et al., 1997). The application of TS-1 in the selective oxidation of aniline to azoxybenzene was first reported by Sonawane et al. (1994) but very few details about the reaction and nature of products were given. Detailed studies were later carried out to investigate the influence of different reaction parameters on aniline oxidation over TS-1 (Gontier and Tuel, 1994; Selvam and Ramaswamy, 1995), showing that TS-1 can be an excellent catalyst for selective oxidation of aniline to azoxybenzene.

In this chapter, a multi-channel membrane microreactor was developed. Zeolites were employed as catalyst and membrane materials and incorporated in the design of the multi-channel membrane microreactor. Selective oxidation of aniline to azoxybenzene over TS-1 was studied whereas hydrophilic ZSM-5 was prepared as a membrane for selective removal of water, which is one of the by-products. Experimental results are presented in this chapter at different reaction parameters.

The product yield and selectivity were then compared with and without water removal. This novel fabrication technology opens up a new horizon to incorporate zeolite in microstructured reactors for various chemical applications.

Aniline   Phenylhydroxylamine (PH)   Nitrosobenzene (NSB)   Nitrobenzene (NB)

Aminophenol (AP)   Azobenzene (AZO)   Azoxybenzene (AZY)
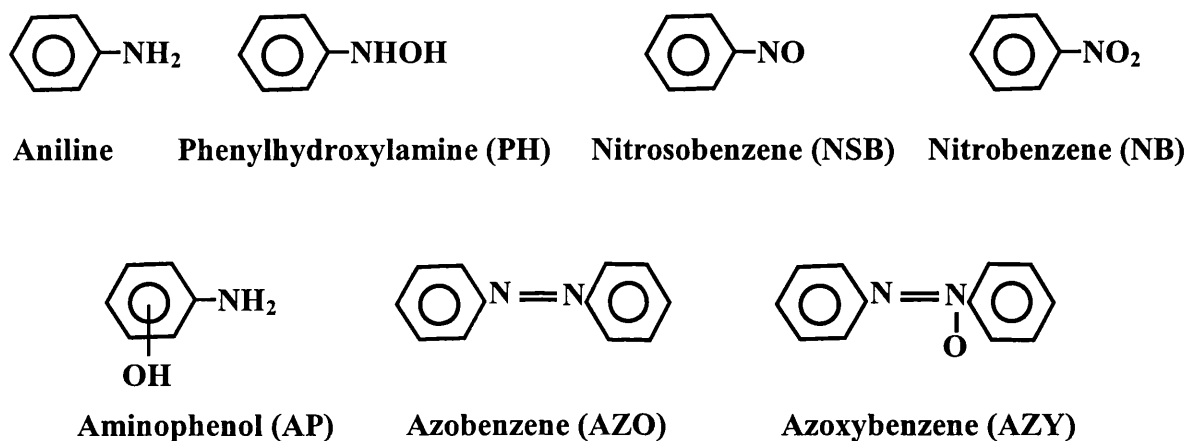
Figure 7.1   **Formulas of the different compounds obtained from aniline oxidation (Gontier and Tuel, 1994)**

7.2   Experimental

7.2.1   Catalyst Preparation

TS-1 nanocrystals were used as the catalysts in the selective oxidation of aniline, which are prepared similarly as the colloidal TS-1 seeds. The synthesis solution was prepared from a mixture containing the silica source, tetraethyl orthosilicate (TEOS), the titanium source, tetraethyl orthotitanate (TEOT) and the organic templating agent, tetrapropylammonium hydroxide (TPAOH) to give a composition 20 TEOS: 0.75 TEOT: 9 TPAOH: 404 H_2O. A clear and homogeneous solution was obtained after stirring for 24 hours at room temperature. The synthesis mixture was then transferred to a 125 ml Teflon autoclave (Parr Scientific Inc.) and heated in an oven (Memmert GmbH Co.) to a temperature of 398 K for 50 hours.

After hydrothermal synthesis, the colloidal zeolites were recovered and purified using centrifugation and ultrasonic treatment. They were stored as colloidal suspensions in deionized, distilled water. The SEM pictures of colloidal suspensions of TS-1 nanocrystals are shown in figure 7.2. It is shown that the TS-1 crystals have an average particle size of 120nm. They are crystalline and have an MFI-type structure. Chemical analyses using XPS indicated that 1.12% of titanium atom was incorporated into the zeolite framework of the catalysts. The crystals possessed a BET surface area of 425 m^2/g as measured by N_2 physisorption (Coulter, SA3100). Finally, the TS-1 nanocrystals were activated for catalytic reaction. The crystals were

first dried overnight at an oven temperature of 338K. They were then crushed into fine powder and calcined in air at 823K for 8 hours to remove all the organic templates with the zeolitic pores.
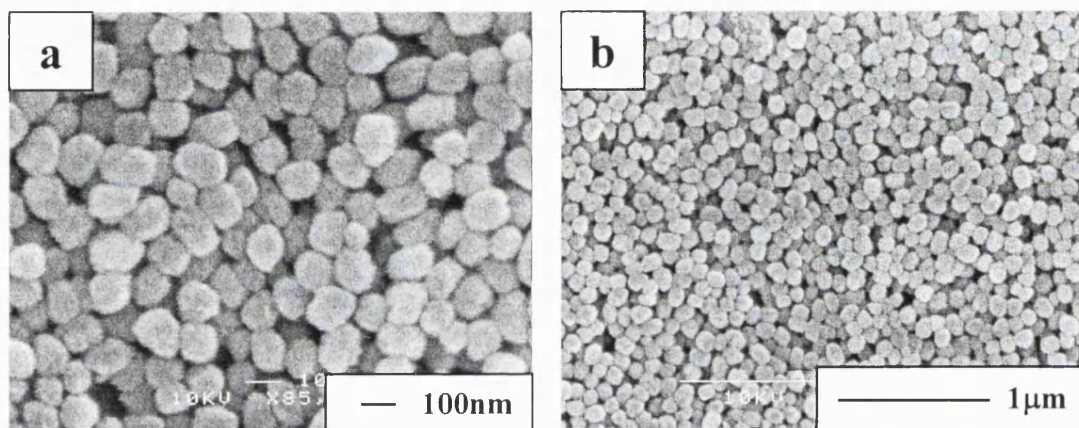
Figure 7.2   (a) SEM picture of TS-1 nanocrystals, regrowth condition: 20TEOS-0.75TEOT-9TPAOH-404H$_2$O, 398K, 50h (b) SEM picture of TS-1 nanocrystals with lower magnification

7.2.2   Selection and preparation of substrate

The subsequent scale up of the single channel microreactor was realized by the fabrication of multichannel stainless steel plate. The material employed in this experiment was porous stainless steel with a nominal pore size of 0.2μm (Mott metallurgical corporation). The plate can serve as the catalyst bed for the reaction and as the porous support of the zeolite membrane allowing transport of material across the plate. Unlike silicon, stainless steel can be fabricated without clean room facilities. It is also chemical resistant and can withstand high temperature applications, providing a low cost alternative for use in microreaction systems.

215

The multichannel stainless steel plate is shown in figure 7.3. The 25mm × 25mm plate consisted of 35 channels with width 300μm and depth 500μm, which was fabricated by electrical discharge micromachining (EDM, AGIE Wirecut 120). The parallel channels setting can be employed to increase the product throughput in the microreaction for chemical synthesis. The porous SS plate was first sonified in water with detergent for 15minutes to remove any oils during the micromachining process. It was sonified in dilute solution of nitric acid (0.05M) until all the rust was removed and a shiny surface obtained. The plate was then rinsed thoroughly with deionized, distilled water and sonified in ethanol to completely remove any water remained on the plate. The plate was then air dried and kept in a cool dry place to prevent any formation of oxide and rust.
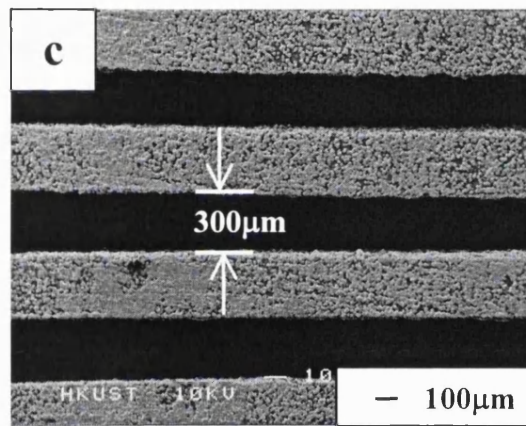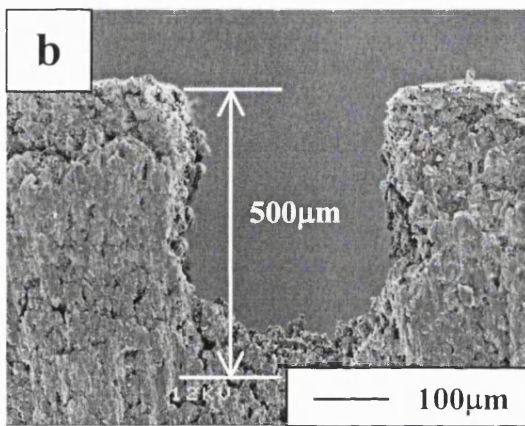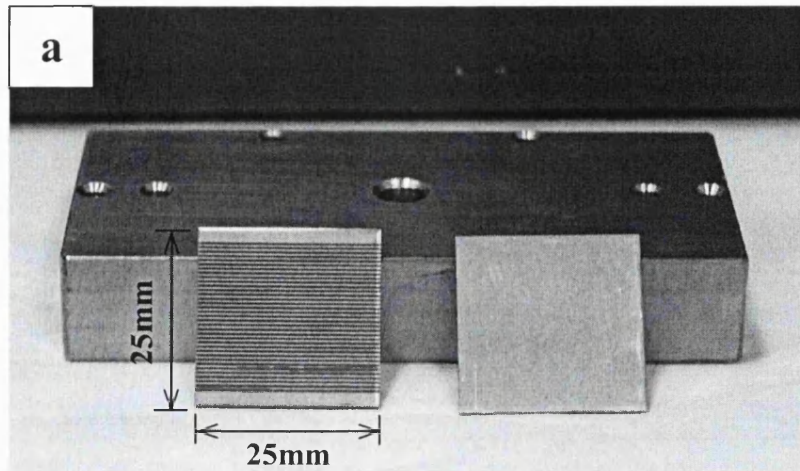
Figure 7.3 (a) A picture showing the front and back view of the multichannel stainless steel plate (b) SEM picture of the microchannel cross section (c) Top view of the stainless steel plate showing multiple channels with a width of 300µm

7.2.3 Membrane preparation

There are two approaches for the preparation of zeolite membranes: in-situ synthesis and seeded secondary growth. The former method allows a controlled

condition so zeolite can nucleate and grow directly from the surface of the porous support. However, this will require a longer synthesis time to obtain the continuous film. A thick coating with multiple crystal layers and randomly orientation will result. A more promising technique will be the synthesis of continuous zeolite film onto seed-coated layers. Chau et al. (2000) has demonstrated the preparation of silicalite-1 film onto porous stainless steel. By chemically modification and seeding of the support surface, this method gives highly reproducible film structure.

In this study, the seeded secondary growth method to prepare the ZSM-5 membrane is employed. The flat surface at the back of the stainless steel plate was first coated with colloidal silicalite-1 seeds prior to hydrothermal synthesis. The zeolite seeds were synthesized from a mixture containing 15 g of fumed silica, 0.85 g of sodium hydroxide (NaOH), and 60mL of 1 M TPAOH solution. The mixture was stirred overnight until a clear and homogeneous solution was obtained. The synthesis mixture then underwent hydrothermal treatment at a temperature of 398 K for 8 hours. The colloidal zeolites were recovered and purified using a series of centrifugation and rinsing steps. The silicalite-1 seeds have a spherical shape and an average particle size of 100 nm. The zeolite has a BET surface area of 420 m^2/g as measured by N_2 physisorption.

The stainless steel support was first brushed with mercapto-3-propyltrimethoxysilane surfactant. A thin layer of colloidal silicalite-1 zeolite seeds in 1wt % of absolute ethanol was then applied onto the surface. The steps were repeated

four times to obtain a complete and uniform coverage of the zeolite seeds onto the support surface. After drying at room temperature overnight, the seeded plate was heat treated at 523 K for 24 hours to produce a better adhesion to the surface.

The ZSM-5 membranes were prepared with a synthesis mixture with a mole ratio of 80TEOS: 10NaOH: 1TPAOH: 8 Al: 20000 H_2O. Al was obtained by heating aluminium sulphate $(Al_3(SO_4)_2)$ with ammonium hydroxide (NH_4OH) and mixed for 2 hours. The mixture was then washed and filtered with distilled, deionized water to obtain the remaining white powder, which was the aluminium source. The powder was then added to the mixture of NaOH, TPAOH with water. A homogenous solution was acquired by 24 hours of mixing for hydrothermal synthesis.

The stainless steel plate was then placed onto a specially designed Teflon holder so that the seeded surface facing downwards. This was to prevent any precipitate or powders from being incorporated into the zeolite film. The hydrothermal treatment was carried out at a temperature of 453 K for 48 hours. The same treatment was repeated thrice to obtain the desired thickness and coverage of the ZSM-5 membrane. The membrane was then activated at 673 K for 48 hours to make sure the TPA^+ organic template was removed from the voids in the zeolite channels.

7.2.4 Catalyst deposition

After hydrothermal synthesis, TS-1 catalysts were introduced onto the stainless steel plate. When compared to the silicon substrate, the direct regrowth of TS-1 crystal layer onto porous stainless steel support was unsatisfactory. Instead, TS-1 synthesized powders were deposited onto the microchannels directly. A thin layer of polydiallydimethyl ammonium chloride (PDAMAC) solution was applied on the surface of the microchannels. The positively charged PDMAC provides a better adhesion of the catalyst powders to attach to the channel wall. The TS-1 powders were first dispersed as a 2wt % solution in distilled, deionized water. The powders were then introduced onto the microchannels drop by drop until 5ml of the solution was added. The catalyst plate was then air dried overnight and heat treated at 623K for 24 hours to remove the remaining PDMAC.

7.2.5 Membrane microreactor unit

The pictures of the membrane microreactor unit are illustrated in figure 7.4. Figure 7.4a displays the top view of the reactor main body, which was made of stainless steel (SS 316). A small hole was drilled at the side for insertion of a thermocouple. The reactant mixture flows through the cavity on the surface of the stainless steel block. Multi flow channels were machined on both sides of the reactor to provide an even distribution of fluids to the catalyst plate in which the reaction

takes place. A square recess was fabricated in the middle of the reactor main body to place the multichannel stainless steel plate. The reaction mixture enters and leaves the unit through the reactor inlet and outlet (figure 7.4b) whereas the middle tubing was connected to vacuum pump for membrane prevaporation. O-rings were placed around the cavity and recess of the reactor body to provide a leak free environment. Figure 7.4c displays the assembled unit with stainless steel catalyst plate fitted in the reactor. The reactor was heated by a copper block fitted with two heating rods as shown (figure 7.4d). The power output of the heating rods was controlled by a K-type temperature controller.
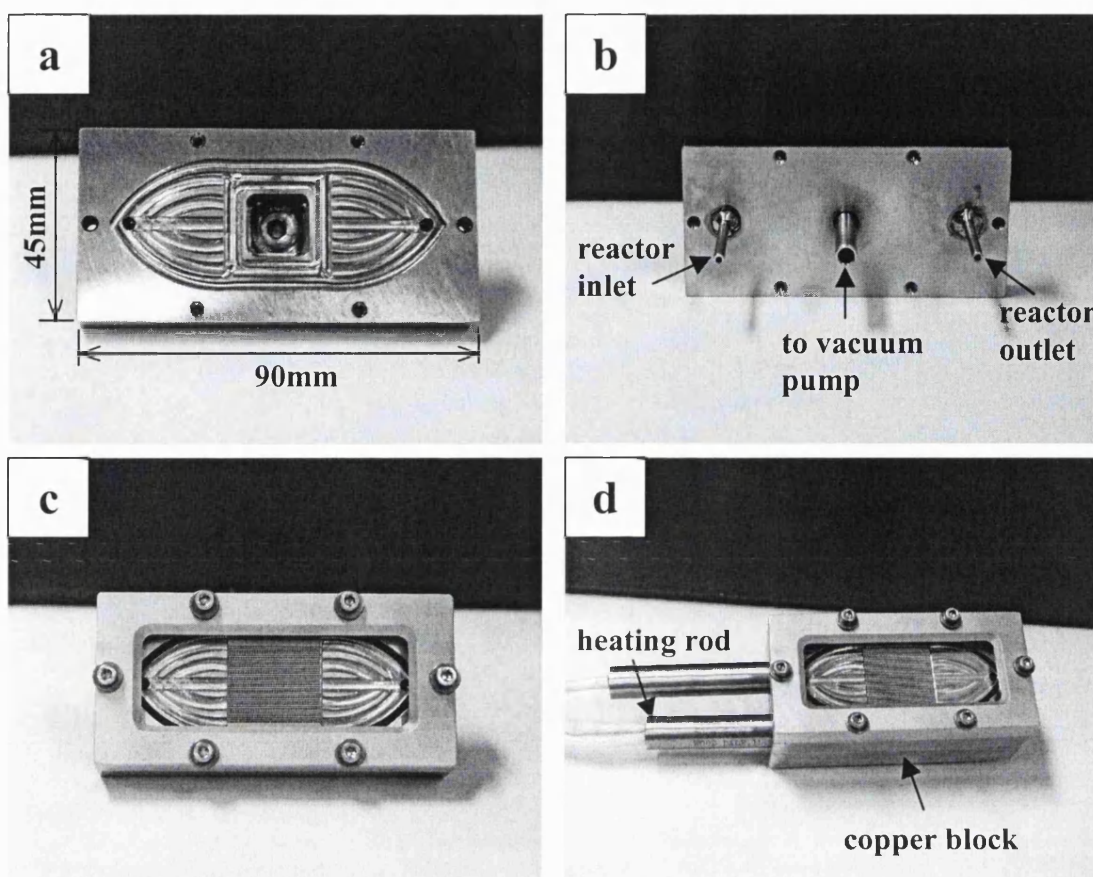
Figure 7.4   Pictures of membrane microreactor unit (a) top view of the reactor main body (b) back view of the reactor body showing inlet and outlet (c) assembled reactor unit and (d) assembled membrane microreactor with heating unit

7.2.6   Assembly of membrane microreactor

The schematic diagram of the assembly of membrane microreactor is illustrated in figure 7.5. Pyrex glass plate (1/8" thick) was employed as the top sealing of the reactor. It was pressed against the reactor with the catalyst plate fitted into the recess. An aluminium gasket was applied to press against the glass plate with the

reactor main body. O-rings were fitted between the glass plate and the reactor to ensure a leak free sealing. The copper heating block can be easily screwed onto the reactor body and provide heating throughout the experiment. During the experiment, the reaction mixture was pumped into the inlet using a syringe pump (Kd Scientific). Fluid flow was then developed through the machined groove whereas reaction took place inside the catalyst plate. The reacted mixture was collected through the reactor outlet and analysed by gas chromatography. A pressure of 125mmHg was pulled from the reactor recess using a vacuum pump (Barnant Company, Edwards Company) for membrane pervaporation. The permeates were collected using a liquid nitrogen cold traps.
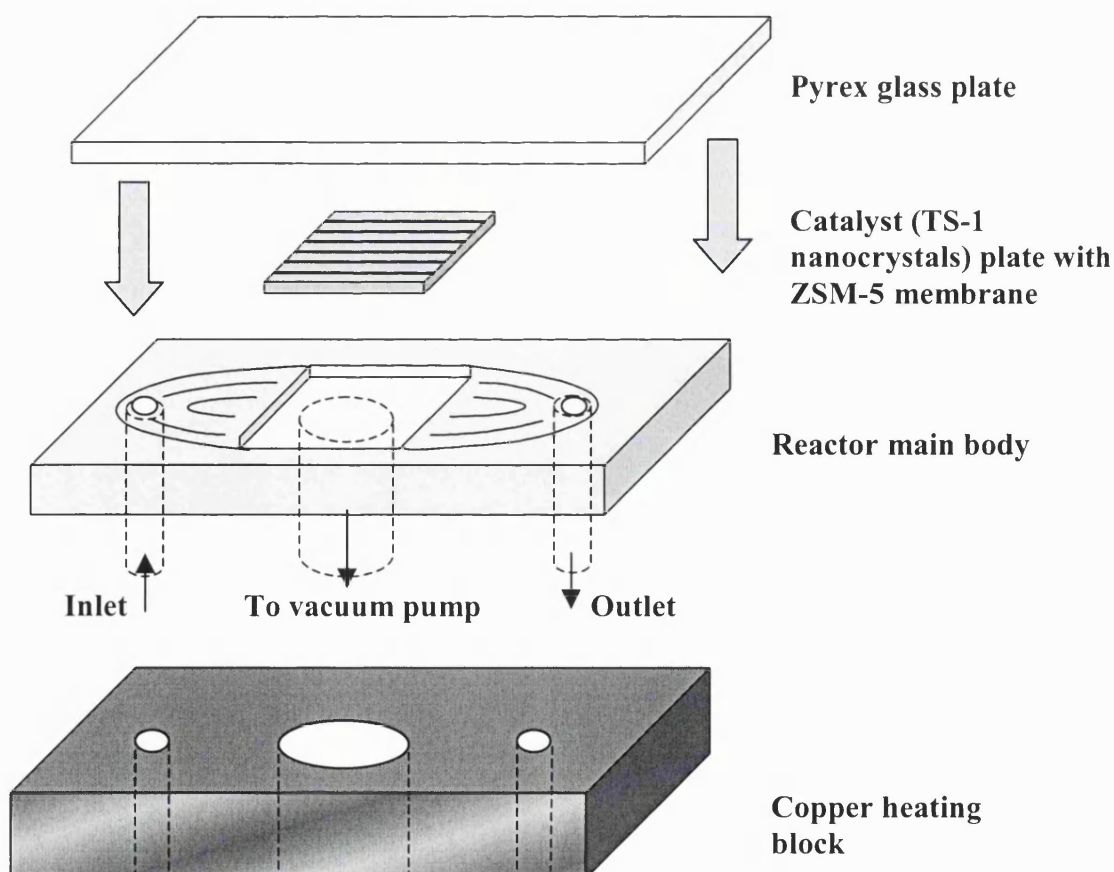
Figure 7.5   Assembly of membrane microreactor

7.2.7 Selective oxidation of aniline

The membrane microreactor system was used to study titanium silicalite-1 catalyzed oxidation reaction using hydrogen peroxide as the oxidizing agent. This set can allow a reaction temperature up to 150°C while the silicon T-channel microreactor was for low temperature application in epoxidation reactions. Hydrophilic ZSM-5, with a maximum free pore diameter of 5.4Å is capable of selective water permeation from a mixture with hydrocarbons. ZSM-5 membrane can be employed for removal of water, which is the side product of the TS-1/H_2O_2 oxidation reaction. As described in chapter 6.4.5, it is suspected that the presence of water will deactivate the catalyst. Another reason for catalyst deactivation is the adsorption of organic compounds on TS-1 active sites.

In order to observe the improvement obtained in the membrane microreactor system, selective oxidation is chosen with a higher reaction temperature. In this study, oxidation of aniline over TS-1 is examined with azobenzene and azoxybenzene as the major products. The by-product water can be continuously removed from the membrane by connecting to a vacuum while TS-1 deposited in the micromachined channels acted as catalyst bed for the reaction. In a typical run of the membrane microreaction, 4.8ml of aniline and 1.2ml of 30wt % hydrogen peroxide were added to 14ml of chloroform, which acted as the solvent of the reaction. The reaction mixture was then introduced into the unit where the reaction took place. The details of the different reaction parameters are listed in table 7.1.

Membrane	ZSM-5 membrane
Catalyst	TS-1 nanocrystals with a loading of ~0.1 g
Oxidizing agent	Hydrogen peroxide
Solvent	Choloroform
Reaction temperature	30, 50, 70, 90 °C
Reactor volume	0.13ml (35×25mm×500μm×300μm) no. of channels × channel length × depth × width
Reactant flowrate	0.5, 1, 2, 4 ml/h
Effective pervaporation area	4 cm^2
Reactant ratio	H_2O_2 / aniline = 0.2
GC analysis	Nickel column (2m × 1/8 inch) packed with Tenax GC 60/80

Table 7.1   Experimental conditions for selective oxidation of aniline in multichannel membrane microreactor

7.2.8   Characterization

Zeolite structural analyses were conducted using X-ray diffraction (XRD) and scanning electron microscopy (SEM). The crystal structure, crystallinity and crystallographic orientation of the ZSM-5 memrbane were determined using a Philips PW 1030 X-ray diffractometer equipped with a CuK X-ray source and graphite monochromator. The X-ray line intensity was obtained for $5° \leq 2\theta \leq 45°$ at a scan rate

of $0.02°$/min and time constant of 0.02. SEM was employed to determine the dimensions of the microchannels, and to measure the thickness of the ZSM-5 membrane coated on the back of the stainless steel plate. The samples were mounted onto aluminium specimen stubs with conducting carbon tape and sputter-coated with a 10 nm layer of gold to reduce sample charging. The zeolite surface morphology and grain size were also determined from analysis of the SEM micrographs. Bulk and surface compositions of zeolites were examined by X-ray photoelectron spectroscopy (XPS, Physical Electronics PHI 5600).

7.2.9 Materials

For TS-1 synthesis, the chemicals used were TEOS (98%, Aldrich), tetraethyl orthotitanate (95%, MERCK-Schuchardt) and TPAOH (1 M, Aldrich). The silicalite-1 seeds were prepared with fumed silica (0.01μm, 99.8%, Aldrich), TEOS and sodium hydroxide (98%, BDH). Aluminium sulphate (98+%, Aldrich) and ammonium hydroxide (28-30%, Fisher Scientific), TPAOH and TEOS were employed for the synthesis of ZSM-5 membrane. The chemicals used for catalyst deposition was polydiallydimethyl ammonium chloride (20 wt% in water with average M_w 200,000–350,000, Aldrich).

For reaction experiments, the chemicals used were aniline (99.5%, Aldrich), hydrogen peroxide (30 wt.%, BDH) and chloroform (99.8%, Aldrich).

7.3   Results and discussion

7.3.1   Membrane characterization

It has been reported that the zeolite films obtained by in-situ synthesis will exhibit [0k0] or [h00]-out-of-plane orientation while a [h0h]-out-of-plane preferred orientation will obtained by secondary growth (Gouzinis and Tsapatsis, 1998; Xomeritakis et al, 1999; Koegler et al. 1997). In this study, the seeded secondary growth method for the preparation of ZSM-5 membranes onto porous stainless steel plate is employed.

The deposition and growth of ZSM-5 zeolite onto a stainless steel support are shown in figure 7.6. Figure 7.6a displays the surface morphology of the ZSM-5 membrane. The zeolites indicated an MFI crystalline structure with a crystal coverage of approximately 6.5×10^{10} crystals/m^2. The crystals were well intergrown with a size of 10μm×15μm forming a continuous zeolite film. The film has a thickness of 25μm with a surface roughness about 5μm (figure 7.6b). XPS indicated a Si/Al ratio of 18.5 for the ZSM-5 zeolites. The zeolite film exhibits great adhesion to the stainless steel support. They are able to withstand harsh and extreme operating conditions showing stable prevaporation performance throughout the experiment.

The XRD analysis in figure 7.6c displays the different orientation of the crystal layer obtained for the membrane. The ZSM-5 crystals on the seeded support

indicate an orientation (101) with (200). Most of the crystals were oriented with their <101> crystallographic axis perpendicular to the support surface because of the secondary growth.
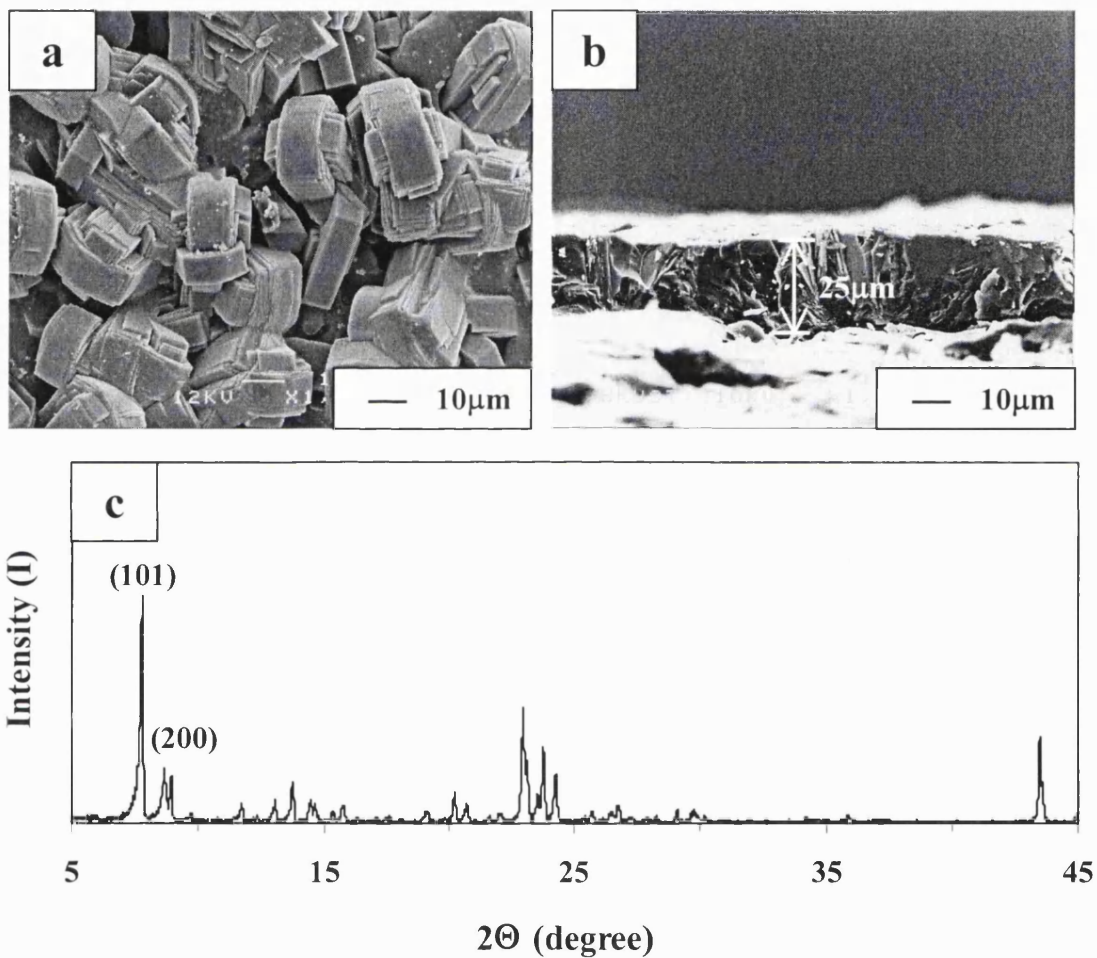
Figure 7.6 (a) Top view of the ZSM-5 membrane grown onto the porous stainless steel support (b) Cross section of the ZSM-5 membrane across the stainless steel plate and (c) Corresponding XRD diagram of the ZSM-5 membrane

7.3.2 Selective oxidation of aniline to azoxybenzene

The oxidation pathway of aniline in the presence of mono oxygen donors is illustrated in figure 7.7 (Selvam and Ramaswamy, 1995). The titanium peroxo complex (IV) delivers reactive oxygen which converts aniline 1 to phenylhydroxylamine 2 and further oxidize to nitrosobenzene 3. Two routes are suggested for the formation of azoxybenzene 5: direct oxidation of azobenzene 4 or reaction between nitrosobenzene 3 and phenylhydroxylamine 2. The first route involves the condensation of nitrosobenzene 3 with aniline 1 to azobenzene 4, followed by subsequent oxidation to azoxybenzene 5. However, it is found that no azoxybenzene was detected after 3 hours under the oxidation reaction of azobenzene (Gontier and Tuel, 1994). It is more likely that azoxybenzene is formed by the direct condensation of nitrosobenzene 3 and phenylhydroxylamine 2.

1	aniline
2	phenylhydroxylamine
3	nitrosobenzene
4	azobenzene
5	azoxybenzene
6	nitrobenzene
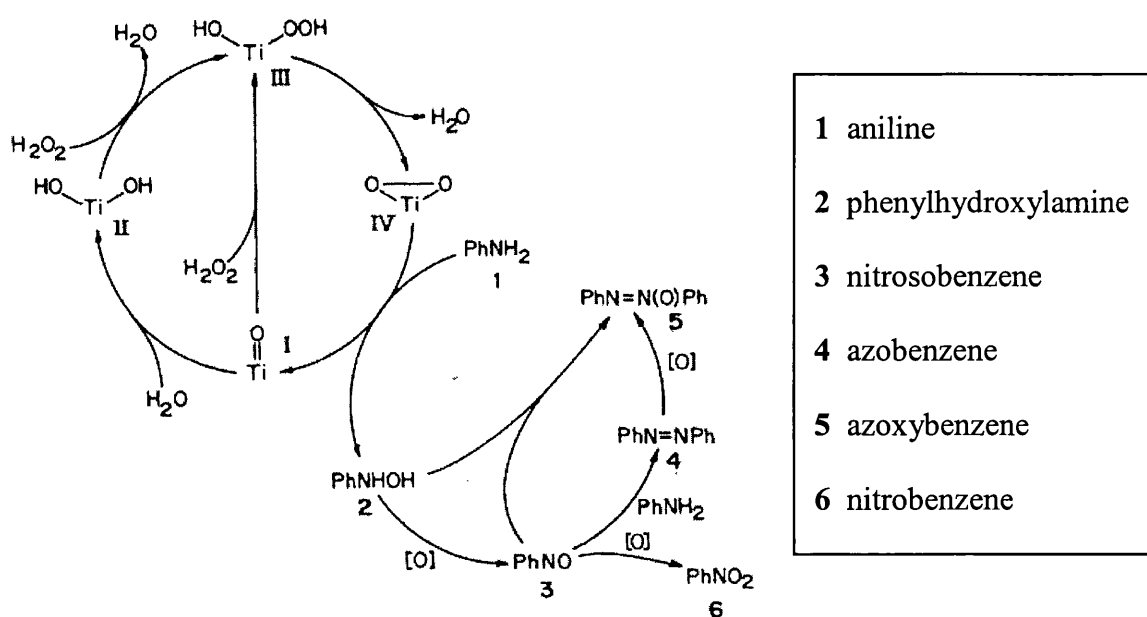
Figure 7.7   Oxidation pathways of aniline (Selvam and Ramaswamy, 1995)

Two main products are observed with aniline oxidation using hydrogen peroxide as the oxidant: nitrosobenzene and azoxybenzene (Gontier and Tuel, 1994). In order to obtain high selectivity of nitrosobenzene, a relatively high H_2O_2/aniline ratio (>3) is required (Tollari et al., 1993). Within the H_2O_2/aniline ratio from 0.1 to1, azoxybenzene is the main product with only traces of nitrobenzene observed (Selvam and Ramaswamy, 1995).

It has been reported that three moles of H_2O_2 are necessitated for the formation of one mole of azoxybenzene (Gontier and Tuel, 1994). The stoichiometric equation of selective oxidation of aniline to azoxybenzene is shown in figure 7.8. In this study, two products in the selective oxidation of aniline are observed: azobenzene and azoxybenzene at a H_2O_2/aniline ratio of 0.2 with azoxybenzene as the main product.
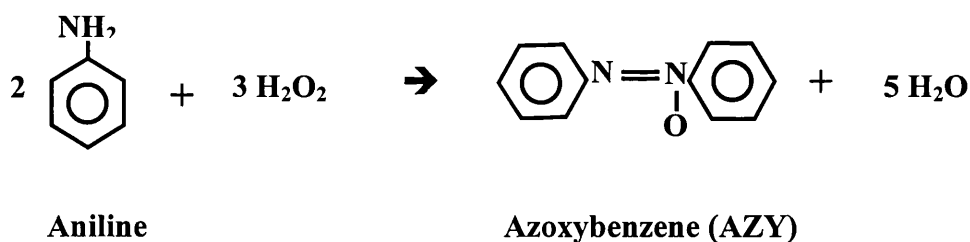
Figure 7.8   Reaction equation of aniline oxidation to azoxybenzene

7.3.3 Membrane microreactor results

The reaction was conducted in the membrane microreactor unit with and without water removal. Four flowrates were studied in the experiment: 0.5, 1, 2 and 4ml/h at a temperature of 343 K. However, it is found that at a flowrate of 4ml/h, the product yields obtained for azobenzene and azoxybenzene were not adequate to observe the difference of product removal. There was no significant improvement in product selectivity towards azoxybenzene. This can be explained by the fact that the residence time attained at such a flowrate was not enough for the reaction mixture to stay in the reactor chamber for effective water removal.

Figure 7.9 illustrates the product yield of azoxybenzene at 2ml/h with a residence time of 234s. The residence time was calculated from the volume of the microchannels within the stainless steel plate (0.13ml) and total liquid flowrate (2ml/h). The average product yield shows an increment of 10% with water removal when compared with the result obtained without membrane prevaporation.
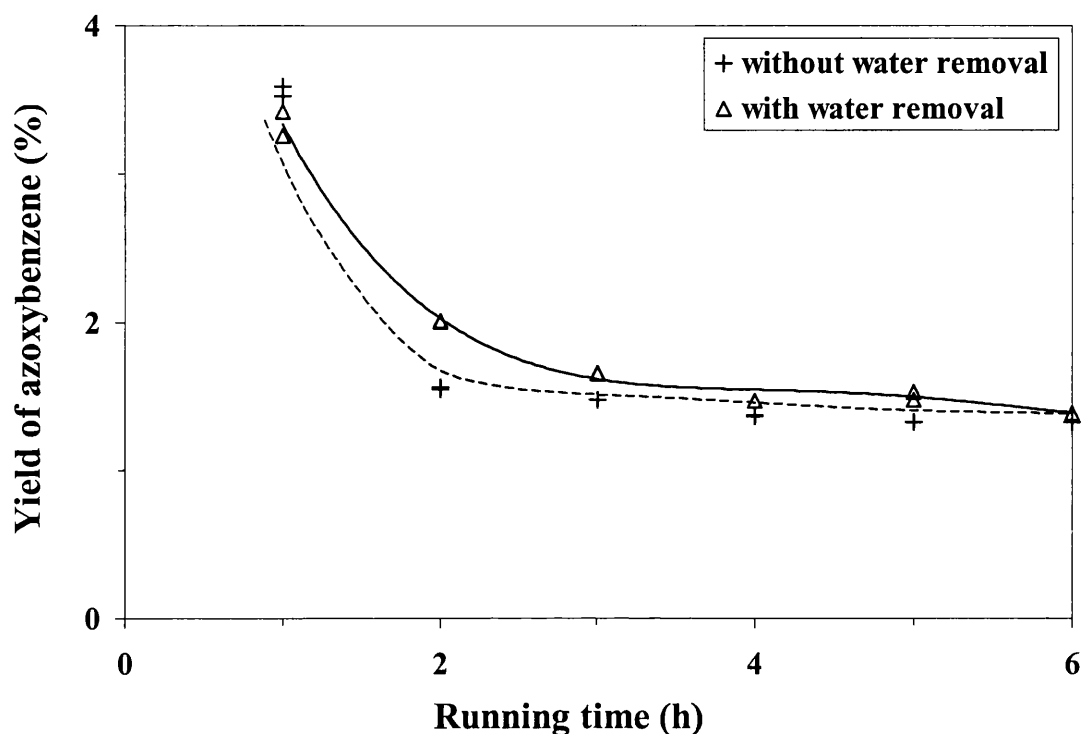
Figure 7.9   **Yield of azoxybenzene against running time at 2ml/h: TS-1**

catalyst = 0.1g, T = 70°C, H_2O_2/aniline=0.2

A lower reactant flowrate (1ml/h) was tested to observe any improvement on the product yield and selectivity (figure 7.10). Improvement on the product yield and selectivity towards azoxybenzene was more pronounced at a longer residence time (468s). The yield of azoxybenzene can go up to 10% with the use of the ZSM-5 membrane. It is believed that the presence of water would poison the TS-1 catalyst leading to catalyst deactivation and thus lower reactivity and product yield. By selectively removal of the side product water, an improvement of 35% on product yield was observed and the effect on catalyst deactivation was lessened (figure 7.10a). A selectivity of 97% towards azoxybenzene was also obtained with product removal and the average selectivity was increased by 2-3% (figure 7.10b).

An increased yield of azoxybenzene was observed with water removal. This can be explained by the fact that the presence of water will reduce the TS-1 activity. Thiele and Roland (1997) have observed the reversible deprotonation of the coordinated water which will convert most titanium sites to an ate complex with coordinated hydrogen peroxide. The ate complex does not form any active sites for reaction when in contact with hydrogen peroxide which increases the tendency for byproduct formation. It is also suspected that the presence of water may induce side reactions thus lowering the product selectivity towards azoxybenzene.

The catalyst deactivation is also caused by the adsorption of organic compounds on Ti sites. Aniline and its reaction intermediates are bigger molecules, which are likely to deposit inside the zeolite pores and will block the TS-1 pores causing diffusional hindrance (Unguina et al., 2000).

It is also interesting to note that the product yield curve seems to tend towards a constant value (figure 7.9 and 7.10a). After a reaction time of 5 hours, a similar product yield was obtained regardless of the use of a membrane for water removal. It may be due to the fact that water removal was less effective after prolonged periods of prevaporation. Uguina and co-workers (2000) have observed that longer reaction times will favour preferential chemisorption of aldehydes (product) versus styrene (reactant) in TS-1 catalysed styrene oxidation. This may be the case for selective oxidation of aniline. The proportion of aniline occluded in the spent catalyst will

decrease, while the amounts of hydroxylamines and azoxy compounds will be enhanced with reaction time.

It can be concluded that there were two mechanisms involved in catalyst deactivation: the presence of water byproduct and adsorption of organic compounds. At high reaction rates (initial running time), water adsorption is predominant causing catalyst deactivation over time while longer reaction times will favour preferential adsorption of product. That is why the catalyst deactivation was reduced with a longer running time.

Although a greater improvement on the product yield and selectivity was observed when the residence time was lengthened, this would only apply at a residence time larger than 500s. At a flowrate lower than 1ml/h (i.e. 0.5ml/h), catalyst initial deactivation was much more significant with reaction rates lower than expected. Difficulties were encountered to evenly distribute the fluid along the multiple microchannels. This will also result in bubble formation causing cavitation.
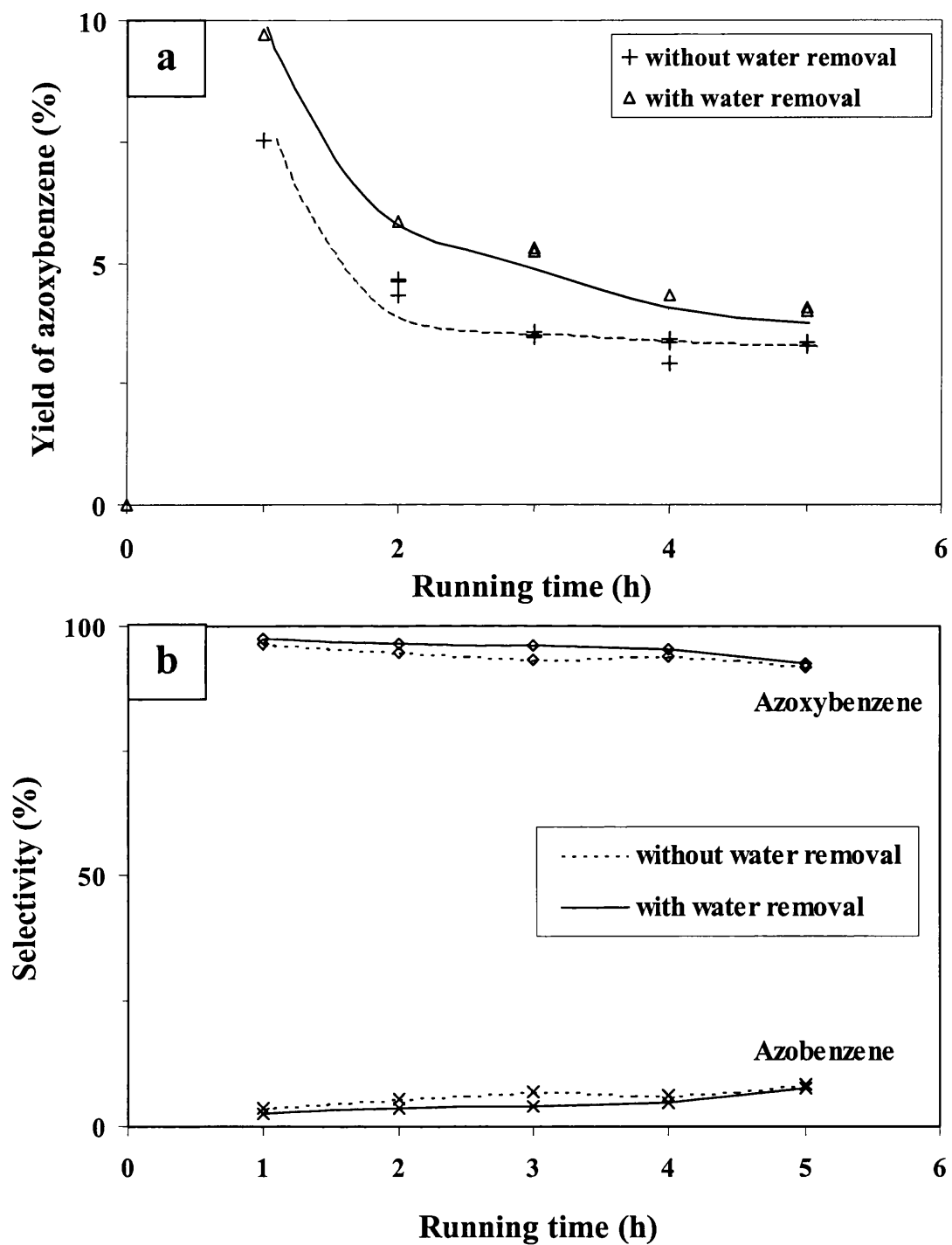
Figure 7.10 (a) Yield of azoxybenzene and (b) product selectivity against running

time at 1ml/h: TS-1 catalyst = 0.1g, T = 70°C, H_2O_2/aniline=0.2

7.3.4 Reactor performance at different temperatures

A flowrate of 1ml/h provides a sufficient time for the reactants to stay in the reactor for effective water removal. An improvement in product yield and selectivity with water removal is observed. Therefore, the optimum flowrate 1ml/h would be employed to study the reactor performance at different operating temperatures. The reaction was carried out at temperatures ranged from 30 to 90°C.

The yield of azoxybenzene was plotted against the running time at four different temperatures: 30, 50, 70 and 90°C (figure 7.11a). It is clearly shown that a higher product yield was attained when increasing the temperatures from 30 to 70°C. However, when the reaction temperature exceeded the boiling point of the solvent (chloroform), the problem of bubble formation was getting worse. This was difficult to overcome and the product yield obtained at 90°C was lower than expected. Product selectivity was observed to be best at an operating temperature of 70°C whereas the selectivity of azoxybenzene was similar at 30 and 50°C (figure 7.11b).

It is known that lower temperature will favour the equilibrium of adsorption. Therefore, high concentration of organic compounds will impose diffusional hindrance thus reducing the catalyst performance. At the same time, higher temperatures would result in larger reaction rate constants (Gontier and Tuel, 1994). Selvam and Ramaswamy (1995) have reported that the reaction temperature has a positive effect on the selectivity of azoxybenzene. The yield and selectivity towards

azoxybenzene was shown to increase with reaction temperature from 30 to 70°C. However, this effect was not observed at a reaction temperature of 90°C. Besides bubble formation, it is hypothesized that high reaction temperatures (90°C) will increase the formation of oligomeric compounds in the reaction medium (Thiele and Roland, 1997). The deposition of oligomeric compounds inside the zeolite pores will block the catalyst active sites. This may also induce side reactions thus reducing product selectivity to azoxybenzene.
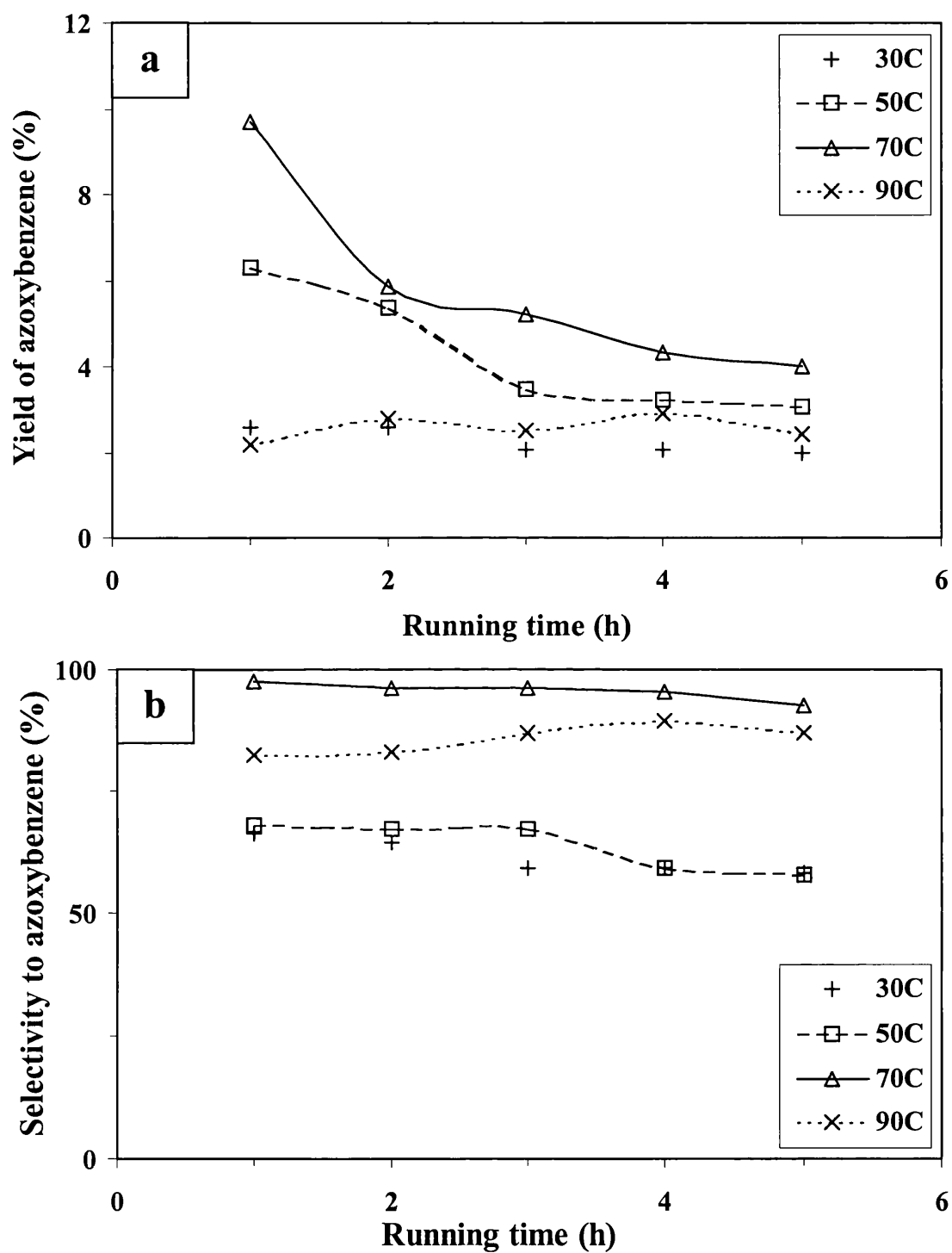
Figure 7.11 (a) Yield of azoxybenzene and (b) product selectivity against running time at different temperatures: TS-1 catalyst = 0.1g, T = 30, 50, 70 and 90°C, H_2O_2/aniline=0.2, flowrate=1.0ml/h with water removal

7.4 Concluding remarks

The application of a multichannel membrane microreactor in the study of selective oxidation of aniline was successfully demonstrated. The high surface area to volume ratio that can be attained in the microreactor ($3000m^2/m^3$) facilitates the selective removal of water by-product, which reduces the effect of catalyst deactivation during the reaction. The improvement in the product yield and selectivity towards azoxybenzene was also observed. The setup can also withstand a reaction temperature up to 150°C.

The design of the reactor system facilitates the combination of separation and reaction in one unit. This concept can be further developed for the *in-situ* production of fine chemicals, enabling isolation of reaction intermediates and pure products. The design also works well for a hazardous reaction system, for the case of aniline, which is highly toxic. The idea of enclosing and integrating the reaction processes enables safer handling of toxic and explosive chemicals.

However, the fabrication procedures of the ZSM-5 membrane and subsequent catalyst deposition are quite lengthy. A possible alternative is the use of a catalytically active membrane (i.e. H-ZSM-5, TS-1 membrane) to shorten the preparation time and improve the catalyst loading. Improvement in the reactor design should be considered to provide a better liquid distribution across the multichannel plate.

CHAPTER 8

Conclusions and Future Work

8.1   Conclusions

Microtechnology has visualized the development of microchemical devices for various chemical and biological applications. Microreactors can help to redeem the main concerns of safety and environmental issues in major chemical plants (Jensen, 2001). They can provide better energy and material utilization, leading to cost reduction and pollution abatement (Gavriilidis et al., 2002). New reaction regimes can be explored by the use of microreactors resulting in improved product yield and selectivity (Ehrfeld et al., 2000).

Catalyst incorporation is a critical task in microreactor fabrication. Metal catalysts can be deposited in microchannels using sputter coating, thermal deposition or chemical vapour deposition (Thomas and Thomas, 1997; Kursawe and Hönicke, 2000). However, these methods are only limited to metal thin film catalysts. Catalyst powders are usually packed or coated on the microchannel. Packing requires a catalyst filter structure and the pressure drop can be severe across the packed bed of catalyst powders in the microchannel (Ajmera et al., 2001). Also, catalyst powders coated onto the channel wall can delaminate during reaction resulting in lost activity and in some cases the detached powder can clog the microchannel.

Incoporating zeolite employs a different strategy, this provides room to improve current disadvantages of catalysts incorporation in microreactors. Zeolites can be grown directly onto microstructured supports providing a strong adhesion to

241

the microchannel. The silica (SiO_2) structure of zeolites can also enable the fabrication of zeolite micropatterns by employing traditional clean room techniques. A precise and localized addition of zeolite materials in a microchannel can be obtained leading to a successful integration of zeolite catalyst and membrane within the design architecture of microchemical devices. Therefore, zeolites can serve as substrates for fabrication in microchemical devices. Their microstructure and chemistry can be tailored for catalysis and separation processes (Bhatia, 1990). They possess great thermal and mechanical stability, which can withstand severe reaction conditions (Feast and Lercher, 1996).

The main objective of this project was to develop the technology and applications of zeolite-based microreactors in catalytic reactions and separation processes. The well-defined flow characteristics in the microchannel enable a better theoretical prediction of the reactor performance through the development of computer simulation models. It is expected to observe an increase in product yield and selectivity with improved mass transfer properties.

However, due to catalyst deactivation and titanium leaching from the zeolite framework, the experimental results reveal that the improvement in product yield in the microreactor is not as expected. The other reason is the presence of internal diffusion resistance within TS-1 catalysts. These findings provide an insight to further understand the microreactor performance and suggesting ways to improve the catalyst and reactor design.

The important findings from this objective are the following:

1. The thesis introduces a novel fabrication procedure to incorporate zeolite in the design of microchemical devices. The technique was based on microelectronic fabrication and zeolite thin film technologies. The ability to control zeolite film thickness and orientation has been demonstrated. High-resolution micropatterns of complex microchannel geometry and network, as well as complex catalyst arrays (size of 3μm) were successfully etched onto zeolite silicon composites. Blueprints for zeolite-based microchemical devices are presented and their structural details were analysed.

2. MFI zeolite has been employed as catalyst, membrane and structural materials in microreactors and microseparators. Zeolite powder coatings, uniform zeolite film growth, localized zeolite growth, and etching of zeolite-silicon composite films were successfully implemented for the fabrication of zeolite catalytic microreactors. Silicalite-1 was prepared as a free-standing membrane in zeolite microseparators.

3. The first prototype of zeolite catalytic microreactor has been successfully fabricated and tested for 1-pentene epoxidation. A simple computational model has been introduced for design and data interpretation to study the

microreactor performance. The modelling result was shown to compare well with the experimental data.

4. The technique to engineer the catalyst microstructure and chemistry has been demonstrated. The data obtained through computer simulation can act as a tool to better understand the catalyst properties and suggest ways of improving the microreactor performance. The catalyst performance can be improved through the addition of crystal growth inhibitors and optimum OH^- /Si ratio in synthesis solution whereas a linear relationship of catalytic activity with titanium loading was obtained. Catalyst short-term deactivation was attributed to the formation of organic compounds and presence of water. Titanium leaching was also observed from the zeolite framework.

5. Further improvement and design modification in the zeolite microreactor was carried out. A multichannel membrane microreactor has been designed and fabricated for the selective water removal in the study of selective oxidation of aniline. The high surface area to volume ratio in the microreactor facilitated the removal of water by-product, thus reducing the effect of catalyst deactivation. An improvement in product yield and selectivity was observed.

8.2   Future Work

The following suggested topics would require further investigation:

8.2.1   Improvement in TS-1 catalytic properties

The mechanism by which titanium is leached from the zeolite framework is unknown. Further studies are to understand the reaction mechanism and improve the titanium loading within the catalyst. Catalyst layers can be micropatterned to increase the surface area exposing the active sites for reaction. A detailed computational model can be established to enhance the microreactor performance.

8.2.2   *In-situ* production of chemicals

The incorporation of zeolite membranes in catalytic reactions can be further studied for *in-situ* production of chemicals, enabling selective removal of reaction intermediates and side products. Chemical reaction and product purification can be combined within the membrane microreactor. It can also be applied to explore new reaction regimes, which cannot be obtained by conventional means.

8.2.3 Scale-out of microreactor

Microreactors can be further applied in the chemical industry for fine chemical production. The annual production throughput can be obtained by repeating the basic units of microreactors to create an on-site, on-demand production network for high value added chemicals. The main task is to improve the microreactor design to achieve uniform flow distribution. Quality control should be carried out during the fabrication of the microreactors to ensure a reliable operation of scale-out systems.

8.2.4 Application of zeolite microchemcial devices

Zeolite-based microchemical devices can find applications in various biological and chemical processes. Zeolite membranes can be employed in the design of microseparators and microcontactors, serving many separation functions in a micro-analytical laboratory. A zeolite micromembrane can also be incorporated in electrochemical and sensor devices. It can act as the proton exchange membrane in a micro fuel cell. For sensor applications, the zeolite membrane can enhance the sensor performance by acting as a selective barrier. Further studies are encouraged to explore the different design and application of zeolite-based microchemical devices.

Bibliography

1. Ahn, W.S., Kang, K.K. and Kim, K.Y., 2001, Synthesis of TS-1 by microwave heating of template-impregnated SiO2–TiO2 xerogels, *Catal Lett*, 72: 229-232.

2. Ajmera, S. K, Losey, M.W, Jensen, K. F. and Schmidt, M. A., 2001, Microfabricated packed-bed reactor for phosgene synthesis, *AIChE*, 47: 1639-1647.

3. Ajmera, S. K., Delattre, C., Schmidt, M. A. and Jensen, K.F., 2002, Microfabricated cross-flow chemical reactor for catalyst testing, *Sensor Actuat B-Chem*, 82: 297-306.

4. Amiridis, M. D., Zhang, T. J. and Farrauto, R. J., 1996, Selective catalytic reduction of nitric oxide by hydrocarbons, *Appl Catal B*, 10:203-227.

5. Arasasingham, R. D., He, G. X. and Bruice, T. C., 1993, Mechanism of manganese porphyrin-catalysed oxidation of alkenes. Role of Mn(IV)-oxo species, *J Am Chem Soc*, 115: 7985-7991.

6. Armor, J. N., 1989, Catalysis with permselective inorganic membranes, *Appl Catal*, 49: 1-25.

7. Armor, J. N., 1999, Advances in chemistry - Part 1 - Catalysis: Recent value future opportunities, *Chem Eng*, 106: 70-74.

8. Arnold, J., Dasbach, U., Ehrfeld, W., Hesch, K. and Löwe, H., 1995, Combination of excimer laser micromachining and replication processes suited for large scale production, *Appl Surf Sci*, 86: 251-258.

9. Atoguchi, T. and Yao, S., 2001, Phenol oxidation over titanosilicalite-1: experimental and DFT study of solvent, *J Mol Catal A-Chem*, 176: 173-178.

10. Auroux, A., 1994, in Imeik, B. and Vedrine, J. C. (Eds), *Catalyst Characterization Physical Techniques for Solid Materails*, Plenum Press, New York.

11. Baerlocher, Ch., Meier, W. M. and Olson, D. H., 2001, *Atlas of zeolite framework types*, 5th Edition, Elsevier.

12. Bein, T., 1996, Synthesis and applications of molecular sieve layers and membranes, *Chem Mater*, 8: 1636-1653.

13. Bellussi, G., Carati, A., Clerici, M. G., Maddinelli, G. and Millini, R., 1992, Reactions of titanium silicate with protic molecules and hydrogen-peroxide, *J Catal*, 133: 220-230.

14. Bellussi, G. and Rigutto, M. S., 1994, Metal ions associated to the molecular sieve framework: possible catalytic oxidation sites, *Stud in Surf Sci and Catal*, 85: 177-213.

15. Bernal, M. P., Coronas, J., Menéndez, M. and Santamaría, J., 2002, Coupling of reaction and separation at the microscopic level: esterification processes in a H-ZSM-5 membrane reactor, *Chem Eng Sci*, 57: 1557-1562.

16. Bhatia, S., 1990, *Zeolite Catalysis: Principles and Applications*, CRC Press, Inc.

17. Biscardi, J.A. and E. Iglesia, 1998, Isotopic tracer studies of propane reactions on H-ZSM5 zeolite, *J Phys Chem B*, 102: 9284-9289.

18. Boudreau, L.C., Kuck, J. A. and Tsapatsis, M., 1999, Deposition of oriented zeolite A films: in situ and secondary growth, *J Membrane Sci*, 152: 41-59.

19. Burkett, S.L. and Davis, M. E., 1994, Mechanism of structure direction in the synthesis of Si-ZSM-5: An investigation by intermolecular ^{1}H-^{29}Si CP MAS NMR, *J Phy Chem*, **98**: 4647-4653.

20. Burkett, S. L. and Davis, M. E., 1995, Mechanism of structure direction in the synthesis of pure-silica zeolites. 1. Synthesis of TPA/Si-ZSM-5, *Chem Mater*, 7: 920-928.

21. Carati, A., Flego, C., Berti, D., Millini, R., Perego, C., Stocchi, B. and Perego, C., 1999, Influence of synthesis media on the TS-1 characteristic, *Stud in Surf Sci and Catal*, 125: 45-52.

22. Caro, J., Noack, M., Kölsch P. and Schäfer, R, 2000, Zeolite membranes - state of their development and perspective, *Microporous Mesoporous Mat*, 38: 3-24.

23. Casanave, D., Giroir-Fendler, A., Sanchez, J., Loutaty, R. and Dalmon, J.-A., 1995, Control of transport properties with a microporous membrane reactor to enhance yields in dehydrogenation reactions, *Catal Today*, 25: 309–314.

24. Chao, K. J., Lin, J. C., Wang, Y. and Lee, G. H., Single-crystal structure refinement of TPA ZSM-5 zeolite, *Zeolites*, 1986, 6: 35-38.

25. Chau, J. L. H., Tellez, C., Yeung, K. L. and Ho, K., 2000, The role of surface chemistry in zeolite membrane formation, *J Membr Sci*, 164: 257-275.

26. Chau, J. L. H., Leung, A. Y. L. and Yeung, K. L., 2002a, Design, fabrication and performance of zeolite micromembranes, ISCRE-17, Hong Kong, August 25-28.

27. Chau, J. L. H., Wan, Y. S. S., Gavriilidis, A. and Yeung, K. L., 2002b, Incorporating zeolites in microchemical systems, *Chem Eng J*, 88: 187-200.

28. Chau, J. L. H. and Yeung, K. L., 2002, Zeolite microtunnels and microchannels, *Chem Comm*, 9: 960-961.

29. Chau, J. L. H., Leung, A. Y. L., Shing, M. B., Yeung, K. L. and Chan, C. M., 2003a, Hydrogen and proton transport properties of nanoporous zeolite micromembranes, in Tang, Z. and Sheng, P. (Eds), *Nano Science and Technology: Novel Structure and Phenomena*, Taylor and Francis, London.

30. Chau, J. L. H., Leung, A. Y. L. and Yeung, K. L., 2003b, Zeolite micromembranes, *Lab-on-a-Chip*, 3: 53.

31. Chen, L.Y., Chuah, G.K., Jaenicke S., 1998, Propylene epoxidation with hydrogen peroxide catalyzed by molecular sieves containing framework titanium, *J Mol Catal A*, 132: 281–292.

32. Cheng, M., Lin, L., Yang, W., Yang, Y., Xu, Y. and Li, X., 1997, Growth of oriented zeolite crystal membranes, *Stud in Surf Sci and Catal*, 105: 2233.

33. Choudhary, V.R., Nayak, V. S. and Mamman, A. S., 1992, Diffusion of straight- and branched-chain liquid compounds in H-ZSM-5 zeolite, *Ind Eng Chem Res*, 31: 624-628.

34. Claus, P., Hönicke, D. and Zech T., 2001, Miniaturization of Screening Devices for the Combinatorial Development in Heterogeneous Catalysts, *Catal Today*, 67: 319-339.

35. Clerici, M.G., 1991, Oxidation of saturated hydrocarbons with hydrogen peroxide, catalysed by titanium silicalite, *Appl Catal*, 68:249-261.

36. Clerici, M. G., Bellussi, G. and Romano, U., 1991, Synthesis of propylene oxide from propylene and hydrogen peroxide catalysed by titanium silicalite, *J Catal*, 129: 159-167.

37. Clerici, M.G., 1993, Catalytic oxidations with hydrogen peroxide: new selective catalysts, *Stud in Surf Sci and Catal*, 78: 21-33.

38. Clerici, M. G. and Ingallina, P., 1993, Epoxidation of lower olefins with hydrogen peroxide and titanium silicalite, *J Catal*, 140: 71-81.

39. Commenge, J. M., Falk, L., Corriou, J. P. and Matlosz, M., 2002, Optimal design for flow uniformity in microchannel reactors, *AIChE J*, 48(2): 345-358.

40. Coronas, J. and Santamaria, J., 1999a, Separations using zeolite membranes, *Sep Purification Meth,* 28: 127–177.

41. Coronas, J. and Santamaria, J., 1999b, Catalytic reactors based on porous ceramic membranes, *Catal Today*, 51: 377–389.

42. Cronstedt, A.F., 1756, Ron och beskrifning om en obekant bärg art, som kallas zeolites. Kongl., *Vetenskaps Acad. Handl*, Stockholm 17: 120-123.

43. Davies, L., McMorn, P., Bethell, D., Page, P. C. B., King, F., Hancock, F. E. and Hutchings, G.J., 2000, By-product formation causes leaching of Ti from redox molecular sieve TS-1, *Chem Comm*, 1807-1808.

44. Davies, L., McMorn, P., Bethell, D., Page, P. C. B., King, F., Hancock, F. E. and Hutchings, G.J., 2001a, Effect of preparation method on leaching of Ti from the redox molecular sieve TS-1, *Phys Chem Chem Phys*, 3: 632-639.

45. Davies, L., McMorn, P., Bethell, D., Page, P. C. B., King, F., Hancock, F. E. and Hutchings, G.J., 2001b, Epoxidation of Crotyl Alcohol Using Ti-Containing

Heterogeneous Catalysts: Comments on the Loss of Ti by Leaching, *J Catal*, 198: 319-327.

46. Davis, M.E. and Lobo, R.F., 1992, Zeolite and molecular sieve synthesis, *Chem Mater*, 4: 756-768.

47. Davis, M.E., 1998, Zeolite-based catalysts for chemicals synthesis, *Microporous Mesoporous Mat*, 21: 173-182.

48. de Aragón, 1998, Space applications of micro/nano-technologies, *J Micromech Microeng*, 8: 54-56.

49. Delannay, F., 1984, Charaterization of Heterogeneous Catalysts, Dekker, New York.

50. den Exter, M.J., van Bekkum, H., Rijn, C.J.M., Kapteijn, F., Moulijn, J. A., Schellevis, H. and Beenakker, C. I. N., 1997, Stability of oriented silicalite-1 films in view of zeolite membrane preparation, *Zeolites*, 19: 13-20.

51. Deubel, D. V., Sundermeyer, J. and Frenking, G., 2000, Theoretical studies of molybdenum peroxo complexes [MoOn(O2)3-n(OPH3)] as catalysts for olefin epoxidation, *Inorg Chem*, 39: 2314-2320.

52. Derouane, E.G., Crehan, G., Dillon, C.J., Bethell, D., He, H. and Derouane-Abd Hamid, S.B., 2000, Zeolite catalysts as solid solvents. 2 Competitive adsorption of the reactants and products in Friedel Crafts acetylation of anisole and toluene, *J Catal*, 194: 410-423.

53. Drago, R.S., Dias, S.C., McGilvray, J.M. and Mateus, A.L.M.L., 1998, Acidity and Hydrophobicity of TS-1, *J Phys Chem B,* 102: 1508-1514.

54. Drost, M. K., Call, C. J., Cuta, J. M. and Wegeng, R. S., 1997, Microchannel evaporator/combustor thermal process, *Microscale Therm Eng*, 1: 321-332.

55. Drost, M. K., Wegeng, R. S., Martin, P. M., Brooks, K. P., Martin, J. L. and Call, C., 2000, Microheater, *Proc 4th Inter Conf on Microreaction Technol, Atlanta*, 308-313.

56. Dutta, K, 1970, Integrated micromotor concept, *Proc Int Conf on Microelectronics Circuits and System Theory*, 36.

57. Ehrfeld, W., Hessel, V. Löwe, H., Schulz, Ch. and Weber, L., 1999, Materials of LIGA technology, *Microsystem Technol*, 5: 105-112.

58. Ehrfeld, W., Hessel, V. and Löwe, H., 2000, *Microreactors: New technology for modern chemistry*, Wiley-VCH, Weinheim.

59. Espinoza, R., Santamariá, J., Menéndez, M., Coronas, J., Irusta, S., 1998, *Rep South Africa Patt Appl Ner* 985093.

60. Fatikow, S. and Rembold, U., 1997, *Microsystem Technology and Microrobotics*, Springer, Berlin.

61. Feast, S. and Lercher, J. A., 1996, Synthesis of intermediates and fine chemicals using molecular sieve catalysts, *Stud in Surf Sci and Catal*, 102: 363-412.

62. Flanigen, E.M., J.M. Bennett, R.W. Grose, J.P. Cohen, R.L. Patton, R.M. Kirchner and J.V. smith, 1978, Silicalite, a new hydrophobic crystalline silica molecular sieve, *Nature*, 271: 512-516.

63. Fogler, H. S., 1992, *Elements of chemical reaction engineering*, Prentice-Hall, Upper Saddle River, USA.

64. Franz, A. J., Quiram, D., Srinivasan, R., Hsing, I. M., Firebaugh, S. L., Jensen, K. F. and Schmidt, M. A., 1998, New operating regimes and applications feasible with microreactors, *Proc 2nd Int Conf on Microreaction Technol, New Orleans*, 33-38.

65. Froment, G. F. and Bischoff, K. B., 1990, *Chemical reactor analysis and design*, John Wiley & Sons, Inc., New York.

66. Funke, H. H., Argo, A. M., Baertsch, C. D., Falconer, J. L. and Noble, R. D., 1996a, Separation of close-boiling hydrocarbons with silicalite zeolite membranes, *J Chem Soc-Farad Trans,* 92: 2499-2502.

67. Funke, H. H., Kovalchick, M. G., Falconer, J. L. and Noble, R. D., 1996b, Separation of hydrocarbon isomer vapors with silicalite zeolite membranes, *Ind Eng Chem Res*, 35: 1575-1582.

68. Gao, H., G. Lu, J. Suo and S. Li, 1996, Epoxidation of allyl chloride with hydrogen pewroxide catalysed by titanium silicalite-1, Appl. Catal. A, 138, 27-38.

69. Gavriilidis, A., Angeli, P., Cao, E., Yeong, K. K. and Wan, Y. S. S., 2002, Technology and applications of microengineered reactors, *Trans IChemE*, 80: 3-30.

70. Gobby, D., Angeli, P. and Gavriilidis, A., 2001, Mixing characteristics of T-type microfluidic mixers, *J Micromech Microeng*, 11: 126-132.

71. Gontier, S. and Tuel, A., 1994, Oxidation of aniline over TS-1, the titanium substituted silicalite-1, Appl Catal A, 118: 173-186.

72. Gouzinis, A. and Tsapatsis, M., 1998, On the preferred orientation and microstructural manipulation of molecular sieve films prepared by secondary growth, *Chem Mater*, 10: 2497-2504.

73. Greenway, G.M., Haswell, S. J., Morgan, D. O., Skelton, V. and Styring, P., 2000, The use of a novel microreactor for high throughput continuous flow organic synthesis, *Sensor Actuat B-Chem*, 63: 153-158.

74. Grzybowska-Swierkosz, B. and Haber, J., 1994, Catalysis, *Annu Rep Prog Chem C*, 91: 395.

75. Hardt, S., Ehrfeld, W., Hessel, V. and Vanden, K.M., 2000, Strategies for size reduction of microreactors by heat transfer enhancement effects, *Proc 4th Inter Conf on Microreaction Technol, Atlanta*, 432-440.

76. Harris, D. C., 1996, *Exploring Chemical Analysis*, W.H. Freeman and Company, New York, 286-287.

77. Haswell, S.J., Middleton, R.J., O'Sullivan, B., Skelton, V., Watts, P. and Styring, P., 2001, The application of micro reactors to synthetic chemistry, *Chem Commun*, 391-398.

78. Hedlund, J., Schoeman, B. and Sterte, J., 1997, Ultrathin oriented zeolite LTA films, *Chem Commun*, 13: 1193-1194.

79. Hedlund, J., Mintova, S. and Sterte, J., 1999, Controlling the preferred orientation in silicalite-1 films synthesized by seeding, *Microporous Mesoporous Mater*, 28: 185-194.

80. Hölderich, W. F. and van Bekkum, H., 1991, Zeolites in organic synthesis, *Stud in Surf Sci and Catal*, 58: 631-726.

81. Hisng, I. M., Srinivasan, R., Harold, M. P., Jensen, K.F. and Schmidt, M. A., 2000, Simulation of micromachined chemical reactors for heterogeneous partial oxidation reactions, *Chem Eng Sci*, 55: 3-13.

82. Hsieh, H. P., 1991, Inorganic membrane reactors, *Catal Rev*, 33: 1-70.

83. Hutchings, G. J., Lee, D. F. and Minihan, A. R., 1995, Epoxidation of allyl alcohol to glycidol using titanium silicalite TS-1: effect of the method of preparation, *Catal Lett*, 33: 369-385.

84. Illgen, U., Schäfer, R., Noack, M., Kölsch, P., Kühnle, A. and Caro, J., 2001, Membrane supported catalytic dehydrogenation of iso-butane using MFI zeolite membrane reactor, *Catal Comm*, 2: 339-345.

85. Ingallina, P., Clerici, M. G., Rossi, L. and Bellussi, G., 1995, Catalysis with TS-1: new perspectives for the industrial use of hydrogen peroxide, *Stud Surf Sci Catal*, 92: 31-39

86. Jacobs, P. A. and Martens, J. A., 1991, Introduction to acid catalysis with zeolites in hydrocarbon reactions, *Stud in Surf Sci and Catal*, 58: 445-496.

87. Jakeway, S. C., de Mello, A. J. and Russell, E. L., 2000, Miniaturized total analysis systems for biological analysis, *Fresen J Anal Chem*, 366: 525-539.

88. Jansen, J. C. and van Rosmalen, G. M., 1993, Oriented growth of silica molecular sieve crystals as supported films, *J Crystals Growth*, 128: 1150-1156.

89. Jansen, J. C., Kashchiev, D. and Erdem-Senatalar, A., 1994, Preparation of coatings of molecular sieve crystals for catalysis and separation, *Stud in Surf Sci and Catal*, 85: 215-250.

90. Jensen, K. F., 1999, Microchemical systems: status, challenges, and opportunities, *AIChE .*, 45: 2051-2054.

91. Jensen, K.F., 2000, Microfluidics module lecture notes.

92. Jensen, K. F., 2001, Microreaction engineering - is small better?, *Chem Eng Sci*, 56: 293-303.

93. Jenzer, G., Mallat, T., Maciejewski, M., Eigenmann, F. and Baiker, A., 2001, Continuous epoxidation of propylene with oxygen and hydrogen on a Pd-Pt/TS-1 catalyst, *Appl Catal A*, 208: 25-133.

94. Johansson, S., Schweitz, J. Å., Westberg, H. and Boman, M., 1992, Microfabrication of three-dimensional boron structures by laser chemical processing, *J Appl Phys*, 72: 5956-5963.

95. Jung, K. T. and Shul, Y. G., 1997, Preparation of transparent TS-1 zeolite film by using nanosized TS-1 particles, *Chem of Mater*, 9: 420.

96. Karnik, S. V., Hatalis, M. K. and Kothare, M. V., 2001, Palladium based micro-membrane for water gas shift reaction and hydrogen gas separation, *5th Int. Conf. Microreaction Tech.*, Strasbourg, France, May, 27-30.

97. Kawahara, N., Suto, T., Hirano, T. Ishikawa, Y., Kitahara, T., Ooyama N. and Ataka, T., 1997, Microfactories: new applications of micromachine technology to the manufacture of small products, *Microsystems Technol.*, 3: 37- 41.

98. Kieboom A .P. G, Moulijn, J. A., Sheldon, R. A., and van Leeuwen, P. W. N. M., 1999, Catalytic processes in industry, *Stud in Surf Sci and Catal*, 123: 29-80.

99. Klein, S. and Maier, W.F., 1996, Microporous mixed oxides – catalysts with tunable surface polarity, *Angew Chem Int Ed Engl*, 35: 2230-2233.

100. Koegler, J. H., Zandbergen, H. W., Harteveld, J. L. N., Nieuwenhuizen, M. S., Jansen, J. C. and van Bekkum, H., 1994, Oriented coatings of silicalite-1 for gas sensor applications, *Stud in Surf Sci and Catal*, 84: 307-314.

101. Koegler, J. H., van Bekkum, H. and Jansen, J. C., 1997, Growth model of oriented crystals of zeolite Si-ZSM-5, *Zeolites,* 19: 262-269.

102. Kokotailo, G. T., S. L. Lawton, D. H. Olson and W. M. Meier, 1978, Structure of synthetic ZSM-5, *Nature*, 27: 437-438.

103. Krull, F. and Endres, H.-E., 1993, Spürnasen: Grundbauelemente der chemischen Mikrosensorik, *Technische Rundschau*, 18: S28-34, 20: S46-52.

104. Krummradt, H., Koop, U. and Stoldt, J., 2000, Experience with the use of microreactors in organic synthesis, *Proc 3rd Inter Conf on Microreaction Technol,* Frankfurt, Germany, 181-185.

105. Kumar, S.B., Mirajkar, S. P., Pais, G.C.G., Kumar, P. and Kumar, R., 1995, Epoxidation of styrene over titanium silicalite molecular sieve TS-1 using dilute H_2O_2 as oxidizing agent, *J Catal*, 156, 163-166.

106. Kursawe, A. and Hönicke, D., 2000, Epoxidation of ethene with pure oxygen as a model reaction for evaluating the performance of microchannel reactors, *Proc of the 4th Inter Conf on Microreaction Technol*, Atlanta, Georgia, 153-166.

107. Kusakabe, K., Kuroda, T., Murata, A. and Morooka, S., 1997, Formation of a Y-type zeolite membrane on a porous α-alumina tube for gas separation, *Ind Eng Chem Res*, 36: 649-655.

108. Kusakabe, K., Kuroda, T. and Morooka, S., 1998, Separation of carbon dioxide from nitrogen using ion-exchanged faujasite-type zeolite membranes formed on porous support tubes, *J Membr Sci*, 148: 13-23.

109. Lai, S. M., Au, L. T. Y. and Yeung, K. L., 2002, Influence of synthesis conditions and growth environment on MFI zeolite film orientation, *Microporous Mesoporous Mater*, 54: 63-77.

110. Lai, S. M., Martin-Aranda, R., Yeung, K. L., 2003, Knoevenagel condensation reaction in a membrane microreactor, *Chem Comm*, 2: 218-219.

111. Lamberti, C., Bordiga, S., Arduino, D., Zecchina, A., Geobaldo, F., Spano, G., Genoni, F., Petrini, G., Carati, A., Villain, F. and Vlaic, G., 1998, Evidence of the presence of two different framework Ti(IV) species in Ti-silicalite-1 in vacuo conditions: an EXAFS and a photoluminescence study, *J Phys Chem B*, 102: 6382-6390.

112. Langhendries, G., De Vos, D. E., Baron, G. V. and Jacobs, P.A., 1999, Quantitative sorption experiments on Ti-zeolites and relation with α-Olefin oxidation by H_2O_2, *J Catal*, 187: 453-463.

113. Lehr, H. and Ehrfeld, W., 1994, Advanced microstructure products by synchrotron radiation lithography, *J de Physique IV*, 4: 229-236.

114. Lerou, J. J. and Ng, K. M., 1996, Chemical reaction engineering: a multiscale approach to multiobjective task, *Chem Eng Sci*, 51: 1595-1614.

115. Lin, Y. S., 2001, Microporous and dense inorganic membranes: current status and prospective, *Sep Purif Technol*, 25: 39-55.

116. Losey, M. W., Isogai, S., Schmidt, M. A. and Jensen, K. F., 2000, Microfabricated devices for multiphase catalytic processes, *Proc of the 4th Inter Conf on Microreaction Technol*, Atlanta, U.S.A., 416-422.

117. Lovallo, M. C., Gouzinis, A. and Tsapatsis, M., 1998, Synthesis and characterization of oriented MFI membranes prepared by secondary growth, *AIChE J*, 44: 1903-1913.

118. Löwe, H. and Ehrfeld, W., 1999, State-of-the-art in microreaction technology: concepts, manufacturing and applications, *Electrochimica Acta*, 44: 3679-3689.

119. Lunsford, J.H., 1987, Synthesis, characterisation and reaction of transition metal complexes in zeolites, *Review in Inorganic Chemistry*, vol 9, no.1.

120. Madou, M., 1997, *Fundamentals of Microfabrication*, CRC Press, New York.

121. Mantegazza, M.A., Petrini, G., Spanò, G., Bagatin, R. and Rivetti F., 1999, Selective oxidations with hydrogen peroxide and titanium silicalite catalyst, *J Mol Catal A*, 146: 223–228.

122. Martin, P. M., Matson, D. W. and Bennett, W. D., 1999, Microfabrication methods for microchannel reactors and separations systems, *Chem Eng Commun*, 173: 245-254.

123. Maspero, F. and Romano, U., 1994, Oxidation of alcohols with H_2O_2 catalyzed by titanium silicalite-1, *J Catal*, 146: 476-482.

124. Matson, D. W., Martin, P. M., Stewart, D. C., Tonkovich, A. L. Y., White, M., Zilka, J. L. and Roberts, G. L., 1999, Fabrication of microchannel chemical reactors using a metal lamination process, *Proc 3rd Inter Conf on Microreaction Technol*, Frankfurt, Germany, 62-71.

125. Maxwell, I. E. and Stork, W. H. J., 1991, Hydrocarbon processing with zeolites, *Stud in Surf Sci and Catal*, 58: 571-630.

126. McMorn, P., Roberts, G. and Hutchings, G. J., 1999, Oxidation of glycerol with hydrogen peroxide using silicalite and aluminophosphate catalysts, *Catal Lett*, 63: 193-197.

127. Meier, W.M. and C. Baerlocher, 1999, Zeolite type frameworks: connectivities, configuration and conformations, in: H. G. Karge and J. Weitkamp (Eds.), *Molecular Sieves: Science and Technology*, Vol. 2, Springer-Verlag, Berlin, 141-161.

128. Menz, W., Mohr, J. and Paul, O., 2001, *Microsystem Technology*, Wiley-VCH, Weinheim.

129. Mitchell, M. C., Spikmans, V., Manz, A. and de Mello, A. J., 2001, Microchip-based synthesis and total analysis systems (μSYNTAS): chemical microprocessing for generation and analysis of compound libraries, *J Chem Soc Perk T 1*, 5: 514-518.

130. Mukhopadhyay, S. M. and Garofalini, S. H., 1990, Surface Studies of TiO_2-SiO_2 Glasses By X-Ray Photoelectron Spectroscopy, *J Non Cryst Sol*, 126: 202.

131. Niemantsverdriet, J.W., 1993, Catalyst characterisation with spectroscopic techniques, *Stud in Surf Sci and Catal*, 79: 363-400.

132. Nishizaka, Y. and Misono, M., 1993, Catalytic reduction of nitrogen monoxide by methane over palladium-loaded zeolites in the presence of oxygen, *Chem Lett* 1295–1298.

133. Nomura, M., Yamaguchi, T. and Nakao, S., 1998, Ethanol/water transport through silicalite membranes, *J Membrane Sci*, 144: 161-171.

134. Notari, B., 1996, Microporous crystalline titanium silicates, *Adv Catal*, 41: 253-334.

135. Olson, D. H., Kokotailo, G. T., Lawton, S. L. and Meier, W. M., 1981, Crystal Structure and Structure-Related Properties of ZSM-5, *J Phys Chem*, 85: 2238-2243.

136. On, D. T., Bonnevoit, L., Bittar, A., Sayari A. and Kaliaguine, S., 1992, titanium sites in titanium silicalites: an XPS, XANES and EXAFS study, J Mol Catal, 74: 233-249.

137. Paul, B, K., Dewey, T. Alman, D. and Wilson, R. D., 2000, Intermetallic microlamination for high-temperature reactors, *4th Int Conf Microreaction Tech*, Atlanta, GA, 236–243.

138. Perego, G., Millini, R. and Bellussi, G., 1998, Synthesis and characterization of molecular sieves containing transition metals in the framework, in: Karge, H. G. and Weitkamp, J. (Eds.), *Molecular Sieves: Science and Technology*, Vol. 1, Springer-Verlag, Berlin, 187-227.

139. Piner, R. D., Zhu, J., Xu, F., Hong, S. H. and Mirkin, C. A., 1999, Dip-Pen Nanolithography, *Science*, 283: 661-663.

140. Post, M. F. M., 1991, Diffusion in zeolite molecular sieves, *Stud in Surf Sci and Catal*, 58: 391-443.

141. Quiram, D. J., Hsing, I. M., Franz, A. J., Jensen, K. F. and Schmidt, M. A., 2000, Design issues for membrane-based, gas phase microchemical systems, *Chem Eng Sci*, 55: 3065-3075.

142. Rebrov, E. V., Seijger, G. B. F., Calis, H. P. A., de Croon, M. H. J. M., van den Bleek, C. M. and Schouten, J. C., 2001, The preparation of highly ordered single layer ZSM-5 coating on prefabricated stainless steel microchannels, *Appl Catal A*, 206: 125-143.

143. Rebrov E.V., de Croon M. H. J. M., Schouten, J. C., 2002, Development of the kinetic model of platinum catalyzed ammonia oxidation in a microreactor, *Chem Eng J*, 90:61-76.

144. Reynaerts, D., Heeren, P.H. and van Brussel, H., 1997, Microstructuring of silicon by electro-discharge machining (EDM) .1. Theory, *Sensor Actuat A-Phys*, 60: 212-218.

145. Richter, Th., Ehrfeld, W., Hessel, V., Löwe, H., Storz, M. and Wolf, A., 2000, A flexible multi-component microreaction system for liquid phase reactions, *Proc 3rd Inter Conf on Microreaction Technol,* Frankfurt, Germany, 636-644.

146. Robertson, J. K., 2001, A vertical micromachined resistive heater for a micro-gas separation column, *Sensor Actuat A-Phys*, 91: 333-339.

147. Rodemerck, U., Ignaszewski, P., Lucas, M., Claus, P. and Baerns, M., 2000, Parallel synthesis and fast screening of heterogeneous catalysts, *Topic Catalysis*, 13: 249-252.

148. Sakuae, S., Tsubakino, T., Nishiyama, Y. and Ishii, Y., 1993, Oxidation of aromatic-amines with hydrogen peroxide catalysed by cetylpyridinium heteropolyoxometalates, *J Org Chem*, 58: 3633-3638.

149. Salomón, M. A., Coronas, J., Menéndez, M. and Santamaría, J., 2000, Synthesis of MTBE in zeolite membrane reactors, *Appl Catal A*, 200: 210-210.

150. Sano, T., Mizukami, F., Takaya, H., Mouri, T. and Wananbi, M., 1992, Growth Process of ZSM-5 Film, *Bull Chem Soc Jpn*, 65: 146-154.

151. Sano, T., Yanagishita, H., Kiyozumi, Y., Mizukami, F. and Haraya, K., 1994, Separation of ethanol/water mixture by silicalite membrane on pervaporation, *J Membr Sci*, 95: 221-228.

152. Saracco, G. and Specchia, V., 1994, Catalytic inorganic-membrane reactors: present experience and future opportunities, *Catal Rev*, 36: 305-384.

153. Sato, S., Yu-u, Y., Yahiro, H., Mizuno, N. and Iwamoto, M., 1991, Cu-ZSM-5 zeolite as highly active catalyst for removal of nitrogen monoxide from emission of diesel engines, *Appl Catal*, 70: L1–L5.

154. Schmidt, K., Ehricht, R., Ellinger, T. and McCaskill, J. S., 1998, A microflow reactor with components for mixing, separation and detection for biochemical experiments, *Proc. of the 2nd Int Conf on Microreaction Technol*, New Orlean, U.S.A., 125-126.

155. Schmidt, I., Krogh, A., Wienberg, K., Carlsson, A., Brorson, M. and Jacobsen, C. J. H., 2000, Catalytic epoxidation of alkenes with hydrogen peroxide over first Mesoporous titanium-coating zeolite, *Chem Commun*, 2157-2158.

156. Schoeman, B. J., Erdem-Senatalar, A., Hedlund J. and Sterte, J., 1997, The growth of sub-micron films of TPA-silicalite-1 on single crystal silicon wafers from low-temperature clear solutions, *Zeolites*, 19: 21-28.

157. Selvam, T. and Ramaswamy, A. V., 1995, Selective catalytic oxidation of aniline to azoxybenzene over titanium silicalite molecular sieves, *Catal Lett*, 31: 103-113.

158. Shea, K. J. and Kim, J. S., 1992, Influence of strain of chemical reactivity, relative reactivity of torsionally distorted double bonds in MCPBA epoxidations, *J Am Chem Soc*, 114: 3044-3051.

159. Sheldon, R. A., 1996, *Applied Homogeneous Catalysis with Organometallic Compounds*, eds. B. Cornils and W. A. Herrmann, VCH, Weinheim, vol. 1, 411.

160. Sheldon, R. A, 1997, Catalysis: The key to waste minimization, *J Chem Technol Biotecnol*, 68: 381-388.

161. Sheldon, R. A., Wallau, M., Arends, I. W. C. E. and Schuchardt, U., 1998, Heterogeneous catalysts for liquid-phase oxidations: Philosophers' stones or Trojan horses?, *Acc Chem Res*, 31: 485-493.

162. Sienel, G., Rieth, R. and Rowbottom, K. T., 1999, *Ullmann's Encyclopedia of Organic Chemicals,* vol. 4, Wiley-VCH, Weinheim.

163. Sonawane, H. R., Pol, A. V., Moghe, P. P., Biswas, S. S. and Sudalai, A., 1994, Selective catalytic-oxidation of arylamines to azoxybenzenes with H_2O_2 over zeolites, *Chem Comm*, 10: 1215-1216.

164. Srinivasan, R., Hsing, I. M., Berger, P. E., Jensen, K. F., Firebaugh, S. L., Schmidt, M. A., Harold, M. P., Lerou, J. J. and Ryley, J. F., 1997,

Micromachined reactors for catalytic partial oxidation reactions, *AIChE J*, 43: 3059-3069.

165. Suzuki, H., 1987, Composite membrane having a surface layer of an ultrathin film of cage-shaped zeolite and process for production thereof, *US Patent* 4699892.

166. Swern, D., 1971, *Organic Peroxides*, vol. 2, Wiley Interscience, New York.

167. Tantanak, D., Vincent, M.A. and Hillier, I.H., 1998, Elucidation of the mechanism of alkene epoxidation by hydrogen peroxide catalysed by titanosilicates: a computational study, *Chem Commun*, 1031-1032.

168. Taramasso, M., G. Perego and B. Notari, 1983, Preparation of porous crystalline synthetic material comprised of silicon and titanium oxide, *U.S. Patent*, 4,410,501.

169. TeGrotenhuis, W. E., Cameron, R. J., Butcher, M. G., Martin, P. M. and Wegeng R. S., 1999, Microchannel devices for efficient contacting of liquids in solvent extraction, *Sep Sci Technol*, 34: 951-974.

170. TeGrotenhuis, W. E., Wegeng, R. S., Vanderwiel, D. P., Whyatt, G. A., Viswanathan, V. V., Schielke, K. P., Sanders, G. B. and Peters, T. A., 2000, Microreactor system design for NASA in situ propellant production plant on Mars, *Proc 4th Inter Conf on Microreaction Technol*, Atlanta, 343-348.

171. Thiele, G. F. and Roland, E., 1997, Propylene epoxidation with hydrogen peroxide and titanium silicalite catalyst: Activity, deactivation and regeneration of the catalyst, *J Mol Catal A*, 117: 351-356.

172. Thomas, J. M. and Thomas, W. J., 1997, *Principles and practice of heterogeneous catalysis*, VCH Publishers, New York.

173. Thompson, R.W., 1998, Recent Advances in the Understanding of Zeolite Synthesis, in: H. G. Karge and J. Weitkamp (Eds.), *Molecular Sieves: Science and Technology*, Vol. 1, Springer-Verlag, Berlin, 1-33.

174. Tollari, S., Cuscela, M. and Porta, F., 1993, Catalytic-oxidation of primary aromatic-amines to the corresponding nitroso-compounds by H_2O_2 and [MO(O)(O_2)_2(H_2O)(HMPA)] (HMPA=hexamethylphosphoric triamide), *Chem Comm*, 19: 1510-1511.

175. Tonti, S., Roffia, P., Cesana, A., Mantegazza, M. and Padovan, M., 1988, *Eur Pat* 314147.

176. Tsapatsis, M., Xomeritakis, G., Hillhouse, H., Nair, S., Nikolakis, V., Bonilla G. and Lai, Z., 1999, Zeolite membranes, *Cattech*, 3: 148-163.

177. Tuel, A., Diab, J., Gelin, P., Dufaux, M., Dutel, J. F. and Taarit, Y. B., 1990, EPR evidence for the isomorphous substitution of titanium in silicalite structure, *J Mol Catal*, 63: 95-102.

178. Turner, C., Shaw, J., Miller, B. and Bains, V., 2000a, Vapour stripping using a micro-contactor, *Proc of the 4th Inter Conf on Microreaction Technol*, Atlanta, Georgia, 106-113.

179. Turner, C., Shaw, J., Miller, B. and Bains, V., 2000b, Solvent extraction using micro-mesh reactors, *Proc of the 4th Inter Conf on Microreaction Technol*, Atlanta, Georgia, 334-340.

180. Uguina, M. A., Serrano, D. P., Sanz, R., Fierro, J. L. G., López-Granados, M. and Mariscal, R., 2000, Preliminary study on the TS-1 deactivation during styrene oxidation with H_2O_2, *Catal Today*, 61: 263-270.

181. van Bekkum, H., Geus, E. R. and Kouwenhoven, H. W., 1994, Supported zeolite systems and applications, *Stud in Surf Sci and Catal*, 85: 509-542.

182. van Bekkum, H., 1998, Zeolite catalysts for the production of organic chemicals, *Proc of 1998 Catalysis and Zeolite Workshop*, Hsinchu, Taiwan.

183. van Koningsveld, H., van Bekkum, H. and Jansen, J.C., 1987, On the location and disorder of the tetrapropylammonium (TPA) ion in zeolite ZSM-5 with improved framework accuracy, *Acta Crystallogr,* B43:127-132.

184. van der Pol, A. J. H. P., Verduyn, A. J. and van Hooff, J. H. C., 1992, Why are some titanium silicalite-1 samples active and others not, *Appl Catal A,* 92:113-130.

185. van der Pol, A. J. H. P. and van Hooff, J. H. C., 1993, Parameters affecting the synthesis of titanium silicalite-1, *Appl Catal A*, 92: 93-111.

186. van Koningsveld, H., van Bekkum, H. and Jansen, J. C., 1987, On the location and disorder of the tetrapropylammonium (TPA) ion in zeolite ZSM-5 with improved framework accuracy, *Acta Cryst*, B43: 127-132.

187. Vayssilov, G. N., 1997, Structural and physiochemical features of titanium silicalites, *Catal Rev – Sci Eng*, 39: 209-251.

188. Vayssilov, G. N., Popova, Z. and Tuel, A., 1997, Catalytic oxidation of anisole over titanium silicalite-1, *Chem Eng Technol*, 20: 33-337.

189. Védrine, J. C., 2000, Combinatorial catalysis and high throughput catalyst testing: conclusions of the workshop on "high throughput catalytic testing: its challenges", *Combinatorial catalysis and high throughput catalyst design and testing, Kluwer, Netherlands*, 467-473.

190. Wachs, I. E., 1992, *Characterization of Catalytic Material*, Butterworth-Heinemann, Boston.

191. Wakao, N. and Kaguei, S., 1982, *Heat and mass transfer in packed beds*, Gordon and Breach Science Publishers, New York, USA.

192. Wan, Y. S. S., Chau, J. L. H., Gavriilidis, A. and Yeung, K. L., 2001, Design and fabrication of zeolite-based microreactors and membrane microseparators, *Microporous Mesoporous Mat*, 42: 157-175.

193. Wan, Y. S. S., Gavriilidis, A., Chau, J. L. H. and Yeung, K. L., 2002, TS-1 zeolite microengineered reactors for 1-pentene epoxidation, *Chem Commun*, 8: 878-879.

194. Wegeng, R.S. and Drost, M.K., 1998, Opportunities for distributed processing using micro chemical systems, *Proc 2nd Int Conf on Microreaction Technol, New Orleans*, 3-9.

195. Wießmeier, G. and Hönicke, D., 1996a, Heterogeneously catalyzed gas-phase hydrogenation of cis,trans,trans-1,5,9-cyclododecatriene on palladium catalysts having regular pore systems, *Ind Eng Chem Res*, 35: 4412-4416.

196. Wießmeier, G. and Hönicke, D., 1996b, Microfabricated components for heterogeneously catalysed reactions, *J Micromech Microeng*, 6: 285-289.

197. Wise, K. D. and Najafi, K., 1991, Microfabrication techniques for integrated sensors and microsystems, *Science*, 254: 1335-1342.

198. Wörz, O., Jäckel, K. P., Richter, Th., and Wolf, A., 1998, Microreactors, a new efficient tool for optimum reactor design, *Proc 2nd Inter Conf on Microreaction Technol, New Orleans*, 183-185.

199. Wörz, O., Jäckel, K. P., Richter, Th. and Wolf, A., 2001, Microreactors, a new efficient tool for optimum reactor design, *Chem Eng Sci*, 56: 1029-1033.

200. Wu, S. Q, Bouchard, C. and Kaliaguine, S., 1998, Zeolite containing catalytic membranes as interphase contactors, *Res Chem Intermediat*, 24: 273-289.

201. Xomeritakis, G., Gouzinis, A., Nair, S., Okubo, T., He, M. Y., Overney, R. M. and Tsapatsis, M., 1999, Growth, microstructure, and permeation properties of supported zeolite (MFI) films and membranes prepared by secondary growth, *Chem Eng Sci*, 54: 3521-3531.

202. Yan, Y. and Bein, T., 1995, Zeolite thin films with tunable molecular sieve function, *J Amer Chem Soc*, 117: 9990-9994.

203. Zaman, J. and Chakma, A., 1994, Inorganic membrane reactors, *J Membr Sci*, 92: 1-28.

204. Zech, T. and Hönicke, D., 2000, Simultaneous screening of catalysts in microchannels: methodology and experimental setup, *Proc 3rd Inter Conf on Microreaction Technol, Springer, Berlin*, 260-266.

205. The IZA Structure Commission, http://www.iza-sc.ethz.ch/IZA-SC/Atlas/data/models/MFI_mod.html, viewed on 5/5/203.

206. Database of zeolite structures, http://www.zeolites.ethz.ch/zeolites, viewed on 5/5/203.

Appendix A1

Calculation of Reaction Constants for 1-Pentene Epoxidation

A1.1   Calculation of external surface area of TS-1 catalyst

External surface area of colloidal silicalite-1

BET surface area for synthesized crystals (before calcination) = $60 m^2 g^{-1}$

Crystal size, $\varepsilon = 100 nm = 0.1 \mu m$

The density of zeolite crystals will remain constant, $\rho = 1.6 \times 10^6$ g m^{-3}

Thus, the external surface area per catalyst weight is inversely proportional to the crystal size, ε:

$$\frac{\text{external surface area}}{\text{catalyst density} \times \text{catalyst volume}} = \frac{4\pi\left(\dfrac{\varepsilon}{2}\right)^2}{\rho \times \dfrac{4}{3}\pi\left(\dfrac{\varepsilon}{2}\right)^3} = \frac{6}{\rho\varepsilon}$$

For TS-1 of crystal size 2μm,

Corresponding surface area per unit mass of catalyst:

$$S_a = 60 m^2 g^{-1} \times \frac{0.1}{2} = 3.00 m^2 g^{-1}$$

Therefore, the surface area per unit mass of catalyst for crystal size, ε can be calculated:

$$S_a = 60 m^2 g^{-1} \times \frac{0.1}{\varepsilon} \tag{A1.1}$$

Crystal size, ε (μm)	External surface area, Sa (m^{2}g^{-1})
2	3.00
2.5	2.40
3	2.00
3.5	1.71
4	1.50

Table A1.1   External surface area for different crystal sizes, ε

A1.2 Calculation of first order reaction constant for 1-pentene epoxidation

First order reaction with respect to hydrogen peroxide

$r' = -k'_1[H_2O_2]$

Catalysts weight, $W = 0.1\text{g}$ (crystal size, $\varepsilon = 2\mu\text{m}$)

External surface area per unit mass of catalyst, $S_a = 3.00 \ m^2g^{-1}$

Total external surface area, $A = 3.00m^2g^{-1} \times 0.1g = 0.30m^2$

Assume first order reaction w. r. t. $[H_2O_2]$,

$$r' = -k'_1[H_2O_2] \tag{A1.2}$$

$$\frac{d[H_2O_2]}{dt} = -k'_1[H_2O_2]$$

$$-\int_{[H_2O_2]_0}^{[H_2O_2]} \frac{d[H_2O_2]}{[H_2O_2]} = k'_1 \int_0^t dt$$

$$\ln\frac{[H_2O_2]_0}{[H_2O_2]} = k'_1 t \tag{A1.3}$$

A graph of $ln\dfrac{[H_2O_2]_0}{[H_2O_2]}$ (obtained experimentally), was plotted against time, t.
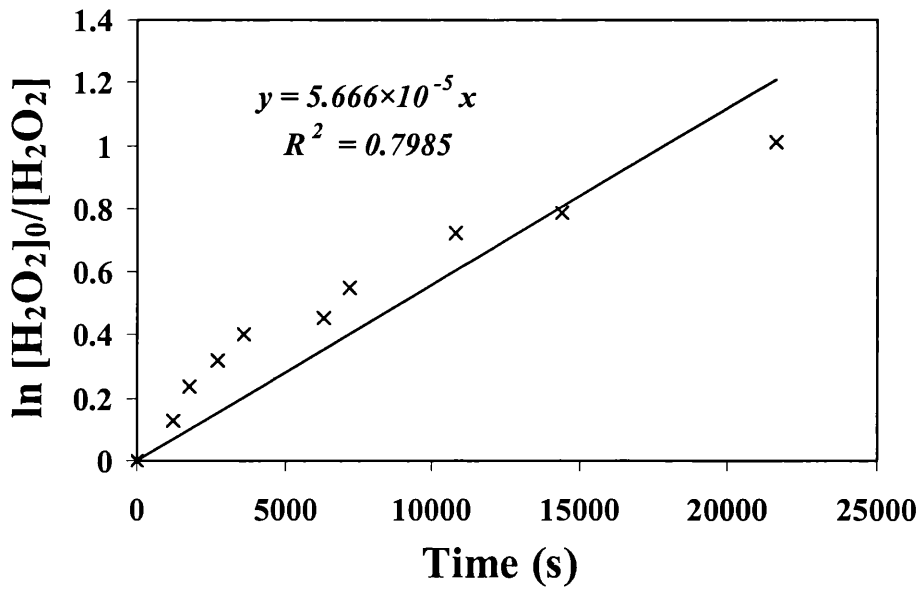
Figure A1.1 Graph of $ln\frac{[H_2O_2]_0}{[H_2O_2]}$ against time, t (s) for first order reaction

Slope of the graph $\quad m = k'_1 = 5.666\times10^{-5}\,s^{-1}$

$$k_1 = k'_1\times\frac{Volume\ of\ batch\ reactor,V}{Total\ external\ surface\ area\ of\ catalyst,A} \qquad (A1.4)$$

$$V = 5\times10^{-5}\,m^3$$

$$k_1 = 5.666\times10^{-5}\,s^{-1}\times\frac{5\times10^{-5}\,m^3}{0.3m^2} = \underline{\underline{9.443\times10^{-9}\,ms^{-1}}}$$

A1.3 Calculation of second order reaction constant for 1-pentene epoxidation

Second order reaction with respect to hydrogen peroxide and 1-pentene

$r ' = -k'_2 [H_2O_2][C_5]$

Catalysts weight, $W = 0.1g$

Assume second order reaction w. r. t. $[H_2O_2]$ and $[C_5]$,

$$r' = -k'_2[H_2O_2][C_5] \tag{A1.5}$$

$$\frac{d[H_2O_2]}{dt} = -k'_2 [H_2O_2][C_5] \qquad \theta_0 = \frac{[C_5]_0}{[H_2O_2]_0}$$

$$[H_2O_2]_0 \frac{d(1-\chi)}{dt} = -k'_2 [H_2O_2]_0 (1-\chi)[H_2O_2]_0 (\theta_0 - \chi)$$

$$\chi = \frac{[H_2O_2]_0 - [H_2O_2]}{[H_2O_2]_0}$$

$$[H_2O_2]_0 \frac{d\chi}{dt} = k'_2 [H_2O_2]_0 (1-\chi)[H_2O_2]_0 (\theta_0 - \chi)$$

$$\int_0^\chi \frac{d\chi}{(1-\chi)(\theta_0 - \chi)} = k'_2 [H_2O_2]_0 \int_0^t dt$$

$$\frac{1}{\theta_0 - 1} \ln \frac{\theta_0 - \chi}{\theta_0 (1-\chi)} = k'_2 [H_2O_2]_0 t$$

Express the above in terms of $[H_2O_2]$ & $[C_5]$

$$\frac{1}{\theta_0 - 1} \ln \frac{\theta_0 - \chi}{\theta_0 (1-\chi)} = k'_2 [H_2O_2]_0 t$$

$$\frac{1}{\dfrac{[C_5]_0}{[H_2O_2]_0} - 1} \ln \frac{\dfrac{[C_5]_0}{[H_2O_2]_0} - \dfrac{[H_2O_2]_0 - [H_2O_2]}{[H_2O_2]_0}}{\dfrac{[C_5]_0}{[H_2O_2]_0} \dfrac{[H_2O_2]}{[H_2O_2]_0}} = k'_2 [H_2O_2]_0 t$$

$$\frac{[H_2O_2]}{[C_s]_0 - [H_2O_2]_0} \ln \frac{\dfrac{[C_s]_0 - [H_2O_2]_0 + [H_2O_2]}{[H_2O_2]_0}}{\dfrac{[C_s]_0}{[H_2O_2]_0} \dfrac{[H_2O_2]}{[H_2O_2]_0}} \times \frac{1}{[H_2O_2]_0} = k'_2 t$$

$$\frac{1}{[C_s]_0 - [H_2O_2]_0} \ln \frac{[C_s][H_2O_2]_0}{[C_s]_0[H_2O_2]} = k'_2 t$$

$$\frac{1}{[H_2O_2]_0 - [C_s]_0} \ln \left(\frac{[H_2O_2][C_s]_0}{[C_s][H_2O_2]_0} \right) = k'_2 t$$

$$\ln \left(\frac{[H_2O_2][C_s]_0}{[C_s][H_2O_2]_0} \right) = k'_2 \left([H_2O_2]_0 - [C_s]_0 \right) t \qquad\qquad \text{(A1.6)}$$

$$\ln \xi = k'_2 \left([H_2O_2]_0 - [C_s]_0 \right) t \qquad \text{where} \qquad \xi = \left(\frac{[H_2O_2][C_s]_0}{[C_s][H_2O_2]_0} \right)$$

$[H_2O_2]$ and $[C_s]$ were experimental values obtained from Iodometric titration and GC analysis respectively.

278

0

-0.2   0   +   5000   10000   15000   20000   25000

-0.4

$\ln \xi$ -0.6 $y = -5.333 \times 10^{-5}x$
$R^2 = 0.8298$

-0.8

-1

-1.2

Time (s)
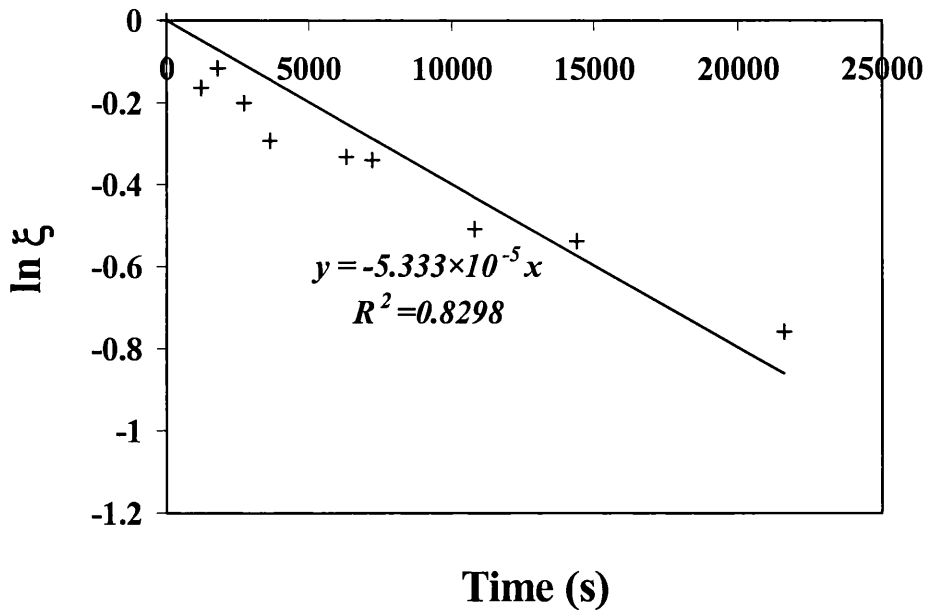
Figure A1.2   Graph of *ln* ξ against time, *t (s)* for second order reaction

Slope of the graph, $m = -5.333 \times 10^{-5} s^{-1} = k'_2 \left([H_2O_2]_0 - [C_S]_0 \right)$

$[H_2O_2]_0 = 330 molm^{-3}$ $[C_S]_0 = 1493 molm^{-3}$

$k'_2 = \dfrac{-5.333 \times 10^{-5} s^{-1}}{(330 - 1493)molm^{-3}} = 4.586 \times 10^{-8} m^3 s^{-1} mol^{-1}$

$k_1 = k'_1 \times \dfrac{Volume \ of \ batch \ reactor, V}{Total \ external \ surface \ area \ of \ catalyst, A}$ (A1.4)

$k_2 = 4.586 \times 10^{-8} m^3 s^{-1} mol^{-1} \times \dfrac{5 \times 10^{-5} m^3}{0.3m^2} = \underline{\underline{7.643 \times 10^{-12} m^4 mol^{-1} s^{-1}}}$
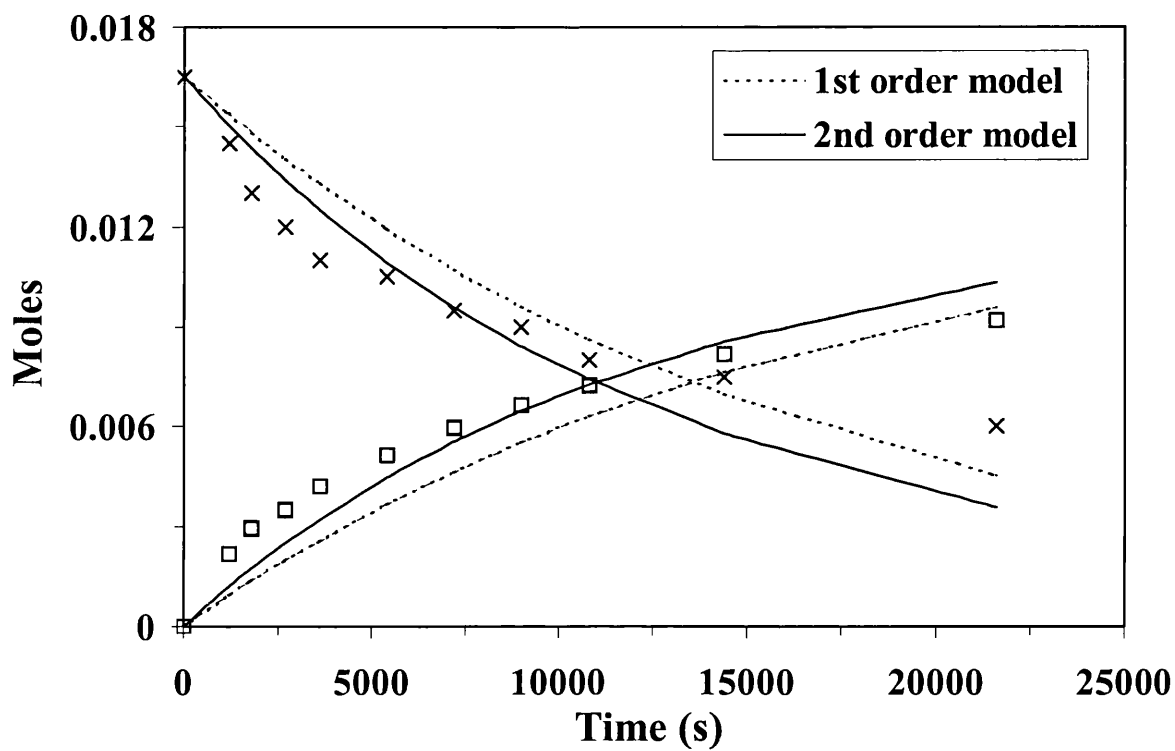
Figure A1.3 Moles of hydrogen peroxide reactant and 1,2-epoxypentane product in the batch reactor as a function of reaction time. ($[H_2O_2]_0 = 0.33$ M, $[C_5]_0 = 1.49$ M, catalyst loading = 2g/L, $\delta = 5$ μm, $\varepsilon = 2$ μm, $\beta = 2.5$ at.%, T = 298 K, x – hydrogen peroxide, □ - 1,2-epoxypentane)

Appendix A2

Calculation of Titanium Content in TS-1 Catalyst

A2.1   Calculation of titanium content, β (%) in TS-1 catalyst from XPS

result
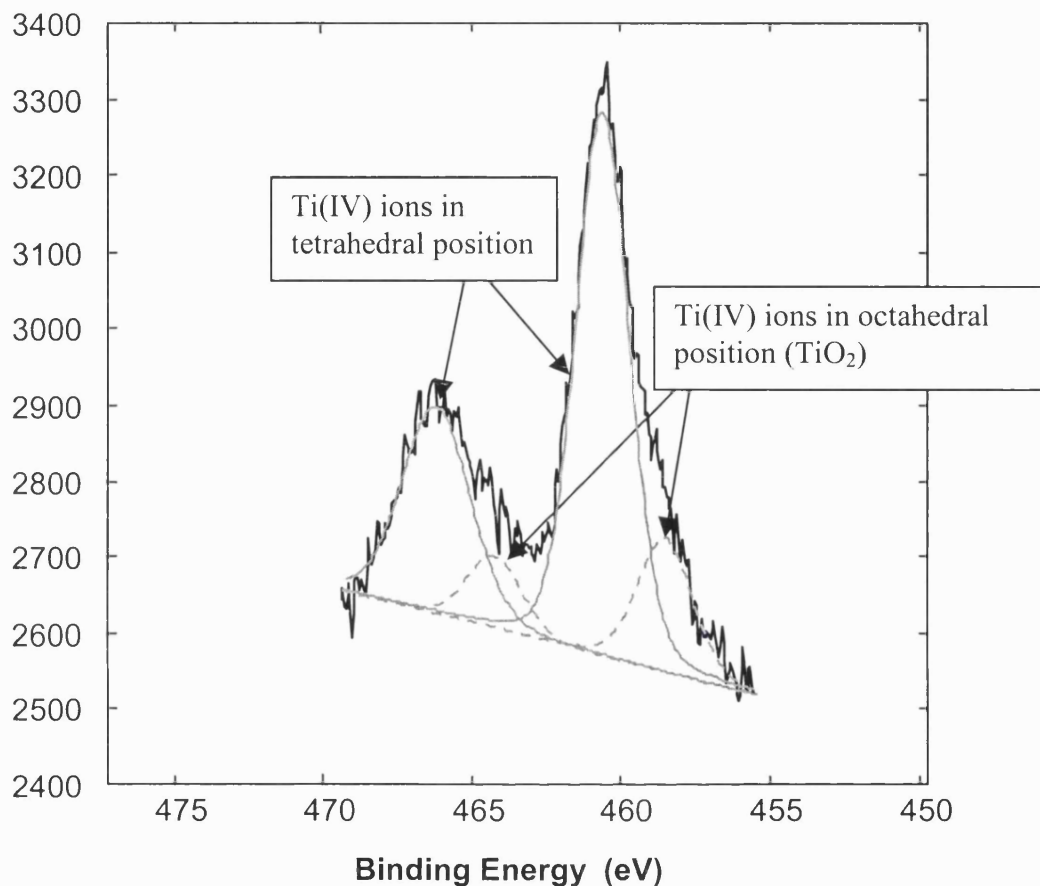
Figure A2.1   X-ray photoelectron spectrum for titanium silicalite-1

The ratio of atomic concentration of Si to Ti is 40.96 from XPS result. Curve fitting was applied to locate the binding energies of Ti 2p (figure A2.1). The area ratios of octahedrally-coordinated Ti(IV) and tetrahedrally-coordinated Ti(IV) were obtained to calculate the atom % of Ti(IV) incorporated with the silicalite framework as shown in table A2.1.

Peak	Position (eV)	Area %
Ti 2p$_{3/2}$ octahedral position	458.49	13.43%
Ti 2p$_{3/2}$ tetrahedral position	460.59	53.24%
Ti 2p$_{1/2}$ octahedral position	464.24	6.71%
Ti 2p$_{1/2}$ tetrahedral position	466.34	26.62%

Table A2.1   Area ratios of Ti 2p binding energies

The incorporation of Ti(IV) in tetrahedral position is calculated in the following:

$$\frac{1}{40.96} \times (53.24\% + 26.26\%) = 1.95\%$$

Appendix A3

Correlation of Titanium Content with Reaction Constant

A3.1 Correlation of titanium content, β (%) with reaction constant, k_2 ($m^4 s^{-1} mol^{-1}$)

The overall yield of epoxypentane was modelled by varying the value of k_2 ($m^4 s^{-1} mol^{-1}$) in the Femlab model at $\varepsilon = 2\mu m$ and $\theta = 4.5$ with a channel width, w of $500\mu m$. The results were tabulated in table A3.1:

k_2 ($m^4 s^{-1} mol^{-1}$)	Theoretical yield, Ψ (%) $\tau = 100$s
2.09E-11	24.12
1.57E-11	19.17
1.31E-11	16.47
1.04E-11	13.59
7.59E-12	10.17
4.18E-12	5.85
2.09E-12	3.06
7.59E-13	1.17
7.59E-14	0.18

A3.1 **Reaction constants of second order reaction, k_2 with the corresponding product yield, Ψ obtained from Femlab model**

The modelled product yields, Ψ (%) were plotted against the corresponding values of k_2 ($m^4s^{-1}mol^{-1}$) as shown in figure A3.1.


$$\Psi = -1E20\ k_2^{\ 2} + 1E10\ k_2$$

$$R^2 = 1$$
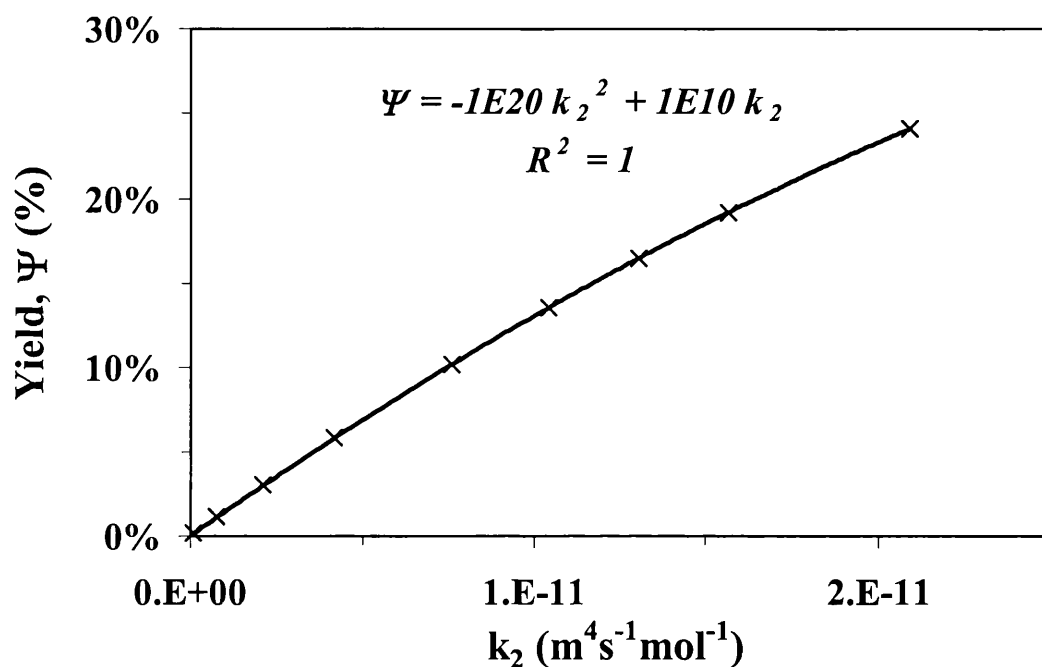
Figure A3.1 Plot of modelled product yields, Ψ (%) against the corresponding reaction constants of second order reaction, k_2 ($m^4s^{-1}mol^{-1}$)

The k_2 ($m^4s^{-1}mol^{-1}$) values can be calculated from the product yield, Ψ (%) by the following equation:

$$k_2 = 9E\text{-}11\ \Psi^2 + 7E\text{-}11\ \Psi \qquad\qquad (A3.1)$$

The experimental value of product yield, Ψ (%) obtained from the catalyst with different titanium content, β (%) was tabulated below. The corresponding k_2 ($m^4s^{-1}mol^{-1}$) values were calculated by using equation A3.1. The k_2 ($m^4s^{-1}mol^{-1}$) values were plotted against titanium content, β (%) in figure A3.2 to find out their correlation.

Titanium content, β (%)	Experimental yield, Ψ (%) $\tau = 100s$	k_2 calculated with equation A2.1 ($m^4s^{-1}mol^{-1}$)
0.88	2.04	1.47E-12
1.39	0.70	4.98E-13
1.52	2.52	1.82E-12
1.74	2.98	2.17E-12
2.13	5.16	3.85E-12
3.48	11.63	9.35E-12

Table A3.2   Titanium content, β (%) and experimental product

yield, Ψ (%) with the calculated k_2 ($m^4s^{-1}mol^{-1}$) values
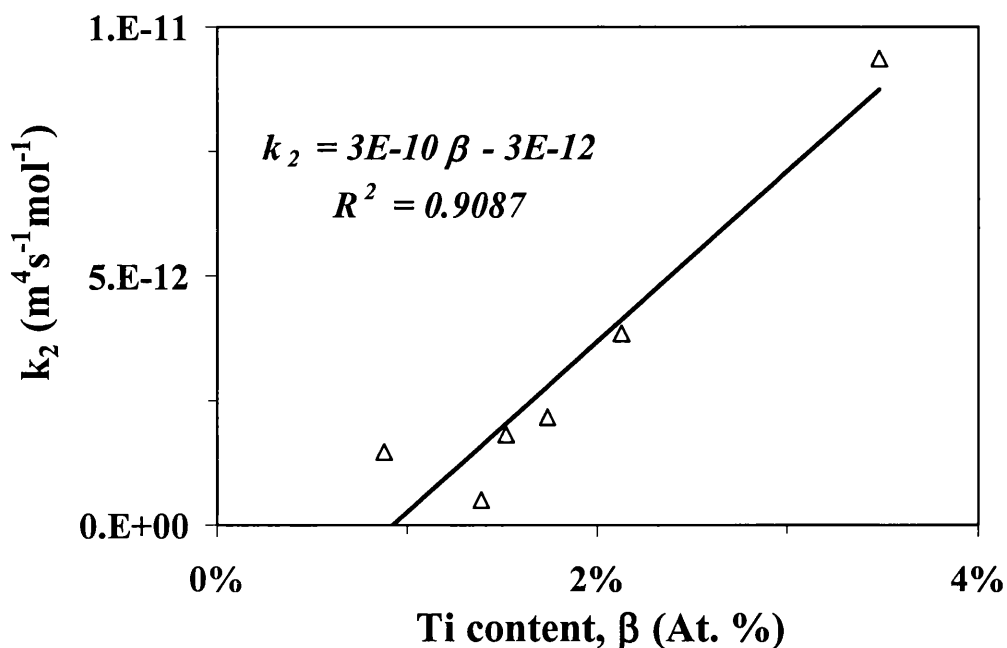
Figure A3.2 Plot of k_2 $(m^4s^{-1}mol^{-1})$ values against titanium content, β $(\%)$

Vayssilov and co-workers (1997) have reported that for TS-1 catalysed oxidation of anisole, catalyst activity is directly proportional to the titanium-content of the catalyst. Therefore, a simple linear relationship between titanium content and kinetic constant was assumed taking into account that TS-1 catalysts with less than 1 at.% titanium content are inactive for the epoxidation reaction.

Equation A3.2 gives the correlation between k_2 values $(m^4s^{-1}mol^{-1})$ with titanium content, β $(\%)$:

$$k_2 = 3E\text{-}10\beta - 3E\text{-}12 \tag{A3.2}$$

Therefore, the corresponding k_2 values $(m^4s^{-1}mol^{-1})$ can be calculated from titanium content, β $(\%)$ using equation A3.2.

k_2	Theoretical yield, Ψ	Theoretical titanium content, β
$(m^4 s^{-1} mol^{-1})$	$(\%)$ $\tau = 100s$	$(\%)$
2.09E-11	24.12	7.517
1.57E-11	19.17	5.862
1.31E-11	16.47	5.035
1.04E-11	13.59	4.208
7.59E-12	10.17	3.306
4.18E-12	5.85	2.223
2.09E-12	3.06	1.562
7.59E-13	1.17	1.141
7.59E-14	0.18	0.924

Table A3.3 k_2 values $(m^4 s^{-1} mol^{-1})$ values with the corresponding yield, $\Psi(\%)$ and titanium content, $\beta(\%)$

The product yield, Ψ (%) was plotted against the calculated titanium content, β (%) which agrees well with the experimental values as shown in figure A3.3.
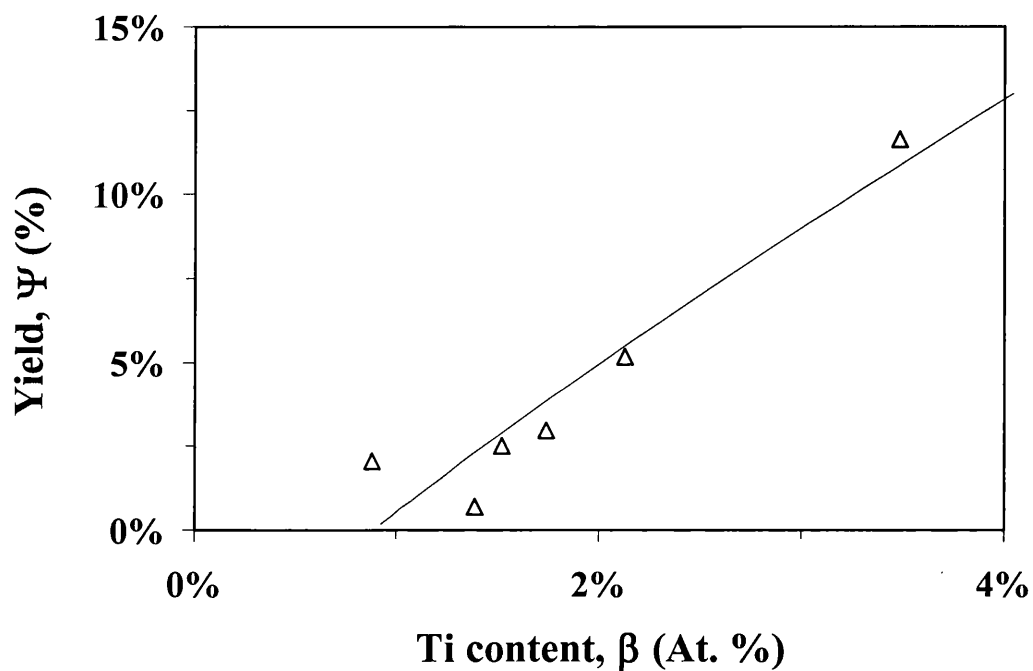
Figure A3.3 1,2-epoxypentane yield as a function of titanium-content at a

fixed residence time of 100s. (w = 500 μm, δ = 5 μm, ε = 2-2.5

μm, $[H_2O_2]_0$ = 0.2 M, θ = 4.5 and T = 298 K)

(symbols – experimental data, lines – model data)

Appendix A4

Calculation of Weisz-Prater Parameter

A4.1 Calculation of Weisz-Prater Parameter

The Weisz-Prater parameter, Φ for first-order reaction is defined by (Froment and Bischoff, 1990, Fogler, 1992),

$$\Phi = \frac{r'(obs)V\rho L^2}{D_{eff}C_{AS}W}$$ (A4.1)

where r' (obs) = observable rate of hydrogen peroxide conversion $(mol\,m^{-3}s^{-1})$

V = reactor volume (m^3)

W = catalyst weight (g)

L = characteristic length, $\varepsilon/6$

C_{AS} = concentration of species A at the external surface of the catalyst $(mol\,m^{-3})$

ρ = catalyst density $(g\,m^{-3})$

$D_{eff(intra)}$ = intra crystal diffusitivity (m^2s^{-1})

Choudhary et al. (1992) have stated that the liquid phase diffusitivities of n-pentanol and n-hexane in H-ZSM-5 zeolites at 293K are 2.6×10^{-15} and 1×10^{-13} m^2s^{-1}. For TS-1 with a pore size of 0.55nm, diffusivity value as low as 1×10^{-17} is also possible (figure A4.1). However, there is no literature value for diffusitivity for TS-1 and 1-pentene. Assumption made is that the value will lie around the above range. The nature and charge of the cation present may also have a distinctive effect on the effective pore diameter of zeolites, which are not considered here for titanium siliclaite-1 (Post, 1991). The calculated Weisz-Prater parameter is an approximation to determine whether the reaction is internal diffusional limited. The range of diffusivity of 1-pentene is taken to be in the range of 5×10^{-13} to 1×10^{-16} m^2s^{-1}.

Weisz-Prater parameter, Φ in batch reactor,

$$\Phi = \frac{\left(\dfrac{330-220}{3600}\right) \times 5 \times 10^{-5} \times 1.6 \times 10^{6} \times \left(\dfrac{2 \times 10^{-6}}{6}\right)^{2}}{1 \times 10^{-16} \times 330 \times 0.1} = 82.3$$

$$\Phi = \frac{\left(\dfrac{330-220}{3600}\right) \times 5 \times 10^{-5} \times 1.6 \times 10^{6} \times \left(\dfrac{2 \times 10^{-6}}{6}\right)^{2}}{5 \times 10^{-13} \times 330 \times 0.1} = 0.016$$

Weisz-Prater parameter, Φ in microreactor,

$$\Phi = \frac{\left(\dfrac{200-180}{100}\right) \times 1.55 \times 10^{-9} \times 1.6 \times 10^{6} \times \left(\dfrac{2 \times 10^{-6}}{6}\right)^{2}}{1 \times 10^{-16} \times 200 \times 7.36 \times 10^{-5}} = 37.4$$

$$\Phi = \frac{\left(\dfrac{200-180}{100}\right) \times 1.55 \times 10^{-9} \times 1.6 \times 10^{6} \times \left(\dfrac{2 \times 10^{-6}}{6}\right)^{2}}{5 \times 10^{-13} \times 200 \times 7.36 \times 10^{-5}} = 0.0075$$
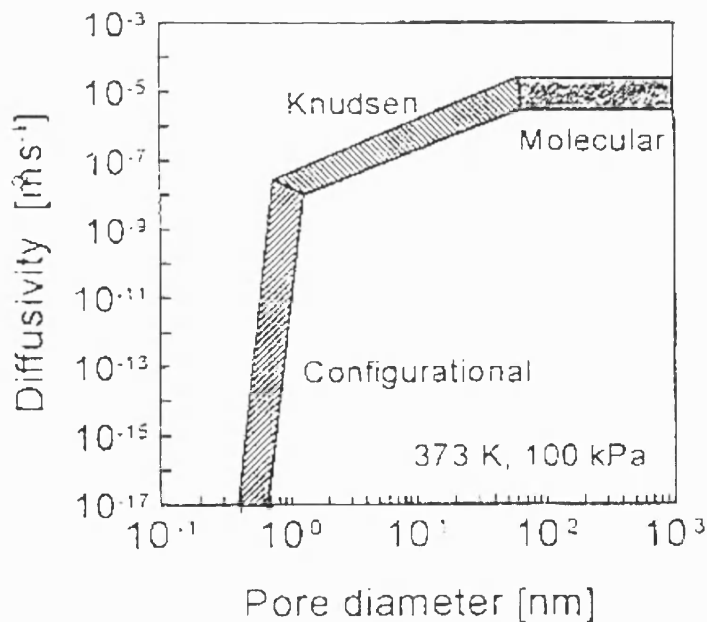

Figure A4.1   Effect of zeolite pore diameter on the order of magnitude of diffusitivities (Post, 1991)

Appendix A5

Calculation of Pressure Drop in Microreactor

A5.1 Pressure drop calculation in microreactor

Pressure drop, $\Delta P = \dfrac{12Ql\mu}{dw^3}$ where (A5.1)

Q = volumetric flowrate (m³s⁻¹) = $\dfrac{volume\ of\ microreactor}{residence\ time}$

V = volume of microreactor = $1.548 \times 10^{-9}\,m^3$

τ = residence time (s) where $\tau = 50\text{-}1000s$

l = length of mixing channel (m) where $l = 0.02m$

μ = viscosity (Nsm⁻²) where viscosity of methanol = $5.4 \times 10^{-4}\ Nsm^{-2}$

d = depth of channel (m) where $d = 250\mu m = 2.5 \times 10^{-4}\,m$

w = width of channel (m) where $w = 50\text{-}1000\mu m = 5 \times 10^{-5} - 1 \times 10^{-3}\,m$

Sample calculation of pressure drop at a residence time of 100s and a channel width, w of 500µm (Jensen, 2000):

At $\tau = 100s$, $w = 500\mu m = 5 \times 10^{-4}\,m$

$$\Delta P = \frac{12Ql\mu}{dw^3}$$ (A5.1)

$$= \frac{12Vl\mu}{\tau dw^3}$$

$$= \frac{12 \times 1.55 \times 10^{-9} \times 0.02 \times 5.4 \times 10^{-4}}{100 \times 2.5 \times 10^{-4} \times \left(5 \times 10^{-4}\right)^3}$$

$$= 0.06428Nm^{-2}$$
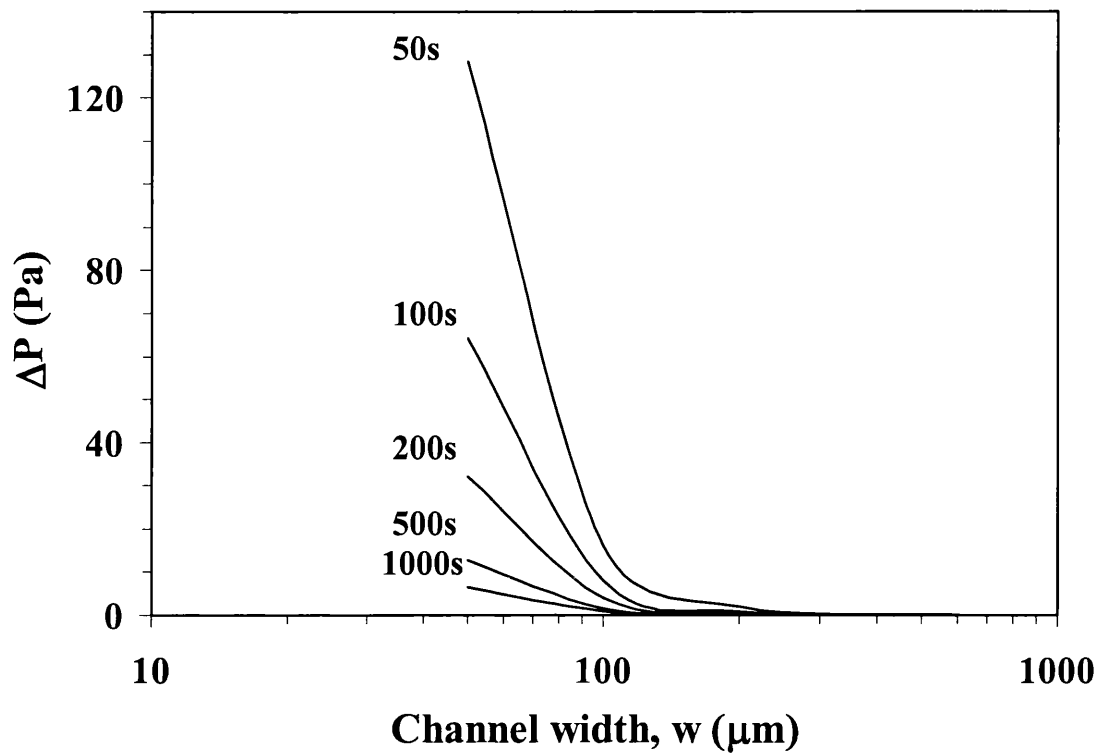
Figure A5.1   Plot of pressure drop against channel width